Actuation System Design Optimization

for Lower Limb Assistive Robotic Exoskeletons

ASIM GHAFFAR

Submitted in accordance with the requirements for the degree of Doctor of Philosophy

The University of Leeds
School of Mechanical Engineering

August 2020

The candidate confirms that the work submitted is his own, except where the work that has formed part of jointly-authored publications has been included. The contribution of the candidate and other authors to this work has been explicitly indicated. The candidate confirms that appropriate credit has been given within the thesis where reference has been made to the work of others.

Chapter 3 of this thesis is based on a jointly-authored journal publication:

Ghaffar, A., Dehghani-Sanij, A.A. and Xie, S.Q., 2020. A review of gait disorders in the elderly and neurological patients for robot-assisted training. *Disability and Rehabilitation: Assistive Technology*, *15*(3), pp.256-270.

The contribution of the candidate in this publication includes the literature survey, data collection, statistical analysis and writing. The contribution of the co-authors includes guidance, supervision and revision.

This copy has been supplied on the understanding that it is copyright material and that no quotation from the thesis may be published without proper acknowledgement.

The right of Asim Ghaffar to be identified as Author of this work has been asserted by him in accordance with the Copyright, Designs and Patents Act 1988.

© 2020 The University of Leeds and Asim Ghaffar

Dedicated to my parents,

who always believed in my ability to be successful.

Acknowledgements

All praise and thanks to Almighty Allah for giving me the courage to accomplish this work sincerely and successfully. During the period of this research work, I have been guided and accompanied by a number of people. I would like to acknowledge all of them for providing me the necessary support and direction.

I would like to express my sincere gratitude to my thesis advisor Professor Abbas Dehghani for his unlimited guidance, assistance and encouragement throughout the work. I am also very grateful to my co-supervisor Professor Shane Xie for his endless support, useful suggestions, reviews and comments. Special thanks to the School of Mechanical Engineering, the Faculty members, staff members and technicians of the School for their support. I would like to extend my sincere thanks to the fellow researchers and colleagues especially Sina Firouzy who provided me with the helpful advice and suggestions throughout this period. I am also extremely grateful to my friends and colleagues for making this journey a source of learning and excitement and for the constructive conversations we had during our coffee breaks.

I would like to express my deepest gratitude to my parents, without their support and guidance, this would have not been possible. The sacrifices they have made throughout, it is their motivation and direction that has eventually took me to this point to achieve this task.

A special mention goes to my wife and my children, Waleed and Zayd. I am deeply indebted to them for their endless love, encouragement and prayers, the patience they had shown can never be underestimated. Although, this period was filled with many ups and downs but their understanding and devotion played a vital role towards fulfilling my research targets.

Finally, I would like to acknowledge my sponsor University of Engineering and Technology Lahore for the financial support provided for a doctorate degree at this prestigious institute. This experience has no doubt given me the opportunity to work with the best people and resources.

Asim Ghaffar
University of Leeds, UK

Abstract

Assistive lower limb robotic exoskeletons are wearable devices that support people with impaired gaits to perform activities of daily living (ADL) independently. The rapid increase in the mobility disorders in the growing population has a significant impact on the demand of wearable devices. Consequently, the requirement to develop efficient wearable devices that meet the needs of the users has increased.

This study is oriented towards developing lightweight, power efficient and powerful assistive robotic exoskeletons with a focus on the actuation aspect. An analysis of the gait pathologies among different categories of patients reveals a significant difference in the spatio-temporal, kinematic and kinetic requirements of the impaired gait subjects as compared to the healthy users. Therefore, suitable powered assistive devices have to be developed to address the demand of the users. Following the assessment of the support requirements of the users, the number of degrees of freedom of the device was identified to evaluate an actuator design solution to determine an optimal motor size and transmission mechanism for a rigid actuation system. Part of this study also includes the elastic actuators that were used in two basic configurations as series and parallel elastic configurations. Elastic element was introduced into the system to reduce the power flow requirements of the actuation system. It was beneficial for the reduction of the actuator size and to increase the efficiency of the system. The spring optimization techniques were explored that lead to a decrease in the kinetic requirements of the system. The analysis showed that a parallel elastic actuator (PEA) was able to reduce significant amount of the power requirements of the system, while series elastic actuator (SEA) has a marginal impact on the overall efficiency of the system.

An actuator design solution was developed for the elastic actuators to determine an ideal solution for the motor and transmission mechanism for an elastic actuation system. Furthermore, the redundancy of an actuation system was also analysed in which the output power of the system is distributed between the two motors. The redundant rigid and elastic systems were investigated. The benefits of an elastic system as a variable stiffness actuator in a dual arrangement were assessed. An optimized design solution for a dual system was developed to evaluate an optimal dual actuation system for a rigid and elastic system.

Based on the outcomes of the actuator design solutions for a rigid and elastic systems in a single and dual arrangements, the optimal actuation systems were implemented and validated using a virtual prototype of an assistive robotic exoskeleton.

Table of Contents

List of Tables

List of Figures

List of Abbreviations

ADL	Activities of Daily living
AT	Ataxia
B	Ball screws
CP	Cerebral Palsy
CMT	Charcot Marie Tooth
CI	Confidence Interval
COG	Center of Gravity
CS	Control Subject
DOF	Degree of Freedom
DP	Diplegia
DF	Dorsi-flexion
ECG	Electrocardiogram
EEG	Electroencephalogram
EMG	Electromyography
H	Harmonic Drive
$\mathbf{H_b}$	Harmonic Drive with a Belt and Pulley Drive System
HP	Hemiplegia
$\mathbf{K_I}$	Integral Gain
L_Ankle	Left Ankle
L_Hip	Left Hip
L_Knee	Left Knee
$\mathbf{K_D}$	Derivative Gain
$\mathbf{K_P}$	Proportional Gain
$\mathbf{k_p}$	Parallel Spring Stiffness
$\mathbf{k_s}$	Series Spring Stiffness
$\mathbf{M_F}$	Multi-factor Optimization

MoCap	Motion Capture
NP	Neuropathy
PEA	Parallel Elastic Actuators
PD	Parkinson Disease
P_b	Belt and Pulley Drive
P_c	Total Power Consumption
PF	Plantar-flexion
PWM	Pulse Width modulation
R_Ankle	Right Ankle
R_Hip	Right Hip
R_Knee	Right Knee
ROM	Range of Movement
REV	Reverse
RMS	Root mean square
RSEA	Rotary Series elastic Actuators
SEA	Series Elastic Actuators
STS	Sit-to-Stand
ST	Stance Phase
SD	Standard Deviation
SW	Swing Phase
U_C	User's Carrying Capacity
V-PEA	Variable-Parallel Elastic Actuator
V-SEA	Variable-Series Elastic Actuator
W_{exo}	Total Weight of the Exoskeleton

List of Publications

Chapter 3 of this thesis is based on a jointly-authored journal publication:

1. Ghaffar, A., Dehghani-Sanij, A.A. and Xie, S.Q., 2020. A review of gait disorders in the elderly and neurological patients for robot-assisted training. *Disability and Rehabilitation: Assistive Technology*, *15*(3), pp.256-270 [https://doi.org/10.1080/17483107.2019.1568594].

The following jointly-authored papers based on the work done in Chapter 4 to 7 are under-preparation and will be ready to be submitted soon.

2. Ghaffar, A., Dehghani-Sanij, A.A. and Xie, S.Q., Optimal design of an Assistive Robotic Exoskeleton Actuation System,

3. Ghaffar, A., Dehghani-Sanij, A.A. and Xie, S.Q., Optimization and Implementation of an Assistive Exoskeleton Actuation System for the Elderly using Series and Parallel Springs.

4. Ghaffar, A., Dehghani-Sanij, A.A. and Xie, S.Q., Optimal Design of Dual actuation system for an assistive robotic exoskeleton,

5. Ghaffar, A., Dehghani-Sanij, A.A. and Xie, S.Q., Modelling of a robotic exoskeleton for investigating the efficiency of an actuation system.

Chapter 1
Introduction

1.1 Background

Ambulation is an important goal of elderly and people having gait difficulties. A number of advances have been made in the field of user oriented robots that integrate robots and humans into a single system. One such system is the exoskeleton robot that can assist humans in their activities of daily living (ADL). An exoskeleton robot can be defined as a mechanical device that is worn outside the human body and is capable of detecting human motion intention through sensors. It integrates human intelligence and robot power and works in coordination with the human movements. The external force is provided by the actuators equipped at the joints of the device, thus an exoskeleton can provide complete assistance to the user. A number of robotic exoskeletons have been developed that are able to provide gait rehabilitation, assistance and can also be used to increase the strength of humans. Many developments have also been made in the field of assistive exoskeletons that can provide support to elderly and other pathological gait users.

The mobility disorders are rapidly increasing worldwide with the growing population that can seriously affect individuals to perform ADL independently. In order to improve mobility, there is a need to develop light weight exoskeleton robots based on the needs of the users that can provide assistance in locomotion. A number of exoskeletons have been developed that can provide assistance to the users in performing the ADL. These exoskeletons available to date will be examined in Chapter 2 highlighting the limitations in each of them.

This research will focus on lower extremity assistive exoskeleton robots and work towards the actuation system design by investigating the technical aspects in the design of an assistive robotic exoskeleton. It will examine the solutions to fulfil the shortcomings in the existing designs and therefore, pushing the boundaries in the field of assistive robotic exoskeleton.

1.2 Motivation

Considering the growing elderly population and people with lower limb impairments, there is a high demand for wearable assistive devices that can provide the required support to perform (ADL) independently. Exoskeletons can significantly increase the level of performance of its users. However, efforts are required to develop better designs that should have some leverage over the existing products. To build a powered exoskeleton, research is required to investigate in a lightweight, portable and safe designs as most of the devices developed so far are bulky in nature which also creates portability issues.

The above aspects could be achieved by carefully considering some key issues. The first and foremost is the user support requirements among different gait impairments. Criteria should be explored to systematically define the assistance requirement among potential end users so that the user's technical and clinical needs could be identified. A comprehensive detail of various types of gait impairments and the biomechanical deviations found in the impaired gaits will be analysed in Chapter 3. Based on the assistance requirement, portable, lightweight and efficient actuation systems could be developed that can provide complete assistance to the user which is the main point of focus of this research. By reducing the size of a motor in an actuation system, the losses in the motor winding increases and vice versa. Therefore, an optimum actuation design solution should be figured out that performs the best trade-off between the selection of the actuation systems in terms of the weight, and power efficiency of the system. Some part of these methods exist in the literature but a complete solution that defines an optimal solution based on specific objective functions regarding assistive robotic exoskeleton cannot be found and there is a need to exploit these areas to develop algorithms that completely define an optimal solution for an actuation system of an assistive robotic exoskeleton. In an actuation system, the type of the transmission system greatly affects the performance of an actuation system and thus for an optimal selection of the transmission systems, comparative studies are required to assess the performance of commonly used transmission systems in the exoskeleton. The transmission systems are modelled in Section 4.3 of Chapter 4 and a comparative study will be obtained to assess the optimum actuation solution.

The power requirement of the system can also be affected by using passive elements at the joints of the exoskeleton actuation system as revealed by the previous studies. However, it was found that the best performance using

a passive element e.g. a spring, could be achieved only when it is optimized to a certain range of a particular parameter in which the performance of the system is maximum. This performance has to be defined with respect to a particular parameter. There is a need to exploit the spring optimization techniques to achieve the best performance of an elastic actuation system. As with case of a rigid actuation system, there is a need to devise an actuation solution for the case of elastic systems. An investigation has to be made to determine the benefits of optimization of the elastic elements together with the best actuator selection techniques. However, it will be noticed in Chapter 5 that the performance could be further increased by varying the stiffness of the spring. Therefore, solutions will also be devised to determine the optimum performance of the actuation system implemented with the variation of the spring stiffness in order to boast the efficiency of the system. One such technique to exercise this is to utilize a dual actuation system that will be addressed in Chapter 6. Depending upon the arrangement of the two motors, different types of redundancies could be executed. In this study the two motors will be arranged to a common shaft in an antagonistic arrangement known as static redundancy in which the torques add up when the two motors move in the same direction and it changes the stiffness of the spring without producing any torque at the output, when they move in the opposite direction. This type of dual actuation concept needs to be explored in the assistive exoskeletons and the benefits of the variable spring stiffness associated with them. Ideal efficiency solutions are needed for this type of system as the author did not find any optimal design solution available in the literature related to the dual actuation system.

Based on the above mentioned concerns for an assistive robotic exoskeleton, this project is linked to several following research questions.

- What should be the best optimal actuation solutions (best actuator combinations) so that the efficiency of the overall system is increased?
- How much compromise should be made in the weight of the exoskeleton in order to make it more power efficient or vice versa?
- What should be the best approach in order to optimize a spring in an elastic actuation system and how to maximize its performance?
- Can a dual actuation system brings benefits in the weight and power efficiency of the system at a cost of adding complexity to the system?

- How much benefit a variable spring stiffness approach can bring in the actuation design solution?

1.3 Aims and objectives

1.3.1 Aim

The aim of the project is to optimize the design (in a virtual environment) of a novel assistive lower limb exoskeleton robot with a focus on its actuation aspects.

1.3.2 Objectives

The objectives of the project will define the steps to be taken in achieving the above aim which are given as follows:

- **To establish the assistance requirements of the potential users of the lower limb exoskeleton robot:** The identification of the support requirement of the end users i.e. finding the degree of impairment of patients is the primary step in the design of an exoskeleton actuation system.
- **To perform dynamic simulations to determine the joint kinematic and kinetic requirements:** The dynamic simulations will be carried out in order to assess the joint torque and power requirements of an assistive exoskeleton. These requirements will be achieved for the common tasks of ADL.
- **To analyse the commercially available motors and transmission systems suitable for an assistive robotic exoskeleton:** A market search of the available motors and transmission systems will be performed that will be best suited for an assistive robotic application.
- **To determine the optimal selection of the actuation system:** An optimal actuation solution will be presented with a focus on a lightweight design, power efficient and powerful system.
- **To evaluate the spring optimization techniques:** Elastic elements will be introduced into the actuation system and methods will be developed to optimize the spring parameters.
- **To assess the optimal solution of an elastic actuation system:** An optimal design solution for a series and parallel elastic actuation system will be evaluated.
- **To establish the variable spring stiffness optimization technique:** To bring variable stiffness solutions to the actuation system, dual actuation optimization techniques will be explored.

- **To investigate the optimal solution for a dual actuation system:** The dual actuation system will be arranged in an antagonistic arrangement and optimal dual actuation system for a rigid and elastic system will be developed.
- **To build a virtual prototype and to validate the mathematical and simulation model:** The virtual prototype of an assistive exoskeleton will be developed with a rigid and elastic, single and dual actuation systems that will also be used for the design verification of the models.

1.4 Scope of this research

This research presents an actuator design solution to obtain a lightweight, power efficient and a powerful system for an assistive robotic exoskeleton actuation system. Actuation systems of the lower extremity exoskeletons in the sagittal plane have only been assessed in this study. The main scope points of this research are as follows:

- To identify the support requirements in elderly and neurological gait patients for the actuation design of an assistive robotic exoskeleton.
- To evaluate an actuation design solution to obtain an optimal rigid actuation system
- To examine the spring optimization techniques and develop an optimal solution for series and parallel elastic actuation system
- To assess the variable spring stiffness in the dual actuation systems and obtain an optimal dual actuation system for assistive robotic exoskeletons.

1.5 Contributions of this research

This research contributes to the assistive medical applications with a focus on providing assistance to the elderly and other pathological gait patients using lower limb exoskeletons. The contributions of this research are summarized below:

- A systematic approach was developed and a general trend was established for the support requirements in the elderly and neurological gait patients.
- An actuator design solution for an assistive exoskeleton that utilizes a significant search space of the motors and transmission systems leading to a lightweight and power efficient design. The most efficient

design was found that uses ballscrews at the knee joint and harmonic drives at the hip and ankle joints.

- The multi-factor optimization technique developed for elastic elements was found to be most suitable to optimize series and parallel springs in an elastic actuator. The optimization algorithm designed for elastic actuators evaluates the optimal design that utilizes harmonic drives at the hip and knee joints and ball screws at the ankle joint in a parallel configuration of the elastic element.
- A variable stiffness actuator can be implemented using a dual actuation system. It has been found that the efficiency of the system is increased by combining elasticity with the redundancy of the actuation system. A further reduction in the power requirements is achieved by designing an actuator solution for dual actuators.
- A successful implementation of a virtual prototype of an assistive robotic exoskeleton using a rigid and elastic actuation system for a single and dual actuators based on the results of the optimal actuator design solutions.

1.6 Outline of the report

The contents of the thesis are organized as follows:

Chapter 1 introduces the background and the motivations in carrying out the project. The aims and objectives were defined and the scope and the contributions of the project were presented.

Chapter 2 provides a comprehensive review of the literature and the work carried out by researchers so far in the field of assistive exoskeleton robots. Different possible areas of the exoskeleton are reviewed and analysed. It includes biomechanical parameters, human robot interaction, actuator technologies and control strategies used in wearable devices. Furthermore, it discusses the strengths and weaknesses of the available exoskeletons.

Chapter 3 focuses on the design requirements of the exoskeleton robots and analyses the assistance required from them. It defines the end users and investigates in detail the assistance required by them. A report on the meta-analysis of the spatio-temporal, kinematic and kinetic gait parameters of elderly and neurological patients are presented and analysed.

Chapter 4 illustrates the optimization algorithm and discusses the types of actuation systems used in the optimal actuator design solution in order to develop an optimal robotic exoskeleton actuation system. The kinematic and

kinetic requirements of the lower limb joints are obtained using an experimental setup. The mathematical and simulation model of the assistive exoskeleton is developed and the modelling of the electric motor and the power transmission systems used in the actuator design solution are discussed. The optimization algorithm is defined to obtain an optimal rigid actuation system of an assistive robotic exoskeleton.

Chapter 5 presents the development of an optimal design solution for the elastic actuators used in an assistive exoskeleton. It discusses the modelling of the series and parallel elastic actuators. Furthermore, the evaluation of spring stiffness using optimization techniques in the elastic actuators are highlighted. The models of the elastic actuators with the optimized elastic elements are used in the actuator design solution to obtain optimal elastic actuation system.

Chapter 6 describes the development of the optimal actuation solution for a dual actuation system. It uses the concept of actuation redundancy to identify a variable stiffness actuator. Different techniques will be formulated to optimize the spring in consideration to the type of manoeuvre it performs. The variable elastic models arranged in a dual actuation system in an antagonistic arrangement are assessed using the developed dual actuator design solution to obtain a lightweight and power efficient dual actuation system. Furthermore, a dual actuation system in a rigid mode without using the elastic elements is also assessed.

Chapter 7 describes a virtual prototype of an assistive robotic exoskeleton actuation system. It examines several models of the DC motor speed control system. The actuation models with different designs were tested and the energy consumed by the virtual prototype of the exoskeleton during the performance of various locomotion tasks is assessed. It also validates the optimal actuation models obtained using the actuator design solutions for a rigid and elastic, single and dual actuation system.

Chapter 8 summarizes the work in this thesis and presents the conclusions drawn from this study. Furthermore, the future challenges are also highlighted.

Chapter 2
Literature Review

2.1 Introduction

A robotic exoskeleton is a mechanical device that is worn outside of the human body and is capable to combine human intelligence and machine power. There are several versions of robotic exoskeletons available in the literature that comes as full body, upper extremity and lower extremity exoskeletons. These devices have been applied in the various fields of military, medicine such as assistance, rehabilitation etc. In military and industrial applications, the exoskeletons can empower the human strength capacities to carry heavy loads [1]. The assistive versions of exoskeletons can provide support to elderly and other paraplegic patients to carry out ADL independently [2, 3]. These devices are expected to work in close collaboration with humans integrating the intelligence of humans with the robot power. The major applications of the exoskeleton robots are summarized below:

- Assistive exoskeletons: These types of exoskeletons are designed to provide ambulation to some patients and elderly population of the society. The major problem faced by these people is the inability to sit, stand or walk independently. By using these exoskeletons, people suffering from paraplegia or quadplegia can have improved quality of life as they can perform activities of daily living.
- Exoskeleton used for rehabilitation purposes: Stroke is a trauma that has affected many people and it can lead to an inability to walk and often the patients can have one or more paralyzed limbs. In order to restore the affected part, it requires rehabilitation treatment to restore gait function and regain the ability to walk independently. The exoskeletons are capable to provide regular gait training to restore the weakened part of the human body.
- Exoskeletons for human power augmentation: Exoskeletons can also be designed to carry heavy loads such as in military applications or to help reduce the burden of the worker in an industry. These types of exoskeletons enhance the power capabilities of humans giving them extra power to achieve the required tasks.

In this study, the exoskeletons that can provide assistance to the humans in their daily life activities will be considered along with the different aspects associated with the wearable devices. This chapter provides a review of the current assistive exoskeletons developed so far and their related technologies. However, it will not consider the areas of exoskeletons that are either outdated or less important. The primary focus will be on the portable, untethered devices that are able to provide assistance to the users. The issues discussed will include the different technological aspects of the exoskeletons. Section 2.2 introduces the biomechanical parameters that should be taken into account when designing an exoskeleton. This will be reviewed in order to develop a better understanding of the dynamic modelling of the exoskeleton performed in the preceding chapters. The sensors that have been observed to be used in exoskeletons will be discussed in Section 2.3. Sensors are a main source of human robot interaction. The actuator technology used will be defined in Section 2.4. These include the actuation design that will include the rigid, elastic and dual actuation systems. Some of the methods related to the control strategies will be discussed in Section 2.5 and some performance indices methods will be reviewed in Section 2.6. Some of the control strategies that have been applied in exoskeletons will be summarized in Section 2.5. Methods to estimate the performance of an exoskeleton will be introduced in Section 2.6. The knowledge gaps and the limitations of the existing devices will be discussed in Section 2.8.

2.2 Biomechanical considerations

Human biomechanical considerations are an important aspect to consider in the design of lower limb exoskeleton robots. These include consideration of the parameters such as maximum joint torque, maximum range of motion, joint velocity and joint bandwidth during the development of the exoskeletons. These parameters help in proposing improved designs of lower limb exoskeleton robots. An exoskeleton design should be able to provide natural movement of the human limb without interference. Ideally, an exoskeleton should possess the following characteristics related to biomechanical kinematics: It should have enough degree of freedom (DOF) to allow unrestricted motion, the maximum torque at the joint should be compatible with that of the human joint torque, and the joint centre of the exoskeleton should be aligned with that of the human joint. Usually, the non-ideal mechanics of the joints makes the design process difficult. Moreover,

human biomechanics change from one wearer to the next. This section will cover the kinematics and kinetic factors that should be considered in the design stage of exoskeleton robots. Before considering these factors, a brief review of biomechanics of human walking will be presented.

2.2.1 Biomechanics of human walking gait

Some basic terminologies related to the human walking will be defined as they are essential in developing the kinematic and kinetic considerations of the lower limb. A human walking can be defined as a method of locomotion using two legs that can alternatively provide support and motion. A human walking gait cycle consists of two phases: swing phase and stance phase [4] and each phase is further subdivided into different subphases. A gait cycle is defined as a successive intervals of repetitive events of walking. It usually starts when one of the foot makes an initial contact with the ground. The phase when a foot makes contact with the ground is known as a stance phase and during the instance when the foot is not in contact with the ground is known as swing phase. Consequently, stance phase starts with the heel strike and ends with the toe off position (also known as foot off). Similarly, swing phase begins with the toe off position and terminates when the same limb strikes the ground again. This is also illustrated in Figure 2.1.

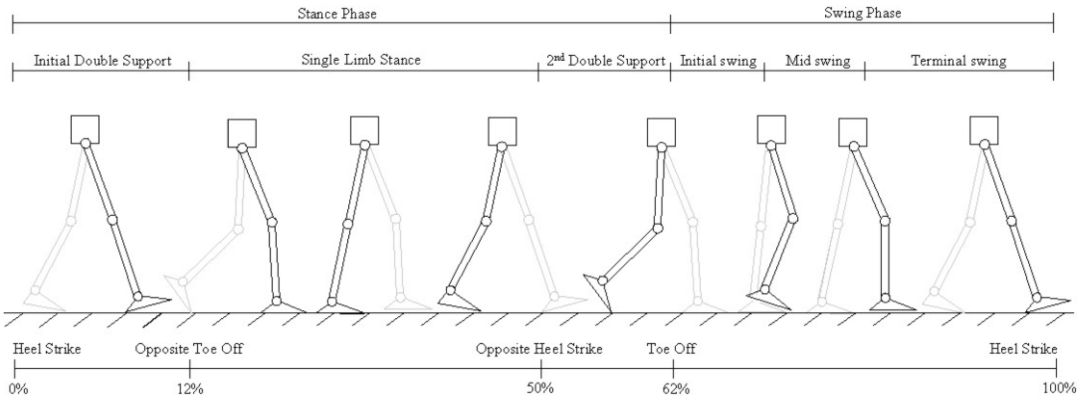

Figure 2.1: Phases of Human walking gait cycle [4]

As mentioned, these phases are further subdivided into eight phases: initial contact that occurs when the heel strikes the ground and happens over 2% of the total gait cycle, following by the initial contact which is the beginning of the loading response. The loading response appears during the period between the initial contact and opposite toe off. This ends the double support phase and the cycle turns into a single limb phase. After the opposite toe-off, the stance leg reaches the mid stance phase that lasts until the heel off of the same foot. The stance phase occupies approximately 60% of the total gait cycle. The heel off occurs symmetrically with the opposite

foot contact and the leg moves into the pre-swing phase which is the second period of double support phase. Following this the cycle enters into the swing phase which is again a single limb support phase, and is further sub divided as initial, mid and terminal swing phase. This has been more clearly depicted in Figure 2.2 adapted from Perry's work [5]. During each gait cycle, there are two periods of single support phase and two periods of double support phase. The percentage of occurrence of each phase depends upon the speed of the walking, thus increasing the single leg phase during faster speed and vice versa (Murray 1967).

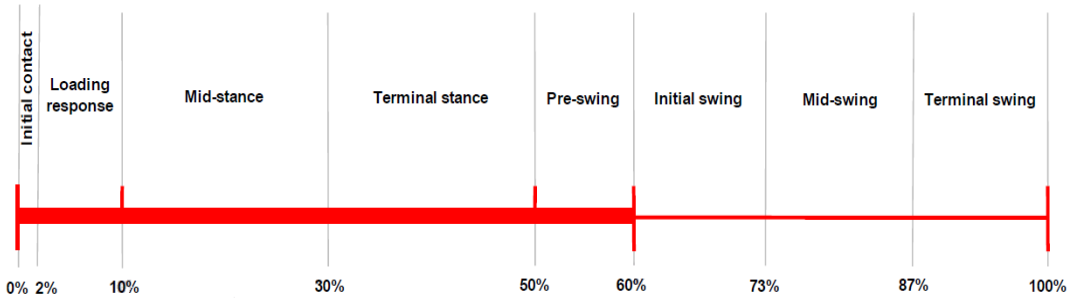

Figure 2.2: Sub-division of Swing and Stance Phase [5]

Some basic terminologies used to define the placement of the foot during the gait cycle will be elaborated as follows. The stride length is defined to be the distance between the two consecutive positions of the same foot. A stride length consists of two step lengths one termed as right step length and the other as left step length. These terms are illustrated in Figure 2.3. These two step length might be different for a pathological gait. Further details will be discussed related to the pathological gaits in Chapter 3. A stride width is defined to be the side by side distance between the left and right foot and usually measured using centre of the heel of each foot. One complete gait cycle consists of two steps, cadence is defined as the number of steps taken per minute and therefore it is the measure of the half cycles. The speed of walking is the distance covered by the body during a specified time. It usually measured in meters/ seconds.

The locomotion of the human body can be defined using three planes: Sagittal plane, Coronal plane and transverse plane shown in Figure 2.3. A sagittal plane is the upright vertical plane that divides the human body into left and right halves. A coronal plane refers to the perpendicular vertical plane that divides the body into front and back portion. A transverse plane is the horizontal plane dividing the body into upper and lower extremities. Human lower limb can be thought of as a 7DOF structure with links and joints. There are 3DOF for the hip joint, 1DOF for knee and 3DOF for ankle

joint [6].The human limb locomotion takes place in the sagittal plane. This includes flexion/extension of hip, knee and ankle joint. The flexion/extension movement of ankle joint is known as dorsi-flexion and plantar flexion of ankle joint. Human balance is maintained through other planes. Movement in the coronal plane includes hip abduction/adduction and ankle eversion/inversion. Hip and knee internal/external rotation takes place along the transverse plane. However, the internal/external rotation of knee is less considerable. It has been observed that the forward walking, the hip joint consumes power, so a power adding source should be incorporated at hip flexion/extension joint, knee joint dissipates power, therefore using a damper or brake can be beneficial and a passive spring element can be used for storing and releasing energy at the ankle joint [6].

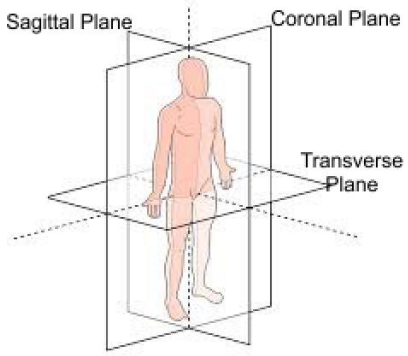

Figure 2.3: Three planes of human locomotion

2.2.2 Kinematic and Kinetic considerations

The biomechanical properties that should be considered in the design process of an exoskeleton include DOF, range of motion (ROM), joint torques, joint velocity and bandwidth.

As discussed in the previous section, human lower limb consists of 7 DOF for each leg, three for hip, two for knee and two for the ankle joint. The hip joint can be modelled as a ball and socket joint, knee joint as condyloid joint and ankle joint as a hinge joint considering two degrees of freedom [7]. The movement in the sagittal plane is responsible for locomotion. The hip flexion/extension is included in all designs of exoskeletons [8] and the limb lies in the plane containing the axis of rotation, therefore, this DOF is not an issue. This is not the case for adduction/abduction and internal/external rotation of the hip joint. In both the cases, the limb is offset from the axis of rotation. The MIT exoskeleton [8, 9] and BLEEX [1] are the only exoskeletons available that possess DOF along hip adduction/abduction and

internal/external rotation. The MIT exoskeleton has taken this issue into account by placing the rotation joint above the knee in the upper part of the limb [10].

The knee joint is considered to have flexion/extension and internal/external rotation but the knee internal/external rotation is found to be very limited so most of the designs of exoskeletons available have only one DOF for the knee joint which is flexion/extension in the sagittal plane. The actuation applied at the ankle joint is also employed at ankle flexion/extension.

Another kinematic parameter to consider is the joint ROM of an exoskeleton. The ROM depends on the type of application e.g. the joint ROM of an exoskeleton used for rehabilitation and assistance purposes is the ROM of that joint during normal walking of a healthy person. The MIT knee exoskeleton has a ROM of 100 degrees knee flexion that is designed for running purposes [11]. These biomechanical properties of the human limb are summarized in Table 2.1.

Table 2.1: Ranges of Biomechanical properties of human limb [7]

Joint / Plane	Hip (°)	Knee (°)	Ankle (°)
Coronal	40/30-35 (adduction/abduction)	---	30-35/15-20 (inversion/eversion)
Sagittal	140/15 (flexion/extension)	120-140/0-10 (flexion/extension)	40-50/20 (dorsi-flexion/plantar-flexion)
Transverse	15-30/60 (medial/lateral)	10-15/30-50 (medial/lateral)	---

It can be observed in Table 2.1 that the maximum range of motion for hip, knee and ankle occurs along the sagittal plane. Knee internal/external rotations are considerably less compared to knee flexion/extension. Maximum range of motion is achieved by hip flexion which is found to be 140°. Since locomotion takes place along the sagittal plane, therefore the movement along this plane only will be point of focus in this research.

An exoskeleton should be capable of providing a movement close to the natural healthy movement of humans as much as possible as well as to assist the wearer during locomotion. This is achieved by applying joint torques of appropriate magnitude and direction. This is important aspect in the design and control of exoskeletons. The walking and running activities of

the human are performed by the motion of the lower limbs in the sagittal plane [11]. All exoskeletons should be designed in such a way so as to provide power to joints in this plane. Zoss et al. pointed out that hip adduction/abduction requires the largest power during motion [1]. Therefore, the assistance must be included in this joint when designing exoskeleton.

For designing the actuation system, gait analysis can be performed that provides the average motion data during locomotion. The gait analysis data fluctuates during the cycle and therefore joint moment also fluctuates [1, 12]. Joint moment represents the nature of actuators to be used in the design process. However, other methods such as optimization method or human motion data model are also used to determine the type of actuation system to be used in each joint [13].

The above parameters described represent the static characteristics. However, locomotion is a dynamic task and therefore joint velocity and bandwidth should also be considered. These parameters were considered by [6, 14] in the design of the actuation system in exoskeletons. These parameters are particularly important so that the actuation system should not only be able to provide the required magnitude of the torque but also with necessary velocity and bandwidth.

There has been observed a lot of variability and uncertainty in human biomechanics. In order to effectively design the actuation system of an exoskeleton, both kinematics and kinetics factors need to be considered. Exoskeletons can be found with variable number of actuated joints and DOF.

2.3 Sensor technologies used in exoskeleton robots

In this section, the advancements and limitations related to the sensor technologies in the exoskeletons will be discussed. Sensors are the necessary components in an exoskeleton design and the main source to measure interaction between human and exoskeleton. Apart from developing improved designs of exoskeletons, there should also be a sophisticated means of determining the wearer’s intention and motion. Sensors play a critical role in the efficient and smooth operation of exoskeletons. They are the first and necessary component in an exoskeleton design. Many control strategies are based on the type of sensors used to obtain information. Every exoskeleton robot found in literature contains some form of sensor to measure the human intention. Based on the exoskeleton control, sensors can be classified into three types: Sensors that measure

signals directly from the human body such as EMG or EEG, sensors that measure the interaction forces between exoskeleton and wearer and sensors that can estimate signals directly from the exoskeleton. The interaction between human and user is a fundamental factor for smooth and efficient operation of the system. They play an important role in monitoring, identification and control of exoskeletons. This section is devoted to the study of the sensors that have been found in different designs of the exoskeleton robots.

2.3.1 Measuring signals from the human body

The first category of sensors are those that measure biological signals from the human body. These include measuring signals such as EMG [15], EEG [16], ECG and EOG. They contain useful information regarding human motion intention. Thus, signals can be measured without any loss of information and delay. Surface electrodes are used to measure the muscular activity during muscular contraction and can directly respond to activity status in human muscle. Although the signals from the EMG are very weak and is sensitive to noises but they are mostly employed in control systems and can be used to estimate intention efficiently . Even if the EMG signals are weak i.e. for the case of elderly patients, they can still be used to determine the human motion intention accurately. The relationship is observed to be linear between EMG signal and joint torque. Apart from the advantages of EMG signals described, there are also some drawbacks as follows. It is difficult to produce an identical signal for one user performing the similar action, muscular activity status could also vary from one user to another implementing the same task, prediction of real time motion is a difficult task as different muscles are involved during a motion [17].

Multiple sensors are operated to obtain human robot information. It is a combination of an array of sensors to determine the interaction between human and robot. HAL 3 and HAL 5 used EMG signals to measure the human motion intention [18, 19]. The electrodes are placed on desired muscles to obtain the required force/torque at joints. Researchers also detect human motion intention by using EMG signals and human musculoskeletal model [20-22]. Human lower limb can be modelled as a 7DOF rigid structure with links and joints. EMG signals are measured at selected points on the muscles of the lower limb.

A lot of work has been highlighted on EEG based exoskeletons. The exoskeletons that used discrete commands of EEG signals i.e. the intended action were investigated by [23] and [24]. These have also been utilized in

exoskeleton control. Invasive brain machine interface and non-invasive brain machine interface are the two types of brain machine interface. The EEG is considered as a type of non-invasive brain machine interface. The EEG based brain machine interface in exoskeletons were employed by [25] and [26]. Hintermuller et al. measured EEG signal at eight electrode positions and the output was transferred to a linear discriminant analysis classifier to distinguish the correct commands of EEG [25]. Apart from many advantages of EEG signals there are also several limitations as well which include high sensitivity, constraints of the evaluating instrument, EEG signals can also merge which are measured from different areas of muscles.

2.3.2 Measuring interaction forces between the human and the exoskeleton

These categories of sensors measure the forces that exist between exoskeletons and humans. Some sensors measure forces directly from the interaction points while others require an additional intermediate sensor placed at the attachment point. LOPES lower limb exoskeleton measures pressure interaction between human and exoskeleton [27]. In this paper, the author used three techniques to measure the efficiency of this sensor. These include: static test, dynamic test and gait training test. In the static test, the subject provided an incremental torque at the hip joint in the stationary condition. A toque was applied at the hip joint in the dynamic test while the subject was standing. Similarly HAL 5 uses the floor reaction force to estimate the position of centre of gravity and that can be used to estimate the human motion intention [28].The intention of the user can be detected through floor reaction force sensors so that the control system provides assistance to the user during walking. As described earlier in this chapter, the walking phase can be divided into two phases, swing phase and stance phase. By estimating the reference pattern for each phase, the exoskeleton will be able to assist the wearer during walking. Sometimes, pressure sensors which are placed on the straps are used to determine the interaction forces between exoskeleton and the wearer. Light in the photosensitive diodes was obstructed with the change in the pressure and thus output current varied accordingly. A force detection system via a force sensor has been used in [29] to detect the physical interaction. The interaction force sensors give the direct information regarding human motion intention.

2.3.3 Measuring signals from exoskeletons

These type of sensor measure signals directly from an exoskeleton. They have an advantage of not requiring an additional interface in the control

system to estimate the wearer's motion. These sensors can be applied directly on the exoskeleton. Sensors may include angle sensors such as encoders which are usually located at hip, knee or ankle joint to measure joint angle, angular acceleration sensors, which are used to obtain the angle, angular velocity and angular acceleration of the joints on which the sensor is located. The inertial measurement sensor is positioned on the leg to predict the motion state of the human [30]. Gyroscope and inclinometers are usually positioned at the back to estimate the angle between upper torso and vertical direction. In BLEEX, force and torque sensors are located at the hip, knee and ankle joint of the exoskeleton to measure the required parameters [31]. The running state can be determined by pressure sensors. These are usually fixed on the sole of the exoskeleton or at the bottom of the crutches. Some other force/pressure sensors that can be used in exoskeleton applications are piezoelectric, strain gauge and capacitive force sensors.

2.4 Actuator designs of Lower Extremity exoskeleton robots

Actuators used in exoskeleton robots are required to provide high torques while operating at high speeds. Therefore, selecting a particular type of actuator is a difficult task as one has to weigh the pros and cons of each type of actuator. Size, weight and power efficiency of actuators have limited the applications of exoskeleton robots. In order to provide high torques requirement, significant amount of size and inertia should be introduced to exoskeleton robots to house the actuators. Electrical, hydraulic and pneumatic are the main actuation modes used in exoskeletons. Elastic actuation systems are also used in exoskeleton robots [32]. Exoskeletons can be classified according to the actuation modes as: hydraulic actuators, pneumatic actuators and electric actuators. An actuator should possess the characteristics such as low inertia, fast response, high precision and safety performance. The first walking exoskeleton was developed in 1969 using pneumatic actuation [33]. A hydraulically actuated full body exoskeleton was introduced by General electric during the same era [34]. The first electrically actuated design was developed by [35] in 1974. The above mentioned actuation modes of exoskeletons also contain some limitations. The main drawback among them were non-back driveability of actuators so elastic actuators became the point of focus that possess special characteristics as high fidelity, low impedance, low friction etc [32, 36]. The primary task in the design of exoskeleton robots is the selection of actuation mode according to the intended application. The mechanism of the exoskeleton is designed

around the actuator and then the associated sensors and power supply is developed. Therefore, the exoskeleton robots are classified according to the actuation mode used.

2.4.1 Hydraulically actuated exoskeleton robots

Hydraulic actuators transmit power via oil and therefore having simple structure, easy to operate and high power output but the issue of oil leakage reduces the overall efficiency and causing environmental pollution. The prime movers or pumps used to pressurized fluid are too heavy and bulky lowering the specific power of these actuators [37]. The BLEEX robot, developed by university of California in 2004 uses hydraulic actuators [38, 39]. BLEEX was initially design for augmentation purposes but introduced with assistive applications in the later versions. BLEEX consists of 7DOF, out of which 4DOF (2DOF at hip, one at knee and one at ankle) require high torque so a two way linear piston type hydraulic cylinder with a diameter of 19.05mm was used. The torques were calculated based on human walking gait analysis. It can also obtain high control bandwidth. Another type of exoskeleton known as Sarcos uses rotary hydraulic actuators that are positioned directly at the powered joint of the exoskeleton [15, 40, 41]. In terms of performances, the hydraulic actuators can supply high power to weight ratio and therefore they are suitable choices for actuation in exoskeletons designed for augmentation purposes. The rotary hydraulic actuators employed in Sarcos exoskeleton has more inner leakage compared to the linear one [31]. BLEEX and Sarcos exoskeletons are shown in Figure 2.4.

Figure 2.4: (a) BLEEX [1] (b) Sarcos [15]

2.4.2 Pneumatically actuated exoskeleton robots

These type of actuators used compressed air as the transmitting medium and therefore they are lighter and cleaner as compared to hydraulic ones

[42]. It has been observed that exoskeletons that used pneumatic actuators would have slower response speed and lower load carrying capacity.

The nurse assisting exoskeleton developed in Japan [43, 44] utilized pneumatic rotary actuators as the actuation mode. This type of robot is used to assist nurse to carry a patient in her arms. It consisted of a full body exoskeleton that employed pneumatic rotary actuators with pressure cuffs in the middle of the thin plates. Figure 2.5(a) elaborates the pneumatic rotary actuator for elbow and knee joint and Figure 2.5(b) illustrates for waist joint. When a pressure is supplied, the plates expand, therefore providing torque and accordingly rotational motion is supplied by the actuators.

Researchers have also designed a flexible device similar to human muscle known as pneumatic muscle. University of Salford developed an exoskeleton that employed this type of actuator in their design [45]. It consists of a flexible reinforced closed membrane attached at both ends.

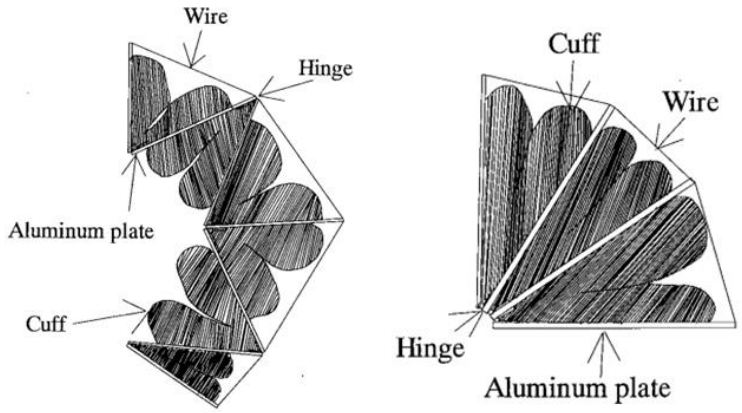

(a) **(b)**

Figure 2.5: Pneumatic rotary actuator (a) for elbow and knee joints (b)waist joint [43]

2.4.3 Electrically actuated exoskeleton robots

The electric actuators can provide a smooth operation with high precision and without any problem of leakage or environmental pollution as is the case with pneumatic and hydraulic actuators. A fundamental limitation of electrical actuators is the need of the transmission element that converts the high speed, low torque output into low speed and high torque to be used in exoskeleton robots. These transmission elements affects back drivability, efficiency, introduces backlash, friction, noise, safety issue and complexity of electrical actuators.

BLEEX exoskeleton also used electrical actuators apart from the hydraulic ones [46]. By comparing the two actuation modes, it can be observed that the electric actuators are more power efficient but are heavier than hydraulic ones [47]. Techniques were also presented in [46] for selecting the appropriate size of the actuators and gearing mechanism. As the requirements of exoskeleton robots are high output torque and low speed, therefore geared electric drives are used in order to satisfy the requirement. The hybrid assistive limb HAL 5 utilized electric actuators. Each electric actuator comprises of a DC servomotor and a harmonic gear drive and therefore they can supply required torque at hip, knee and upper body joints. Most of the lower limb exoskeletons such as REX, Ekso, ReWalk, Indego, HAL used electrical actuation system with two degrees of freedom per leg. The electric motor is used with a suitable form of the transmission system such as harmonic drives, ball screws, chains and sprockets and belt drive system. Since the devices are untethered, therefore portability and thus battery technology usually limits the efficiency of an electric actuator. Therefore, focus is mainly onto the development of efficient actuators that can reduce the size of the battery and prolong the operational time of the system.

2.4.4 Elastic Actuation System

There are certain drawbacks using traditional non-backdrivable actuators such as friction, backlash, noise of the gears etc. For these reasons, researchers are developing another type of actuator that introduces elasticity into the system using a conventional spring or other form of the elastic element to overcome some of the limitations with the traditional actuation systems. It can combine the following advantages: energy storage due to spring mounted in the device, shock tolerance, lower inertia and more stable force control [32, 35]. Therefore, elastic actuation systems have been used in many exoskeletons and orthosis. Human cognition of Florida institute developed rotary series elastic actuator (RSEA) shown in Figure 2.6 [48, 49]. It was used to drive a power assist lower extremity exoskeleton robot having 5 DOF on each leg, out of which three of them are active. The RSEA consists of a brushless DC motor with a harmonic reducer. The gear reducer can convert the rotary motion into linear motion. Encoders are placed on the actuator to detect the position and torque output. Another type of SEA converts the rotary motion into linear motion by using some conversion mechanisms such as gear and rack, ball screws or belt and transmission mechanism. This kind of actuator is used in knee-ankle foot robot developed

by university of Singapore [50]. Further details regarding the elastic actuation systems will be elaborated in Chapter 5.

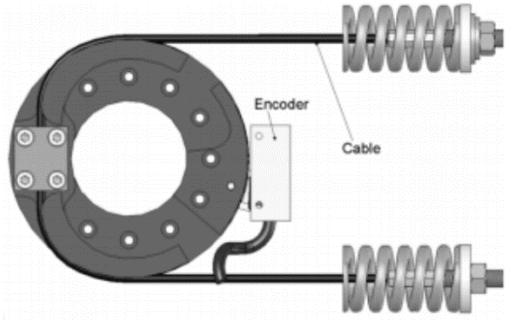

(a)

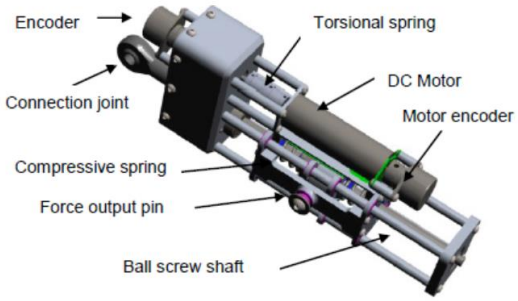

(b)

Figure 2.6: (a) Rotary series elastic actuator (b) Series elastic actuator that converts rotary into linear motion [17]

The common form of actuation mode used in assistive exoskeleton robots is electrical whereas hydraulic and pneumatic actuators are rare. Research is being focussed in developing efficient systems to improve the performance of the actuators. In the mechanical design, the selection of actuator is the fundamental part and actuators should be able to offer enough moments in the normal actions.

2.4.5 Dual Actuation Systems

In recent years, techniques have been introduced to vary the stiffness of the spring as the variation of the spring stiffness can bring reduction in the power requirement of the system [51]. These type of systems require two motors, one can be used to vary the stiffness of the spring and the other one to rotate the joint. However, with this design the system become heavy since the stiffness adjustor motor cannot be used to rotate the joint and vice versa. An alternate approach to use the dual actuation system is the antagonistic arraignment of the system in which both motors can be utilize to rotate the

joint and varying the stiffness of the spring depending upon the direction of rotation of the two motors. Electric motors can allow this type of setup, details of which will be mentioned in Chapter 6.

In order to allow the stiffness of the system to be varied, either the spring used should be of non-linear characteristics or the mechanism should be designed to vary the stiffness of the spring in a non-linear manner [52-54]. Figure 2.7 shows a cross coupled agonistic/antagonistic configuration of the mechanism in which the stiffness of the spring could be made non-linear. However, the control of this type of actuation system is more complicated.

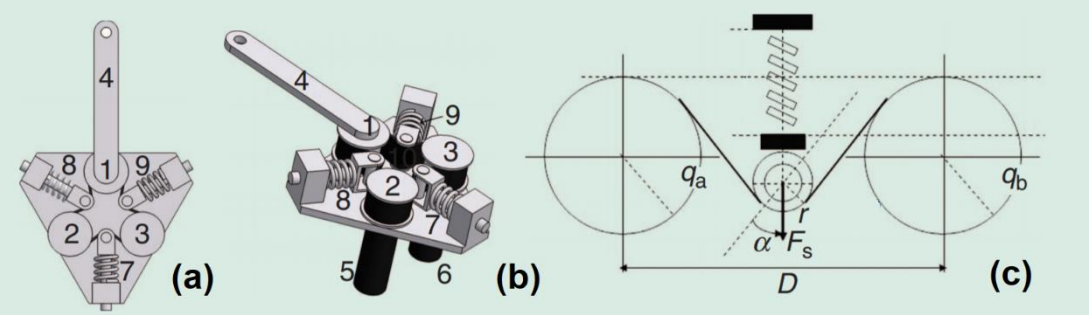

Figure 2.7: (a) and (b) represent the CAD models of a variable stiffness actuator, (c) describes the configuration of the mechanism to form the spring non-linear [55]

There are other such methods reported in the literature that utilized the mechanical structure in order to vary the stiffness of the spring [54, 56, 57]. Some of the elastic elements have also been reported to be used in the actuation system to use in the variable stiffness actuator [56]. Figure 2.8 shows a mechanically adjustable compliance actuator in which the stiffness of the spring can be achieved by vary the pretension in the spring. Further details specifically related to the dual antagonistic arrangement of the actuation system will be explained in Chapter 6.

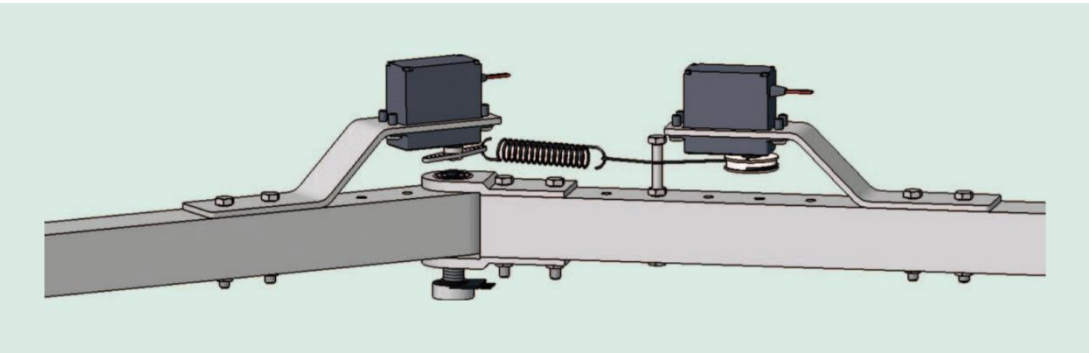

Figure 2.8: Mechanically Adjustable Compliance and controllable equilibrium position actuator [57]

There are several methods that exist regarding actuator design selection [58-60]. Wang et. al proposed an optimization framework to tackle a solution for torque controlled series elastic actuator [61]. The approach developed in the aforementioned studies were derived similar to [62] that have been used in the modelling of hybrid electric vehicles where the objective was to minimize the fuel consumption of the system.

2.5 Control strategies in Lower Extremity Exoskeleton robots

There are a variety of exoskeleton control strategies found in the literature. A control strategy should be such that it is able to provide effective and natural movement assistance to the exoskeleton. A control system in an exoskeleton provides mechanical power to the user and receives intended motion from the wearer. Generally, control systems can be divided into three types: high level control, middle level control and low level control. High level control infers human intention and determine the control strategy. Middle level control maps joint responses based on user intention and the low level control manages the actuators to produce the desired joint torques. The high level control is the core intelligence of the exoskeleton. The general block diagram of the human exoskeleton control system is shown in Figure 2.9. The diagram depicts that the human and exoskeleton works in cooperation with each other. The assistive function defined produces a reference torque which inputs into the controller to obtain a signal to drive the actuator. The output from the actuator produces joint torque to the exoskeleton and human body. The interaction torque is applied to the wearer as the external assistance.

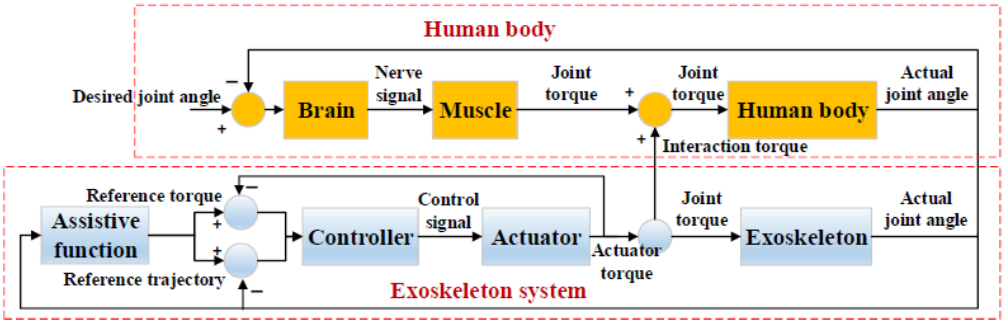

Figure 2.9: Block Diagram of human exoskeleton cooperation system [63]

This section will describe some of the high level control strategies that have been found in lower limb exoskeletons throughout the literature. The control strategies discussed are: Sensitivity amplification method, in which the

user's force is reduced by an amplification factor, Predefined gait trajectory, in which users follow a defined path, Model based control, in which modelling of the exoskeleton dynamic system is performed and Predefined action based on gait pattern, which uses gait phase transitions to control the exoskeleton.

2.5.1 Sensitivity Amplification control algorithm

This algorithm was usually employed in exoskeletons for augmentation applications. It was based on the inverse dynamic model of the exoskeleton and therefore, it required high accuracy of the model. The force/torque exerted by the user is reduced to some amplification factor [64] so the force exerted by the user will approach to zero when the controller is accurately following the user's movement. The disadvantage with this type of method is that the controller can also amplify disturbance signals that could lead to instability. Berkeley lower extremity exoskeleton (BLEEX) and Naval Aeronautical Engineering Institute exoskeleton suit (NAEIES) uses sensitivity amplification method based controllers [64, 65]. The inverse dynamics of BLEEX was modelled as based on three distinct gait phases. Single support with 7 DOF serial link mechanisms, double support with 3 DOF links, double support with one foot flat, 3DOF for the flat foot leg and 4 DOF for the other one. Sensors detect the number of DOF of each leg and the controller implements the algorithm [64].

An adaptive sensitivity amplification technique was presented in [66] based on reinforcement learning. In this method, the sensitivity factors are measured online to handle the variations in interaction dynamics. Impedance algorithm was implemented in [65] to control NAEIES. It utilized multi axis force sensors to measure the interaction forces between human and exoskeleton. These forces were used to generate the desired trajectory and by selecting appropriate values of impedance parameters, these force values could be reduced.

2.5.2 Model based control system

In this strategy, the desired exoskeleton action is based on human exoskeleton model. The model can be divided into two types as dynamic model and muscle model based control. In dynamic model based control, the human body can be modelled as rigid links and joints. Mathematical model, system identification and artificial intelligent method is used to obtain the dynamic model of the system. In mathematical modelling, the exoskeleton is modelled theoretically based on physical characteristics of

the system. It is sometimes difficult to obtain the theoretical model of the system, therefore, system identification method is employed. In BLEEX, least square method is used to determine the parameters of the dynamic model based on input output data pairs [67]. Artificial intelligent method is used to obtain non-linear dynamic models [68]. The second method to obtain human exoskeleton model is muscle model control. This model estimates muscle forces generated as a result of muscle limb movement as a function of muscle neural activities and joint kinematics. It takes EMG signal as input and estimates the required force [69].

The human exoskeleton model also requires a series of sensors for kinematics and dynamic variables. Some assistive exoskeletons such as HAL, ABLE and WPAL used this strategy in their control. In [2], HAL is developed to support the paralyzed leg and the bioelectrical signals of the weakened leg could still be detected. The control method used consists of a command signal, which triggers the motion support of the HAL and torque generation, which produces an assistive torque to move the affected leg smoothly. The control method in WPAL was based on dynamic equation [70]. The analysis of the dynamic characteristics is necessary for an effective control model. Force sensors were utilized to measure the interaction forces between human and WPAL and these forces were used to understand the intention of the wearer.

2.5.3 Predefined gait trajectory control method

In this technique, the desired gait trajectory is recorded from a normal healthy person and then replayed in an exoskeleton. The trajectory was parametrized for different postures. The assistance provided by this control method usually targets quadriplegic or paraplegic patients. Many assistive exoskeletons found in literature used this control technique. In [28], HAL was described that used bioelectrical signals for assisting method. It is difficult to measure EMG signals from paraplegic patients so another interface is required. The desired joint trajectory was pre-recorded from a healthy person and is estimated through real time intention estimator. The control algorithm computes the human intention using floor reaction force (FRF) sensors that detect the centre of gravity (COG) shift during walking. The effectiveness of the algorithm was validated through experiments. In eLEGS, a finite state machine was used to estimate the motion of the legs [71]. The controller in Vanderbilt exoskeleton was based on three motion states: sit, stand, walk and within each state are two modes for pause and transition.

The joint angle in each state is predefined based on the recorded gait trajectories from healthy persons [72].

There are many other techniques that have been used in exoskeleton control, for example, a predefined action has been specified based on the expected gait event. This is different from predefined gait trajectory control in which the exoskeleton follows an already defined path from a healthy individual. In predefined action based on gait pattern control method, the exoskeleton provides assistance based on devices such as springs or pneumatic cylinders and operates by activation/deactivation of these devices. Belforte et al. controls the device by switching the pneumatic actuators on/off for each joint [73]. The enrolling of these devices was predefined based on clinical gait analysis. Sasaki et al. developed a power assist wear for locomotion in which pressure of the actuators is increased or decreased according to the gait pattern [16]. There is also a fuzzy control strategy that have been employed in exoskeleton control[74]. This technique is useful when it is difficult to obtain a dynamic model of the system. A fuzzy control consists of a fuzzification block that translates the input, a fuzzy rule block that contains knowledge of controlling the device, an interface mechanism that decides which rule should be adopted and a de-fuzzification block which converts the results into the desired form. Lower limb assist exoskeleton [75] and EXPOS [76] used this strategy to control the exoskeleton. Apart from the above techniques, a combination of two or more above mentioned techniques have also been utilized in exoskeleton control. BLEEX used sensitivity amplification technique during leg swing phase and a position controller is enabled when it enters the stance phase.

2.6 Performance Measurement of Exoskeleton robots

Different methods have been proposed to measure the performance of the exoskeleton robots. The performance measures indicate the acceptability of the exoskeleton by the wearer. Some common methods used to measure the performance are the following: measuring the metabolic cost, analysis of the gait biomechanics and muscular activity analysis. Some common objectives of the exoskeleton robots are the reduction in metabolic cost and muscular torques generated by the wearers.

It is also important to understand the biomechanics of human walking in the design of lower limb exoskeletons. A human leg contains 7 DOF having 3DOF at the hip, 2DOF at the knee and 2DOF at the ankle joint. All movements take place in the sagittal plane. It has been demonstrated that

during slow speed movement, power at the hip joint is positive, power at knee is negative i.e. dissipating whereas power at the ankle varies between positive and negative side [77]. Therefore, for powered lower limb exoskeletons, there should be a source of adding power at the hip joint, a means of dissipating power at the knee and an elastic passive device of storing and realising energy at the ankle position if the exoskeleton is designed for slow speed movements.

Many improvements had been made in the mechanical design of the exoskeleton robots but only few studies take account the effect of human kinesiology on the wearable devices and many designs were rejected due to the high physical energy demands [33, 78]. There are number of performance measurement methods found in the literature. This section will discuss these evaluation methods and will demonstrate the performance of some exoskeletons based on these methods.

2.6.1 Measuring the metabolic cost

There have been many measurement methods presented to measure the metabolic energy expenditure of the wearer [79, 80]. The effectiveness of the exoskeleton was analysed by measuring the energy expenditure of the wearer with and without the exoskeleton. It includes measuring the oxygen consumption, the carbon dioxide production and the nitrogen excretion. There are number of commercial devices available to measure the metabolic parameters such as the K4 telemetric system [81]. The metabolic cost was first measured by MIT exoskeleton study followed by various other researchers but the results were undesirable as the metabolic expenditure was increased by wearing the exoskeleton robot. Only in some of the lower limb orthoses, the metabolic cost was decreased by wearing the assistive device [82]. The increase in the metabolic energy usage is due to change in the users gait and walking patterns. A further exploration needs to be performed in order to reduce the metabolic energy consumption while wearing the exoskeleton.

2.6.2 Analysing the gait biomechanics

Gait biomechanical analysis is an important assessment method that includes measuring variables such as gait kinematic variables, temporal spatial variables, physiological variables etc. Out of these, temporal spatial parameters are the frequent assessment method used to measure the performance of the exoskeletons. The temporal spatial parameters include distance parameters, cadence, stride length and walking speed. Distance

parameters include step length which is the distance that one foot travels in front of the other foot during each step, stride length which is the distance one part of the foot travels between the same instant in two consecutive gait cycles and step width which is the measure of the medio-lateral separation of the feet. Generally a gait cycle can be divided into two phases, stance phase and swing phase. Stance phase refers when the foot is in contact with the floor whereas swing phase refers when it is not. The gait biomechanics were analysed on orthoses developed by [83], AAFO developed by [84],and HAL developed by [18] to assess their performances. The variables such as stability, gait speed, step length etc. were used to measure the effectiveness of these devices. In most of these exoskeletons, it was shown that the gait biomechanics of the wearer were improved. On the other hand, there were some exoskeletons such as [85] in which the biomechanics of walking were negatively affected.

2.6.3 Analysing the muscular activity

Another indicator to measure the performance of the exoskeletons is the muscular activation level. It is the direct measure of the torque imposed by the corresponding joint of the muscle. HAL 3 [18] and [86] used this technique to evaluate the exoskeletons. The results showed that the muscle activation level was decreased by using the exoskeletons. Therefore, the user is applying lower force/torque to achieve the same activity.

2.7 Examples of lower extremity exoskeletons for gait assistance

Some of the assistive exoskeletons found in the literature up to date and is currently being under research are the following: Rewalk, Indego, Ekso, Exo-H2, REX, HAL/HAL-3, ROBIN, Mina, WPAL and the MINDWALKER. This section will describe the key technologies of the above mentioned exoskeletons.

2.7.1 Rewalk

Rewalk manufactured by ReWalk robotics in year 2006 as shown in Figure 2.10 (a). It has one actuated joint at hip and one at knee while the ankle joints are passively controlled. It incorporates DC motors for the actuated joints, Lithium ion rechargeable batteries, sensors and a computer control system [87]. The variation in the centre of gravity is detected by a tilt sensor to estimate the walking phase. A wrist watch style wireless communicator and truck position is used to control the Rewalk exoskeleton. It cannot

maintain balance control and therefore crutches are required to keep balance. It can be used in four movement modes as sit stand, stand sit, walk or climbing stairs. The device is customized and fit for all sized patients [88].

(a) **(b)**

Figure 2.10: (a) Rewalk Exoskeleton [3] (b) HAL by Cyberdyne Inc. [28]

2.7.2 HAL

The Hybrid assistive limb developed by Tsukuba University and Cyberdyne shown in Figure 2.10 (b) comes with different versions as full body, lower limb and one limb models. These models are oriented for different users with different applications. One leg version is targeted for patients with hemiplegia. Full body or lower limb is developed for paraplegic patients [89]. Similarly, it is developed for a variety of applications such as rehabilitation, assistance and augmentation purposes. The lower limb model has three actuated DOFs, one at hip, one at knee and one at ankle. These joints are actuated by DC servo motors and harmonic gear drives. In HAL, EMGs are used to predict the human motion intention and the electrodes are located along the device's frame [90].

2.7.3 Indego

The Indego which was designed by researchers at Vanderbuilt University in 2012 is shown in Figure 2.11 (a). It consists of actuated joints at hip and knee only which are powered by brushless DC motors with a 24:1 gear reduction. The ankle joint is not present in Indego, so it has to be used in conjunction with an ankle foot orthosis. It is designed to provide gait training and assistance to people with paraplegia. Angular position sensors are measured by potentiometers. Balance is maintained by forearm crutches. It has six movement modes as sit, stand, and walk and within each phase are

two states that enable the wearer to pause or transition between modes. Control is based on user's body positions.

(a) **(b)**

Figure 2.11: (a) Indego by Parker Hannifin corporation [91] (b) eLEGS by Ekso Bionics [92]

2.7.4 eLEGS

eLEGS also known as Ekso developed by Ekso Bionics in 2012 was the first clinical robotic exoskeleton (powered exoskeleton for walking assistance) as shown in Figure 2.11 (b).The device is made of carbon fibre and steel and it uses gestural based control. Hip and knee joints are actuated and powered by DC motors. The ankle joints are passive. It is able to perform sit to stand, stand to sit and straight walking movements. Like in ReWalk and Indego, it also requires crutches to maintain balance. Usually kinematic and force sensors are employed in Ekso that take output from human muscles in order to power the exoskeleton.

2.7.5 Rex

Rex was developed by Rex Bionics in 2007 and it is the first device that enables the wearer to walk freely and independently without using crutches. It comes with two versions Rex P, which denotes personal use and Rex Rehab, designed to be use by therapists. It has five actuated joints, three at hip, one at knee and two at ankle joint . The device consists of four double tethered leg straps, an upper harness and back support. It is controlled by a joystick which is integrated to the unit and is one of the heaviest exoskeleton found in literature as shown in Figure 2.12(a).

(a) **(b)**

Figure 2.12: (a) REX by Rex Bionics [93] (b) MINA by Institute of Machine Cognition [94]

2.7.6 MINA

The MINA exoskeleton was developed by Institute of human and Machine cognition in 2011 and was addressed to paraplegic patients. At first, there seems to be no additional advantage of MINA over ReWalk and Ekso. It consists of only one movement mode i.e. walking with real time speed adjustments. The walking is achieved by two actuated joints at hip f/e and knee f/e and a passive joint at hip ab/ad and hip int/ext rotation. There are four attachment points of MINA exoskeleton, one at torso, and three points at each leg: thigh, shank and foot as shown in Figure 2.12(b) .Like other exoskeletons, it also requires crutches to maintain balance [49]. MINA is only available for research purposes yet as no version of it is ready for home or domestic use.

2.7.7 WPAL

The wearable power assist locomotor (WPAL) has two actuated joints at hip and knee and is aimed to provide a safe and natural walking ability to paraplegic users [95]. It is developed with three walking modes, apart from straight normal walking, there is curve walking mode where one step is shortened to allow turning and a slow walking mode where step lengths are shortened to facilitate with rough terrain. A clinical trial on five paraplegic subjects was tested to estimate the gait trajectory and all of them showed improved demonstration when using the WPAL.

2.7.8 MindWalker

The Mindwalker exoskeleton provides assistance for the movement of the individuals with lower limb disabilities. It includes two actuated joints at hip, flexion/extension and abduction/adduction and one at knee flexion/extension. The ankle joints are passively actuated. It is depicted in Figure 2.13. Linear joint actuators are used for actuation that were custom designed and back drivable. The control system consists of multi-layer scheme triggered by centre of mass displacements and pushbuttons to start or stop the process. The reference positions were defined based on the healthy subjects.

Figure 2.13: The Mindwalker Exoskeleton [96]

Though marked differences exists among the exoskeletons reviewed above, there are also many common features that can be derived from these devices. A summary of the comparison of the available assistive exoskeletons are shown in Table 2.2. Almost all of the exoskeletons presented provide 1-6 DOF in the sagittal plane to actuate hip, knee and ankle joint which is also sometimes actively actuated to allow dorsiflexion and plantar flexion. With the exceptions of few, almost all of them required crutches or walkers in order to maintain balance and stability. Many of them measure joint angles and contact forces to access gait performance.

Table 2.2: Comparison of Available Assistive Exoskeletons

Exoskeleton	Maneuvers	Speed (m/s)	Battery life (hrs)	Exo. Weight (kg)	Power con. (W)	Actuation system
ReWalk [3]	• sit to stand • stand to sit • level walking • inclined walking • stairs ascend	0.6	3-4	20.9	28V	Electric Motors
Indego [91]	• sit to stand • stand to sit • walking	0.22	2-3	12.3	117	Two Brushless DC motors
Ekso / eLEGS [92]	• sit to stand • walking • stand to sit	0.89	4	20.4	N/A	Electric motors at hip and knees and a passive spring at the ankles
HAL [97]	• sit to stand • walking • stand to sit	N/A	1	15	N/A	DC servo motors with harmonic gears
Rex Bionics [93]	• sit to stand • standing (without crutches) • walking • stair ascend • stair descend	Too slow	1	38	480	DC motors Maxon RE 40
MINA [94]	walking	0.2	N/A	N/A	N/A	DC brushless motor BN34-25EU-02
MINA v2 [49]	N/A	N/A	2.5	34	192	Allied motion HS02303 with linear ball screw
WPAL [70]	• walking • turning • slow walking for uneven surfaces	N/A	N/A	N/A	N/A	DC servomotor (Maxon) coupled with a harmonic reducer gear
MINDWALKER [61]	walking	N/A	N/A	28	N/A	Series elastic actuators
WSE [98]	• walking • sitting • standing	N/A	N/A	N/A	N/A	Vexta servo motors AHX5100KC servo motor
ALEX I [99]	N/A	N/A	N/A	N/A	N/A	DC motors and a 1:10 gearhead at hip
ATLAS [100]	N/A	1	N/A	6.5	N/A	Brushless Maxon motors coupled with a harmonic drive

Table 2.2: Comparison of Available Assistive Exoskeletons (Cont.)

BLERE [101]	N/A	N/A	N/A	N/A	N/A	Servo motors (EC flat 90, Maxon) and harmonic reducers
WOTAS (Upper limb) [102]	N/A	N/A	N/A	N/A	N/A	Maxon DC flat brushless motor EC 45

2.8 Gap of Knowledge

Many studies have been recorded on exoskeleton robots since its first development in 1960. There have been a number of advances achieved in the development of lightweight actuators, long lasting power supplies and efficient transmission. The components of an exoskeleton such as sensors, actuators, controllers, power supplies and materials will improve to make the exoskeleton design highly efficient.

As mentioned, the assistive exoskeletons need to be portable and untethered. A portable device means reducing the size/weight of the power components to keep an acceptable size and mass of the device. This requires finding an exoskeleton actuation solution in order to develop lightweight, power efficient and powerful actuators. Based on the literature review performed, all the assistive exoskeletons developed so far require crutches to maintain balance with the exception of Rex Bionics. On the other hand, adding additional DOFs makes Rex Bionics much heavier and bulky as compared to the other assistive exoskeletons. To this date, no assistive robotic exoskeleton exists that does not require any crutches to maintain balance and is lightweight, although the user of the device does not carry any of the exoskeleton weight but a larger device comes with a trade-off by using a larger battery or a power inefficient system and consequently requires the need to develop weight efficient batteries and/or power efficient actuators. Furthermore, not much work has been done on the dual actuation concept to develop a power efficient system for an assistive exoskeleton. Therefore, the motivations of this research is to fill this gap of knowledge by developing an actuation solution to implement a design for an assistive robotic exoskeleton that is lightweight, power efficient and has a powerful system to carry a user of up to 100kg. To further reduce the power requirements of the system, passive elements will be introduced with a fixed and variable stiffness in the actuation system design and the concept of dual actuation will be implemented to develop a power efficient system for an assistive robotic exoskeleton.

2.9 Summary

In this chapter, previous research has been analysed in the areas of the assistive exoskeleton robotics. Prior to the discussion of the technological aspects of the robotic exoskeletons, biomechanical parameters were investigated. The biomechanics of human walking and gait cycle was reviewed. Some of the key components of the exoskeleton were discussed and analysed. A general overview was performed for the available technologies to measure the interaction between the human and the exoskeleton. Technologies related to the exoskeleton actuation systems were analysed and the benefits of several types of the systems were assessed. It was observed that mostly electrical actuators were employed in assistive exoskeleton robots nevertheless, several versions of exoskeletons exist that utilized hydraulic and pneumatic actuators. Some of the advantages of using elastic actuation systems were investigated and the available elastic actuators in the exoskeletons were demonstrated. Furthermore, the benefits and prior work performed using dual actuation concept were analysed. Several techniques related to human-exoskeleton control were presented. Parameters that measure exoskeleton performances were also reviewed. A report on the available assistive exoskeletons and their strengths and limitations were also highlighted.

Chapter 3
Support Requirements for Robot Assisted Training

3.1 Introduction

In this chapter, support requirements for robot assisted training will be considered for the elderly and neurological gait disorder patients. Neurological conditions are the most common causes of gait disorders that affect people to perform activities of daily living independently [103]. These common conditions and the diseases associated with them include Parkinson disease (PD) which progresses over time and mostly found in older people [104], group of Ataxia (AT) patients are included that are mostly linked to difficulty in balance and walking [105, 106], people with a condition known as cerebral palsy (CP) is also a part of this study which is found in young children. This is due to the loss of proper muscle coordination in CP patients [107]. Limited sagittal plane motion and crouch gait is associated with CP [108]. Group of neuropathy patients are included that are linked to nerve problems causing weakness. A group known as Charcot Marie tooth (CMT) disease also falls under neuropathy group that linked to damage to the peripheral nerves is also a part of this study [109-111]. There are some conditions apart from the above described cases that lead people to hemiplegic (one side affected) or diplegic gait (both sides affected) [112]. Major incidences reported by elderly population are the frequent falls and as a result of its consequence, some aspects of the movement are affected [113]. They are described as the principal causes of the accidental deaths in the elderly [103]. There is also a slight divergence of gait associated with ageing and this irregularity can also lead to an impaired gait as a result of falls [114].

The assessment of gait impairment requires a clear distinction of pathological findings from the normal. To the authors' knowledge, no previous study has been done that takes into account a wide variety of neurological gaits together with the elderly gait to assess the biomechanical gait deviations associated with them. The aim of this study is to highlight the biomechanical gait deviations associated with elderly and neurological patients. The knowledge of these deviations is important so that robot assisted devices could be designed based on the needs of the individual users. As mentioned before, an assistive exoskeleton is a wearable device that is provided with actuators at the joints and is worn by the human [115].

An exoskeleton is able to assist the user based on its requirements. It has been observed that a simple use of cane can significantly improve gait parameters when compared with those walking without a cane [116]. Therefore, with the use of exoskeletons, the level of performance is greatly increased [63]. There is a need to develop a systematic approach and to thoroughly investigate the biomechanical gait parameters of elderly and neurological patients to highlight the assistance required in each category. The study forms a basis in evaluating the assistance requirement among different clinical population. There has been a lack of study highlighting the lower limb support requirement by the end users of the robot assistive devices which emphasises the need of this study. The requirements of the users identified through this study will set up a design criteria for robot assisted devices, which is critical in order to make sure the devices to be developed are fit for purpose.

In this chapter, the methodology to collect and analyse the data of the categories under consideration will be discussed followed by the discussion of the criterion to assess the quality of the studies involved. The outcomes of the kinematic and kinetic parameters of the elderly and neurological patients will be presented in Section 3.3. This will be followed by a detailed discussion on the support requirement among different categories of users for robot assisted training by analysing the difference in the spatio-temporal, kinematic and kinetic parameters of the lower limb joints.

3.2 Methodology

3.2.1 Literature Search Process

The articles in this study were obtained from various electronic database sources including Science Direct, Springer Link, Web of Science, Medline and PubMed. The search was systematically performed by the author during the month of July-August 2017 reporting studies on biomechanical gait parameters of elderly and neurological patients. The search was restricted to articles published during the year 1985-2017. The keywords used for the search were Elderly, Parkinson, Ataxia, Cerebral Palsy, Charcot Marie Tooth, Neuropathy, Hemiplegia, Diplegia, Gait parameters, Kinematic and Kinetic characteristics, Robot assisted training, and Exoskeleton robots. The Boolean operator used –AND/OR. Full text articles were selected from the aforementioned duration.

3.2.2 Data Collection Process and Criterion

A total of 2245 records were identified from all of the mentioned database sources, out of which 1843 were obtained after removing duplicates. The total records initially screened for abstract/title were based on the question 'Did the study reported at least one of the biomechanical areas of interest?' The articles that remained relevant after initial screening were reviewed for full text (n=102) and excluded those that were not containing the required sufficient data. Studies were selected based on the inclusion/exclusion criteria shown in Table 3.1. The selection of the studies was completed after reading full texts. Studies with a focus on spatio-temporal, kinematic and kinetic parameters were selected.

Table 3.1: Inclusion and Exclusion Criteria for Studies

Inclusion criteria	**Exclusion criteria**
Studies reporting elderly and neurological gaits in comparison to a healthy control group	Studies that did not compare elderly or neurological gait with the normal individuals
Studies that include a barefoot biomechanical analysis	Studies that did not include a barefoot analysis or including an analysis using an assistive device
Studies have full text available	Studies that did not report at least one outcome measure of interest
Outcome measure of interest-	Studies that include elderly people with a previous known disorder
(a) Spatio-temporal parameters (gait speed, stride length and cadence)	Studies that include pathological gaits other than neurological origin
(b) Kinematic variables of hip, knee and ankle (peak flexion/extension and ROM)	
(c) Kinetic variables of hip, knee and ankle (peak flexion/extension moment)	

3.2.3 Search Results

The flowchart of the extensive literature search is outlined step wise in Figure 3.1. Studies were included in the review if they reported at least one parameter of interest in the three biomechanical areas of interests.

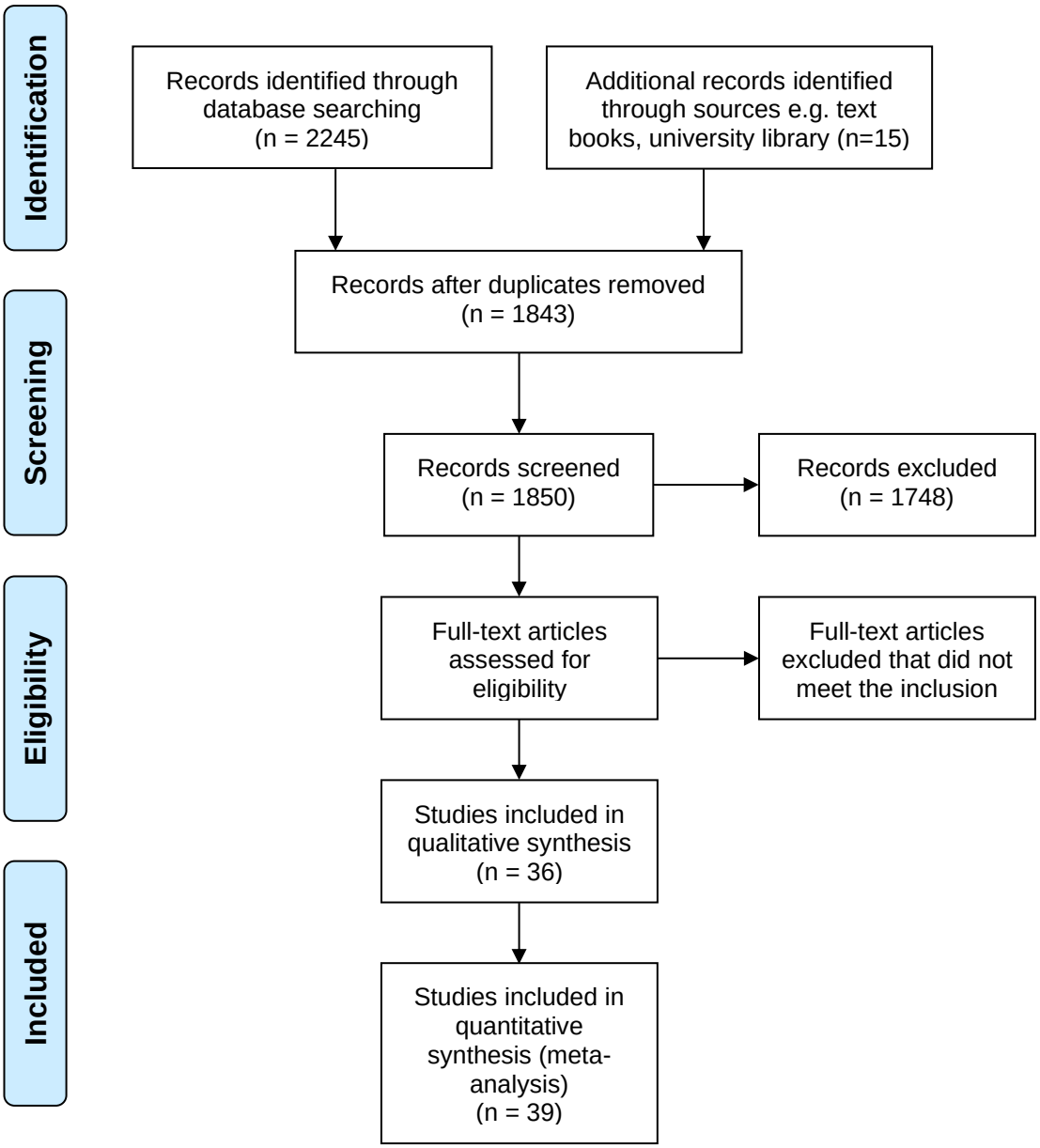

Figure 3.1: Flowchart outlining literature search process

3.2.4 Assessment of Quality of Studies

The quality of the studies were assessed using a quality assessment tool developed by Downs and Black [117]. The overall scoring was done on 27 aspects however 11 questions in the Downs and Black assessment tool were found not relevant to the current assessed articles. Therefore, a modified version of this tool was obtained which included 16 domains and the quality of the study was classified as poor (1-6/16), fair (7-12/16) and good (>12/16). A typical example of the overall score of a study for each domain obtained during the assessment is shown in Table 3.2. The complete Table is presented in Appendix D.

Table 3.2: Study Quality Assessment (Downs and Black [117])

Downs and black questions	Anderson et al. [118]	Judge et al. [119]	Kerrigan et al. [120]	Kerrigan et al. [121]	Peppe et al. [122]	Ferrain et al. [123]	Roiz et al. [124]	Ferrarin et al. [125]
1	Y	Y	Y	Y	N	N	Y	N
2	Y	Y	Y	Y	Y	Y	Y	Y
3	Y	Y	Y	Y	Y	Y	Y	Y
4	NR	NR	NR	NR	NR	NR	NR	NR
5	N	Y	Y	Y	Y	Y	Y	Y
6	Y	Y	Y	Y	Y	Y	Y	Y
7	N	Y	Y	N	Y	Y	Y	Y
8	NR	NR	NR	NR	NR	NR	NR	NR
9	NR	NR	NR	NR	NR	NR	NR	NR
10	N	N	Y	N	N	N	Y	N
11	UTD	Y	Y	N	Y	Y	Y	UTD
12	UTD	Y	Y	UTD	Y	Y	UTD	UTD
13	UTD	UTD	NR	Y	Y	Y	UTD	UTD
14	NR	NR	NR	NR	NR	NR	NR	NR
15	NR	NR	NR	NR	NR	NR	NR	NR
16	Y	Y	Y	Y	Y	N	Y	Y
17	NR	NR	NR	NR	NR	NR	NR	NR
18	Y	Y	Y	N	Y	N	Y	N
19	NR	NR	NR	NR	NR	NR	NR	NR
20	UTD	Y	Y	Y	Y	Y	Y	Y
21	UTD	UTD	N	Y	UTD	Y	Y	Y
22	UTD	UTD	UTD	Y	UTD	UTD	UTD	UTD
23	NR	NR	NR	NR	Y	NR	NR	NR
24	NR	NR	NR	NR	UTD	NR	NR	NR
25	UTD	UTD	UTD	UTD	Y	Y	Y	Y
26	NR	NR	NR	NR	NR	NR	NR	NR
27	NR	NR	NR	NR	NR	NR	NR	NR
Total score	6	11	12	10	13	11	13	9

*Y=1, N=0, NR=not relevant, UTD=unable to determine

3.2.5 Data Extraction

Following the assessment of the quality of studies, the process of data extraction was performed. All the extracted data from studies were entered into tables for easy comparison and grouping. Demographic characteristics of participants (number of participants, age, height, weight), and inclusion/exclusion criteria used by this study were recorded. If the data from any study was identified as missing, an attempt was made to contact the authors for the missing data but if the authors did not respond, the articles

were excluded from the review. Studies that reported the outcome measure of interest were included for statistical analysis.

3.2.6 Statistical Analysis

The data was transformed into standardized units for comparison and analysis. The demographic variables were calculated as means with standard deviations. The meta-analysis using forest plot was performed on each individual outcome measure which is reported in the results section. Since the selected articles contained participants from different neurological conditions and the sample size was also not equally distributed, therefore random effect model was used in the forest plot that computes the combined effect of the distribution. The results were reported as mean differences with 95% confidence intervals and *p* values. The heterogeneity was calculated using the I^2 statistic.

3.3. Results

3.3.1 Search Results

There were 2245 articles that were initially obtained when performing the search, however only 39 articles were finally selected for review. There were reasonable backgrounds for excluding the articles such as inappropriate title, use of inappropriate comparison groups, unsuitable study design, missing data and other irrelevant data. Several studies investigated on more than one study area. Spatio-temporal characteristics were reported by most of the studies, however there were only few studies that recorded kinetic variables.

3.3.2 Quality of Studies

The majority of studies selected in the review were of good quality as assessed by the assessment tool of Downs and Black [117] given in Table 3.2. No study obtained an overall score of less than 6. Few studies fell under a score of fair while majority of studies were having a score of more than 13. The difference between the fair and good quality studies was due to the fact that some of them reported the exact value of *p* rather than reporting the approximate values. Additionally, they described the demographic and exact sites of the selected participants.

3.3.3 Characteristics of Subjects

The participants included in this study were categorized as elderly group, neurological group and the comparison healthy control group. The elderly participants included were fit without any previous known disorder. The

characteristics of the participants are reported in Table 3.3. The participants that form part of the comparison group were the age matched control group without any previous known disorder. The gait data from physically fit individuals were used as a reference benchmark to obtain the level of impairment among different groups.

Table 3.3: Demographic data of participants from included studies

Demographics	**Elderly** Mean ± SD	**Pathological** Mean ± SD	**Normal** Mean ± SD
Number of Subjects (n)	90	647	676
Age (years)	76.3 ±5.28	42.61 ±7.6	41.78±5.1
Height (m)	1.61 ±8.7	1.63 ±10.9	163.41±8
Weight (kg)	66.4 ±11.7	72.91 ±13.56	65.69±11.53

3.3.4 Subject Recruitment Strategy

The subjects were recruited from a variety of sources as documented by the studies. These included hospitals, community outpatients and volunteers. The healthy subjects recruited in some cases were on voluntary basis.

3.3.5 Outcome Results

The variables of interest found in the majority of studies were spatio-temporal, kinematic and kinetic parameters. These variables are discussed in detail in the next section.

3.3.6 Spatio-Temporal Characteristics

3.3.6.1 Gait Speed

Gait speed was reported by four studies for elderly [118-121] and many of them described for different neurological patients. These include ten studies for Parkinson [122-131], five for Ataxia [106, 128, 132-134], four for Cerebral palsy [108, 135-138], three for Charcot Marie Tooth [139-141], four for Neuropathy [142-145], four for Hemiplegia [116, 146-148] and four for Diplegia group [149-152]. The meta-analysis report on gait velocity for elderly showed a significant difference when compared with the young group. The gait velocity in elderly was reported as significantly lower than the young control group. The heterogeneity among the studies were I^2=4% (Figure 3.2a). When gait velocity was observed among different neurological patients, it was reported significantly lower in all of the patient group types. The overall heterogeneity among the neurological group was reported as I^2=92% (Figure 3.2b).

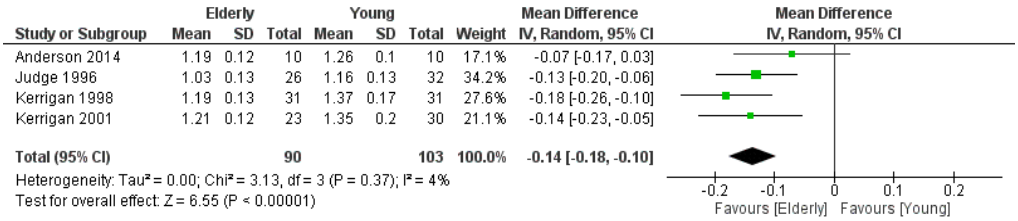

(a) Forest Plot: Gait Velocity-Elderly vs Young

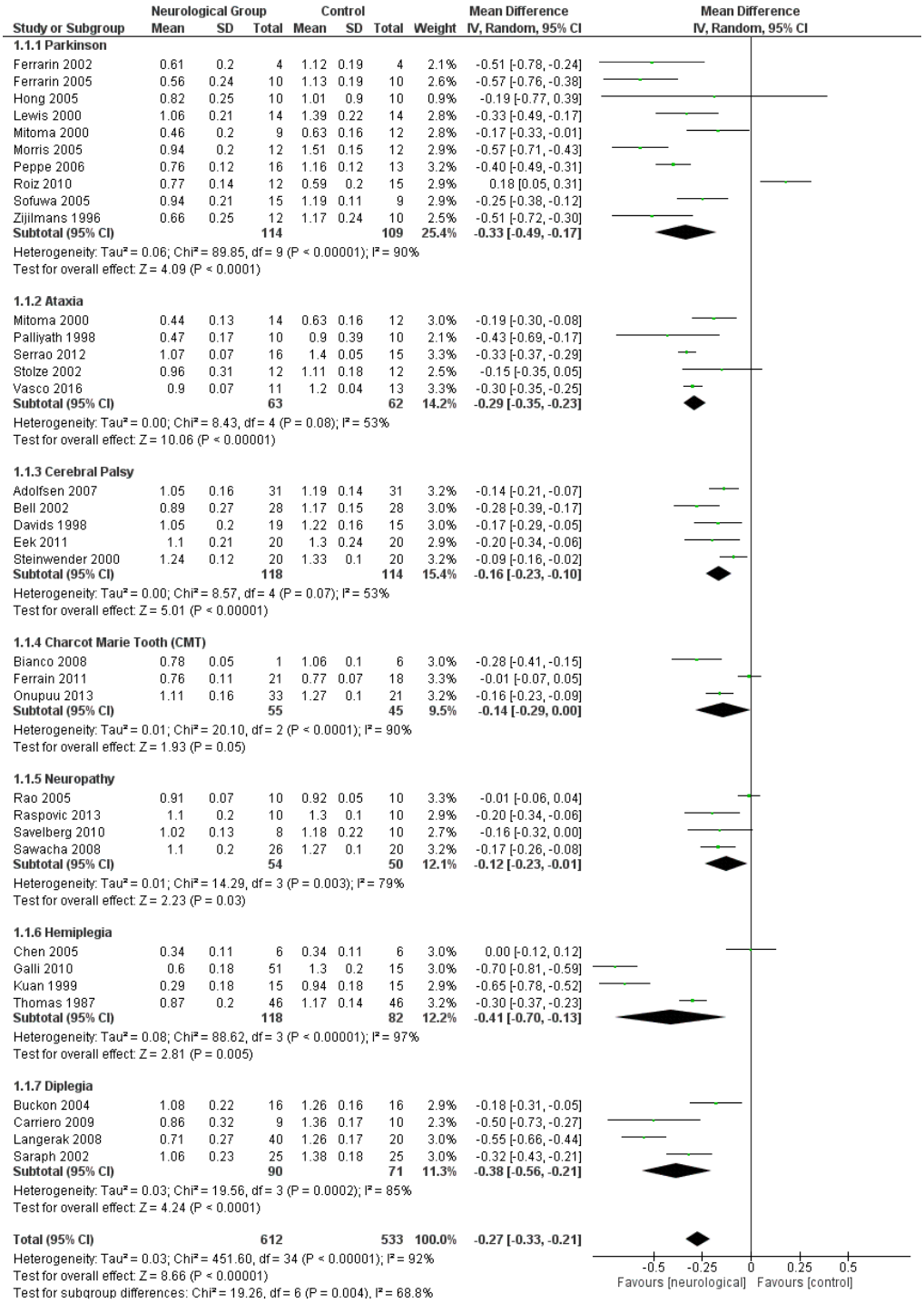

(b) Forest Plot: Gait Velocity-Neurological vs Healthy

Figure 3.2: Meta-analysis report for gait velocity comparing (a) elderly with young group and (b) neurological with healthy group.

3.3.6.2 Stride Length and Cadence

By observing the studies in the elderly group [118-121], the meta-analysis report on stride length recorded significantly lower value in the elderly group (Figure 3.3a) whereas cadence was observed to be higher in elderly patients (Figure 3.4a). The heterogeneity among the studies for stride length and cadence were less I^2 = 5% and I^2 = 21% respectively. These parameters when observed in the neurological group, it was reported as significantly lower when compared to the healthy control group. Only CMT and hemiplegia group showed insignificant difference in the stride length as observed in Figure 3.3b whereas the cadence in the cerebral palsy patients was reported to be higher than the healthy group (Figure 3.4b). The overall heterogeneity among the neurological patients were 90% for stride length and I^2 = 79% for cadence.

3.3.7 Kinematic Characteristics

3.3.7.1 Hip Range of Movement

The meta-analysis report on hip ROM included three studies for elderly group [119-121] and the individual studies for neurological group included Parkinson [123-125, 128-131], Ataxia [106, 128, 132-134], Cerebral palsy [108, 135-137], Neuropathy [143, 153], Hemiplegia [147, 148, 154]and Diplegia [150-152, 155]. The studies on the elderly group reported lower ROM (mean difference as -1.79, 95% CI -5.63 to 2.05, p = 0.36) as compared to the young group with I^2 = 78% heterogeneity but it was not reported to be significant (Figure 3.5a). The seven studies that reported for Parkinson disease [123-125, 128-131] also observed a significant lower hip ROM in the elderly group, though the heterogeneity was I^2 = 64%. The five studies for Ataxia group [106, 128, 132-134], four for Cerebral palsy [108, 135-137], three for hemiplegia [147, 148, 154] and four for diplegia group [150-152, 155] reported a difference that was not significant. Only two studies were found for neuropathy group [143, 153] that recorded a significant lower ROM in the elderly group. The meta-analysis report showed an overall significant difference in the neurological patients as compared to the age matched healthy group (Figure 3.5b).

3.3.7.2 Knee Range of Movement

The knee joint was reported by three authors [119-121] for the range of movement and observed a significant difference between elderly and young group. It was recorded to be significantly lower in the first group with a heterogeneity of I^2 = 0% (Figure 3.6a). The meta-analysis report on the

neurological group also suggested a significantly lower range of motion in the patients group. Only studies by [106, 128, 133, 134] for Ataxia and [149-152, 155] for Diplegia group showed no significant difference whereas the studies for Parkinson [123, 125, 128-131], Cerebral palsy [108, 135-137], Neuropathy [143, 153] and Hemiplegia [147, 148, 154] observed a significant lower range of motion at the knee joint. The overall heterogeneity among the neurological studies were I^2 = 90% (Figure 3.6b).

3.3.7.3 Ankle Range of Movement

The studies on the ankle ROM for elderly [119-121] and neurological patients [106, 108, 123, 125, 128-130, 132-137, 143, 147, 152-155] reported a significant lower value in the elderly and neurological group as compared to the healthy control group. In the neurological group, the meta-analysis report on all subgroup types suggested a lower ROM except Ataxia group in which no significant conclusion can be drawn. The heterogeneity among the studies in the elderly group was less I^2 = 0% (Figure 3.7a) but a high variability has been observed in the neurological group has I^2 = 79% (Figure 3.7b).

3.3.8 Kinetic Characteristics

The kinetic variable of interest was joint moment. The studies reported for the elderly group for the peak flexion moment at hip, knee and ankle joint were not sufficient to perform a meta-analysis. Regarding the neurological group, three studies reported for Parkinson [123, 125, 130] at the hip and ankle joint and observed a significant lower peak joint moment. The heterogeneity was I^2 = 0% in both cases. No conclusion can be drawn for CP [135, 136, 138] at the hip and ankle joint, however it showed a significant higher peak flexion moment at the knee joint [136, 138]. Studies for diplegia [149, 152] showed a significant lower peak moment at hip and ankle whereas no significant conclusion can be drawn at the knee joint. There were only two studies [142, 143] found for neuropathy patients at the ankle joint and showed a significant lower peak ankle dorsiflexion moment. Overall the meta-analysis report on the kinetic variables suggested no significant difference at the hip (Figure 3.8) and knee flexion moment (Figure 3.9) but a significant lower peak ankle dorsiflexion moment (Figure 3.10). There was also a lot of variability observed among the studies for peak flexion moment (I^2 = 98%, I^2 = 99% and I^2 = 89% for hip, knee and ankle joint respectively).

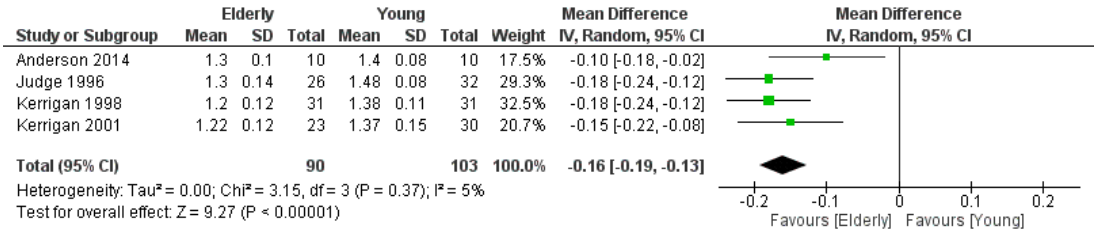

(a) Forest Plot: Stride Length – Elderly vs Young

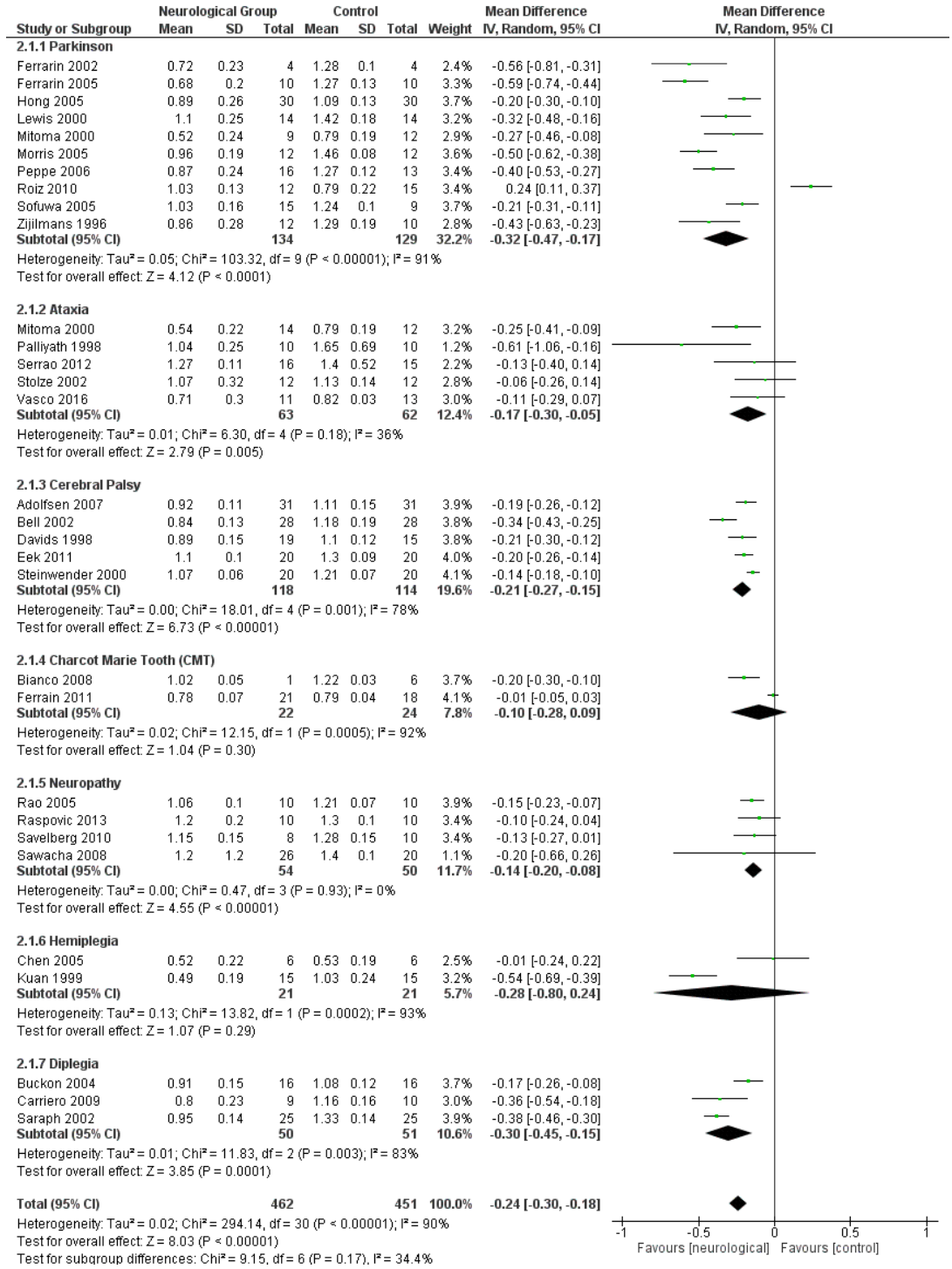

(b) Forest Plot: Stride Length – Neurological vs Healthy

Figure 3.3: (a) Meta-analysis report for stride length comparing (a) elderly with young group and (b) neurological with healthy group.

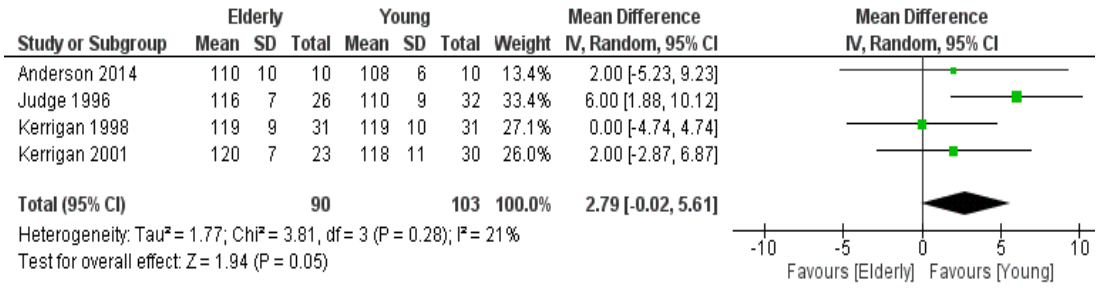

(a) Forest Plot: Cadence – Elderly vs Young

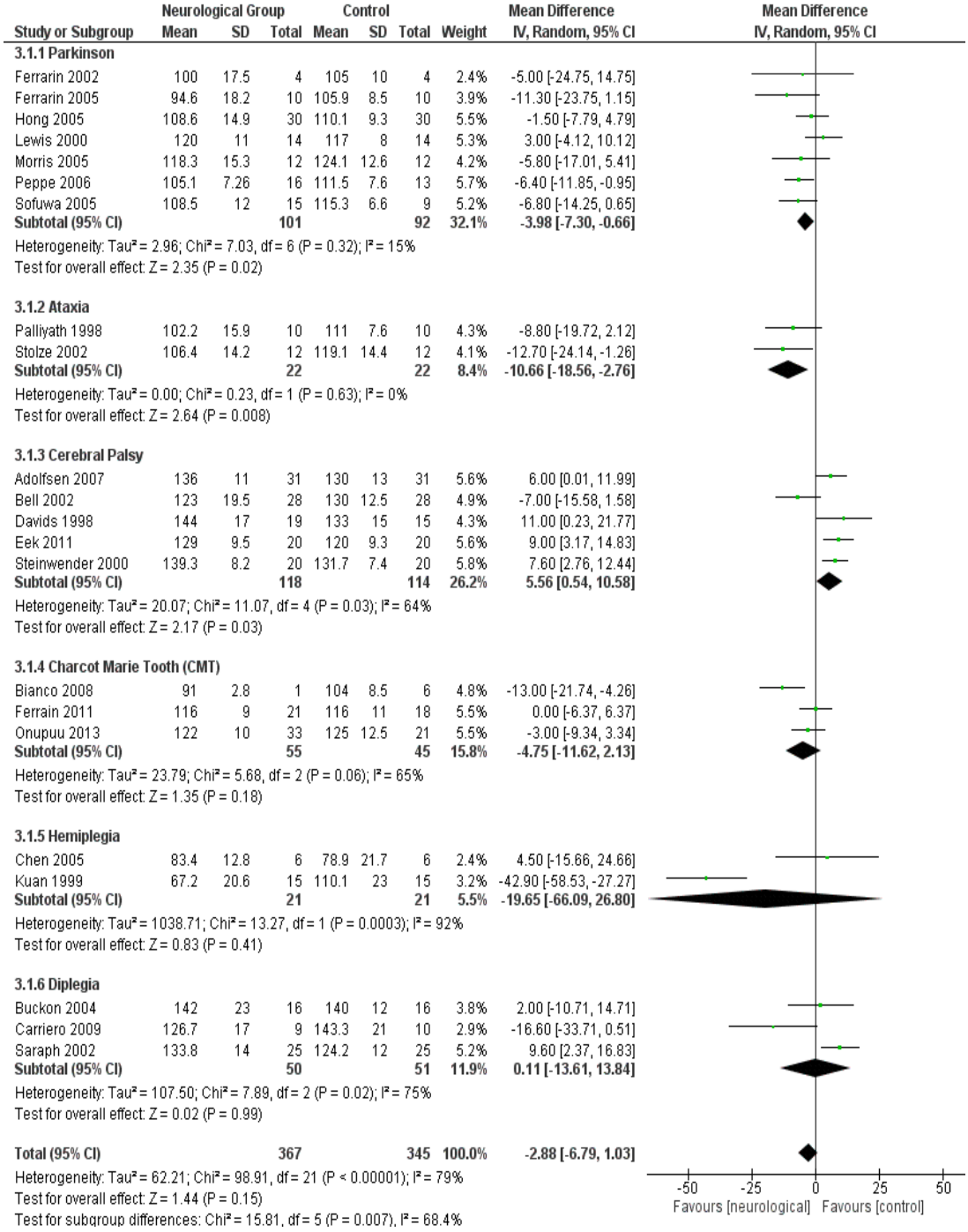

(b) Forest Plot: Cadence – Neurological vs Healthy

Figure 3.4: Meta-analysis report for cadence comparing (a) elderly with young group and (b) neurological with healthy group.

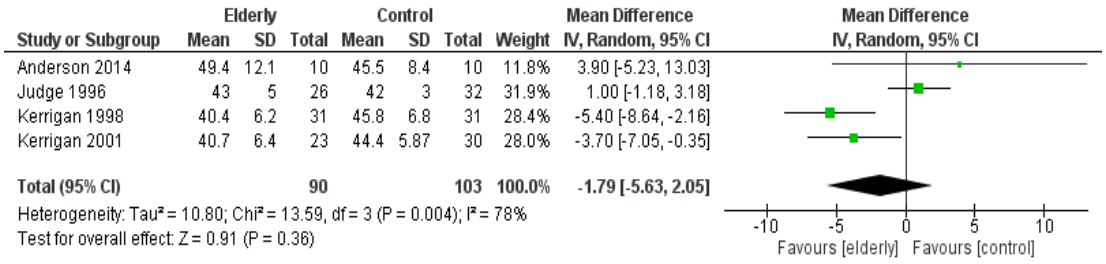

(a) Forest Plot: Hip Range of Movement – Elderly vs Young

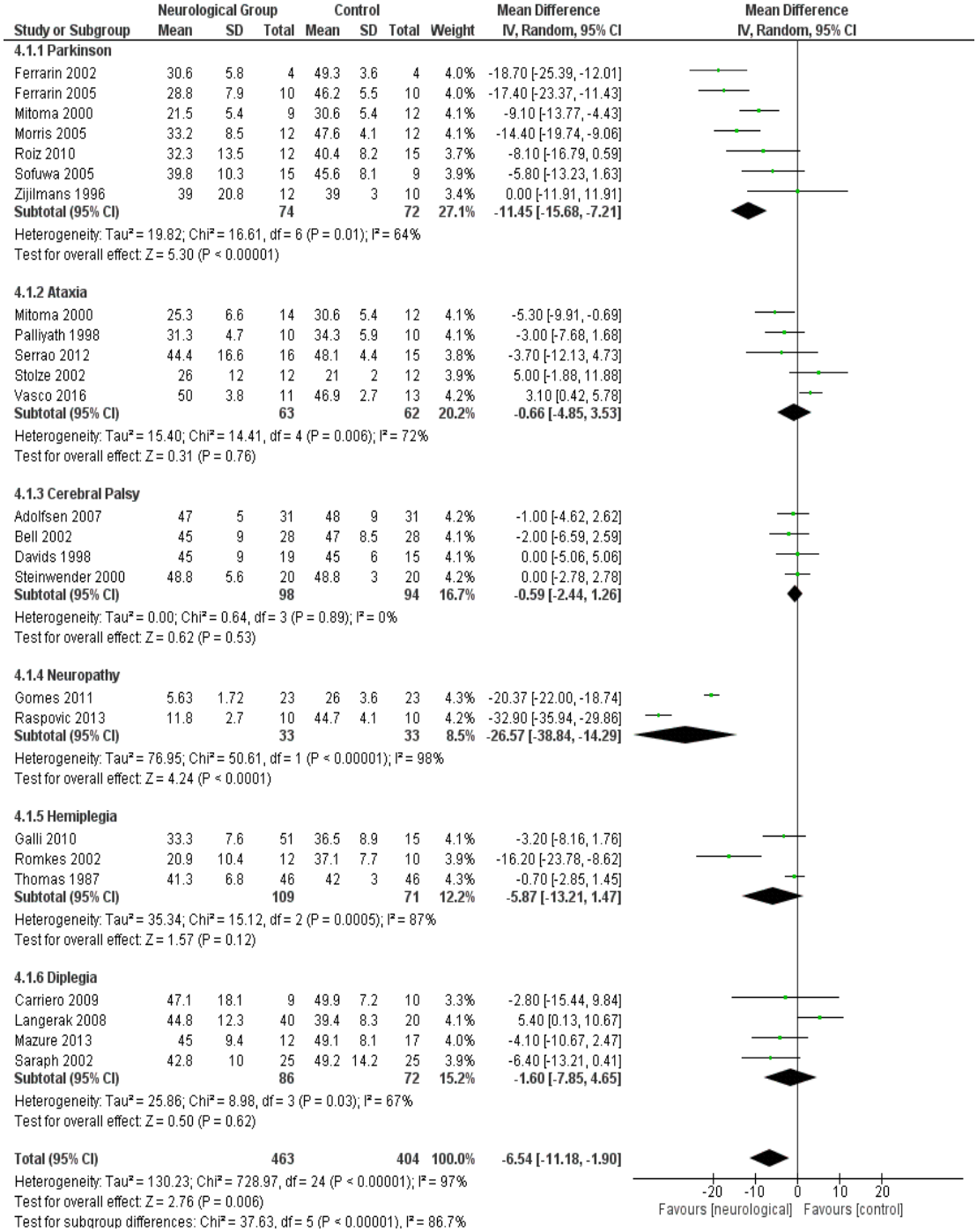

(b) Forest Plot: Hip Range of Movement – Neurological vs Healthy

Figure 3.5: Meta-analysis report for hip ROM comparing (a) elderly with young group and (b) neurological with healthy group.

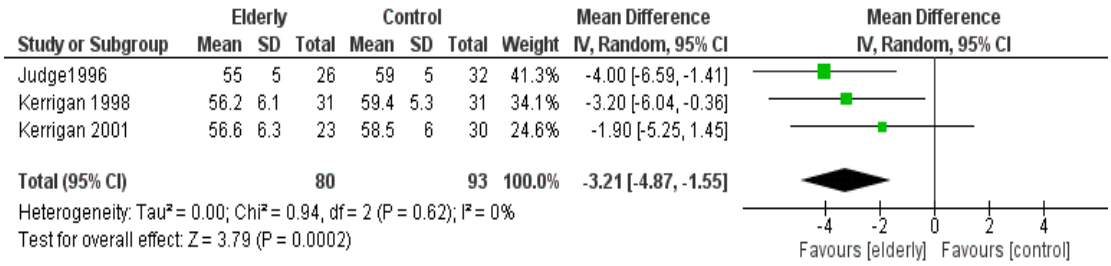

(a) Forest Plot: Knee Range of Movement – Elderly vs Young

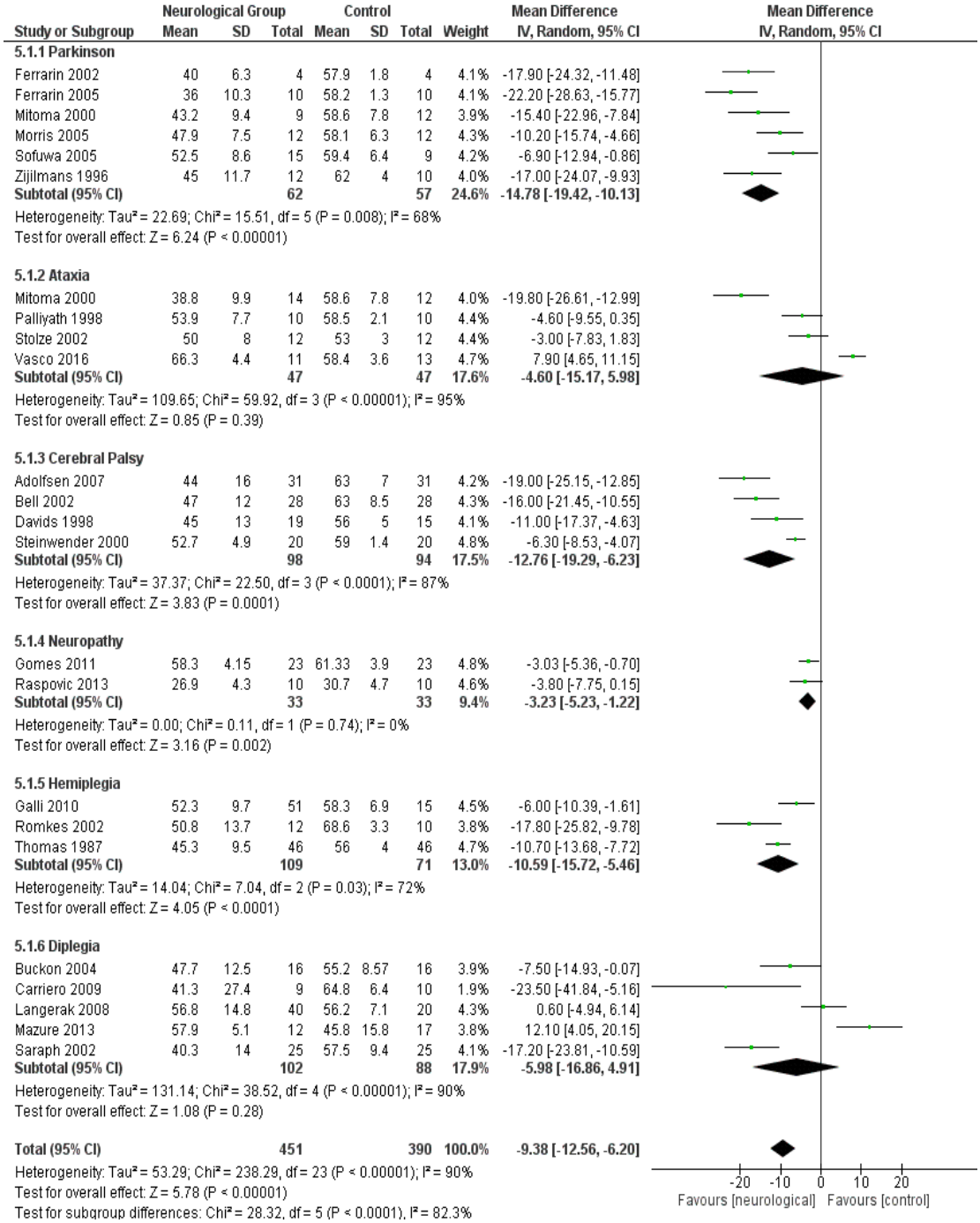

(b) Forest Plot: Knee Range of Movement – Neurological vs Healthy

Figure 3.6: Meta-analysis report for knee ROM comparing (a) elderly with young group and (b) neurological with healthy group.

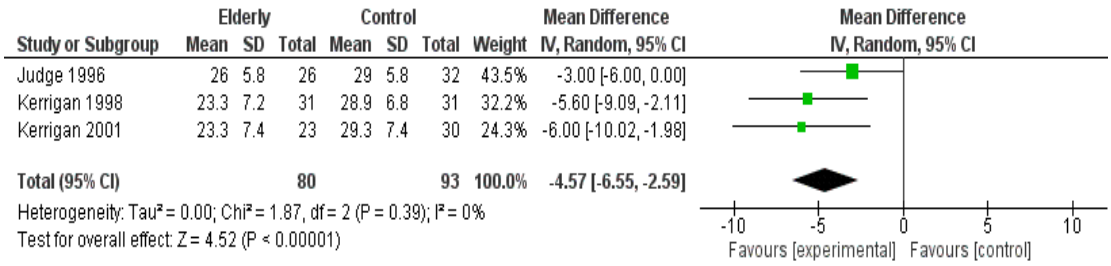

(a) Forest Plot: Ankle Range of Movement – Elderly vs Young

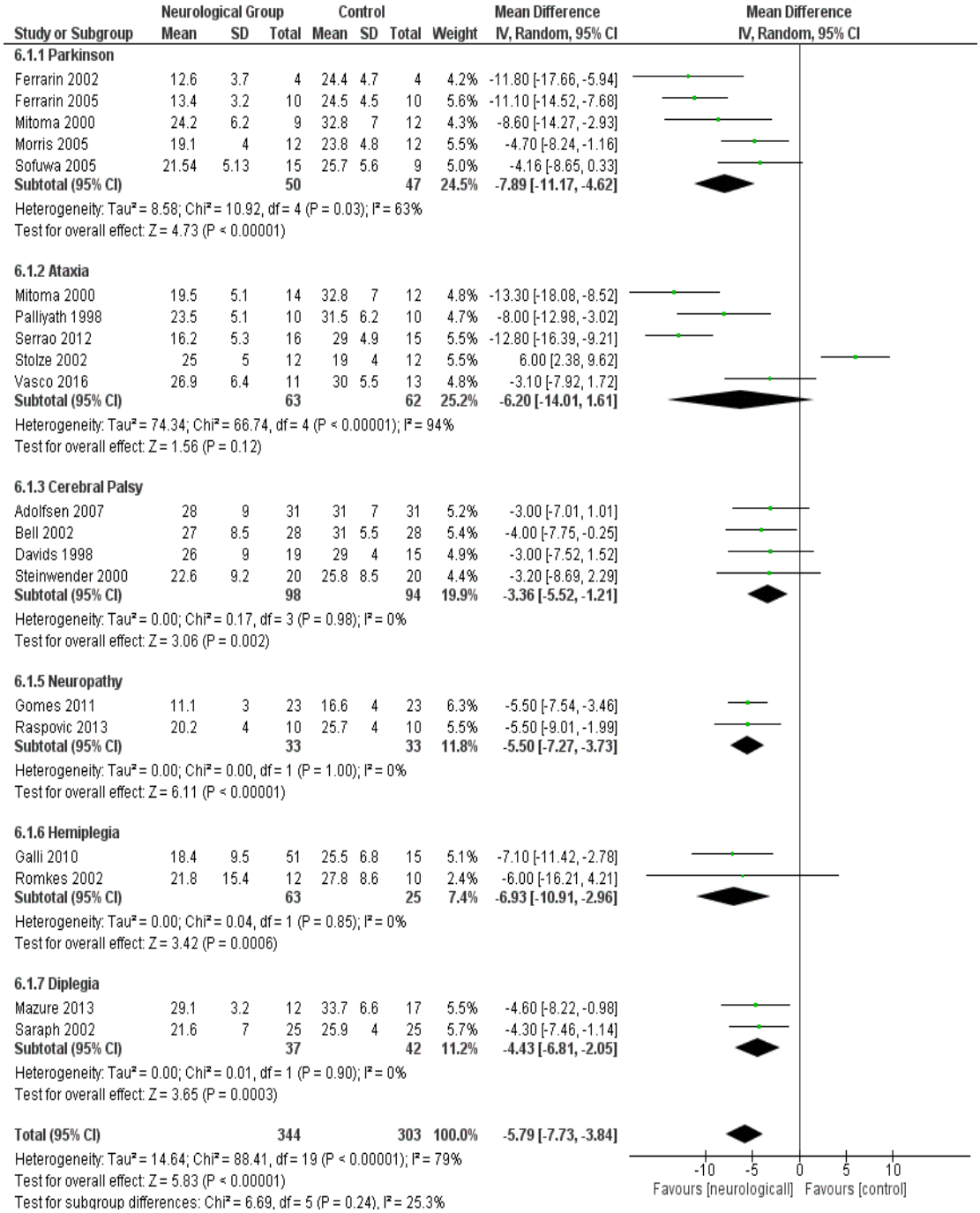

(b) Forest Plot: Ankle Range of Movement – Neurological vs Healthy

Figure 3.7: Meta-analysis report for ankle ROM comparing (a) elderly with young group and (b) neurological with young group.

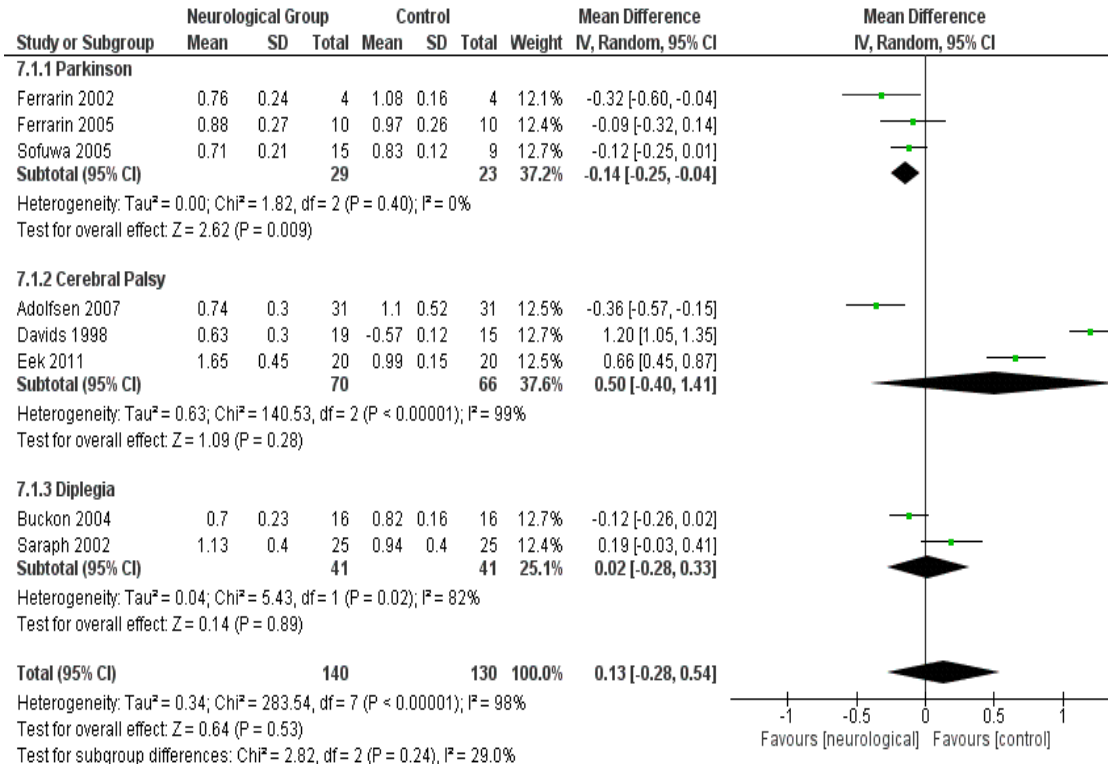

Forest Plot: Peak Flexion Moment at Hip – Neurological vs Healthy

Figure 3.8: Meta-analysis report for peak flexion moment at hip comparing neurological with healthy group. A negative mean difference in Parkinson indicates a lower value of peak flexion moment at hip. Results do not favour any group in cerebral palsy and diplegia

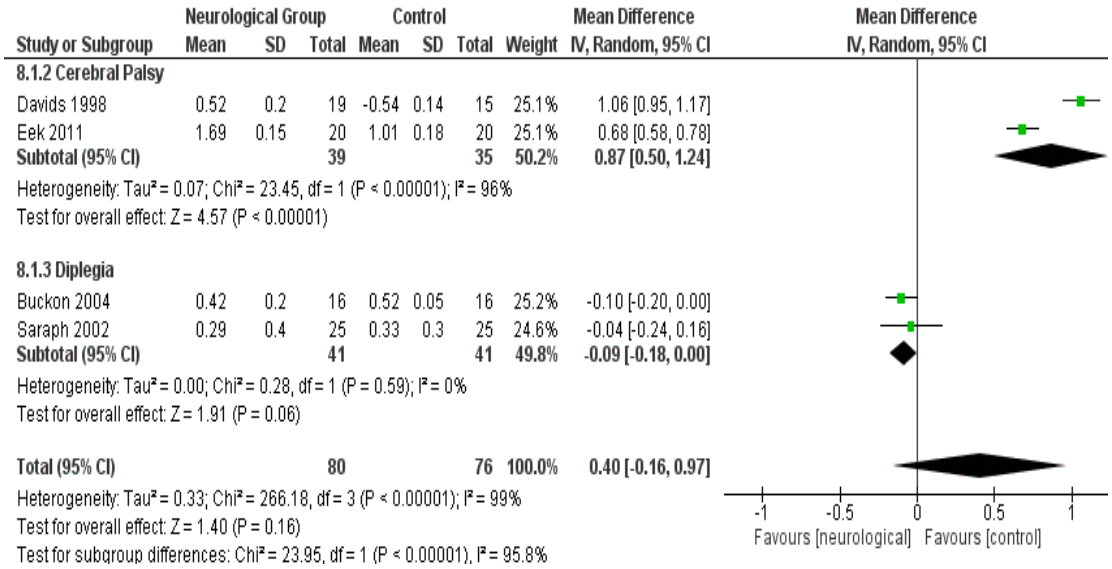

Forest Plot: Peak Flexion Moment at Knee – Neurological vs Healthy

Figure 3.9: Meta-analysis report for peak flexion moment at knee comparing neurological with healthy group. A positive mean difference in cerebral palsy indicates a higher value of peak flexion moment at knee. Results do not favour any group in diplegia

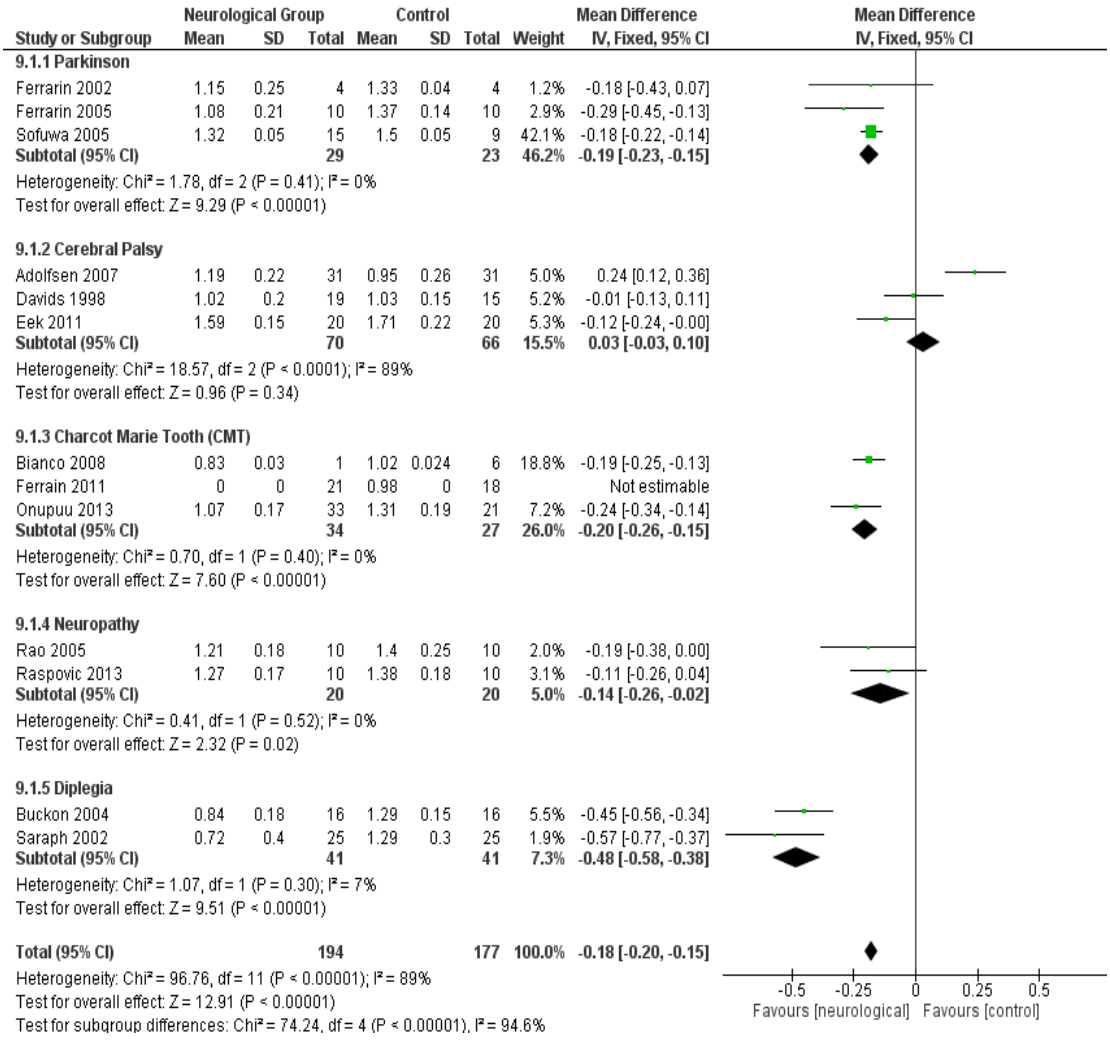

Forest Plot: Peak Dorsi-Flexion Moment at Ankle – Neurological vs Healthy

Figure 3.10: Meta-analysis report for peak dorsi-flexion at ankle comparing neurological with healthy group. A negative mean difference indicates a lower value of peak dorsi-flexion moment in the neurological group

3.4. Discussion

This study is a comprehensive analysis of the biomechanical alterations in elderly and neurological patients. The gait pattern was analysed in comparison with the healthy groups in terms of spatio-temporal, kinematic and kinetic characteristics and highlighted the support requirement in each category of the deviated gait. From the above findings and results, it appeared that there was a degree of agreement in reporting most of the spatio-temporal, kinematic and kinetic variables of various gait impairment types, though some inconsistency and variability has also been observed in describing certain parameters among the authors. The inconsistency among the studies could be as a result of different measurement approaches employed, varied number, age, mass and gender of subjects, the reference

frame used, etc. It has been observed that there are difficulties in categorising patients as some of them do not match a single set of gait pattern. An improper coordination in any one of the input source can lead to gait impairment [112]. For better understanding, it would be appropriate to explore the parameters according to the review findings and results discussed above. From meta-analysis of the spatio-temporal parameters, it could be suggested that participants of Parkinson's disease walked slower than CMT and Neuropathy patients but faster than participants of Diplegic gait. The main reason for slow gait speed in Parkinson disease (PD) is the disorder in the regulation of stride size [104, 156]. A large variation of gait speed, stride length and cadence exists in studies of Hemiplegic gait. The walking speed of Hemiplegic patients were directly related to the stage of motor recovery [157]. In elderly gait, the three spatio-temporal parameters of interests showed a decreasing trend that indicates a decline in the gait performance at older age. In cerebral palsy patients, the deterioration of the gait pattern was suggested to be responsible for decrease in spatio-temporal variables [158]. The overall results of the meta-analysis for the spatio-temporal characteristics showed a decreasing trend in elderly and neurological patients that indicates the need of the patients to use the robot assisted devices so that the deviations among them could be minimized. The study of these deviations in spatio-temporal parameters will also be helpful in the design of robot assisted devices.

The results obtained for the kinematics of hip, knee and ankle joints also showed some degree of inconsistency among them but the overall results of the meta-analysis favoured elderly and neurological patients i.e. a decrease in hip, knee and ankle ROM is recorded and hence the need of robot assisted devices is highlighted. However, there could be several reasons of ROM decrease that may, in some cases, increase the level of discomfort by using assistive devices. The meta-analysis report on the hip ROM of elderly showed a decrease in the ROM as it is reported that even a small reduction in hip ROM alters gait in elderly [118]. In order to produce the same output, there is a large contribution required from hip extensors [118] and small contribution from knee extensors and ankle flexors [159]. Knee ROM in elderly also showed a significant reduction and the studies also reported an increase in the knee extension angle during mid stance and a decrease during the swing phase [119-121]. The decrease in the ankle is associated with the ankle dorsi-flexion (DF) and plantar-flexion (PF) muscles weakness [119, 121]. The ROM of the Parkinson disease was observed to be significantly affected at the later stages of the disease. Knee flexion was

usually observed to be increased in advanced stages of Parkinson [160]. Change in knee extension caused an overall reduction in the ROM of knee. Studies of the kinetic parameters showed a lot of variability among them in reporting most of the parameters. In Parkinson's disease, more abnormalities were observed in kinetic profiles than the kinematics with the moments reaching peaks that were significantly different from the healthy group [161]. The peaks of the moment profile in Parkinson disease were observed to be different from normal, hip showed a prolonged and increase in the flexion moment, peaks of the knee extension moment were observed to be lowered [125]. The ankle ROM was reduced during push off and recorded a reduction of PF at toe off [127, 129, 130]. In PD patients, it was reported that there was an increase of PF moment at heel strike and a reduction before push off [125]. Studies of the Ataxic gait showed a lot of variability among them. A lack of inter joint coordination was suggested to be the main reason for gait impairment in Ataxic gait [132]. Studies documented on the kinematic and kinetic changes in ataxic gait observed the changes in stepping and lack of coordination of limb motion [105, 106]. This may lead to lurching in unusual directions. Ataxic patients showed less hip flexion at toe off [133]. The ROM in ataxic patients was reduced [106, 128, 134] and the effects were correlated with clinical severity. Vasco et al. pointed out a decrease in knee flexion at heel contact and mid stance and an increase in the flexion during swing [133]. Changes in the kinematics of ankle joint were appeared to be significant in Ataxic gait even at moderate speed [128]. Limited sagittal plane motion and crouch gait is associated with CP [108]. Hip demonstrated a delay in shifting from extension to flexion moment. Hip extension was appeared to be reduced during mid stance [135]. There existed at least eight different clusters of gait; [162] and [150] used Principal Component Analysis (PCA) to classify gait patterns in CP. Ballaz et al. established a correlation between higher gait speed and ankle ROM [163]. Peak ankle PF and knee flexion at initial contact were observed to be decreased [135]. The increase in the moment of knee flexors was explained by [164] due to the large moment required for hip extension during walking. Although findings of the kinematic and kinetic variables for CMT were not significant to perform a meta-analysis report but it showed excessive hip extension in [139]. The CMT patients showed a delay in the peak DF in the terminal stance associated with the weakness in the ankle plantar flexors [141]. Two distinct gait patterns were reported in CMT, a steppage pattern and a clumsy pattern [165]. A delay in the peak value of ankle DF is a common finding in CMT patients [141]. The results of the findings of the

hemiplegia and diplegia group showed a significant difference at the ankle joint and therefore favours the need of the use of an assistive device.

The findings reported in this chapter will be helpful in proposing the design criteria for lower limb robot assisted training. By observing the torque deviations involved in different impaired gaits, maximum deviated value of the joint torque could be determined. This would indicate a threshold requirement of elderly and neurological gaits, hence a general support requirement from the robotic assistive devices is established. It was also noticed that the torque and angle profile of the lower limb joints varies to a large extent among different categories of gait impairments so it was not possible to group patients with similar gait characteristics based on the joint angular displacement and torque profile. Even subjects belonging to the same category of neurological gait significantly differ among each other. A significant difference was reported in the spatio-temporal, kinematic and kinetic variables in elderly and neurological patients, hence the need for robot assisted devices is highlighted. However, deviations in few parameters were observed to be insignificant.

3.5. Summary

The work presented in this chapter is of great importance in analysing the design requirements of robotic assistive devices. It outlines the requirements among different types of gait impairments that will be beneficial in the design of assistive devices to help users complete the activities of daily living independently. The gait deviations in spatio-temporal, kinematic and kinetic parameters among elderly and neurological groups were identified. A systematic approach was developed to organise the gait data according to the alterations in the biomechanical parameters related with the various gait pathologies. The study was able to gather evidences of gait malfunctions in different categories of patients and established a general trend in the support requirements among them. The work performed is helpful to define the end users of the robot assistive devices by investigating the support required for them in the spatio-temporal, kinematic and kinetic parameters involved in locomotion. It has been observed that the gait of elderly significantly differs when compared it with the normal gait and hence efficient assistive devices need to be developed that can assist them in performing ADL.

Chapter 4
Optimal Rigid Actuation System

4.1 Introduction

This chapter presents an optimal rigid actuation system for an assistive robotic exoskeleton using an optimization framework so that a power efficient, lightweight and powerful system could be obtained. This introduces a great challenge for the exoskeleton actuator design. Choosing the best combinations of existing technologies such as motors and transmission systems in an actuation system is not a trivial task. As mentioned in Chapter 3, there was a need to develop assistive technologies in order to support the users involved with the pathological gait. In this chapter, the optimal actuation system will be investigated for an assistive robotic exoskeleton for elderly users. The assistive exoskeleton reported in this study will have an actuated DOF at the hip, knee and ankle joint. An optimization framework will be described to determine the most efficient and lightweight combinations in a rigid actuation system.

It has been recorded that the gait of elderly significantly differs from the normal gait in the kinematic and kinetic parameters [166]. This change in the movement of the gait results in the frequent falls of the elderly [167] and is addressed in [103] as one of the main causes of accidental deaths among them. There are several versions of the exoskeletons that are specified in the literature such as ReWalk [168], Indego [169], Ekso [170], HAL [19], Mina [49], Mind walker [55] and Rex Bionics [171]. These assistive exoskeletons assist their users in performing their daily tasks independently. Some of the exoskeletons developed are light-weight but require crutches to maintain balance and hence, compromise on the insufficient actuation of the joints. Rex on the other hand, does not require any crutches to maintain balance but is described as one of the heaviest assistive exoskeleton available to date. The performance of the lower limb exoskeletons is restricted by the mechanical design and the actuators limits [63]. In this study, the focus will be on the electrical actuators as previous studies have shown several advantages of using electric actuators over hydraulic and pneumatic actuators [47, 172].

Based on the analysis mentioned in Chapter 2 and explicitly described above, there is a strong need to develop the actuation systems of an

exoskeleton that should be lightweight, since weight is the main factor limiting the use of the exoskeleton as well as it should be power efficient as the assistive devices will need to be portable in order to support ADL. Therefore, by developing a power efficient system, the size of the battery and hence the weight can be reduced. Some questions encountered during the design of an assistive robotic exoskeleton actuation system are, how much compromise should be made in the weight of the exoskeleton in order to make it more power efficient or vice versa? What should be the best combination of the motor and transmission system so that the efficiency of the overall system is increased? Therefore, a multi-factor optimization strategy needs to be developed for assistive robotic exoskeleton actuation system that will perform the optimization based on a number of factors. These factors include the total weight, total power and the user carrying capacity of the exoskeleton. A number of actuator design candidates will be selected and an assessment criterion will be implemented to determine the most efficient and suitable actuator candidate. Hence, the primary purpose of the work presented in this chapter is to provide a framework that will design a lightweight, efficient and a high power system for a rigid actuation system of an assistive robotic exoskeleton.

In this chapter, the requirements of the rigid actuation system of an assistive exoskeleton will be specified in Section 4.2. The experimental setup to obtain the kinematic data of the required movements to perform ADL i.e. sit to stand and level ground walking will be discussed and the kinetic model of the exoskeleton will be explained. The kinetic model of the exoskeleton will be developed by introducing the inertial parameters of the exoskeleton. The kinetic model of the exoskeleton will be validated using a simulation model that was developed in SolidWorks using SolidWorks motion analysis. The selection and modelling of the components will be illustrated. The optimization algorithm will be applied in Section 4.8 for a single joint as well as for a multi-joint system. The results obtained using a mathematical and simulation model of the assistive exoskeleton will be reported and finally the optimal actuation system will be formulated using an optimization algorithm for an assistive robotic exoskeleton actuation system.

4.2 System Requirements

The exoskeleton was intended to be designed for elderly people in order to support them to perform ADL independently. The primary manoeuvres necessary to perform the ADL are level ground walking and sit to stand operations. These manoeuvres are performed in the sagittal plane. In order for the exoskeleton to perform these manoeuvres, actuating the movements in the sagittal plane is necessary i.e. three DOFs will be actuated. These include hip flexion/extension (F/E), knee flexion/extension (F/E) and ankle dorsiflexion/plantar flexion (DF/PF). Actuating these DOFs will be sufficient to realize level ground walking and sit to stand operation [61]. In the optimization algorithm, the rigid actuation system for an assistive robotic exoskeleton will be optimized considering multiple parameters which include,

- The total power consumption of the exoskeleton
- The total weight of the exoskeleton
- The ability of the system to carry a user of up to 100kg. However, these are based on the requirement to provide 50% support to the user.

In order to perform the ADL independently by the user and to maximize the performance of the exoskeleton, it is also expected that the user did not require any crutches while performing the desired manoeuvres. The optimization algorithm will minimize the total weight and power consumption of the exoskeleton with its defined user carrying capacity. These parameters will be compared with the parameters of the Rex Bionics as specified in [93]. Rex Bionics is described as the only assistive exoskeleton available to date that does not require any crutches, however it is much heavier as compared to other available exoskeletons. The weight of the Rex Bionics is given to be 38 kg, the total power consumption obtained as 480 W and the user carrying capacity to be 100 kg. The design parameters of the Rex Bionics were scaled during the comparison process so that it reflects the conditions and requirements similar to this system e.g. 50% support, three DOFs etc and therefore, the scaled power consumption and user carrying capacity was 140W and 50 kg respectively, considering six actuators with 50% support The initial weight of the exoskeleton in the optimization algorithm was kept equal to 38 kg and hence, the mass of the exoskeleton was compared with the full mass of the Rex Bionics. It should be noted that some of the parameters of Rex Bionics were explicitly obtained from the literature but some of them were calculated based on other given parameters. For example, the total power consumption of Rex Bionics was calculated based

on the voltage (29.6 V) and current (16.5 A) of the given battery and the duration (1 hour) it can support the exoskeleton. The design requirements reported during the human gait data analysis are listed in Table 4.1. The details regarding the evaluation of human gait biomechanics is given in the next section.

As can be observed in Table 4.1, the most power demanding joint during sit to stand operation was the knee joint, hip joint estimated similar requirements during each phase, however ankle joint reported high torque and power during the stance phase. It should be noted that the knee torque and power during stance phase was zero. This is because of the knee locking mechanism that was considered during the manoeuvre. The knee locking mechanism also restricted the movement of the hip joint during the stance phase and as a result the hip power was observed to be zero because of the negligible movement of the hip joint during this phase. A similar trend was also noticed at the ankle joint during the stance phase where the power was limited because of the restricted movement of the joint.

Table 4.1: Design requirements of Assistive Robotic Exoskeleton Actuation System at Hip, Knee and Ankle Joint

Maneuver	Sit to Stand			Swing Phase			Stance Phase		
Joint	Hip	Knee	Ankle	Hip	Knee	Ankle	Hip	Knee	Ankle
Peak Torque (Nm)	25.6	96.2	24.6	30.1	16.7	2.5	28.8	0	65.1
RMS Torque (Nm)	16.0	59.1	19.8	15.6	10.2	2.0	14.9	0	38.4
Peak Power (W)	8.3	24.6	1.5	2.7	7.2	0.6	0	0	1.6
RMS Power (W)	4.4	14.1	0.6	1.5	4.1	0.3	0	0	0.6

4.3 Human Gait Data Analysis

4.3.1 Experimental Setup

In order to assess the design requirements during sit to stand and level ground walking, a healthy subject performed the required manoeuvres. Ethical approval was already available for the research group. Markers were placed at certain points on the subject and a number of cameras were recording the position of the markers while the subject was performing the desired manoeuvres. The speed of performing the required manoeuvres were kept similar to the speed of the Rex Bionics. Five trails were obtained

by the subject for each of the manoeuvre. The points where markers were placed on the lower limb of the subject were described as the common points between the user and the exoskeleton and therefore, the kinematic data of these points will be used in the dynamic model of the exoskeleton. The gait data that was obtained in the motion capture experiment was compared with the data collected by D. Winter [173].

Figure 4.1(a)-(c) shows the trajectory of the angular displacement recorded at hip, knee and ankle joints respectively during swing phase of the gait cycle. Figure 4.1(d) shows the angular displacement during single support stance phase of the ankle joint. The joint angles were obtained for each of the lower limb joint during each phase of the manoeuvre. However, for illustration purpose only some of the profiles are shown as all of them follow the similar pattern.

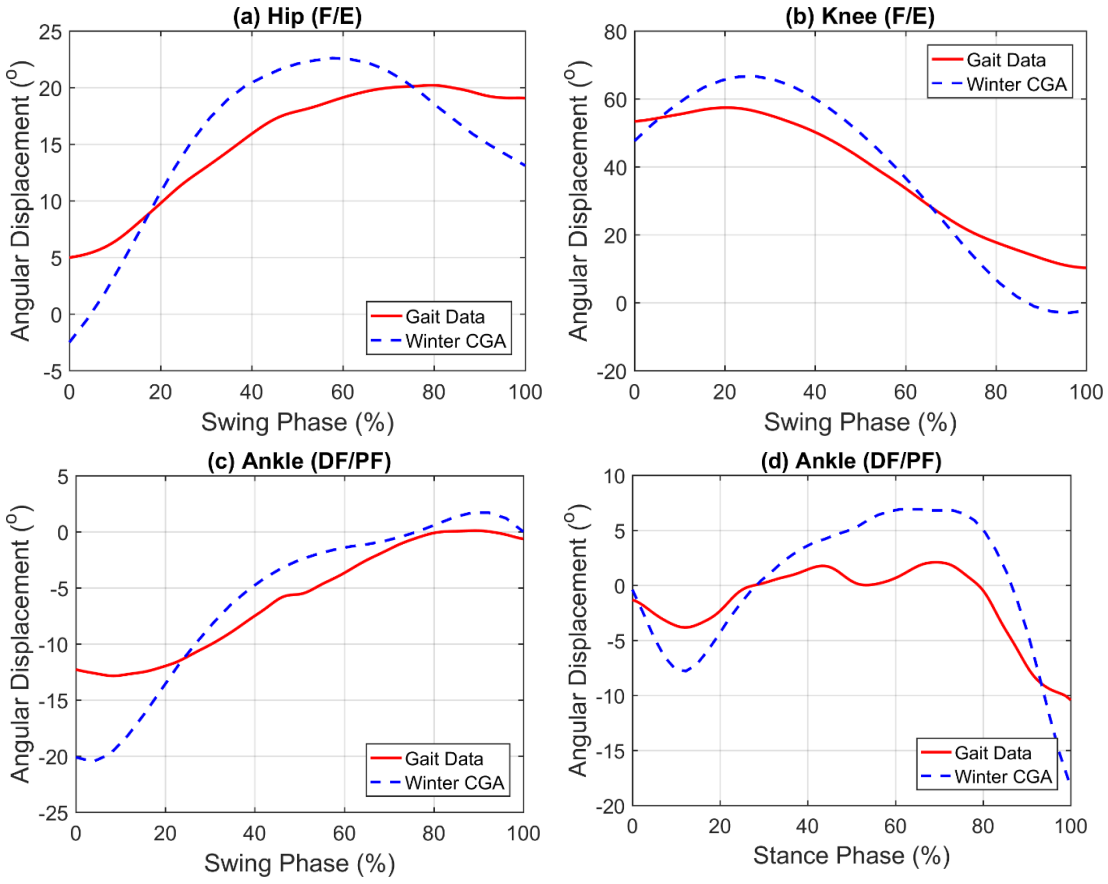

Figure 4.1: Average joint angular displacement data of the five trails during (a) swing phase of the hip joint (b) swing phase of the knee joint, (c) swing phase of the ankle joint and (d) stance phase of the ankle joint of a healthy subject compared with the data of D. Winter.

The solid line represents the gait trajectory while performing the experiment with the healthy subject and dotted lines represent the gait data reported by [173] during the swing phase. The experimental gait data shown in Figure 4.1 has been obtained after filtering the raw data of the markers linear positions and computing the kinematic model to obtain the joint angular displacements. As can be observed, the gait patterns during swing and stance phase at each of the lower limb joints was obtained similar to the gait profiles of [173]. However, the ROM at each of the joints is observed to be slightly reduced. This is in accordance with [178] since the gait pattern was recorded at a slow speed to match the gait speed of Rex Bionics as compared to the speed of the gait collected by [173]. Hence, the ROM of the joints was slightly reduced during slower gait speed.

4.3.2 Data Processing

The raw data collected using markers placed at certain points on the healthy subject was processed and analysed to derive the position, velocity and acceleration of the specified points that were finally presented into the exoskeleton model to compute the exoskeleton joint torque and power. The marker data was processed using Butterworth filter with a low pass bandwidth of 10Hz. The value of the cut-off frequency was selected to be 10Hz as it does not eliminate any motion component of the human body [174]. After the data was filtered, the numerical differentiation of the marker data that represents the sampled position of the point during the particular interval was performed to obtain the velocity and acceleration of each point. The position, velocity and acceleration were incorporated into the kinematic model of the exoskeleton as explained in the next section.

4.4 Dynamic Modelling of the Exoskeleton

After the marker data was processed, the geometric parameters of the exoskeleton were taken into account to estimate the kinematic model of the exoskeleton. The kinematic model of the exoskeleton was evaluated by considering the dimensions of the exoskeleton links. The details of obtaining the kinematic model were derived from [172], description of which have been given in Appendix A. Therefore, the markers positions, velocities and accelerations were translated into the joint angular displacement, angular velocity and angular acceleration. These values were fed into the kinetic model of the exoskeleton to compute the joint torque and power of the lower limb during the desired manoeuvres. The kinetic model of the exoskeleton was formulated taking into account the inertial parameters. The details

regarding the determination of the inertial parameters of the exoskeleton can also be found in Appendix A. The block diagram of the dynamic modelling of the exoskeleton can be visualized in Figure 4.2.

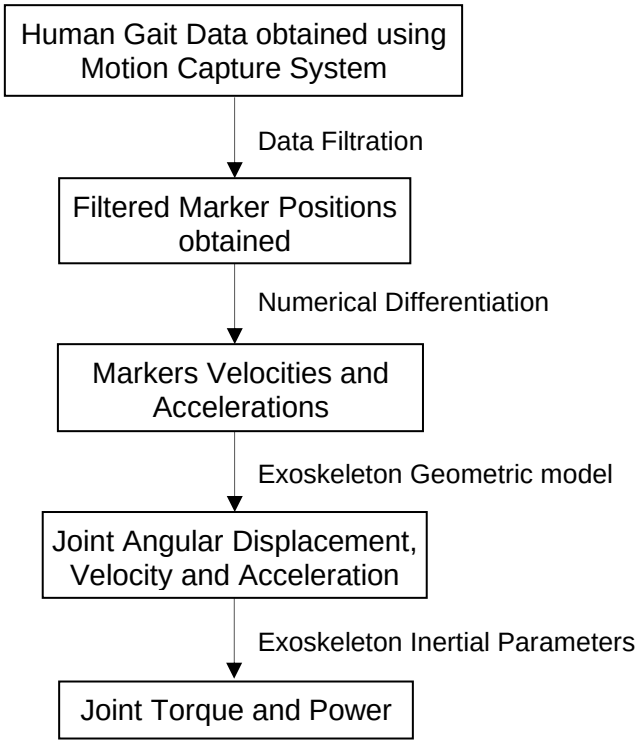

Figure 4.2: Block Diagram of the Dynamic Modelling of the Assistive Exoskeleton

During the calculation of the weight of the user, the total weight was divided into the upper part and the lower part of the body. The weight of the upper part was considered to be a point mass located at its centre of gravity. The centre of gravity of the upper part of the body mass has been calculated in Appendix A. The mass of each lower part of the body has been added at the centre of gravity of each respective exoskeleton link in the dynamic model of the system.

4.5 Simulation Model

The exoskeleton dynamic model was validated using SolidWorks motion analysis toolbox. A model of the lower limb exoskeleton shown in Figure 4.3 was developed in SolidWorks to perform the validations of the mathematical model [172]. It consisted of a hip part, the shin part and the ankle and foot. The desired manoeuvres were simulated using this model. The acquired marker data explained in the previous section was presented into this model in order to assess the joint torque and power. These joint torque and power

were compared with the joint torque and power estimated from the kinetic model of the exoskeleton.

Figure 4.3: Model of the Lower Limb Exoskeleton representing the hip, knee and ankle joint.

4.6 Components Selection

This section explains the components that were selected to be used in the optimization algorithm for assistive robotic exoskeleton actuation system. The optimization algorithm consists of a list of motors and the transmission systems that have been produced by an extensive market search. The list has been collected from different manufacturers of motors and transmission systems. The spreadsheet of motors and the transmission systems contained the required parameters that define the model of the motor and the transmission system. These parameters were extracted from the datasheets provided by the manufacturers. The modelling of motors and the transmission systems will be explained later in Section 4.7. For the selection of motors, the focus was limited only to the electric motors as it has been found to be most suitable for this kind of application [172]. They are compact, reliable, noiseless and easy to control as well as having high efficiency, control precision and a high power to weight ratio [63]. Electric motors are considered to be 92% more power efficient than the hydraulic ones [47].

The motors that were included comes in different power ranging from 25W to 250W in the candidates motors list. However, some of them were high

power motors greater than 300W. The list represented a good state of the art, most suitable for assistive exoskeleton actuation system. The complete list of the motors included in the optimization algorithm has been recorded in Appendix B, part of which is shown in Table 4.2. Motors were incorporated from different suppliers such as Maxon, Kollmorgen, Allied motion, Parker Hannifin, Aerotech, Printed Motors, Moog, Portescap etc. The motors included comes in different designs. Both brushed and brushless motors were assessed. Pan cake motors and some slim motors were also part of the list. Frameless motors were also considered.

Table 4.2: An excerpt of the motors market search with the given parameters (Complete table can be found in Appendix B)

Manufacturer	Model no.	Rated Power (W)	Rated Torque (Nm)	Weight (kg)	Torque constant (Nm/A)
Maxon	EC 45	70	0.92	0.09	0.13
Moog	BN 17 15IP03	90	0.15	0.19	0.02
Allied motion	MF 76008	280	4	0.2	0.26
Pittman Amtek	EC033A-3	34	0.19	0.24	0.07
Portscap	30GT2R82	82	0.09	0.31	0.04
Allied motion	MF 76020	440	13	0.43	0.33
Maxon	RE 40	150	0.655	0.48	0.21
Kollmorgen	TBM-6051A	160	5.7	0.571	0.19
Printed Motors Works	GPN 9	94	3.0	0.65	0.05
Kollmorgen	T 4412	120	2.03	0.68	1.06
Moog	BN 23	227	1.57	0.74	0.03
Kollmorgen	QT 3102	263	3.39	0.91	0.61
Printed Motors Works	GPN 12	200	3.57	1.2	0.09
Aerotech	BMS 100	133	2.26	1.5	0.38
Heinzmann	SL 120 1NFB	250	40	1.8	0.16

In the market search of motors, power was defined as the variable to select the motor size criterion. Therefore, the motors that satisfy the power requirements were selected in the candidates motors list. Although, after initial simulations the lowest power range motor included were turned out to be incapable to perform the task and the larger motors were not considered the optimal one. Consequently, after preliminary simulations, some of the motors in the candidates motor list were ruled out and the list was refined to those motors that falls within the defined range of the application requirements. These motors also appear in different weights ranging from 0.05kg to 4kg but again during the preliminary analysis of results, some of them were ruled out based on their masses because either they were too heavy/bulky or they were incapable to perform the required task. Hence, the final list consisted of 200 motors that were structured in the optimization algorithm, although the list gets further refined after few simulations to reduce the run-time of the optimization algorithm.

Similarly, different transmission systems were investigated to be included in the candidates transmission system list. As electric motors have high speed and low power, therefore suitable form of the transmission system is essential. Some of the transmission systems were excluded in the preliminary stages e.g. Spur gears do not provide enough transmission ratio and a zero backlash connection. Worm gears with high transmission ratio are not back driveable [175]. Pulleys with timing belts and sprockets chains were also not considered as they do not provide enough transmission ratio. However, during the preliminary analysis, it was recorded that these transmission systems can be used in combination with other transmission system types e.g. Harmonic drives. Harmonic drives have certain advantages in terms of inherent high stiffness, nearly zero backlash, low transmission error and high torque density [1]. However, as a drawback they are sensitive to bearing drag, low efficiency and poor back drivability. Ball screws were also considered to have a high torque density, high efficiency and good back driveability. Power transmission system can be cable based, linkage based, gear based or hybrid based [99]. The transmission systems finally included in the candidates transmission system list were harmonic drives, ball screws, belt and pulley drive, chains and sprockets. Ball screws were used in a slider crank linkage mechanism as will be explained later [172].

Different suppliers of the included transmission systems were investigated to form a list of the candidates transmission systems. Strain gears were

selected from different manufacturers with different torque capacities and weights. Similarly, ball screws were recorded from different suppliers. The ball screws were used with different pitch sizes and diameter. There were 20 ball screws that were investigated with various pitch size ranging from 2 mm to 12.7 mm and diameters ranging from 10 mm to 16 mm. As described earlier, ball screws were used in a slider crank mechanism, therefore different configurations of the ball screws in a slider crank mechanism were also determined in order to use them in the optimization algorithm. A complete list of transmission systems of harmonic drives and ball screws can be found in Appendix C. However, an excerpt of the harmonic drives and ball screws are shown in Table 4.3 and Table 4.4 respectively.

Table 4.3: An excerpt of the market search of harmonic drives used in the optimization algorithm (For complete table, please refer to Appendix C)

Type	Rated Torque (Nm)	Moment of Inertia x10-6 (kgm^2)	Repeatable peak torque (Nm)	Average Torque (Nm)	Weight (kg)
CSD-14-50-2A	4	2.1	12	4.8	0.06
CSD-17-100-2A	16	5.4	37	27	0.1
CSG-14-50-2A	7	3.3	23	9	0.09
CSG-17-100-2A	31	7.9	70	51	0.15
CPL-17-50-2A	16	4.9	34	26.0	0.10
CPL-20-160-2A	40	11.2	92	49.0	0.14
FB-25-100-2	39	36.0	52	52.0	0.50
FR-20-128-2	40	32.0	67	49.0	0.30
SHG-17-50-2A	21	7.9	44	34.0	0.18
SHG-25-160-2A	87	41.3	229	140.0	0.48

As can be observed in Table 4.3, harmonic drives comes with a variety of range of transmission ratios, torques and weights. Similarly, Table 4.4 highlighted some of the Ball screws with different pitch diameter and size. The parameters of the ball screws in the slider crank linkage mechanism

were altered to obtain different configurations of the Ball screws in the slider crank linkage mechanism. Some of them can be observed in Table 4.4. These parameters will be explained in detail in Section 4.7.2.

Table 4.4: An excerpt of the market search of Ball screws shown for various configurations (For complete table, please refer to Appendix C)

r_p (m)	r_d (m)	γ_d (rad)	moment of Inertia (kg-m^2)	max h (m)	weight for the max length (kg)	weight per length (kg/m)
Type: SKF SD 12x2						
0.082568	0.083111	1.850049	0.000288	0.075073	0.084643	0.887814
0.084222	0.087333	1.850049	0.000288	0.080809	0.087253	0.887814
0.090699	0.091556	2.158391	0.000288	0.104694	0.072548	0.887814
0.093344	0.095778	2.158391	0.000288	0.112801	0.074859	0.887814
0.09599	0.1	2.158391	0.000288	0.121091	0.077183	0.887814
Type: SKF SD 14x4						
0.080913	0.078889	1.850049	0.000288	0.069438	0.111686	1.208414
0.085408	0.083111	2.158391	0.000288	0.089145	0.092519	1.208414
0.088053	0.087333	2.158391	0.000288	0.0968	0.095622	1.208414
0.097943	0.095778	1.850049	0.000288	0.082492	0.13639	1.208414
0.099321	0.1	1.850049	0.000288	0.0876	0.139913	1.208414
Type: SKF SD 12x5						
0.082568	0.083111	1.850049	0.000288	0.075073	0.084643	0.887814
0.084222	0.087333	1.850049	0.000288	0.080809	0.087253	0.887814
0.090699	0.091556	2.158391	0.000288	0.104694	0.072548	0.887814
0.093344	0.095778	2.158391	0.000288	0.112801	0.074859	0.887814
0.09599	0.1	2.158391	0.000288	0.121091	0.077183	0.887814
Type: SKF SD 16x10						
0.082568	0.083111	1.850049	0.000288	0.075073	0.150477	1.578336
0.084222	0.087333	1.850049	0.000288	0.080809	0.155116	1.578336
0.090699	0.091556	2.158391	0.000288	0.104694	0.128975	1.578336
0.093344	0.095778	2.158391	0.000288	0.112801	0.133082	1.578336
0.09599	0.1	2.158391	0.000288	0.121091	0.137215	1.578336

4.7 Torque and Power Calculation of the Actuator Components

After selecting the components for the actuation system of assistive robotic exoskeleton in the optimization algorithm, the torque and power requirements were derived for the particular candidate actuator and compared with the speed-vs-torque graph of the motors to establish if the particular candidate actuator is capable to perform the required task. The investigation of electric actuators in [1] is the basis of the torque and power requirements derived in this study for motors and the harmonic drives. In the developed model, the motor efficiency and inertia has also been taken into account.

4.7.1 Modelling of Electric Motor

In this section, the model of a motor will be developed. The total torque applied at the rotor of the motor T_m is given by Eq. (4.1).

$$T_m = T_r + J\ddot{\theta}_m + c\dot{\theta}_m \tag{4.1}$$

In Eq. (4.1), T_r is the output torque of the motor, *J* is the inertia of the mechanical parts including motor, shaft and the connecting parts, *c* is the viscous damping of the motor. $\dot{\theta}_m$ and $\ddot{\theta}_m$ represents the required angular velocity and angular acceleration respectively.

As mentioned earlier, the instantaneous torque a motor can provide should fall within the allowable limits of the motors. These include the winding limit, the temperature limit, and the current limit of the motor as explained in Figure 4.4. As can be observed in the Torque-vs-Speed graph of the motor, the required motor torque must lie below the winding line and the current line. Eq. (4.3) can be used to calculate the motors winding line which is derived as follows.

$$T_{max} = K_t I_{max} = K_t(V_{max} - K_e\dot{\theta}_m)/R \tag{4.2}$$

As,

$$K_m = K_t/\sqrt{R}$$

And,

$$K_e = K_t$$

Therefore, Eq. (4.3) can be written as:

$$(T_{max})_{winding} = \frac{K_t}{R}V_{max} - K_m^2\dot{\theta}_m \tag{4.3}$$

Where $K_t, K_m,\ K_e,\ R$, and V_{max} represent the torque constant, motor constant, back EMF constant, resistance and maximum allowable voltage respectively. It can be observed from the motor's winding line in Figure 4.4 that the instantaneous torque decreases with the increase in the speed of the motor.

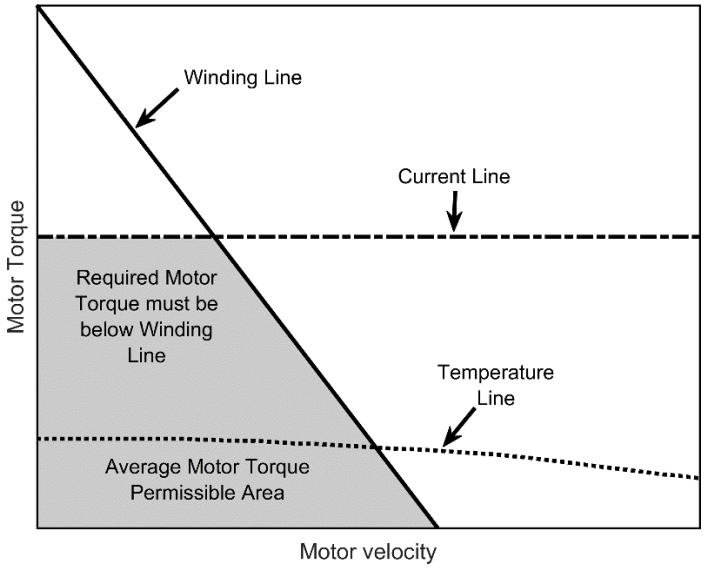

Figure 4.4: The Torque-vs-speed graph of an electric motor illustrating the limit lines and the permissible area for the motor's torque [1].

Apart from the winding line, the torque of a motor is also limited by the current line. This could be either the amplifier's peak current or the motor's maximum current, whichever is lower. The maximum allowable current of the motor was determined from the datasheet provided by the manufacturer. Therefore, Motor's current limit is determined by Eq. (4.4).

$$(T_{max})_{current} = K_t I_{max} \tag{4.4}$$

Where I_{max} is the maximum current that can be provided by the power supply and the controller.

Finally, the torque of the motor is also limited by the overheating of the components and therefore, the average motor's torque should lie underneath the temperature line given by Eq. (4.5).

$$(T_{max})_{temp} = K_m \sqrt{\frac{\Delta T_{max}}{TPR} - D\dot{\theta}_m^2} \tag{4.5}$$

Where ΔT_{max} is the maximum temperature change a motor can hold, TPR is the thermal resistance of the motor and D is the motor's viscous damping coefficient.

Similarly, the power consumption of the motor (P) can be obtained from Eq. (4.6).

$$P = \begin{cases} \frac{T_m^2}{K_m^2 \gamma} + T_m \dot{\theta}_m & P \geq 0 \\ \frac{T_m^2 \gamma}{K_m^2} + T_m \dot{\theta}_m & P < 0 \end{cases} \quad (4.6)$$

Where γ includes the amplifier and other electronic systems efficiencies. The effect of the amplifier efficiencies has also been taken into account while calculating the power consumption of the actuators.

The values described in the equations were obtained from the datasheets of the motors. However, there were some parameters that were not explicitly mentioned in the manufacture's datasheets. Therefore, those values were derived e.g. some of the manufacturer's did not provide the values for the temperature line but instead provided with a graph so those values were extracted from the provided graph. The required values were included in the list of motors market search as provided in Appendix C in order to be used by the optimization algorithm. For illustrative purposes, only important parameters of the electric motors were highlighted.

4.7.2 Modelling of Transmission Systems

As explained in Section 4.6, the model of the selected transmission systems will be developed so they can be utilized in the optimization algorithm. The modelling of harmonic drives, ball screws, belt and pulley drive and sprockets chain systems will be discussed in this section.

4.7.2.1 Harmonic Drives

The torque can be calculated using Eq. (4.7) for harmonic drives .

$$T_m = \begin{cases} \frac{T_r}{nN} & P \geq 0 \\ \frac{nT_r}{N} & P < 0 \end{cases} \quad (4.7)$$

Where T_m denotes the output torque of the motor and T_r represents the required torque at the joint, n is the harmonic drive efficiency and *N* is the transmission ratio obtained from Eq. (4.8).

$$\begin{aligned} \dot{\theta}_m &= N\dot{\theta}_r \\ \ddot{\theta}_m &= N\ddot{\theta}_r \end{aligned} \quad (4.8)$$

In Eq. (4.8), $\dot{\theta}_m$ and $\ddot{\theta}_m$ are the angular velocity and angular acceleration of the motor, $\dot{\theta}_r$ and $\ddot{\theta}_r$ represents the required angular velocity and angular acceleration of the joint respectively. The power for harmonic drives can be calculated using Eq. (4.7) and Eq. (4.8). Figure 4.5 shows a strain wave gear for illustration purpose.

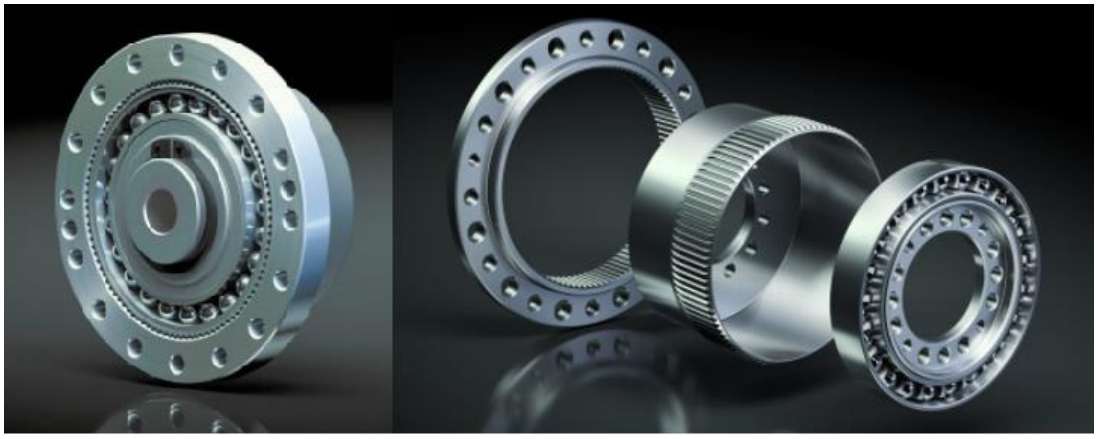

(a) (b)

Figure 4.5 (a) Strain gear (b) Components of a strain gear

Another consideration that must be taken into account when using harmonic drives is the no load starting torque. This is the minimum amount of torque required to overcome friction between the gearing mechanism. Therefore, the torque must be equal to the no load starting torque value when the system is forward driven. Similarly, when it is back driven, the amount of torque must be reduced by the no load starting torque value. The effect of no load starting torque has been taken into account in the optimization algorithm.

In this study, a fixed value of the efficiency of a harmonic drive has been estimated as can be observed in the previous studies [1, 172]. However, the efficiency quoted by the manufacturers only applies at the rated torque. So using a constant efficiency might not be the best approach because as the torque approaches zero, the efficiency will also be zero. In one of the aforementioned studies, the efficiency of the harmonic drive was calculated at each discrete point of the joint trajectory using the manufacturers graphs, however, the values calculated at each point of the trajectory did not significantly differ along the joint trajectory and hence a fixed value, although it will have the above mentioned limitations but it can be considered for the case of harmonic drives.

4.7.2.2 Ball Screws

The modelling of the ball screws in a slider crank linkage mechanism will be discussed in this section. It should be noted here that the transmission ratio is not constant in these types of transmission systems but a function of the joint angle. As the ball screws convert the rotary motion into a linear motion, therefore a slider crank linkage mechanism has been used to convert the linear motion back into the rotary motion at the joints of the exoskeleton. As

described earlier, the ball screws that were investigated in this study comes with various pitch sizes and diameters. The diameter affects the strength of the mechanism and pitch size has an impact on the dimensions and transmission ratio of the system.

The schematic of the ball screw in a slider crank linkage mechanism can be observed in Figure 4.6. The motor and the ball screw are connected at the opposite ends of the mechanism. The four design parameters that determine the dimensions of the mechanism are r_d, r_p, γ_d and γ_p. By varying these parameters, ball screws can be configured with various combinations.

The geometrical and force equations using an inverted slider Ball screw mechanism are shown in Eq. (4.9) to Eq. (4.14). These equations were used to convert the joint velocity, acceleration and torque to those of the motor. The symbols used here have been shown in Figure 4.6.

$$L = \sqrt{(r_p^2 + r_d^2 - 2r_p r_d Sin\,\alpha} \tag{4.9}$$

$$r_f = \frac{r_p r_d Sin\,\gamma}{L} \tag{4.10}$$

$$N = \frac{\dot{\theta}_m}{\dot{\theta}_r} = \frac{2\pi r_f}{p_i} \tag{4.11}$$

Where p_i in Eq. (4.10) is the pitch size of the Ball screw.

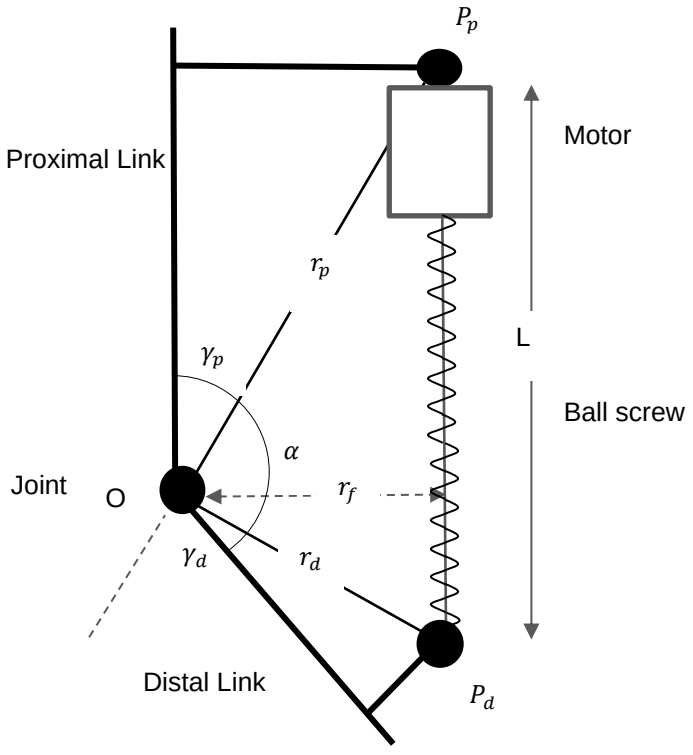

Figure 4.6: Schematic of the Ball screw in a slider crank linkage mechanism

The screw force F can be given by Eq. (4.12) as

$$F = \frac{2\pi}{p_i} n T_m \tag{4.12}$$

The required torque depends on the screw force F and r_f, Hence Eq. (4.13) gives,

$$Tr = F\ x\ r_f \tag{4.13}$$

Therefore, substituting Eq. (4.12) into Eq. (4.13) yields the required motor torque.

$$T_m = \frac{p_i}{2\pi n r_f} T_r \tag{4.14}$$

As mentioned earlier, the design parameters can be varied to create a list of various configurations of the ball screws. For a given ball screw with a specific pitch size and diameter, the four design parameters were modified so that various configurations of a particular ball screw can be realized. However, these design parameters were limited by device constraints e.g. space limitation, avoiding singular positions of the device and an allowable size. The configurations obtained were then tested with the load applied to the ball screw. If the mechanism was not able to bear the required load, it was eliminated. Similarly, this was applied to all the selected ball screws with various pitch sizes and diameters. The final candidate ball screw list contains 20 ball screws with their various configurations. The complete list is presented in Appendix C. A part of this list is illustrated in Table 4.4 with the dimensions of the design parameters and their masses. The masses were evaluated from the material density and the dimensions of the ball screws.

4.7.2.3 Belt and Pulley Drive System

Belt and pulley drive system has been used in combination with other transmission types e.g. harmonic drives in this study. The equations discussed in Section 4.7.2.1 for harmonic drives and Section 4.7.2.2 for ball screws are equally applied for the case of belt and pulley drive system. The difference would be that the efficiency of the belt and pulley drive system is considered to be 98% [176].

Figure 4.7 Timing Belt Pulley

The primary requirement of the belt and pulley drive system is that the belt should not slip over the pulley. To overcome this, the toothed belt drives are used as shown in Figure 4.7. The diameter of the pulley and the centre to centre distance between the pulleys is to be selected so that the required angle of contact between the belt and pulley should be sufficient.

Belts and pulley drive systems consists of a driving pulley and the driven pulley. By varying the sizes of these pulleys, different transmission ratios could be obtained. The driving pulley can also be combined with multiple driven pulleys to achieve a larger reduction ratios. The moment of inertia and mass of the pulleys will be determined from the dimensions and density of the material used. Due to the size limitation of the actuation system, the maximum ratio of a belt and pulley drive is limited to 1:2.5. Different combinations of the belt and pulley drive system were created to achieve a reduction ratio from 0.4 to 2.5.

4.7.2.4 Chains and Sprockets

Chains and sprockets were also used to combine them with other transmission types to obtain the optimal reduction ratio discussed in the previous section. Chain and sprocket systems can also be used to vary the transmission ratio. The modelling method discussed in the previous sections were also applied to the chains and sprockets similar to the belt and pulley drive system. The efficiency of the chain and sprockets system is also considered to be 98%.

The sprockets comes with various sizes and torque carrying capacities. They can have various designs as simplex, duplex and triplex as shown in Figure 4.8. The system can have multiple sprockets to obtain a better transmission ratio. However, due to the size limitations of the exoskeleton

actuation system, chains and sprockets alone cannot provide a high transmission ratio. Therefore, these types of transmission systems were also used in combination with the other types to achieve the desired transmission ratio.

In this study, an optimal transmission ratio of the actuation system was obtained during the initial iterations of the algorithm. The optimal transmission ratio was then matched with the available transmission systems. In some cases it was achieved with only the harmonic drive or the ball screws as the transmission types without the need to combine with other transmission types e.g. chain and sprockets or belts and pulleys drive system. However, in some cases, these transmission systems were combined with the harmonic drives in the optimization algorithm to achieve the desired transmission ratio.

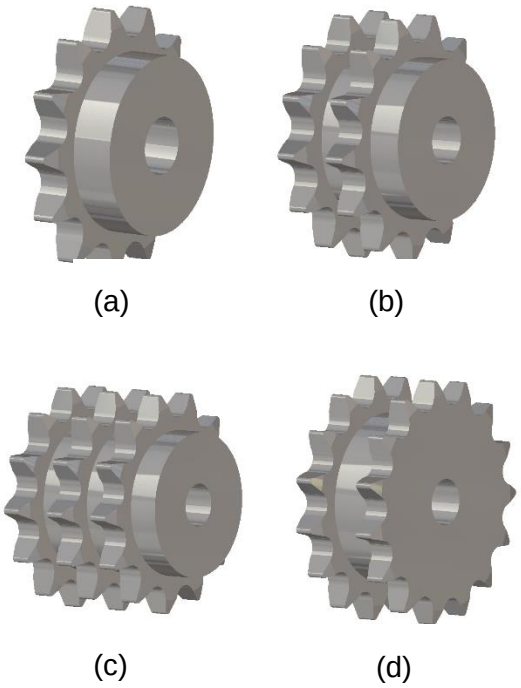

Figure 4.8: Various Designs of the Sprockets (a) Simplex (b) Duplex (c) Triplex (d) Double Strand

4.8 Optimization Algorithm for Assistive Robotic Exoskeleton Rigid Actuation System

In this section, the optimization algorithm will be explained that is applied on a rigid actuation system of an assistive robotic exoskeleton. The method has been adapted from [172] and a similar approach has been developed for an assistive robotic exoskeleton actuation system. The algorithm will be able to

determine the optimized motor and transmission system pair that will minimize the total weight of the exoskeleton, the total power consumption and maximize the user carrying capacity of the assistive exoskeleton. The algorithm will be initially applied at a single joint of the lower limb exoskeleton and then multi joint algorithm will be explained.

4.8.1 Algorithm Applied at a Single Joint

As mentioned, the algorithm is initially applied at the knee joint to determine the optimized actuation system at the joint. Using the data obtained by motion capture system for sit to stand and level ground walking, the algorithm computes the kinematic and kinetic model of the exoskeleton joints taken into consideration the geometric and inertial parameters as explained in Section 4.4. Therefore, once the joint torque and power requirements were evaluated, the algorithm selects the given motor from the candidate motors list. The selection of a motor is followed by the selection of a transmission system from the candidate transmission systems list. The given transmission system model will be used to convert the joint torque, velocity and acceleration into motor torque, velocity and acceleration. The models of the transmission systems employed in the optimization algorithm has been already explained in the previous section. Once the motor torque, velocity and acceleration has been assessed for a given motor and transmission system, the torque speed curve will be compared with the winding line, current line and the temperature line of the respective motor. If the given candidate actuator satisfied these motor's limits, the objective function of that particular actuator candidate will be calculated according to Table 4.5.

The mathematical expression of the objective function O_f is given in Eq. (4.15).

$$O_f = \left(0.3 \times \frac{U_c}{\max\,(U_c)}\right) - \left(0.5 \times \frac{P_c}{\max\,(P_c)}\right) - \left(0.7 \times \frac{W_{exo}}{\max\,(W_{exo})}\right) \quad (4.15)$$

Where U_c is the user carrying capacity of the exoskeleton, P_c represents the total power consumption and W_{exo} is the total weight of the exoskeleton. In the formulation of the objective function, the normalized values for each of the variables were used. On the other hand, if the candidate actuator violated the motor's limits, that particular actuator was eliminated. The flowchart of the algorithm to calculate the optimum actuator at a single joint is shown in Figure 4.9.

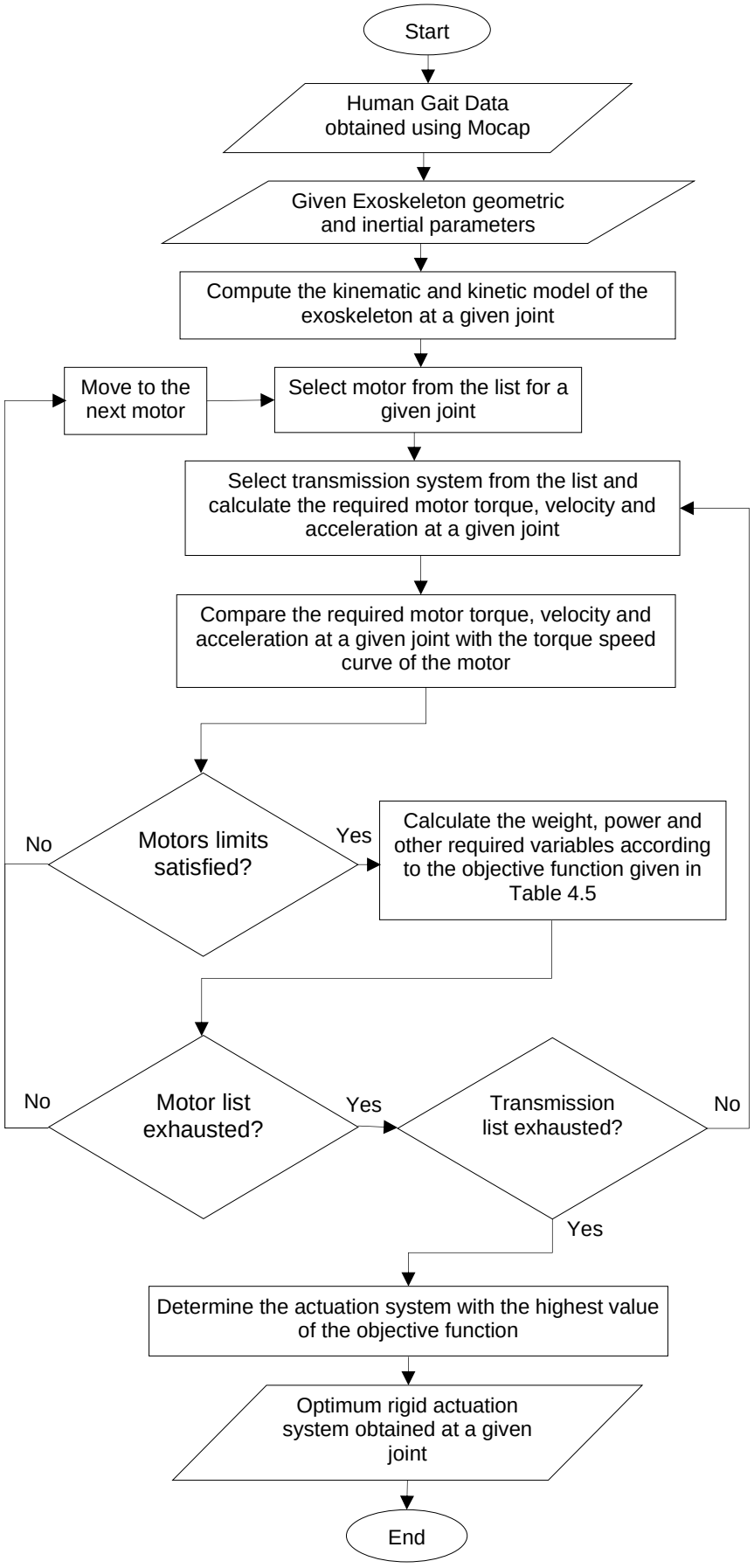

Figure 4.9: Flow chart of the Optimization Algorithm for a Rigid Actuation System at a single joint

Table 4.5: Weightage given to each variable in the objective function to assess different candidate actuators in the optimization algorithm

Variables	Weightage of the variable in the objective function
Power consumption	-0.5
Mass of the exoskeleton	-0.7
User carrying ability	0.3

As mentioned previously, the objective function was calculated taken into account the total power consumption, the total weight and the user carrying capacity of the exoskeleton. Different weightage has been used for each of the variables as shown in Table 4.5. As can be observed in the table, a higher weightage has been given to the variable that corresponds to the total weight of the exoskeleton. The weightages given to each variable were selected after performing the preliminary simulation i.e. during the preliminary analysis, the algorithm was run with fewer motors but it included a large range of power capacities. This identified the suitable power range of motor to be used. Furthermore, the preliminary results were obtained with different weighting factors of the variables. In some cases, the weighting factor was slightly modified to produce an overall more efficient system. The variables desired to be reduced were given a negative weighting factor. Moreover, the total power consumption was evaluated considering the combined power consumption of the three joints. This point will be investigated in detail in Section 4.9.3. As the algorithm initially applied at the knee joint (since knee joint was the middle joint of the lower limb), therefore in order to calculate the total power consumption, the power of the hip and ankle actuators also needs to be determined. To account for this, the optimization algorithm assumed the most lightweight actuators at the hip and ankle joints and calculated the total power consumption by considering the assumed actuators at the hip and ankle joint. Both sit-to-stand (STS) and level ground walking movements were defined in the total power consumption. It has been recorded in [177], that the number of sit to stand movements per day of older healthy adults is 70 movements and the time spend upright is 360 mins. As an STS movement in Rex Bionics takes 6 seconds [93], therefore the ratio of time spent during sit to stand as compared to the level ground walking on daily basis is 7:360 mins. This ratio has been taken into consideration when processing the power consumption of the actuator during sit to stand and level ground walking. Similarly, the total weight of the exoskeleton was estimated using the weight of the knee

actuator and the weight of the assumed actuators at the hip and ankle joints. It should be noted that the weight of the housing, connectors and other parts has also been taken into account. This also included weight of the computer and the power supply of the exoskeleton. The algorithm then adds the weight of the exoskeleton links (the weight of each link is considered as a point mass taken at its centre of gravity) and other parts with the total weight of the actuators (the weight of the actuators is also considered as a point mass to be placed at the required location in the exoskeleton model) to obtain the total weight of the exoskeleton for a given candidate actuator and the dynamic model of the exoskeleton was rebuilt accordingly. The user carrying capacity of 100 kg has been considered in the objective function of the candidate actuators to match the user capacity of Rex Bionics. The weight of the upper part of the user was considered as a point mass and the mass of the lower parts was added to the mass of the respective exoskeleton links at each of their centre of gravity as explained during the dynamic modelling of the exoskeleton. When the objective function of a particular candidate actuator has been calculated, the mass of the upper and lower part of the user was eliminated to obtain only the total weight of the exoskeleton.

The procedure of the optimization algorithm discussed above will be repeated for all the motors and the transmission systems in the list. The objective function will be calculated for each of the candidate actuator at a given joint. When the algorithm finished computing it for all the motors and transmission systems, the candidate actuator with the highest value of the objective function will be the optimized actuator at the knee joint at this stage.

4.8.2 Multi-Joint Algorithm for Lower Limb Assistive Robotic Exoskeleton

The algorithm discussed in the previous section was implemented to a single joint. Multi-joint algorithm discussed in this section will be applied such that all the three joints of the lower limb assistive exoskeleton could be solved. It takes into account the weight, power consumption and the user carrying capacity of the actuators from all joints of the lower limb to solve for the optimum actuator at a given joint. The flowchart of the multi-joint algorithm is illustrated in Figure 4.10.

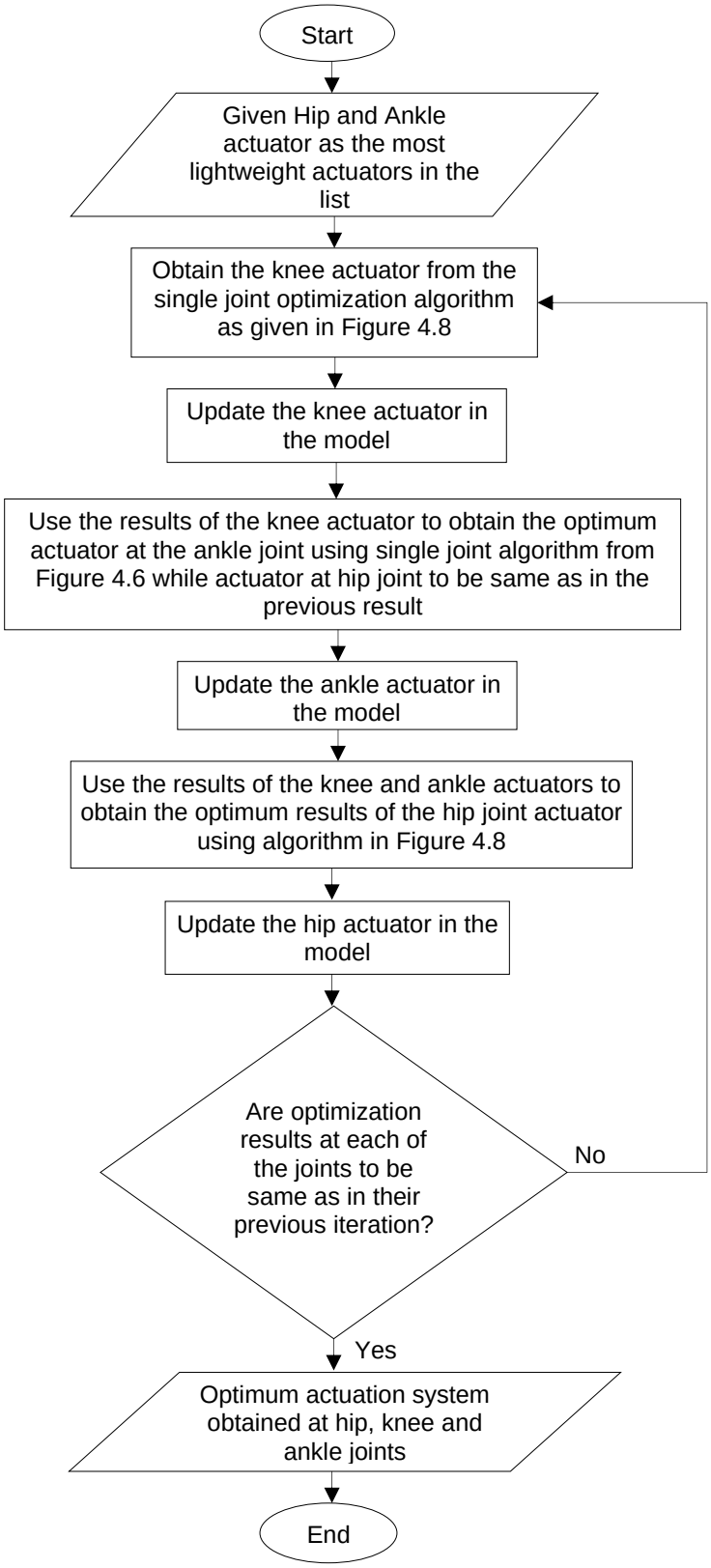

Figure 4.10: Flow chart of the Multi-Joint Algorithm

As mentioned earlier, the single joint algorithm was initially applied at the knee joint by assuming the most lightweight actuators at the hip and ankle joints. The multi-joint algorithm takes into account the results of the knee actuator from the single joint algorithm, updates the dynamic model of the

exoskeleton according to the results of the knee actuator and applies the algorithm at the ankle joint. At this point, hip actuator remains unchanged i.e. the most lightweight actuator assumed from the candidate actuators list. The ankle actuator evaluated during this step will be used in the next stage to solve for the hip actuator. Therefore, the exoskeleton model will be re-structured to replace the knee and ankle actuator estimated from the previous phases to solve for the hip actuator. Finally, the hip actuator obtained will be used in the next stage to solve again for the knee actuator. On this instance, the knee actuator will be solved with the hip and ankle actuators that were assessed during the previous steps by updating the exoskeleton model. The multi-joint algorithm continues to repeat until the actuators stop to change at each iteration at each of the joint of the lower limb of assistive robotic exoskeleton.

4.9 Results and Discussion

In this section, results of the rigid actuation system for lower limb assistive robotic exoskeleton based on the design requirements and optimization algorithm will be discussed. The profiles of the human gait will be visualized followed by the kinematic and kinetic requirements of the exoskeleton. The results of the rigid actuation system will be reported with different transmission systems used in the optimization algorithm.

4.9.1 Exoskeleton Dynamic Manoeuvres and its Validation with SolidWorks

The kinetic model of the exoskeleton was utilized to obtain the torque and power at each of the lower limb joints of the exoskeleton during the required manoeuvres i.e. sit to stand and level ground walking. The torque and power requirement was presented separately for each phase of the task i.e. sit to stand, swing phase and stance phase of the gait cycle. The stance part was only shown during the single support phase as the requirements during the double support phase were not significant [103]. Therefore, to reduce the running time of the optimization algorithm, double support part of the stance phase was not included. The results obtained from the kinetic model of the exoskeleton were validated using the simulation model explained in section 4.5. Similar geometric and inertial parameters and motion inputs of sit to stand and level ground walking were given to the simulation model to obtain the kinetic requirements at the joints of the exoskeleton model.

4.9.1.1 Hip Joint

The trajectories of the kinetic requirements at the hip joint during each phase of the required manoeuvres is shown in Figure 4.11(a)-(f). Results obtained from both the theoretical and simulation models have been illustrated. It has been observed that the torque and power demand of the hip joint was recorded to be high during sit to stand phase as compared to the other phases. The torque and power patterns can also be observed to be similar for the theoretical and simulation model during this phase. The kinetic requirements during swing and stance phase were similar. The power during stance phase of the hip was zero since the angular velocity was very low. This is because of the knee locking mechanism that will be explained in the next section. Similar patterns with some minor deviations were revealed between theoretical and simulation models during the swing and stance phases.

4.9.1.2 Knee Joint

The gait patterns can be observed in Figure 4.12(a)-(f) for the knee joint during the three phases of the tasks. The torque and power requirement were also recorded to be high at the knee joint during sit to stand as compared to the swing and stance phase of the gait cycle.

The gait trajectories of the theoretical and simulation model were also defined to be identical. The kinetic requirements of the knee joint were high during sit to stand but during the swing phase it was recorded to be low when compared with the swing phase of the hip joint. The torque and power requirement at the knee during stance phase was zero as the user was assumed to be moving with straighten knee during the stance phase and hence the knee joint was considered to be locked during this phase. The knee locking was proved to be beneficial in terms of reducing the energy requirements of the system [179].

4.9.1.3 Ankle Joint

The kinetic gait patterns at the ankle joint during sit to stand, swing and stance phase are shown in Figure 4.13 (a)-(f). The torque and power requirements examined by the simulation model have also been illustrated. Similar patterns were observed for both cases. Ankle joint was recorded to be less demanding during the swing phase but a higher requirement during single support stance phase was established at the ankle joint.

The similarity of the kinetic gait patterns during the three phases between the theoretical and simulation model indicates the integrity of the model that

will be used in the optimization algorithm to determine the optimum actuation system in an assistive robotic exoskeleton. Although some differences can be observed in the joint torques and power trajectories between the two models. These variations could be as a result of the slight differences in calculating the moment of inertia of the exoskeleton links between the two models.

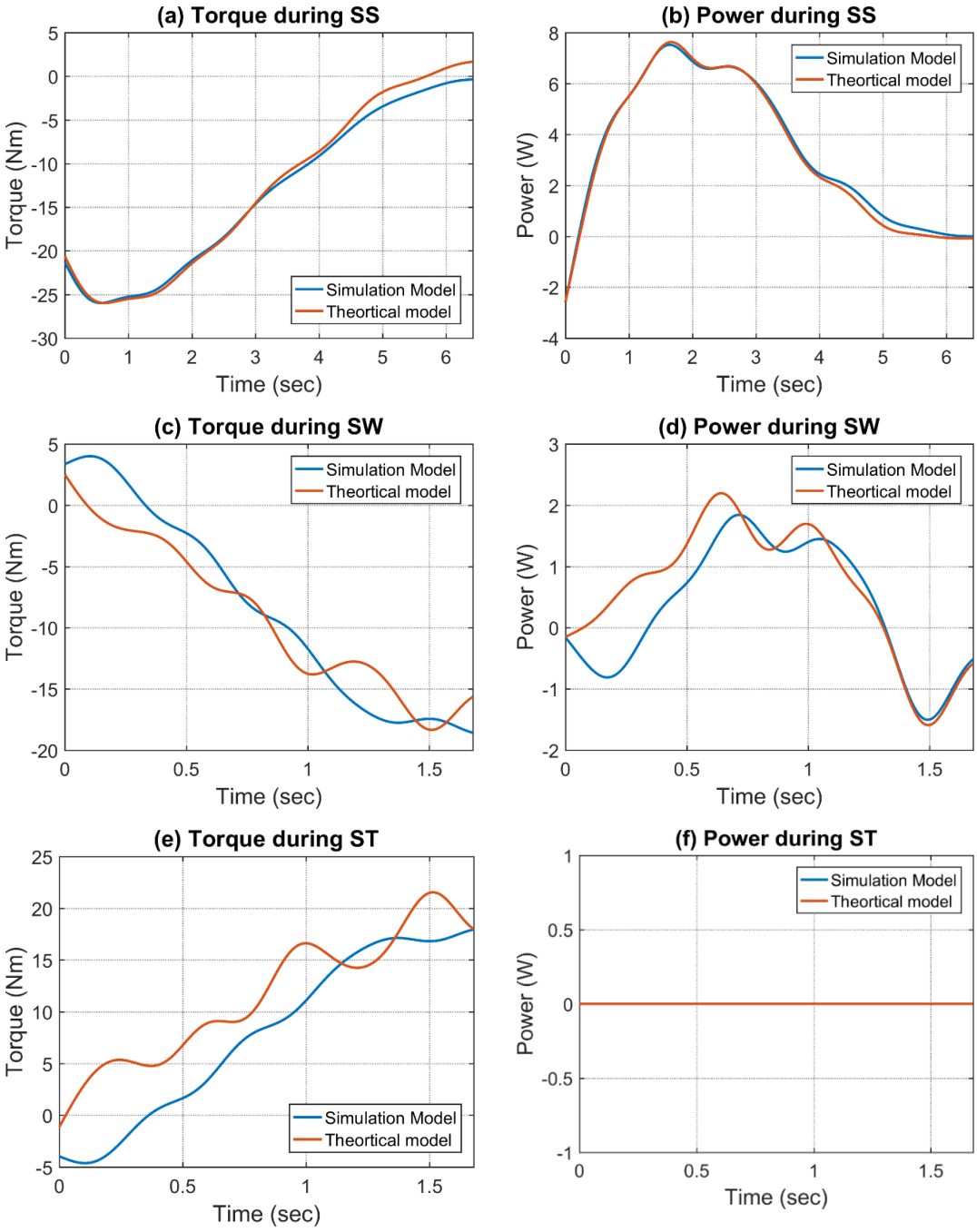

Figure 4.11: Torque and power joint trajectories at the hip during sit to stand (STS), swing (SW) and stance phase (ST) of the theoretical and simulation model. Figures (a), (c) and (e) show the torque trajectory of the joint and Figures (b), (d) and (f) represent power trajectories of the joint during the three manoeuvres.

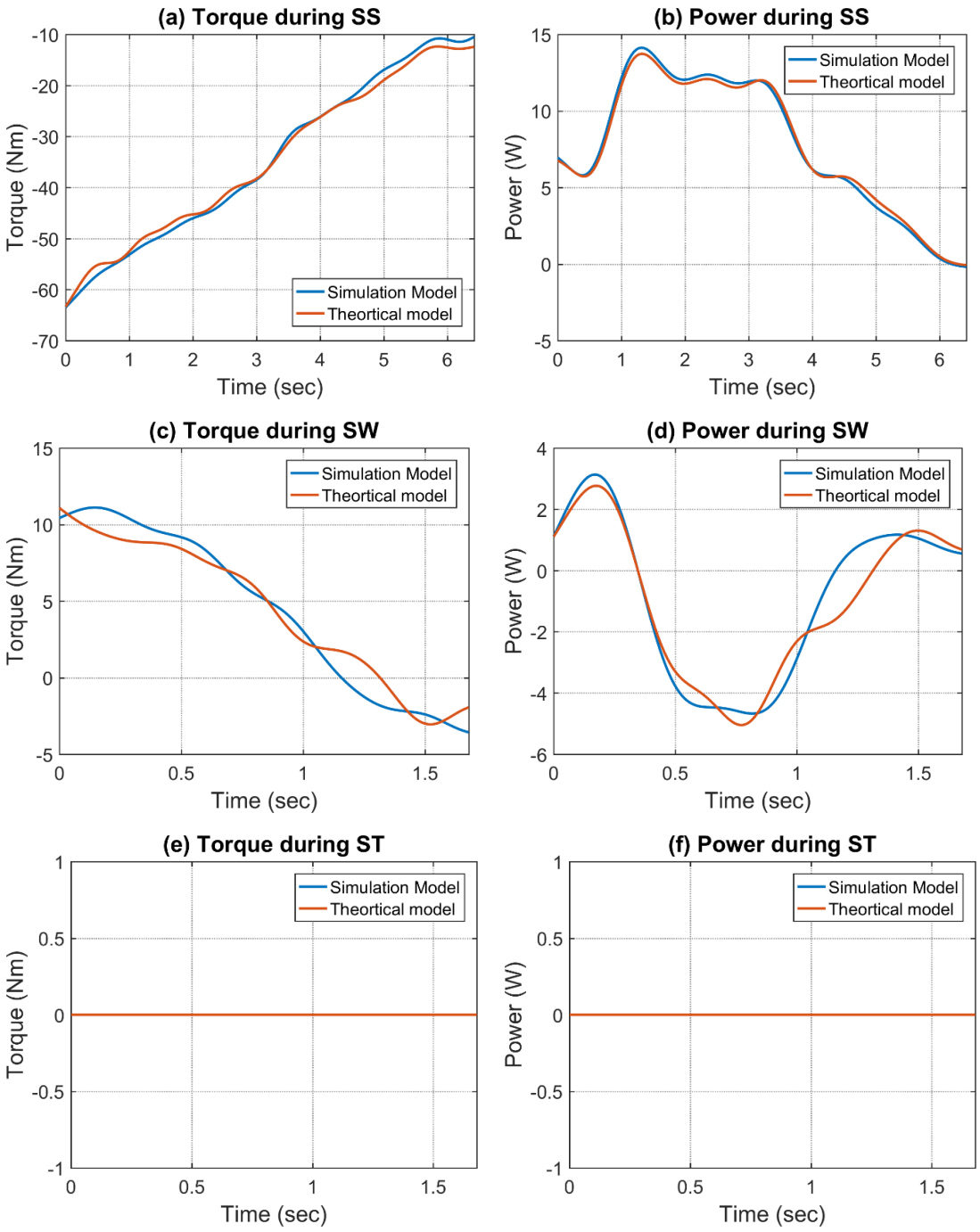

Figure 4.12: Torque and power joint trajectories at the knee during sit to stand (STS), swing (SW) and stance phase (ST) of the theoretical and simulation model. Figures (a), (c) and (e) show the torque trajectory of the joint and Figures (b), (d) and (f) represent power trajectories of the joint during the three manoeuvres.

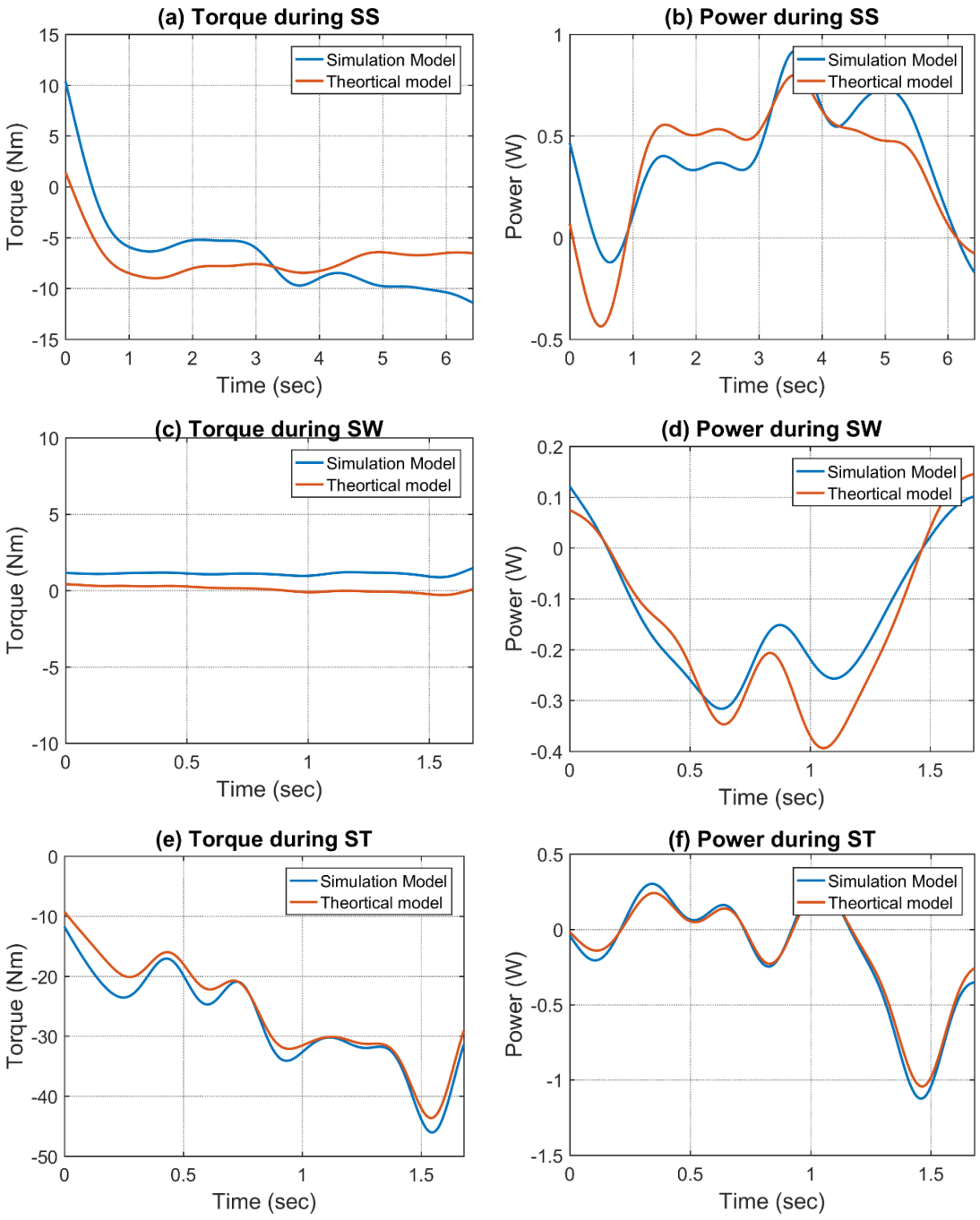

Figure 4.13: Torque and power joint trajectories at the ankle during sit to stand (STS), swing (SW) and stance phase (ST) of the theoretical and simulation model. Figures (a), (c) and (e) show the torque trajectory of the joint and Figures (b), (d) and (f) represent power trajectories of the joint during the three manoeuvres.

4.9.2 Power Consumption by the Assistive Exoskeleton Actuation System

In order to obtain the optimum rigid actuation system, one of the parameters that was considered in the optimization algorithm was the power consumption of the actuation system. Figure 4.14 to Figure 4.16 complied

the absolute and relative total power consumption for a few combinations of the actuators at hip, knee and ankle joint of the exoskeleton and each figure represents the results for a specific type of the transmission system. These results were recorded from the optimization algorithm that determines the optimum actuation system and will be explained later. The total power consumption refers to the sum of the power consumption of the hip, knee and ankle actuator of the assistive robotic exoskeleton.

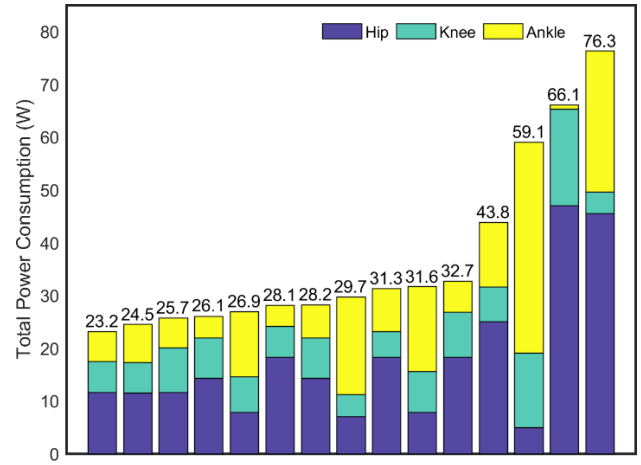

(a)

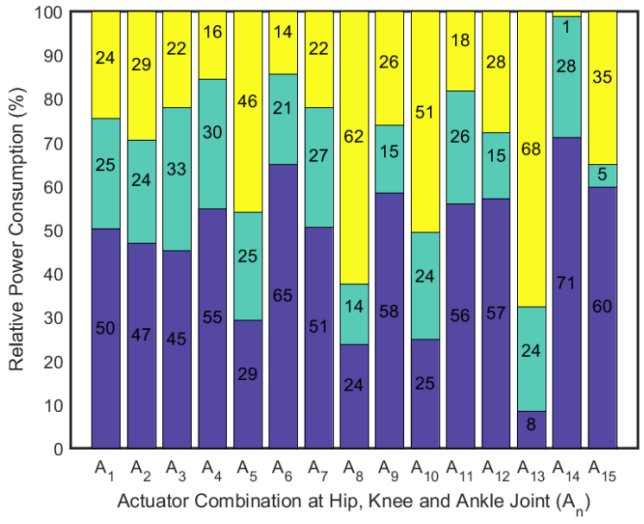

(b)

Figure 4.14: (a) Absolute and (b) Relative average total power consumption of the actuators compared with the individual power consumption of each of the lower limb actuators. The results are shown for the system using harmonic drives as the transmission mechanism. Note that for some systems, the relative power does not add up to 100 % since the values were rounded to nearest integers.

Figure 4.14 illustrates the results of the average total power consumption by the joint actuators when harmonic drives were used as the transmission system. By a careful consideration of Figure 4.14, the average total power consumption was recorded to be high if the actuators were selected based on minimizing the individual power consumption of the joint actuator e.g. in the actuator combination A_{14}, hip actuator was selected with the smallest power consumption, however, the power consumption of the knee and ankle actuator from that particular combination was quite high and therefore, the total power consumption was recorded to be high for this particular combination of actuators at hip, knee and ankle joint. On the other hand, the actuator combination A_1, will have the minimum amount of total power consumption even though the power consumption of the hip actuator was higher as compared to the power consumption of the hip actuator of A_{14}. Therefore, it can be said that the power consumption of the individual actuator at a joint should not be considered but the total power consumption that includes the average power consumption of all the actuators of the lower limb should be the parameter to be taken into account. This also applies to the weight of the exoskeleton since the point of focus is to minimize the total weight of the exoskeleton. Therefore, the total weight of all three actuators should be considered when calculating the weight factor in the objective function.

Similarly, by observing Figure 4.15 that represents the power consumption of the actuators when harmonic drives were used in combination with belt and pulley drive as the transmission system and Figure 4.16 that represents the actuators with the ball screws as the transmission system, it also indicates that the total power consumption should be the selection parameter in the objective function of the optimization algorithm and not the power consumption of the individual joints.

The smallest power consumption by the individual joints along with the total power consumption is shown by the right three bars (A13 to A15) in Figure 4.14 to Figure 4.16 with (a) shows the absolute values of the power consumption & (b) indicates the relative power consumption. Actuator combination A13 represents the total power consumption when the hip actuator was selected with the minimum power consuming actuator. Similarly, actuator combination A14 and A15 indicates the total power consumption when knee and ankle actuators respectively were selected as the ones that consumes less power. As it can be seen that the total power consumption for these cases is very high. On the other hand, the actuator

combination A1 in the figures represents the actuators with the lowest value of the total power consumption. The results using belt and pulleys as the only form of the transmission system were not shown as the power consumption were recorded to be very high. However, those actuators also showed a similar trend.

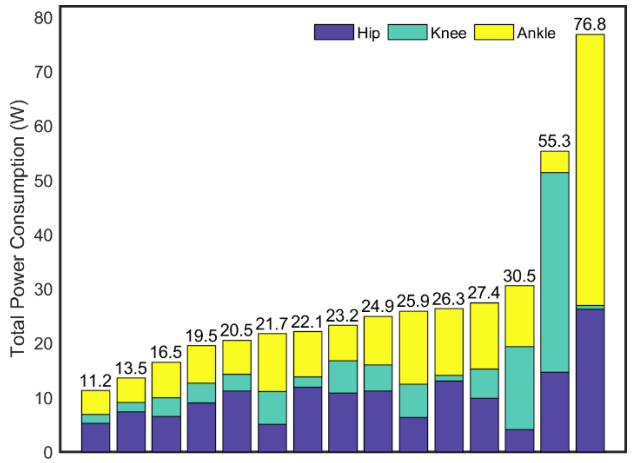

(a)

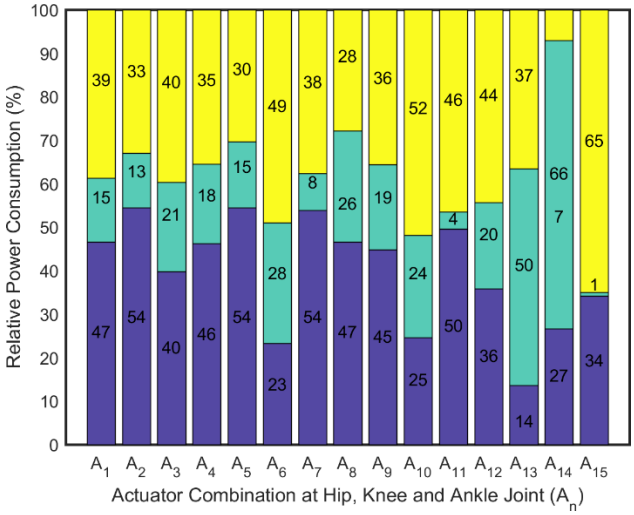

(b)

Figure 4.15: (a) Absolute and (b) Relative average total power consumption of the actuators compared with the individual power consumption of each of the lower limb actuators. The results are shown for the system using harmonic drives in combination with a belt and pulley drive system as the transmission mechanism. Note that for some systems, the relative power does not add up to 100 % since the values were rounded to nearest integers.

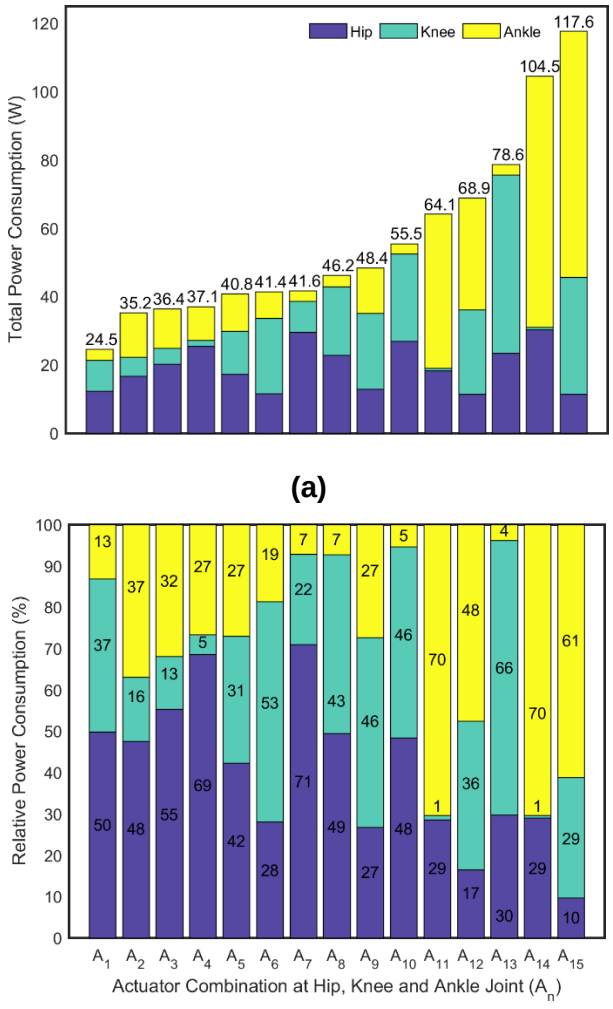

Figure 4.16: (a) Absolute and (b) Relative average total power consumption of the actuators compared with the individual power consumption of each of the lower limb actuators. The results are shown for the system using ball screws as the transmission mechanism. Note that for some systems, the relative power does not add up to 100 % since the values were rounded to nearest integers.

4.9.3 Optimal Rigid Actuation System

The optimization algorithm described in Section 4.8 was applied to determine the optimal rigid actuation system for assistive robotic exoskeleton. The results were separately analysed for each type of the transmission system. However, the results are presented such that two of the lower limb joints have the same transmission system. The optimized actuation system evaluated for each type of the transmission system employed are shown in Tables 4.6 to 4.12. The results have been compiled at each joint of the lower limb and for each iteration of the optimization

algorithm. The single joint algorithm was initially applied at the knee joint and then multi-joint algorithm was applied to perform the actuator optimization at the other joints. The three variables that determine the optimum actuation system for assistive exoskeletons are also shown in the table of results.

Table 4.6 elaborates the outcomes of the optimization algorithm when motors were used in conjunction with the harmonic drives as the transmission mechanism. When single joint algorithm was applied, the optimum actuator at the knee joint was obtained as shown and the hip and ankle actuators illustrated at this stage were the assumed actuators that were the most lightweight actuators in the candidates actuators list. The values of the variables used in the objective function i.e. total power consumption explained in the previous section, total weight of the exoskeleton calculated according to Section 4.4 and the user carrying capacity mentioned in Section 4.2 are also shown.

Table 4.6: Results of the optimal rigid actuation system shown for each iteration of the optimization algorithm when harmonic drives were used as a type of the transmission system at each of the lower limb joint actuators.

Joint Optimization	Candidate Actuator			P_C (W)	W_{exo} (kg)	U_C (kg)	O_f
	Hip	Knee	Ankle				
Knee joint	Maxon ECX16M with CSD-14-50-2A	Allied motion MF60020 with CPL-20-160-2A	Maxon ECX16M with CSD-14-50-2A	11.6	25.8	100	N/A
Ankle joint	ECX16M with CSD-14-50-2A	Allied motion MF60020 with CPL-20-160-2A	Allied motion MF76008 with CPL-25-160-2A	18.3	25.5	100	N/A
Hip joint	Allied motion MF76008 with CSD-20-160-2A	Allied motion MF60020 with CPL-20-160-2A	Allied motion MF76008 with CPL-25-160-2A	25.9	25.6	100	0.47
Knee joint	Allied motion MF76008 with CSD-20-160-2A	Allied motion MF60020 with CPL-20-160-2A	Allied motion MF76008 with CPL-25-160-2A	25.9	25.6	100	0.47
Ankle joint	Allied motion MF76008 with CSD-20-160-2A	Allied motion MF60020 with CPL-20-160-2A	Allied motion MF76008 with CPL-25-160-2A	25.9	25.6	100	0.47

* P_C=Average Total Power consumption, W_{exo}=Total Weight of the exoskeleton and U_C= User's carrying capacity with 50% support and O_f=Objective function

The results of the knee actuators were updated in the optimization algorithm and was then applied to the ankle joint. Finally the optimized actuator at the hip joint was obtained with the values of the variables of interests shown. As mentioned in Section 4.8.2, the algorithm was applied again at the knee and

ankle joint until the last three iterations did not change. The last three rows in Table 4.6 describes the optimum rigid actuation system at the hip, knee and ankle joint when harmonic drives were utilized as the transmission system.

Before applying optimization algorithm on the system where belts and pulley drives were combined with the harmonic drives to be applied as the transmission system, results were illustrated in Table 4.7 where only belt and pulley drive mechanism were used as the transmission system. The results, however, were not favourable as the system was unable to carry a user of 100kg. Even with the reduced user carrying capacity of the system, the actuators obtained were heavy and consumed a large amount of power. Therefore, it was not feasible to use belts and pulley drives exclusively as the transmission system. However, when they were combined with the harmonic drives, favourable results were obtained as shown in Table 4.8. Any last three rows could describe the optimum results obtained at hip, knee and ankle joints.

Table 4.7: Results of the optimal rigid actuation system shown for each iteration of the optimization algorithm when only belt and pulley drive mechanism were used as a type of the transmission system at each of the lower limb joint actuators.

Joint Optimization	Candidate Actuator			P_C (W)	W_{exo} (kg)	U_C (kg)	O_f
	Hip	Knee	Ankle				
Knee joint	Maxon ECX16M with a ratio 1:0.4	Parker Hannifin K1781008Y with a ratio 1:2.6	Maxon ECX16M with a ratio 1:0.4	48.8	36.2	5.2	N/A
Ankle joint	ECX16M with a ratio 1:0.4	Parker Hannifin K1781008Y with a ratio 1:2.6	Parker Hannifin K1781008Y with a ratio 1:2.6	710	45.9	6.1	N/A
Hip joint	Parker Hannifin K1781008Y with a ratio 1:2.6	Parker Hannifin K1781008Y with a ratio 1:2.6	Parker Hannifin K1781008Y with a ratio 1:2.6	1252	56.5	11.5	0.01
Knee joint	Parker Hannifin K1781008Y with a ratio 1:2.6	Parker Hannifin K1781008Y with a ratio 1:2.6	Parker Hannifin K1781008Y with a ratio 1:2.6	1252	56.5	11.5	0.01
Ankle joint	Parker Hannifin K1781008Y with a ratio 1:2.6	Parker Hannifin K1781008Y with a ratio 1:2.6	Parker Hannifin K1781008Y with a ratio 1:2.6	1252	56.5	11.5	0.01

* P_C=Average Total Power consumption, W_{exo}=Total Weight of the exoskeleton and U_C= User's carrying capacity with 50% support and O_f=Objective function

Table 4.8: Results of the optimal rigid actuation system shown for each iteration of the optimization algorithm when harmonic drives combined with a belt and pulley drive mechanism were used as a type of the transmission system at each of the lower limb joint actuators.

Joint Optimization	Candidate Actuator			P_C (W)	W_{exo} (kg)	U_C (kg)	O_f
	Hip	Knee	Ankle				
Knee joint	Maxon ECX16M with CSD-14-50-2A and a transmission ratio of 1:0.4	Maxon EC45 with CPL-20-160-2A and a transmission ratio of 1:400	Maxon ECX16M with CSD-14-50-2A and a transmission ratio of 1:0.4	7.9	25.7	100	N/A
Ankle joint	ECX16M with CSD-14-50-2A and a transmission ratio of 1:0.4	Maxon EC45 with CPL-20-160-2A and a transmission ratio of 1:400	Maxon EC45 with CSD-14-50-2A and a transmission ratio of 1:400	17.3	24.9	100	N/A
Hip joint	Maxon EC45 MF76008 with CSD-20-160-2A and a transmission ratio of 1:400	Maxon EC45 with CPL-20-160-2A and a transmission ratio of 1:400	Maxon EC45 with CSD-14-50-2A and a transmission ratio of 1:400	26.3	24.8	100	0.49
Knee joint	Maxon EC45 MF76008 with CSD-20-160-2A and a transmission ratio of 1:400	Maxon EC45 with CPL-20-160-2A and a transmission ratio of 1:400	Maxon EC45 with CSD-14-50-2A and a transmission ratio of 1:400	26.3	24.8	100	0.49
Ankle joint	Maxon EC45 MF76008 with CSD-20-160-2A and a transmission ratio of 1:400	Maxon EC45 with CPL-20-160-2A and a transmission ratio of 1:400	Maxon EC45 with CSD-14-50-2A and a transmission ratio of 1:400	26.3	24.8	100	0.49

* P_C=Average Total Power consumption, W_{exo}=Total Weight of the exoskeleton and U_C= User's carrying capacity with 50% support and O_f=Objective function

Table 4.9 represents the results with the ball screws as the transmission mechanism. Different configurations of the ball screws are illustrated in Table C.2 to C.4 in Appendix C. During the second iteration for each of the joint, optimum results were established. A slight increase in the power consumption of the actuators with these types of transmission system was observed.

In Table 4.6-4.9, results were elaborated using similar types of the transmission systems at all joints of the lower limb. It was observed that the motors from the same manufacturers were obtained at each of the lower limb joints for each combination of the transmission system. Based on the particular type of the transmission mechanism, the torque and power of the

joint varies and the motor best suited at one particular joint basically suited at all of the three lower limb joints with only a slight model variation by the multi-joint algorithm. It also appeared that the weight and power consumption increased with each iteration. This is because initially the most light weight and efficient actuators were assumed at the hip and ankle joint when assessing the actuators at the knee joint. Later on, the actuators at the hip and ankle were assessed and the total weight and power consumption were changed accordingly.

Table 4.9: Results of the optimal rigid actuation system shown for each iteration of the optimization algorithm when ball screws were used as a type of the transmission system at each of the lower limb joint actuators.

Joint Optimization	Candidate Actuator			P_C (W)	W_{exo} (kg)	U_C (kg)	O_f
	Hip	Knee	Ankle				
Knee joint	Maxon ECX16M with ball screw configuration no. 1	Allied motion MF76008 with ball screw configuration no. 190	Maxon ECX16M with ball screw configuration no. 1	25.9	24.1	100	N/A
Ankle joint	ECX16M with ball screw configuration no. 1	Allied motion MF76008 with ball screw configuration no. 190	Allied motion MF60020 with ball screw configuration no. 11	35.2	24.5	100	N/A
Hip joint	Allied motion MF95008 with ball screw configuration no. 42	Allied motion MF76008 with ball screw configuration no. 190	Allied motion MF60020 with ball screw configuration no. 11	56.5	25.5	100	0.32
Knee joint	Allied motion MF95008 with ball screw configuration no. 42	Allied motion MF76008 with ball screw configuration no. 190	Allied motion MF60020 with ball screw configuration no. 11	56.5	25.5	100	0.32
Ankle joint	Allied motion MF95008 with ball screw configuration no. 42	Allied motion MF76008 with ball screw configuration no. 190	Allied motion MF60020 with ball screw configuration no. 11	56.5	25.5	100	0.32

* P_C=Average Total Power consumption, W_{exo}=Total Weight of the exoskeleton and U_C= User's carrying capacity with 50% support and O_f=Objective function

After evaluating the results using similar types of the transmission systems at all joints of the lower limb, results were achieved by using different types of the transmission systems at the joints e.g. harmonic drives were used at the hip joint whereas ball screws were employed at the knee and ankle joints

etc. The results of the optimization algorithm when different types of the transmission systems were applied at the hip, knee and ankle joint are shown in Appendix E in Tables E.1 to E.3.

At the first stage, harmonic drives and ball screws were applied at the joints. Table E.1 illustrates the results for this particular combination of the transmission system. These results are not shown for each iteration but only the final actuation systems at each of the joints are illustrated. The results are interpreted for each possible combination of the two transmission systems at hip, knee and ankle joints. Table E.2 depicts the results of the rigid actuation system when the transmission systems employed were ball screws and the harmonic drives were used in combination with the belts and pulley drive system. The results evaluated are the final actuation systems from the optimization algorithm for each possible combination at the lower limb joints of the assistive exoskeleton. Finally, Table E.3 illustrates the results with either the ball screws as the transmission mechanism or belt and pulley drive only as the form of the transmission system. The comparison of the power consumption and the weight of the actuators obtained using different combinations of the transmission systems are explained the next section.

4.9.4 Weight and Power Analysis of the Assistive Robotic Exoskeleton with Different Transmission Systems used in the Optimization Algorithm

Figure 4.17 to 4.19 represents the total weight and average power consumption of the exoskeleton actuation system assessed using the optimization algorithm. These results were compared with the weight and power consumption of the Rex bionics, details of which were mentioned previously. Figure 4.17 shows the weight and power consumption of the exoskeleton using different combinations of the actuators, illustrated for the case when either the harmonic drive or ball screws were used as the transmission system at each of the joints of the lower limb of the exoskeleton. It is evident from Figure 4.17 that the weight and power consumption of the exoskeleton was significantly reduced as compared to the Rex Bionics for all combinations of the transmission systems. The most lightweight actuation system was realized when harmonic drives were applied at the hip and knee joint and ball screws were employed at the ankle joint. On the other hand, the lowest power of the system was recorded when harmonic drives were utilized at each of the joints of the lower limb. It should be noted that the scaled value of power consumption of Rex Bionics was

used in Figure 4.17 - 4.19 but the weight of the Rex Bionics used for comparison purpose was 38 kg since an extra weight was added to the exoskeleton in the optimization algorithm so that the initial weight of the exoskeleton before optimization was equal to total weight of Rex Bionics.

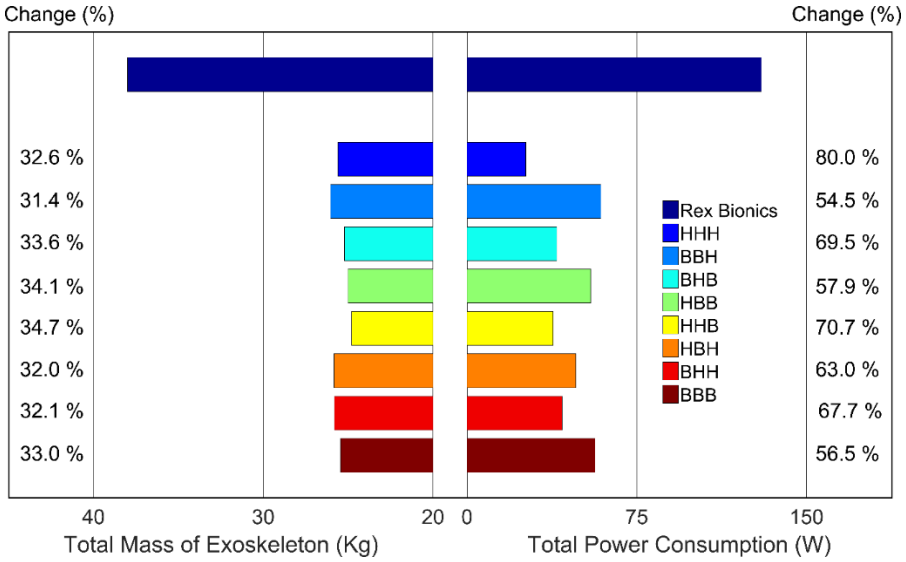

Figure 4.17: The total mass and average power of the exoskeleton for each different combinations of the transmission systems used in the joint actuators compared with the mass and power of the Rex Bionics. The transmission system used were either the harmonic drives (H) or the ball screws (B) represented in the actuator symbols as first, second and third letter that corresponds the mechanism at the hip, knee and ankle joint respectively.

Figure 4.18 illustrates the power and weight comparison when either the ball screws in an inverted slider mechanism was used or harmonic drives in combination with the belt and pulley drive system were employed. There was a further reduction that was recorded as compared to the previous transmission system combinations. The smallest power consumption and the light weight system were evaluated when the harmonic drive combined with belt and pulley drive were operated at the hip and knee joint and ball screw in an inverted slider mechanism at the ankle joint.

A third type of combination was applied when either only belt and pulley drive system or ball screws in an inverted slider mechanism were used and the results are depicted in Figure 4.19. The outcomes by using belt and pulley drives only did not bring any favourable results for any possible combination of the transmission system at the joints of the lower limbs. Therefore, the use of the belt and pulley drive system alone is not beneficial in terms of the weight and power consumption of the exoskeleton.

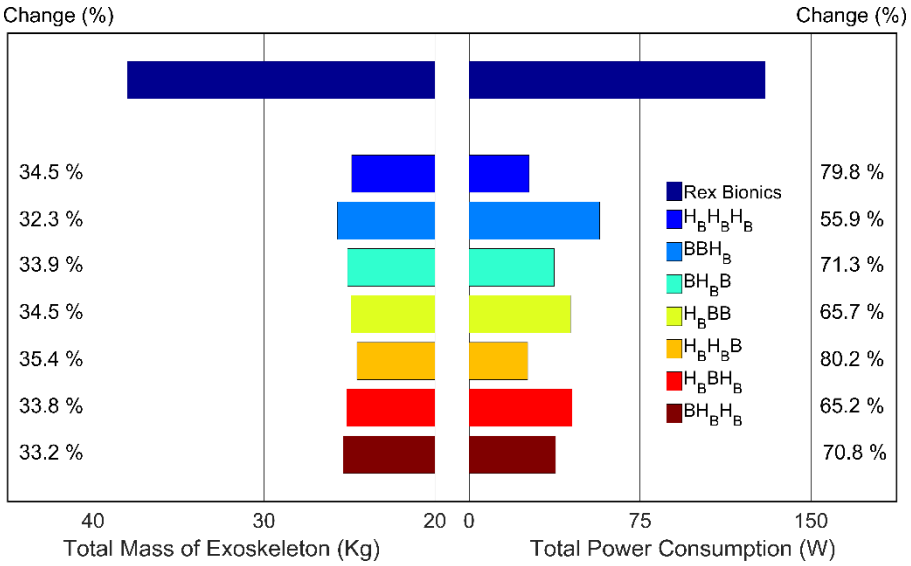

Figure 4.18: The total mass and average power of the exoskeleton for each different combinations of the transmission systems used in the joint actuators compared with the mass and power of the Rex Bionics. The transmission system used were either the harmonic drives combined with a belt and pulley drive H_B or the ball screws in an inverted slider crank mechanism B, represented in the actuator symbols as first, second and third letter that corresponds the mechanism at the hip, knee and ankle joint respectively.

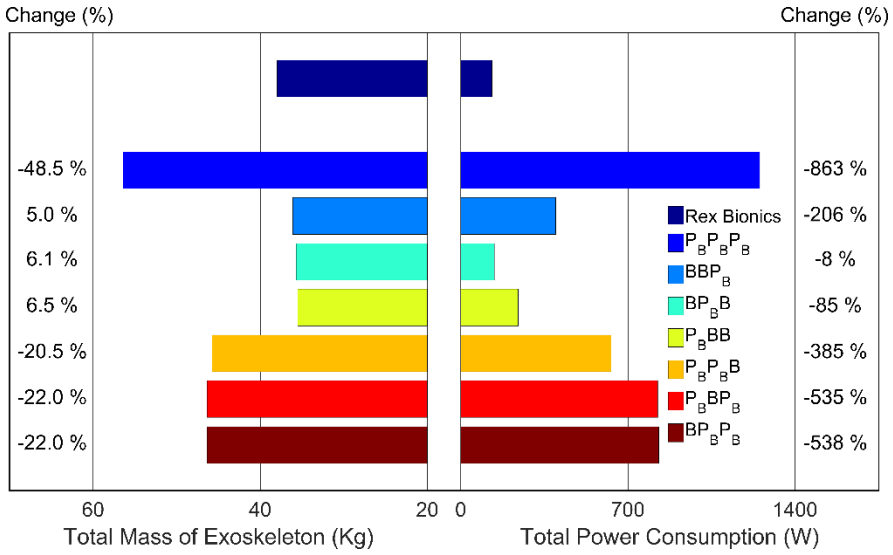

Figure 4.19: The total mass and average power of the exoskeleton for each different combinations of the transmission systems used in the joint actuators compared with the mass and power of the Rex Bionics. The transmission system used were either the belt and pulley drive P_B or the ball screws in a slider crank mechanism B, represented in the actuator symbols as first, second and third letter that corresponds the mechanism at the hip, knee and ankle joint respectively.

By a careful consideration of Figures 4.17 to 4.19, the maximum reduction in the total weight and power consumption of the exoskeleton were evident with the use of harmonic drives combined with belt and pulley drive at the hip and knee joint and ball screw at the ankle joint. The reduction was 35 % and 80 % in terms of total weight and power consumption of the exoskeleton respectively as compared to the weight and power consumption of Rex Bionics. Therefore, the actuator (Maxon EC45 with harmonic drive CPL-20-160-2A as the transmission mechanism combined with a belt and pulley drive in a combined ratio of 1:400) at the hip joint, (Allied motion MF60020 with a ball screw mechanism in a configuration no. 11 given in Appendix C) at the knee joint and (Maxon EC45 with harmonic drive CPL-20-160-2A as the transmission mechanism combined with a belt and pulley drive in a ratio of 1:400) at the ankle joints is described as the optimum actuation system for a rigid system in an assistive robotic exoskeleton.

4.10 Summary

In this chapter, an optimal rigid actuation system of an assistive robotic exoskeleton was presented. By using the optimization framework reported for an assistive exoskeleton actuation system, a power efficient and a lightweight system was obtained. The design requirements and constraints for an assistive exoskeleton were stated in Section 4.2 that includes the number of actuated DOFs, the weight and power required and the kinematic and kinetic requirements of the system. The kinematic and kinetic requirements were obtained by the healthy human trails performing the required manoeuvres. The dynamic and simulation modelling of the exoskeleton was performed and reported in Section 4.4 and 4.5, the results of these modelling were the joint torque, speed and acceleration. The motor torque, velocity and acceleration were assessed through modelling of motors and transmission systems in Section 4.7.

The optimization framework that was developed for assistive exoskeletons was described in Section 4.8 that uses the exhaustive list of motors and transmission systems along with the kinematic and kinetic model of the exoskeleton to evaluate the optimized actuation system. The results of the exoskeleton dynamic manoeuvres and the optimization algorithm were reported in Sections 4.9.2 and 4.9.4. It was established that the sit to stand operation was the most energy demanding phase for the actuation system. By using the optimization algorithm, an actuation system with much less power consumption and light weight system was analysed. Using elastic

elements could also be beneficial in reducing the energy requirements as they can store energy during less demanding phases and could be utilized during high demanding phases. The results were assessed with the parameters of the Rex Bionics. A comparison of the weight and power efficiency of the actuation system for different transmission systems were recorded in Section 4.9.5. It was described that the weight and power consumption of the system was reduced with the use of harmonic drives combined with the belt and pulley drive system as the transmission mechanism at the hip and knee joint and ball screws as the transmission system at the ankle joint.

Chapter 5
Optimization of Series and Parallel Elastic Actuation System

5.1 Introduction

In this chapter, an optimal design of an elastic actuation system equipped with series and parallel springs has been evaluated for an assistive robotic exoskeleton. Weight and power are the main considerations in a robotic exoskeleton that need to be reduced. The use of series and parallel elastic elements can help to reduce these requirements in exoskeletons robots. Choosing the best actuator design for an elastic actuation system is not a trivial task. This also applies to the selection of the strategies to optimize the elastic elements in an elastic actuation system. The work assessed in the previous chapter consisted of an optimization of a rigid actuation system. In this chapter, the optimum design for the elastic actuators for assistive exoskeletons will be established. An elastic actuator can allow deviations from its own equilibrium position depending upon the external forces applied on it. The effect of the elastic elements on the kinetic requirements of the system needs to be further exploited in order to make the overall design more compact, lightweight and power efficient. This work demonstrated the optimized strategy to determine the spring stiffness of a series and a parallel elastic actuators and then further evaluate the optimum elastic actuation systems for an assistive robotic exoskeleton.

Several studies that use the concept of series and parallel elastic elements in robotic orthosis have been recorded [61, 180-185]. However, fewer applications of parallel elastic actuators (PEA) were revealed as compared to series elastic actuators (SEA). The elastic elements can have a significant effect on the kinetic requirements of the lower limb joints. It has been noticed in [186] that adding a parallel spring can reduce the peak torque and power at the hip and ankle joint. On the other hand, a series spring is able to reduce the power and energy consumption at the ankle joint [186, 187]. The reduction in the power consumption of HAL by using passive mechanisms was discussed by [188]. In order to achieve the optimum results, the stiffness of the spring needs to be adjusted for a particular parameter of interest [189, 190]. The spring parameter optimization to reduce power and energy requirements has been investigated by several studies and reported some of the spring optimization criteria [187, 189-193]. The optimal stiffness

of the spring based on peak power and energy consumption was studied by [194]. It was found in [187] that the spring stiffness should be adjusted for the case of SEA with respect to the minimum energy at the hip and knee joint and minimum peak power at the ankle joint. However, the approach used in [187, 194] was based on powered prosthetic devices. It has been noticed in the previous studies that the sit to stand maneuver is the most power consuming phase among the activities of daily tasks [195]. The stiffness of the spring needs to be optimized taking into account both sit to stand and normal walking operation. It has been recorded in the findings described above that a spring can reduce the high torque and power demand on the motor. There is a need to develop an approach to optimize the stiffness of the spring for assistive exoskeleton applications. The effect of an optimum spring stiffness on the torque and power requirements of the system needs to explored.

This part of the research presented an optimization technique to determine the optimal elastic actuation system using series and parallel springs. The optimum elastic actuation system will be evaluated by choosing the ideal combination of motors and transmission systems and by applying the optimum spring stiffness. This approach will be designed for SEA and PEA. It should be noted that only fixed spring stiffness will be considered in this design. Choosing an optimization approach for the motor and transmission systems needs a careful consideration among different design parameters. There has to be an acceptable level of compromise that should be made in one variable to achieve better results for another variable. Therefore, a need for an optimum approach to design the elastic actuation systems of assistive robotic exoskeletons is essential.

The kinematic and kinetic requirements of an elastic actuation system will be discussed in Section 5.2.1. This will be followed by explaining the selection of the components used in the optimization framework of elastic actuators. The modelling of series and parallel elastic actuators will be presented in Section 5.2.4. After the models of elastic actuators were presented, the optimization strategies will be specified for series and parallel springs in Section 5.2.5. A simulation model of an assistive exoskeleton was utilized to determine the kinetic requirements of the elastic actuators presented in Section 5.2.6. The optimization framework will be demonstrated in Section 5.2.7. The results using different spring optimization techniques are reported in Section 5.3. Kinetic results of the lower limb exoskeleton joints using

elastic actuators are assessed. Furthermore, the optimal elastic actuation systems will be established.

5.2 Methodology

5.2.1 Kinematic and Kinetic Requirements of the System

The kinematic and kinetic requirements of the system were explained in detail in Section 4.2 and 4.3 of Chapter 4. These requirements will have to be fulfilled using an elastic actuation system in this work for an assistive exoskeleton.

5.2.2 Components of an Elastic Actuation System

The components used in the optimization algorithm for the elastic actuation system will be explained in this section. As previously mentioned in Chapter 4, a market search of motors and transmission systems were carried out and a spreadsheet was obtained that included motors and transmission systems from different manufacturers. The list was incorporated with motors of different power ranges. A preliminary analysis was conducted for the motors and transmission systems in order to be used in an elastic actuation system. As the requirements of an elastic actuation system were different (less) from a rigid system, therefore only those motors and transmission systems were included that falls under the threshold of the torque and power requirements of elastic system while others were eliminated as they were too bulky or not suitable to be used in the elastic actuation system. The kinetic requirements for an elastic actuation system will be reduced through spring stiffness optimization and therefore, some of the motors were further discarded to refine the components list. Full details regarding the selection of motors and transmission systems can be found in Section 4.6.

A torsional spring connected in series or in parallel with the motor and the transmission system was used in the elastic actuators optimization algorithm. A spring can store energy during the operation when it is not needed and can release the accumulated energy when required. Therefore, the springs can reduce the amount of strength required by the actuator. Furthermore, they can also be used in a sets of two or more springs arranged concentrically for high load requirements. An optimized value of the spring stiffness is calculated for each of the joint prior to its use in the optimization algorithm. The spring is also considered to be made of a single material throughout with a fixed stiffness. Thus, the physical compliance of the spring cannot be changed during its operation.

5.2.3 Modelling of Electric Motor and Transmission Systems

The modelling of the electric motor and the transmission systems that were used in the optimization algorithm for elastic actuators were explained in Section 4.7. Since the motors and transmission systems used in the elastic actuators were similar to the rigid actuators, therefore the modelling of these systems will not be discussed here. However, as these systems will be used together with the elastic elements therefore, some modifications in the design will be required. Figure 5.1 shows the basic concept of the ball screw when combined with the series spring.

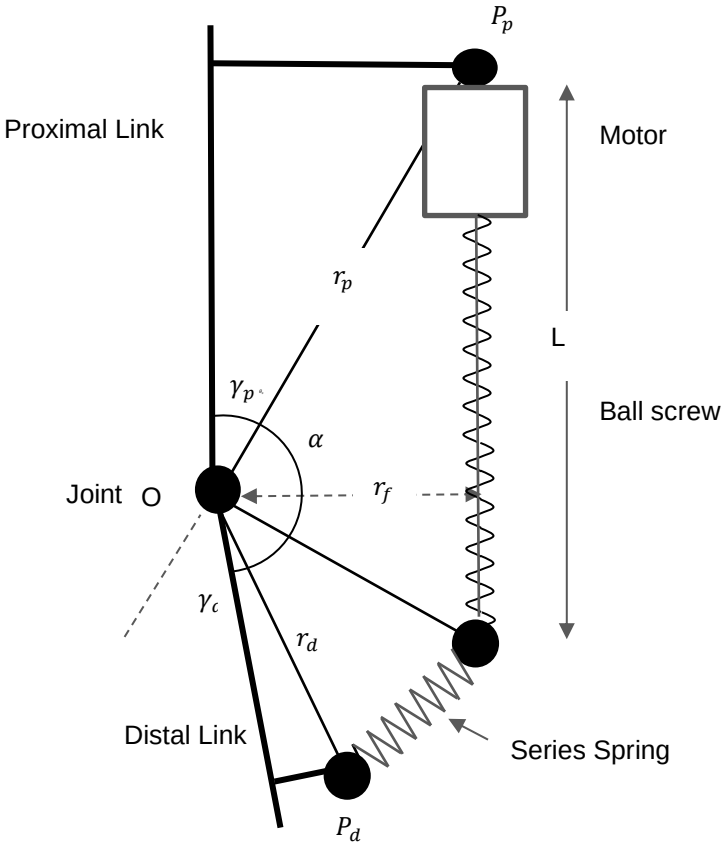

Figure 5.1: Schematic of the Ball screw slider crank mechanism with a series spring

As mentioned previously, this type of configuration of the ball screw can only be used with a hollow structure of the motor. The system shows a linear helical spring that was used with ball screws in the optimization algorithm. The kinetic model of the motors and transmission systems were used along with the model of series or parallel springs as explained in the next section.

5.2.4 Model of SEA

In this section, the power requirements regarding the use of series elastic actuators will be presented. The basic advantage of adding a series spring is to reduce the amount of power required by storing the energy and reusing it during power demanding moments. Although, SEA can reduce the power demand of the motor but it does not reduce the torque requirement of the motor [196]. Figure 5.2 represents the schematic of the SEA.

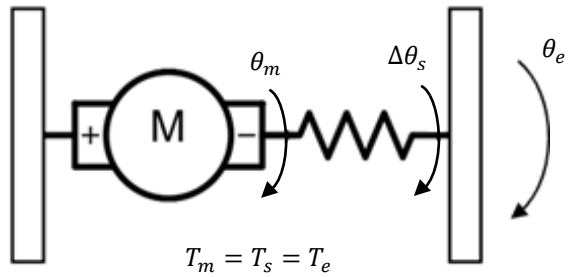

Figure 5.2: Model of a series elastic actuator to determine the kinetic requirements of the system

Motor power can be calculated as

$$P_m = T_m \dot{\theta}_m \tag{5.1}$$

Where T_m is the motor torque and $\dot{\theta}_m$ is the motor angular velocity. The motor angle θ_m is calculated as the difference between the total external angle θ_e and the spring angle $\Delta\theta_s$ given by Eq. (5.2).

$$\theta_m = \theta_e - \Delta\theta_s \tag{5.2}$$

The torque produced by the spring is given by Eq. (5.3)

$$T_e = K_s \Delta\theta_s \tag{5.3}$$

Where K_s is the stiffness and the deflection of the spring $\Delta\theta_s$ is given by the difference between the equilibrium angle of the spring $\Delta\theta_o$ and its instantaneous angle calculated from Eq. (5.2).

$$\Delta\theta_s = \Delta\theta_o - (\theta_m - \theta_e) \tag{5.4}$$

Using $\Delta\theta_s$ from Eq. (5.4) in Eq. (5.3)

$$\theta_s = \theta_o - \frac{T_s}{K_s} \tag{5.5}$$

Substituting in Eq. (5.2)

$$\theta_m = \theta_e - \Delta\theta_o + \frac{T_s}{K_s} \tag{5.6}$$

Taking derivative of Eq. (5.6) results in Eq. (5.7)

$$\dot{\theta}_m = \dot{\theta}_e + \frac{\dot{T}_s}{K_s} \tag{5.7}$$

Finally, by using Eq. (5.7) in Eq. (5.1) gives the motor power using SEA as

$$P_m = T_m(\dot{\theta}_e + \frac{\dot{T}_s}{K_s}) \tag{5.8}$$

The required peak power of the SEA is calculated as

$$P_m = \max\left(\left|T_m(\dot{\theta}_e + \frac{\dot{T}_s}{K_s}\right|\right) \tag{5.9}$$

The objective will be to determine the spring stiffness that gives the minimum value of the required peak power. In order to estimate the required energy consumption, the RMS power will be used given by Eq. (5.10).

$$P_{rms} = \sqrt{\frac{\sum_{i=1}^{n}(P_i)}{n}} \tag{5.10}$$

Where P_i is the power required by SEA at the *ith* instant. The value of P_i is calculated from Eq. (5.8) for each instant *i*.

5.2.5 Model of PEA

A PEA can be used to reduce the amount of torque required, thus reducing the need of a large transmission system. However, it also provides benefits in terms of the power requirements. The schematic of a PEA is illustrated in Figure 5.3.

The power requirement of the PEA can be calculated as,

$$P_m = T_m\,\dot{\theta}_e \tag{5.11}$$

Where T_m is the motor torque and $\dot{\theta}_e$ is the system angular velocity. The total torque T_e produced will be the sum of the motor torque T_m and spring torque T_p. Thus motor torque can be given by Eq. (5.12).

$$T_m = T_e - T_p \tag{5.12}$$

The spring torque T_p can be calculated using Hooke's law

$$T_p = K_p \Delta\theta_e \tag{5.13}$$

Where K_p is the parallel spring stiffness and $\Delta\theta_e$ is the change in the angular displacement of the spring given by the spring initial angle $\Delta\theta_o$ and the system angular displacement θ_e as

$$\Delta\theta_s = \Delta\theta_o - \theta_e \tag{5.14}$$

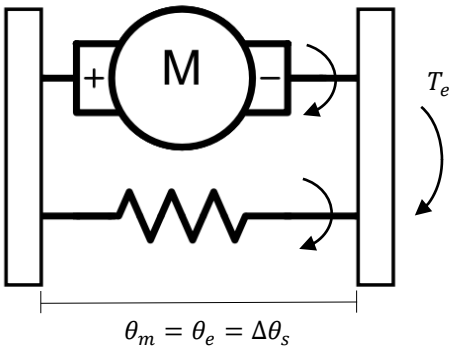

Figure 5.3: Model of a parallel elastic actuator to determine the kinetic requirements of the system

Therefore, using Eq. (5.14) in Eq. (5.13) gives

$$T_p = K_p(\Delta\theta_o - \theta_e) \tag{5.15}$$

Substituting Eq. (5.15) in Eq. (5.12) gives the torque required in PEA.

$$T_m = T_e - K_p(\Delta\theta_o - \theta_e) \tag{5.16}$$

In Eq. (5.16), when θ_e is equal to the spring equilibrium angle $\Delta\theta_o$, the spring torque is zero. Finally, the power required can be obtained by using Eq. (5.16) in Eq. (5.11) results in Eq. (5.17).

$$P_m = \left(T_e - K_p(\Delta\theta_o - \theta_e)\right)\,\dot{\theta}_e \tag{5.17}$$

The peak and rms value of torque and power can be calculated using Eq. (5.18) to Eq. (5.21)

$$(T_m)_{peak} = \max\left(\left|T_e - K_p(\Delta\theta_o - \theta_e)\right|\right) \tag{5.18}$$

$$T_{rms} = \sqrt{\frac{\sum_{i=1}^{n}(T_i)}{n}} \tag{5.19}$$

$$(P_m)_{peak} = \max\left(\left|\left(T_e - K_p(\Delta\theta_o - \theta_e)\right)\,\dot{\theta}_e\right|\right) \tag{5.20}$$

$$P_{rms} = \sqrt{\frac{\sum_{i=1}^{n}(P_i)}{n}} \tag{5.21}$$

In Eq. (5.19), T_i is the torque at *ith* instant and is calculated using Eq. (5.16). Similarly, P_i in Eq. (5.21) is the power at *ith* instant and is derived from Eq. (5.17).

5.2.6 Evaluating the Optimized Spring Stiffness

The stiffness of the spring will have to be optimized in order to use it in an elastic actuation system. The optimized stiffness for a series spring K_s and a

parallel spring K_p will be obtained using brute force search method [197] for each of the minimization criterion. The torque and power required by the motor significantly differs depending upon whether the stiffness of the spring was optimized for peak torque or peak power of the motor. Consequently, it was decided to optimized the value of the spring stiffness for each of the parameter separately. The spring stiffness was optimized based on five spring optimization criteria. The equilibrium angle for the case of PEA will also be optimized to further reduce the torque and power requirements. The first parameter was the peak torque T_{peak} i.e. the stiffness of the spring was determined such that the peak torque requirement of the system was minimized. Similarly, the stiffness of the spring was also optimized for P_{peak} minimization criterion. The root mean square (RMS) value of torque and power was also taken into account as it represented the total amount of torque and power consumed during the entire process. Therefore minimum T_{rms} and P_{rms} criteria were used. It was noticed during the spring optimization that by adapting the spring stiffness for one parameter decreases the value of that particular parameter e.g. optimizing the spring stiffness for T_{peak} minimization decreases the value of T_{peak} at the joint but on the other hand, it increases the values of other parameters i.e. T_{rms}, P_{peak} and P_{rms} for that particular spring stiffness. To overcome this problem, a multi-factor optimization criterion for the spring stiffness was developed that minimizes the values for all the parameters with a slight trade-off in each value of the parameter. The multi-factor optimization criterion was calculated using Eq. (5.22).

$$M_F = T_{rms}/\max(T_{rms}) + P_{rms}/\max(P_{rms}) + P_{peak}/\max(P_{peak}) + T_{peak}/\max(T_{peak}) \quad (5.22)$$

Where $\max(T_{rms})$, $\max(P_{rms})$, $\max(P_{peak})$ and $\max(T_{peak})$ is the maximum RMS torque and power and peak power and torque respectively across the gait cycle. The series spring stiffness K_s was only optimized based on the P_{peak} and P_{rms} and multi-factor optimization criteria since in series spring the amount of torque remains unchanged. The values of the optimized stiffness for series and parallel springs for cases of minimizing different parameters will be determined before performing the optimization of the elastic actuation system. The algorithm to determine the optimized spring stiffness is illustrated in Figure 5.4.

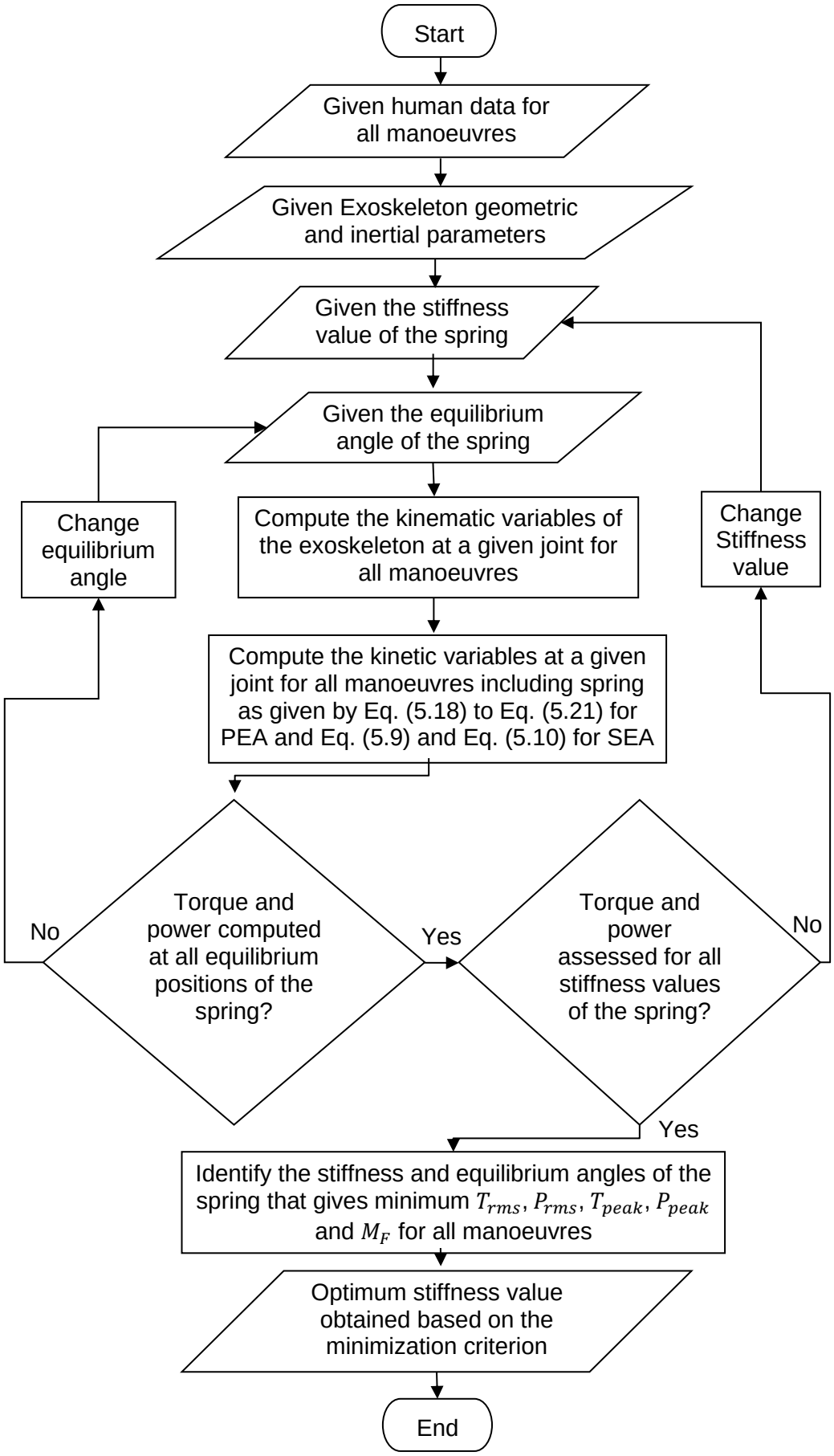

Figure 5.4: Flow chart of the algorithm to optimize the spring for a given joint for all manoeuvres

After incorporating the exoskeleton geometric and inertial parameters, the stiffness of the spring was selected starting from 0 to 2000 Nm/rad and the equilibrium angle from 0 to 360 (deg). The algorithm then computes the kinematic and kinetic variables at a given joint for all the maneuvers. Eq. (5.18) and Eq. (5.19) is used for T_{peak} and T_{rms} minimization criteria respectively for PEA. Similarly Eq. (5.20) and Eq. (5.21) was used for P_{peak} and P_{rms} minimization criteria. In order to determine the optimized stiffness for SEA, Eq. (5.9) and Eq. (5.10) was used for P_{peak} and P_{rms} criteria respectively. For optimizing the spring stiffness using the developed multi-factor optimization criterion, Eq. (5.22) was used for PEA and SEA. The above procedure is repeated until the algorithm has finished computing it for all the given stiffness range and the equilibrium angle using all of the optimization criteria.

It should be noted that the spring stiffness value and the equilibrium angle were considered to be fixed and do not change during sit to stand operation as well as swing and stance phase of the gait cycle, therefore, similar value for spring stiffness and equilibrium angle was used throughout for each of the three maneuvers. The same procedure is repeated for all lower limb joints i.e. hip, knee and ankle to calculate the optimum spring stiffness at each of the joint.

5.2.7 Simulation Approach

The kinematic and kinetic model developed for an assistive exoskeleton using elastic actuators was validated using simulations performed in SolidWorks. A model of the exoskeleton shown in Figure 5.5 was given the required actuators movements along with the series or parallel springs at each of the lower limb joints by fetching the data of the required maneuvers. The torque and power requirements were simulated using both series and parallel springs at the actuators. Figure 5.5 is shown for the case of PEA only however both PEA and SEA were analyzed using this model. The simulations were performed using torsional springs at each of the lower limb joints. The developed model using elastic actuators was used to obtain the torque and power requirements of the joints during sit to stand, swing and stance phase of the gait cycle. These torques and powers were compared with the kinetic requirements obtained using Eq. (5.8) for SEA and Eq. (5.16) to Eq. (5.17) for PEA.

Figure 5.5: Simulation model consisting of parallel spring at each of the joints

5.2.8 Optimization Algorithm of the Elastic Actuators

In this section, the framework of the optimization algorithm for the elastic actuation system in an assistive robotic exoskeleton will be discussed. After integrating the motors and the transmission systems with the desired springs of appropriate stiffness, the optimal elastic actuation system was evaluated using the optimization algorithm for elastic actuators elaborated in Figure 5.6. The algorithm determines the optimal actuation system initially at the knee joint and then proceeds towards the hip and ankle joint and it continues to repeat this cycle until the optimized elastic actuators for the case of PEA or SEA were revealed at each of the three joints. As the algorithm computes the total weight and power of the system, it assumes the most lightweight actuators at the hip and ankle joint while performing the optimization at the knee actuator. This method is explained in detail in Chapter 4 under Section 4.6.

For a given joint, the optimization algorithm computes the kinematic and kinetic requirements of the system depending upon whether the actuation system consisted of PEA or SEA with the given exoskeleton geometrical and inertial parameters. For the case of PEA, it uses Eq. (5.15) and for SEA, it uses Eq. (5.17) with the optimum spring stiffness and equilibrium angle mentioned in the previous section. It should be highlighted that the stiffness

and equilibrium angle of the spring were selected with the spring optimized for the multi-factor criterion. After the kinetic model was obtained by incorporating the type of the elastic system, the algorithm selects a motor from the list at a given joint while assuming the most light weight actuators at the other joints. Similarly the transmission system was also included and the required motor torque, velocity and acceleration were evaluated using the transmission system model specified in Section 5.2.3. The required torque, velocity and acceleration of the motor were then compared with the torque speed curve of the motor (details mentioned in Chapter 4, Section 4.3) to verify if the given candidate elastic actuator satisfies the motor limits. If the given candidate elastic actuator does not satisfy the motor limits, it moves to the next candidate in the list but if it satisfies, a score is calculated for that candidate elastic actuator from the objective function given by Eq. (4.15) that includes the total weight, total power and the user carrying capacity of the exoskeleton. Different weightage was given to each parameter and the normalized values of these variables were included in the objective function. A negative weightage was given to the weight and power in the objective function since a smaller value for these variables was desired. After estimating the score of a given candidate elastic actuator, it moves to the next motor and repeats the above procedure to calculate the score for the next particular candidate actuator. After computing it for all motors, it moves to the next transmission system in the list until all the motors and the transmission systems are exhausted. Lastly, it determines the elastic actuation system with the highest score calculated from the objective function.

The elastic actuator with the highest score will be the most optimized actuator at this phase at a given joint i.e. knee joint since the algorithm was initially applied at this joint. The above procedure is repeated at the ankle joint by taking the knee actuator from the previous step and hip actuator as the previously assumed one. Similarly, the optimized hip actuator was assessed using similar procedure as described above with the knee and ankle actuator updated from the previous steps. The algorithm keeps on repeating until all actuators were obtained similar to their previous iteration at each of the lower limb joints.

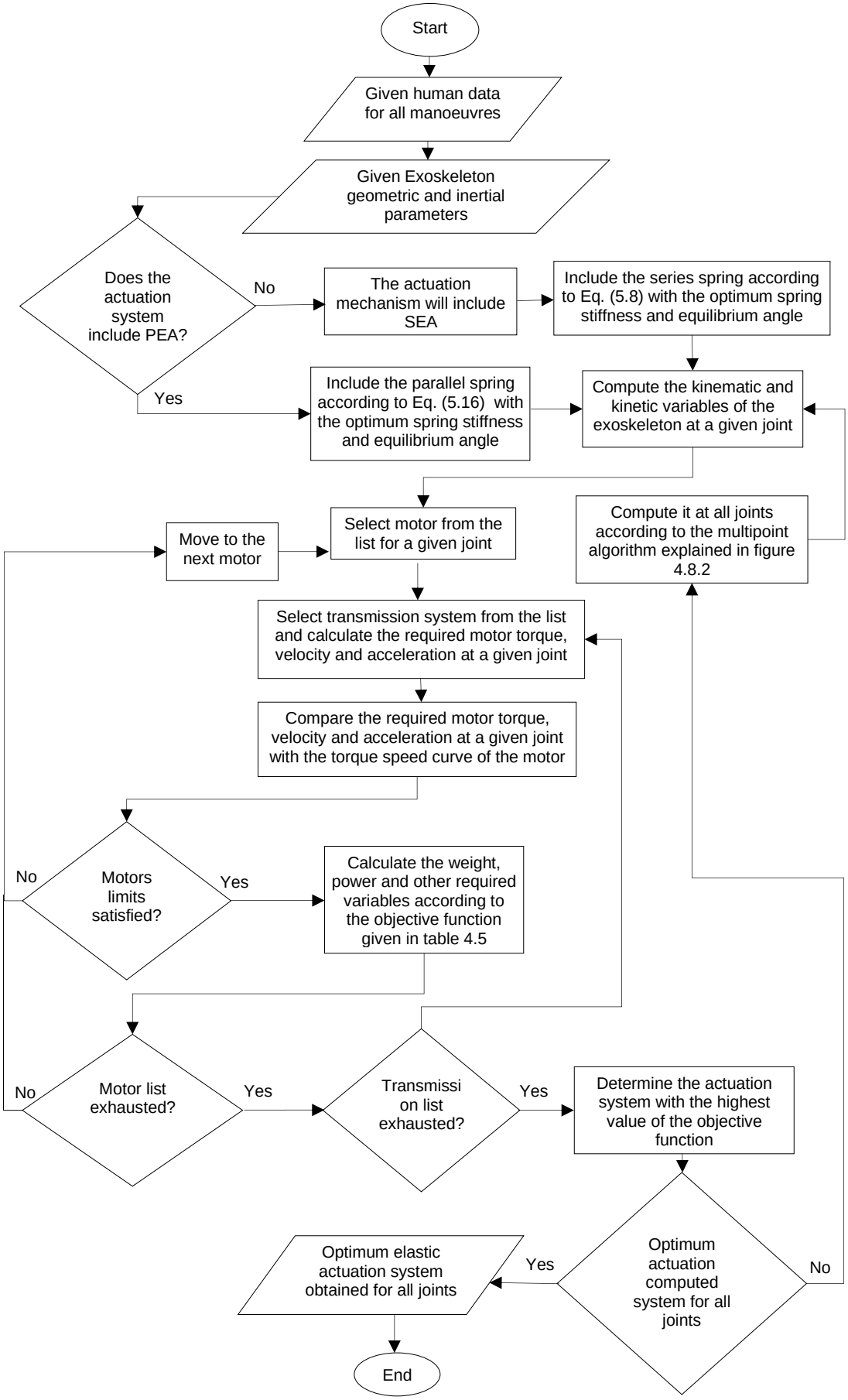

Figure 5.6: Flow chart of the optimization algorithm of an elastic actuation system

5.3 Results and Discussions

The optimization algorithm for elastic actuators discussed in the previous section was used to determine the optimum actuation system using PEA and SEA for an assistive exoskeleton. The optimum spring stiffness using the described minimization strategies will be discussed, followed by the torque and power analysis of the joints in the elastic actuators. The results using the simulation model will also be presented. The kinetic trajectories of the lower limb joints during sit to stand, swing and stance phase of the gait are recorded in Section 5.3.4. The optimal elastic actuation system and the analysis in terms of weight and power of the exoskeleton will be specified in Sections 5.3.5 and 5.3.6.

5.3.1 Spring Stiffness Optimization

The results of the optimized spring stiffness for different minimization criteria are tabulated in Table 5.1. The equilibrium angle of the spring was also elaborated in case of PEA. It can be observed that the optimized spring stiffness for SEA was higher as compared to the spring stiffness in case of PEA. This is because in PEA, the spring has to follow the whole length of change of the actuator during its operation and hence a lower value of spring stiffness is desired. On the other hand, a higher value of spring stiffness is estimated in SEA but even the higher value of spring stiffness did not achieve favorable results in SEA as will be discussed in the next section. The optimized value can be found between 20 to 25 Nm/rad at the hip joint for the case of PEA and equilibrium angle between 13 to 15 deg. The stiffness value for the knee was observed to be higher for peak torque and power case. At the ankle joint, the torque minimization case favored higher stiffness values whereas the power minimization case indicated a lower value. The overall optimization suggests a smaller value of the spring stiffness for PEA.

The spring stiffness optimization in SEA recorded a higher value especially for knee and ankle joint. A higher value of stiffness at the hip joint can be observed during P_{rms} minimization criterion. It is revealed in Table 5.1 that each parameter is best minimized at a particular value of the spring stiffness. A slight change in the spring stiffness and equilibrium angle of PEA significantly changes magnitude of the desired variables.

Table 5.1: Optimized spring stiffness and equilibrium angle of PEA and SEA for different spring optimization criteria

PEA	Hip		Knee		Ankle	
	K_p (Nm/rad)	θ (deg)	K_p (Nm/rad)	θ (deg)	K_p (Nm/rad)	θ (deg)
Minimizing τ_{peak}	24	14	33	36	87	18
Minimizing τ_{rms}	21	13	20	6	66	22
Minimizing P_{peak}	22	16	25	39	7	13
Minimizing P_{rms}	20	14	15	38	1	36
Multi-factor Optimization M_F	21	15	22	36	28	22
SEA	K_s (Nm/rad)		K_s (Nm/rad)		K_s (Nm/rad)	
Minimizing P_{peak}	217		656		1598	
Minimizing P_{rms}	876		1534		576	
Multi-factor Optimization M_F	521		656		1478	

5.3.2 Torque and Power Requirements using Series and Parallel Springs

In this section, the torque and power requirements in series and parallel elastic actuators will be specified for each of the lower limb joints and a comparison will be established with the kinetic requirements of the rigid actuator. The rigid actuation system requirements were derived from Chapter 4 during each of the maneuver. The results were identified for several spring minimization criteria.

5.3.2.1 Hip Joint

The torque and power requirements at the hip joint using PEA and SEA as compared to the rigid actuator is elaborated in Figure 5.7. All the four variables of interest were shown during each of the minimization criterion. When optimizing the spring stiffness for the case of T_{peak}, it resulted in a significant reduction of torque and power for all minimization cases. The maximum reduction was observed in the RMS power P_{rms} of the hip joint during sit to stand which was 78% lower as compared to a rigid actuator. A

significant reduction was also attained during the optimization of T_{rms} minimization criterion. The results indicated a large reduction in T_{rms} with a trade-off in the values of the peak torque T_{peak} and other parameters. The cases of power minimization were also applied to SEA but the outcomes reflected that SEA was unable to reduce any significant amount of torque and power. In PEA, the P_{peak} and P_{rms} minimization cases resulted in a decrease in the required amount of torque and power. The maximum decrease was estimated for the case of P_{rms} during sit to stand with 91 % reduction in P_{rms} as well as a significant reduction in other variables. The multi-factor optimization recorded an amount of reduction in all of the parameters as compared to the rigid actuation system but with a slight increase in the values as compared to the previous individual minimization cases.

5.3.2.2 Knee Joint

The stiffness of the spring in SEA and PEA for different cases of minimizations at the knee joint are demonstrated in Figure 5.8. For the case of minimizing T_{peak} spring stiffness optimization, it was recorded a significant reduction in case of peak torque and other variables during sit to stand but during swing and stance phase, there was a considerable amount of increase in torque and power requirements. This is because a fixed value of spring stiffness is considered for all phases of activities. Similar results have been observed for other cases as well i.e. an increase in torque and power requirement during swing and stance phase in PEA. When spring stiffness was optimized for the T_{rms} minimization case, the T_{rms} decreased with a large increase in T_{peak} and P_{peak} of the actuation system. SEA results did not suggest any benefit in the torque and power requirements at the knee joint. PEA decreased the torque and power during sit to stand but increased them during swing and stance phase as compared to a rigid actuation. The multi-factor optimization also indicated a reduction during sit to stand operation but a slight increase during swing and stance phase of the gait. The torque and power during the stance phase is zero because the knee joint was considered to be fixed during this phase to make it more power efficient [198].

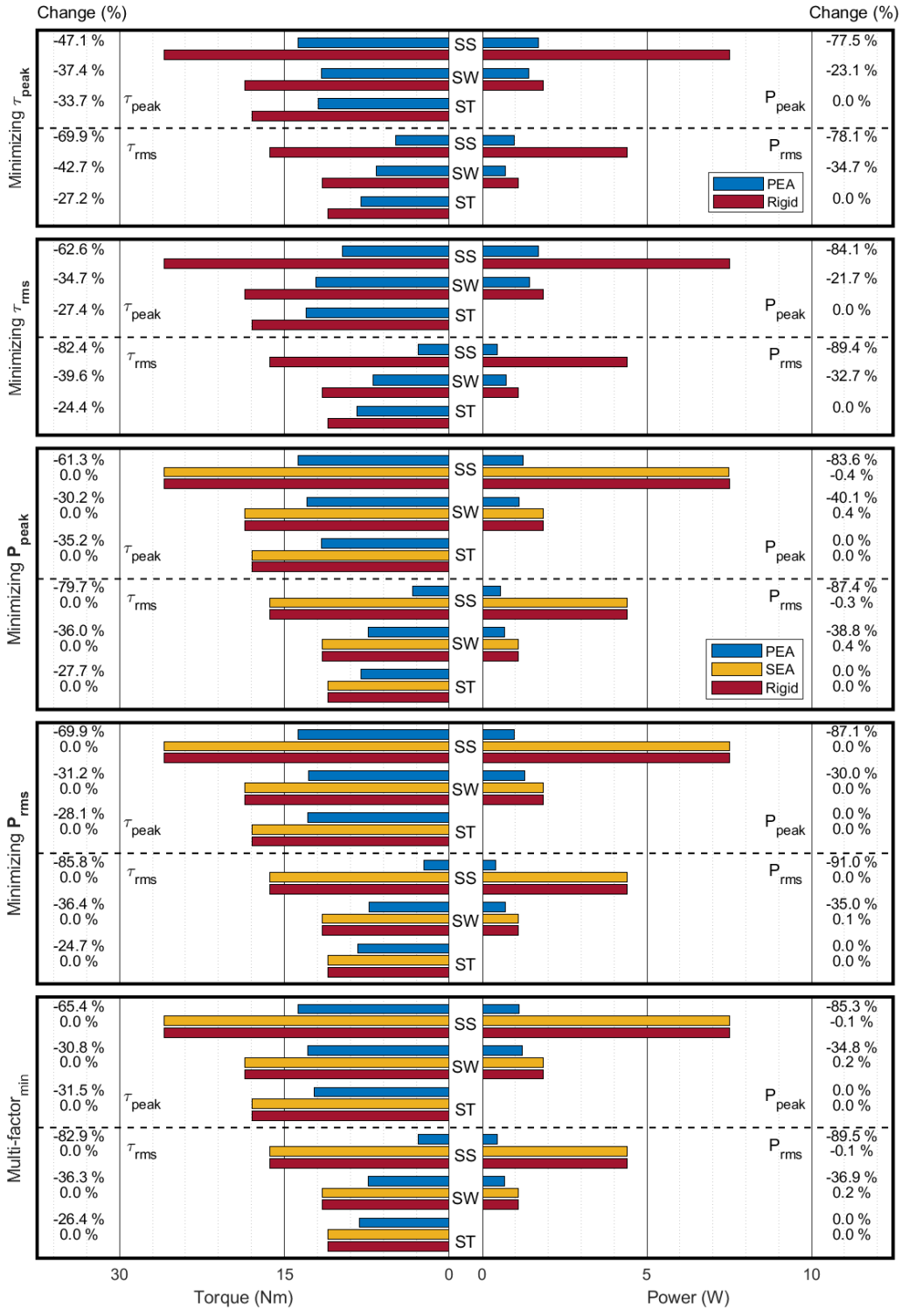

Figure 5.7: Torque and Power requirements at the hip joint during sit to stand (SS), swing (SW) and stance (ST) phase of the gait for PEA, SEA and rigid actuation system. The values of the variables T_{peak}, T_{rms}, P_{peak} and P_{rms} are shown with the spring stiffness and equilibrium angle optimized for each type of the minimization criterion.

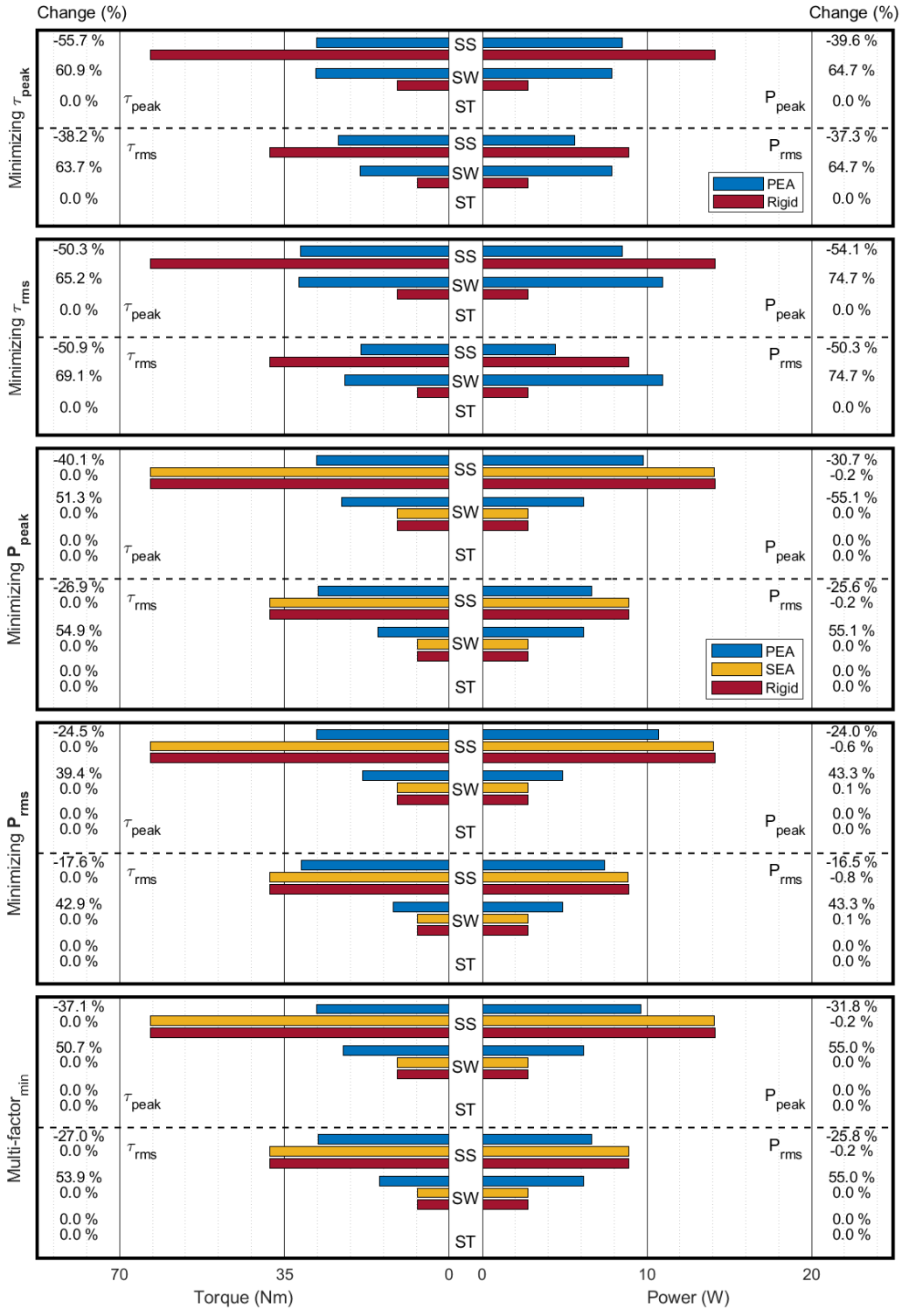

Figure 5.8: Torque and Power requirements at the knee joint during sit to stand (SS), swing (SW) and stance (ST) phase of the gait for PEA, SEA and rigid actuation system for various minimization criteria. The values of the variables T_{peak}, T_{rms}, P_{peak} and P_{rms} are shown with the spring stiffness and equilibrium angle optimized for each type of the minimization criterion.

5.3.2.3 Ankle Joint

At the ankle joint, PEA increased the amount of torque and power during sit to stand and swing phase but decreased a considerable amount during stance phase of the level ground walking. The peak value of torque and power was also observed to be decreased in the stance phase. When minimizing the ankle joint for the case of T_{peak} minimization of spring stiffness, results were reflected similar in all cases i.e. in PEA, torque and power was higher during sit to stand and swing phase but significantly lower during stance phase. Similar results have been recorded for the T_{rms} minimization case. During P_{peak} and P_{rms} minimization cases, there was a reduction in the peak and RMS power but the peak torque and RMS torque were not having any noticeable difference from the rigid actuation. The amount of power reduction in SEA can be observed to be negligible. The multi-factor optimization reduces the peak torque during sit to stand and swing phase as well as in other variables but the difference is not significant in most of the cases of SEA as illustrated in Figure 5.9.

Although the torque and power requirement was noticeably reduced by PEA but SEA did not produce any substantial difference in the kinetic requirements of the joints. Although previous studies have shown a decrease in the power requirement at the ankle joint using SEA but the operational constraints of [186, 189] compared to this work were different. Firstly, the speed requirements were matched as the walking speed of the Rex Bionics as mentioned previously. For the current exoskeleton model i.e. model without using crutches, the walking speed has to be matched with Rex Bionics that is found to be very slow [171]. At slow speed, SEA did not bring any benefits in the power requirements of the actuation system [187]. The second reason was because of the usage of a fixed stiffness actuator for each operation of sit to stand and level ground walking and hence, it was unable to reduce the requirements. It could be suggested that using a variable stiffness for each manoeuvre might bring a considerable difference but will increase the cost and complexity of the system. This is also true for the case of PEA. The performance of the PEA could be further increased if a variable stiffness actuator will be used. The previous studies showed using variable stiffness for each instant of gait was not power efficient [199]. Therefore, it can be said that by means of a fixed stiffness for each particular manoeuvre, it is possible to bring benefits in the power requirement for SEA. This area will be explored in Chapter 6 using dual actuation systems. As only fixed stiffness actuators with the slow walking speed was considered,

therefore, it did not prove any benefit in case of SEA. But, the torque and power requirement was substantially reduced using PEA.

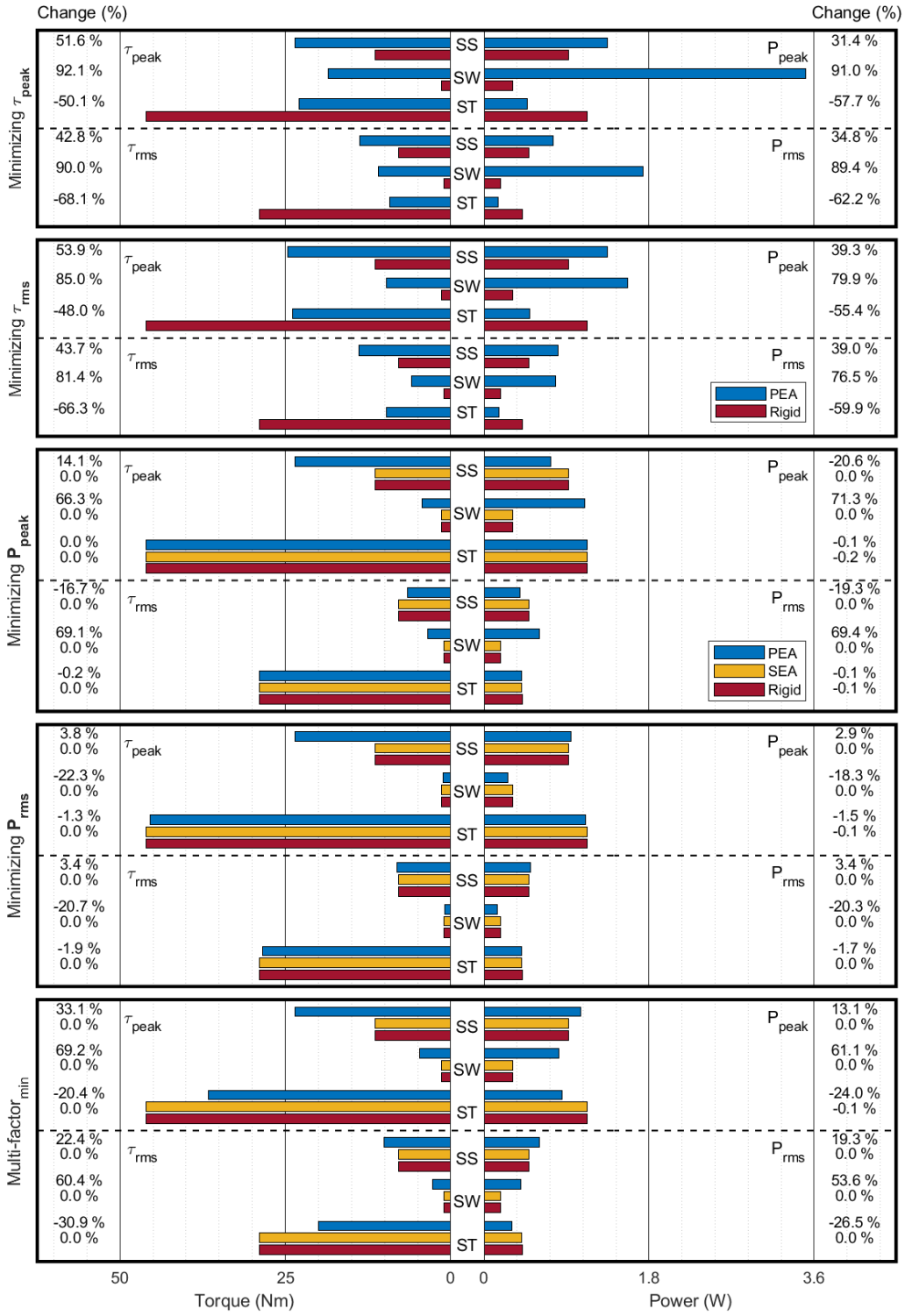

Figure 5.9: Torque and Power requirements at the ankle joint during sit to stand (SS), swing (SW) and stance (ST) phase of the gait for PEA, SEA and rigid actuation system for various minimization criteria. The values of the variables T_{peak}, T_{rms}, P_{peak} and P_{rms} are shown with the spring stiffness and equilibrium angle optimized for each type of the minimization criterion.

5.3.3 Model Validation of an Elastic Actuator

The developed kinetic model using elastic actuators will be validated using the simulation model shown in Figure 5.5 that was developed in SolidWorks modelling software. The motions specified to the simulation model were similar as given to the previous developed parametric elastic model at each of the joints using a motor and a torsional spring by means of the SolidWorks Motion Analysis Toolbox. The results were separately analyzed for each maneuver at each of the lower limb joints of the assistive exoskeleton. Similar spring stiffness and equilibrium angle were given to both of the systems. For the purpose of validation, only multi-factor spring stiffness optimization criterion was considered and the results were illustrated only for the case of parallel elastic actuators (PEA).

The results are elaborated in Figure 5.10 that represents the torque and power trajectories for each of the maneuver at the hip joint. As visualized, the trajectories are similar during each of the maneuver with only a slight variation between the two models. Figure 5.11 that illustrates this for the knee joint, also reflects identical results of the torque and power requirements between previously developed parametric model and the simulation model. A slight negligible deviations in the peak values are noticed. These variations in the peak values are also recorded at the ankle joint as depicted in Figure 5.12. By observing similar patterns between the developed kinetic model (which is mentioned as MATLAB model in the figures) and the simulation model, the integrity of the model is confirmed that will be later used to determine the optimum elastic actuation systems for an assistive robotic exoskeleton.

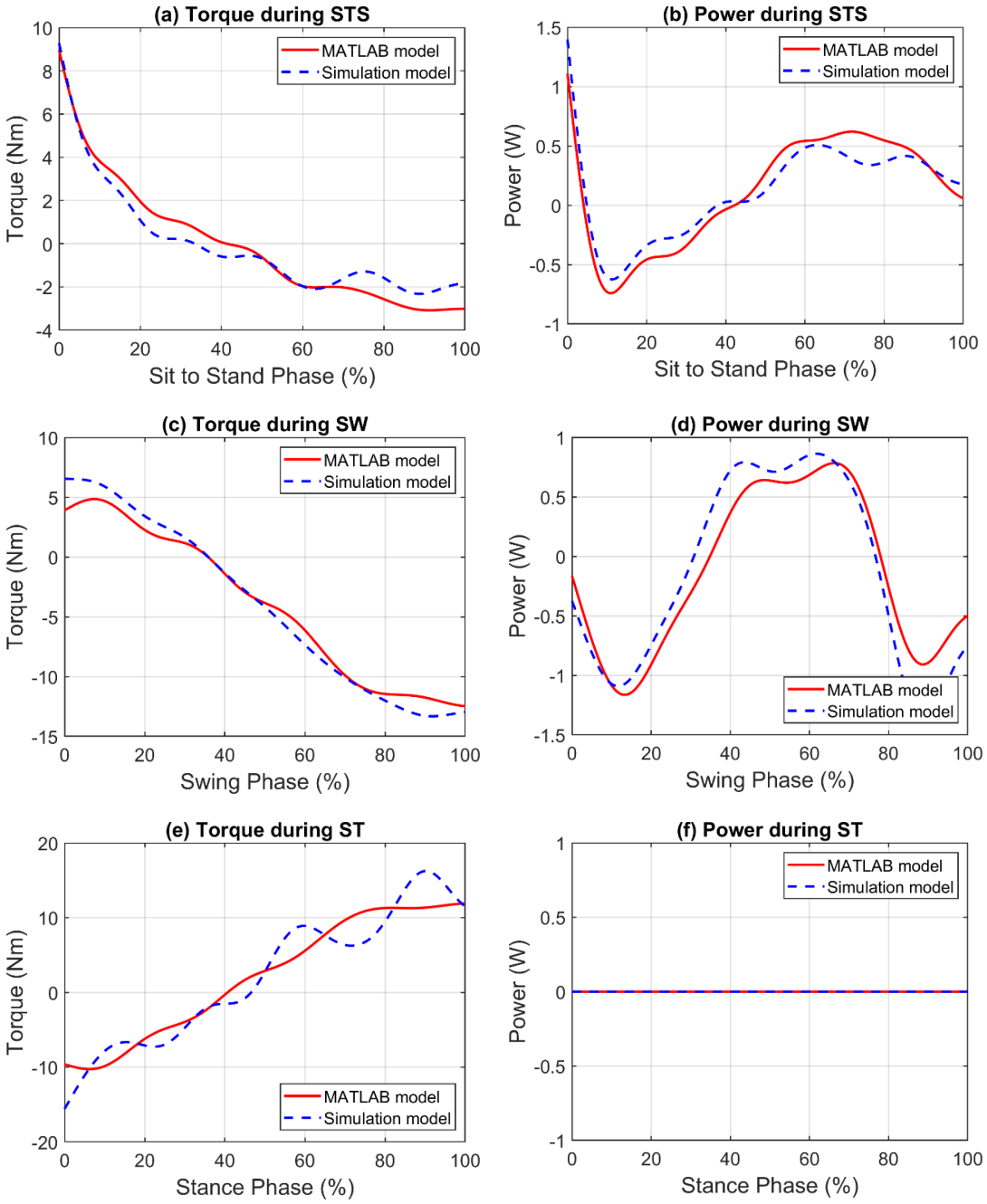

Figure 5.10: Torque and power joint trajectories at the hip during sit to stand (STS), swing (SW) and stance phase (ST) of the theoretical and simulation model using PEA. Figures (a), (c) and (e) display the torque trajectory of the joint and Figures (b), (d) and (f) represent power trajectories of the joint during the three manoeuvres.

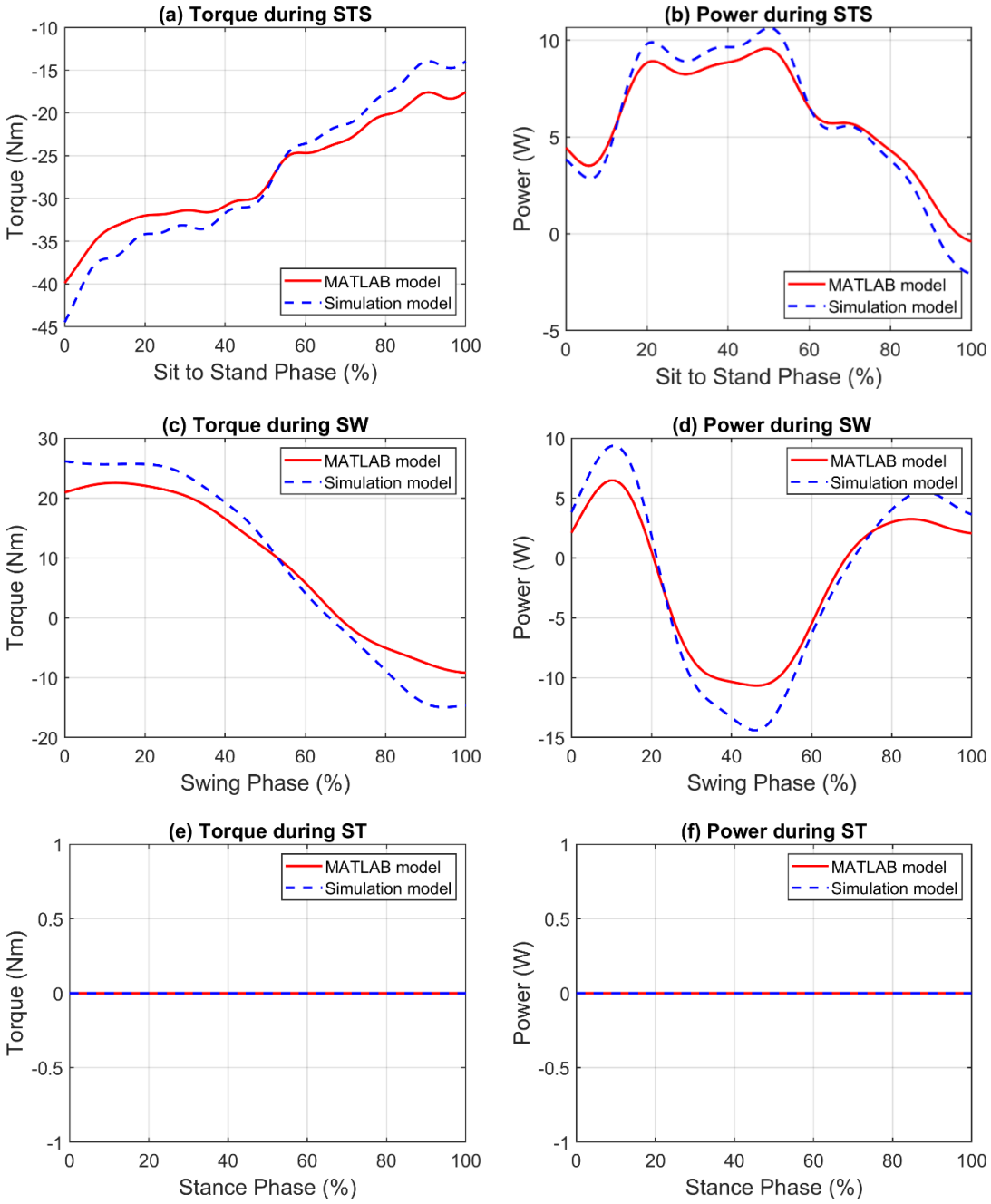

Figure 5.11: Torque and power joint trajectories at the knee during sit to stand (STS), swing (SW) and stance phase (ST) of the theoretical and simulation model using PEA. Figures (a), (c) and (e) display the torque trajectory of the joint and Figures (b), (d) and (f) represent power trajectories of the joint during the three manoeuvres.

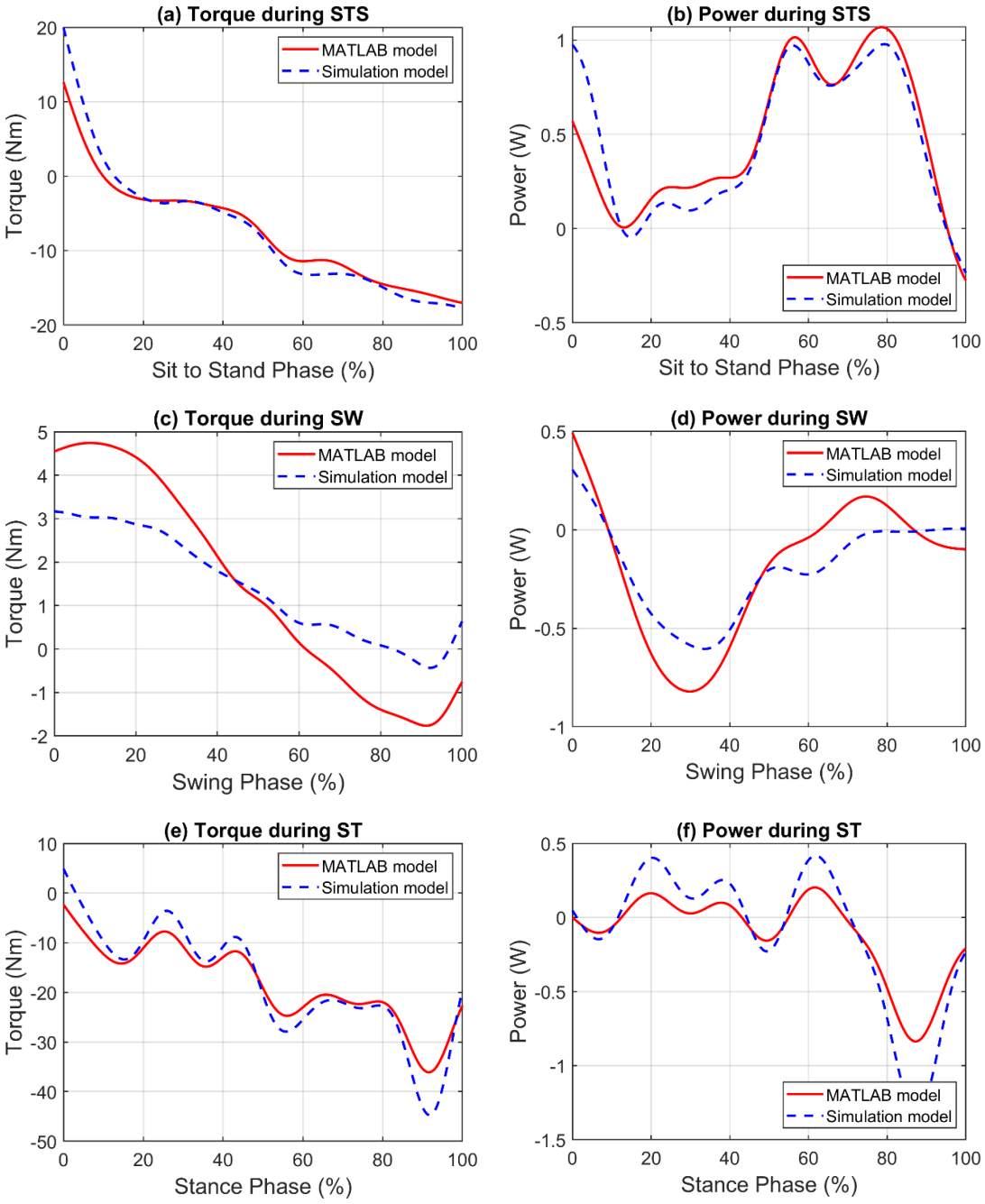

Figure 5.12: Torque and power joint trajectories at the ankle during sit to stand (STS), swing (SW) and stance phase (ST) of the theoretical and simulation model using PEA. Figures (a), (c) and (e) display the torque trajectory of the joint and Figures (b), (d) and (f) represent power trajectories of the joint during the three manoeuvres.

5.3.4 Kinetic Results of the Lower Limb Joints of the Exoskeleton using Elastic Elements

Using the optimum spring stiffness assessed for the cases of PEA and SEA for each of the minimization criterion discussed in Section 5.3.2, the trajectories of the torque and power requirements of lower limb joints will be analyzed for each criterion. The results will be separately recorded for every single phase of the maneuver. Similar to the rigid actuation system, the double support in the stance phase is not included in the results to reduce the running time of the optimization algorithm for elastic actuators.

5.3.4.1 Parallel Elastic Actuators (PEA)

Results using parallel actuators are presented in Figures 5.13 to 5.15 for hip, knee and ankle joints. These results provide the torque and power requirements at each of the joints.

5.3.4.1.1 Hip Joint

The torque and power trajectories using a parallel elastic actuator at the hip joint can be examined in Figure 5.13. The patterns of the maneuvers were recorded for each of the parallel spring optimization criterion. The maximum difference between the rigid and the parallel elastic actuation system was visualized during the trajectory of sit to stand maneuver. All the spring optimization criteria were able to bring significant reduction in the torque and power during the trajectory with a slight variation among them. The torque and power was also recorded to be reduced at the hip joint during swing and stance phase of the gait cycle. The trajectory obtained using the developed multi-factor spring optimization criterion was observed to be running in between the trajectories of the other spring optimization criteria. This shows that it was able to reduce the requirements for all spring parameters considered with only a marginal compromise in each of them. The power during single stance phase at the hip joint is zero because of the knee locking mechanism as previously explained.

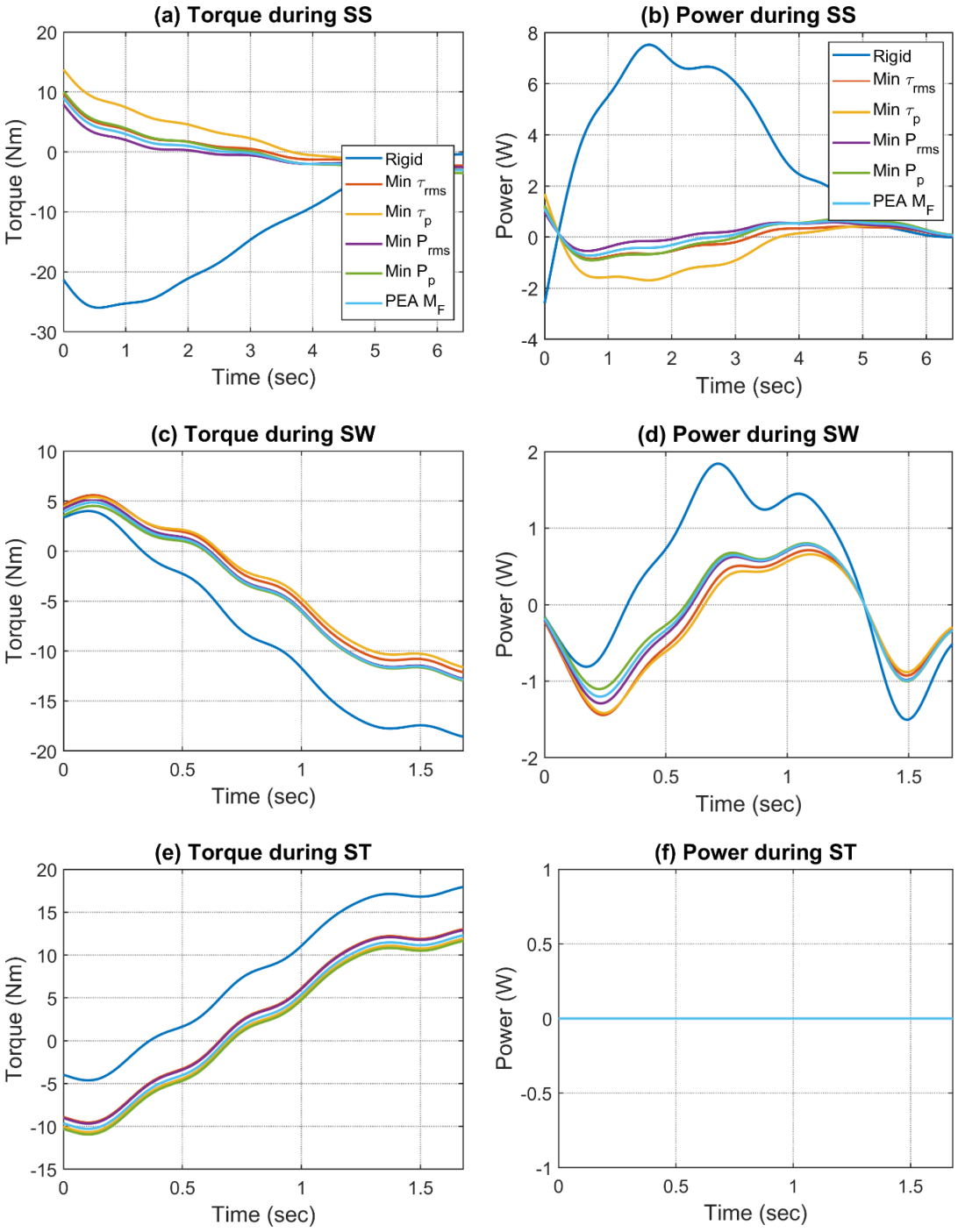

Figure 5.13: Torque and power trajectories at the hip joint during sit to stand (SS), swing (SW) and stance (ST) phase. Figures (a), (c) and (d) display the torque trajectory of the joint and Figures (b), (d) and (f) represent power trajectories of the joint during the three manoeuvres. These trajectories are shown for the case of PEA by using each of the spring optimization strategies and compared with the trajectory for the rigid actuation system.

5.3.4.1.2 Knee Joint

A large variation has been observed at the knee joint comparing the results of the different spring optimization criteria for PEA as illustrated in Figure 5.14. During sit to stand, the torque and power trajectories recorded a reduction as compared to the trajectories of the rigid actuation system. The maximum reduction was noticed during T_{peak} spring minimization criterion. The trajectory during this case follows approximately the same value during the whole trajectory. At the stance phase, the trajectories for each of the minimization criterion stick to a higher value as compared to the rigid actuation system. A larger variation was reflected during T_{rms} minimization and the smallest deviation was recorded in P_{rms} minimization criterion. The requirements during the stance phase were reported to be zero at the knee joint since the knee joint was considered to be locked during this phase. This was explained in the previous chapter.

5.3.4.1.3 Ankle Joint

Considering the torque and power requirements at the ankle joint, noticeable dissimilarities occur among the different spring optimization criteria as recorded in Figure 5.15. In some cases, the requirements were observed to be decreased while an increase was noticed in other cases. During the swing phase, the trajectories of different spring optimization criterion reflected a higher value in the torque and power but they followed a significant reduction during the stance phase.

In the elastic actuators using parallel springs, the multi-factor spring optimization criterion showed an overall balanced reduction during the whole trajectory at each of the joints. In [187], the spring stiffness was optimized based on minimizing energy requirements at the hip and knee joint but at the ankle joint, it was optimized to minimize the peak power. In our work, a multi-factor optimization approach was used that takes into account the peak and RMS values of torque and power simultaneously to achieve better reductions. Therefore, in the optimization algorithm for parallel elastic actuation system, a spring stiffness optimized using the developed multi-factor criterion was employed.

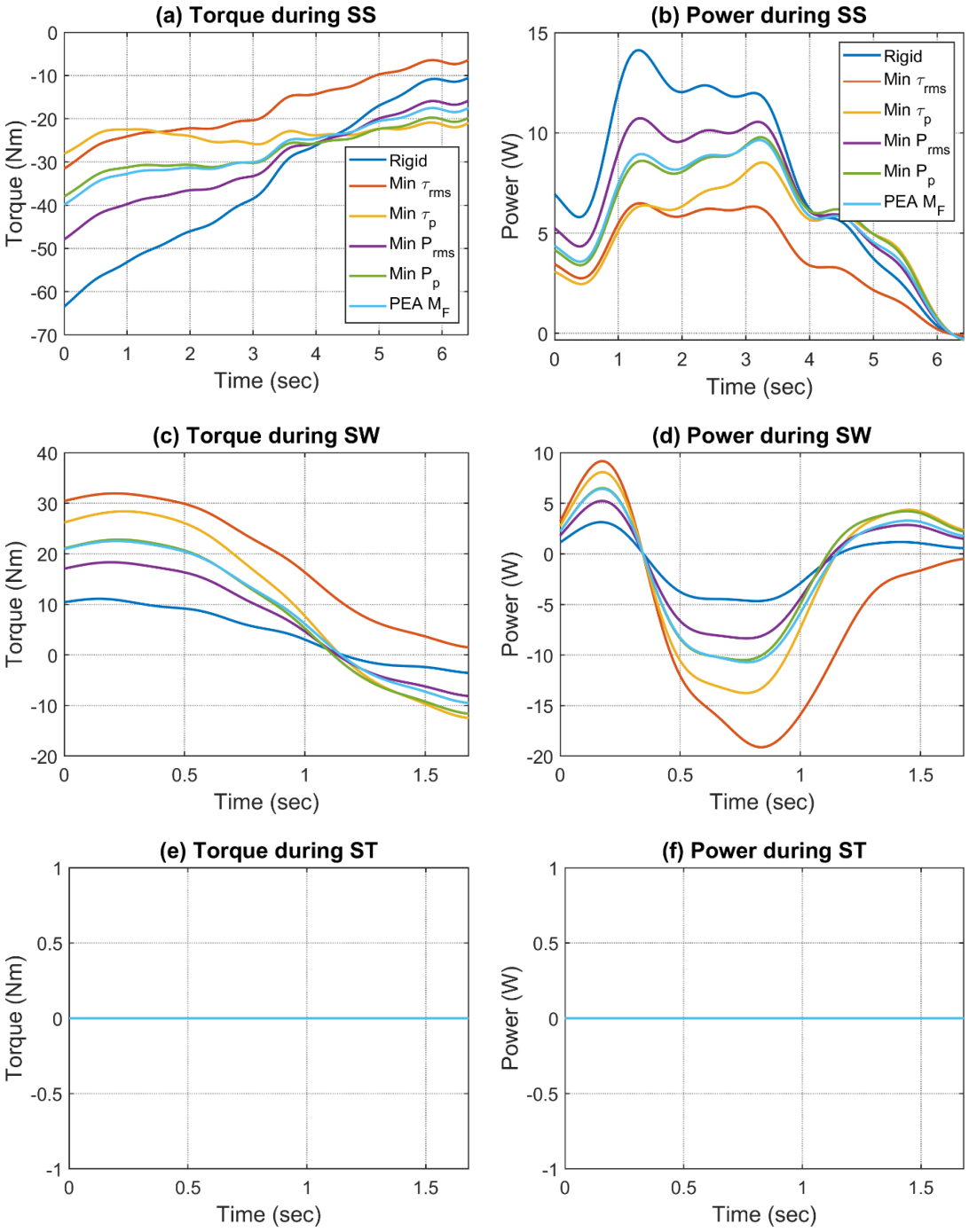

Figure 5.14: Torque and power trajectories at the knee joint during sit to stand (SS), swing (SW) and stance (ST) phase. Figures (a), (c) and (d) display the torque trajectory of the joint and Figures (b), (d) and (f) represent power trajectories of the joint during the three manoeuvres. These trajectories are shown for the case of PEA by using each of the spring optimization strategies and compared with the trajectory for the rigid actuation system.

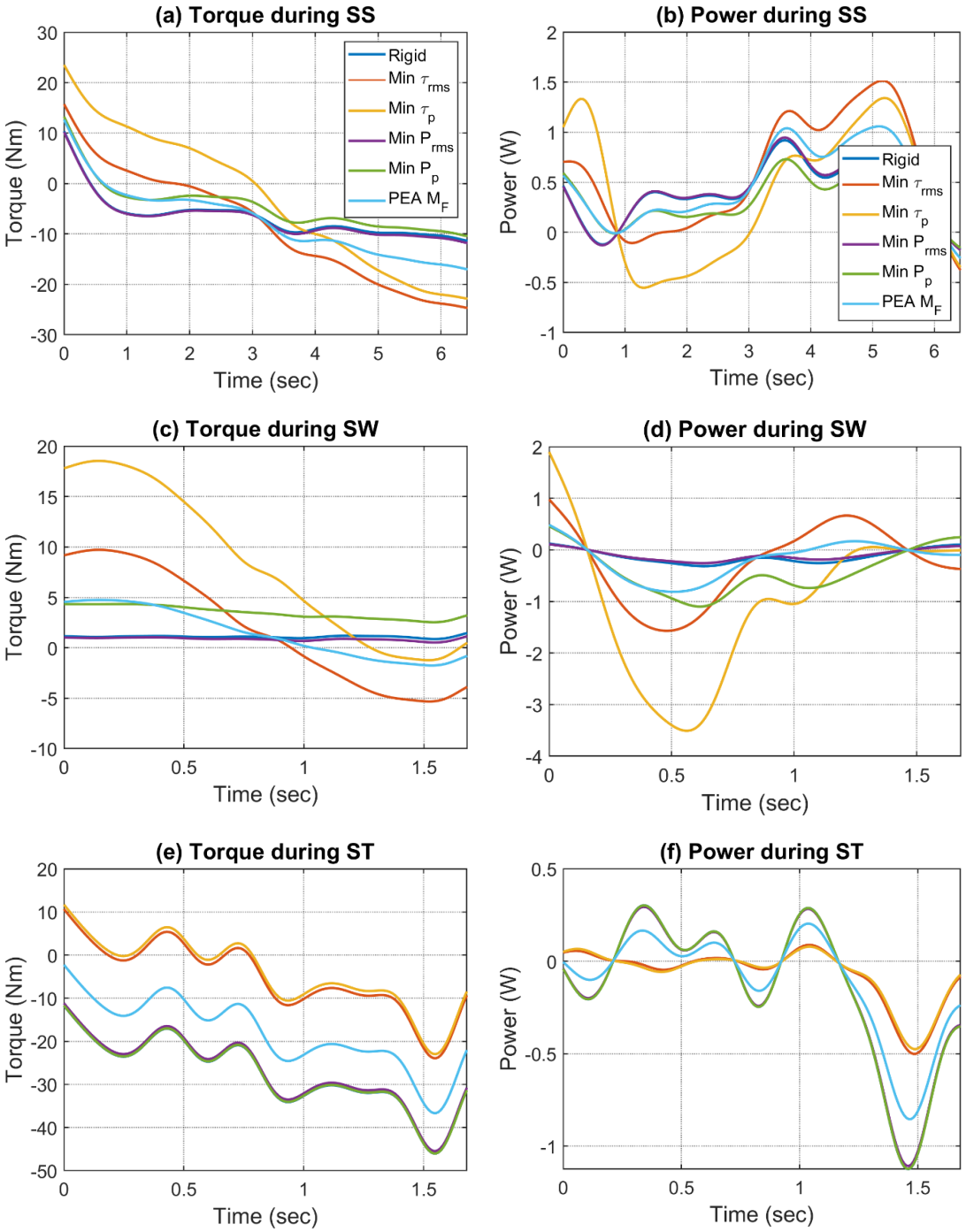

Figure 5.15: Torque and power trajectories at the ankle joint during sit to stand (SS), swing (SW) and stance (ST) phase. Figures (a), (c) and (d) display the torque trajectory of the joint and Figures (b), (d) and (f) represent power trajectories of the joint during the three manoeuvres. These trajectories are shown for the case of PEA by using each of the spring optimization strategies and compared with the trajectory for the rigid actuation system.

5.3.4.2 Series Elastic Actuators (SEA)

The kinetic variations at the hip, knee and ankle joint using the series elastic actuator are presented in Figures 5.16 to 5.18 respectively. It examined the torque and power assessed for all of the series spring minimization criteria. However, unlike PEA, it was recorded that a series spring did not bring any reductions in the requirements. There has only been a slight variation observed at the knee joint but it was not significant. As mentioned previously, this could be due to the slow walking speed and because of the fixed spring actuators used. The effects of the variable stiffness actuators will be explored in Chapter 6.

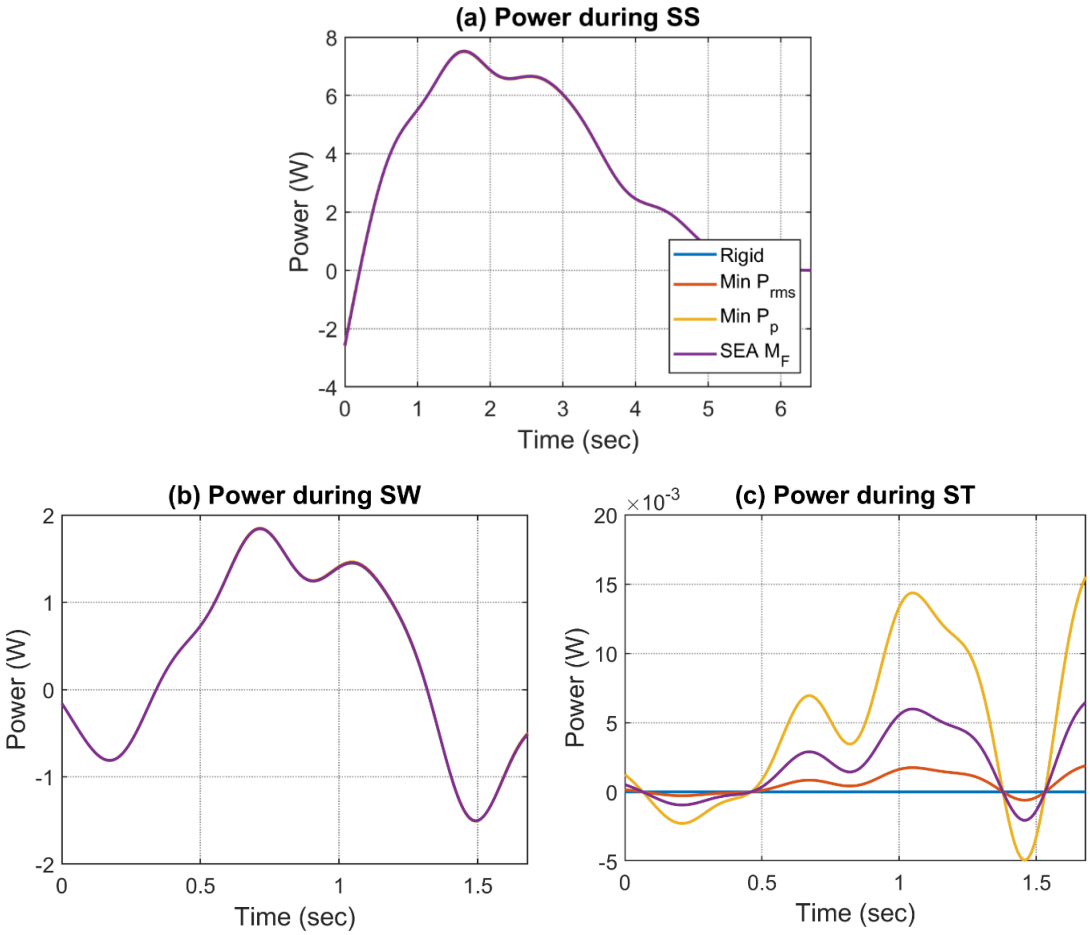

Figure 5.16: The power trajectory at the hip joint during (a) sit to stand (SS), (b) swing (SW) and (c) stance (ST) phase. These trajectories are shown for the case of SEA by using the three spring optimization strategies and compared with the trajectory for the rigid actuation system during the three manoeuvres.

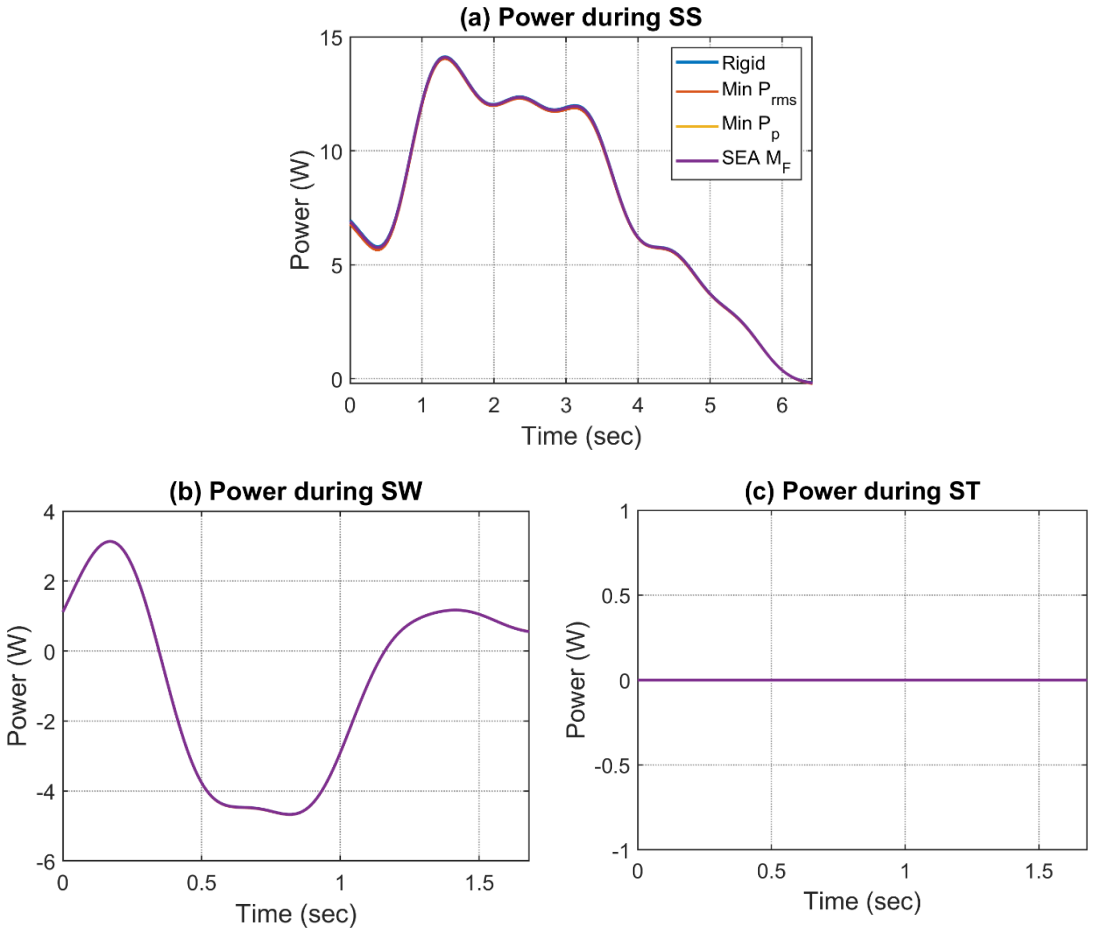

Figure 5.17: The power trajectory at the knee joint during (a) sit to stand (SS), (b) swing (SW) and (c) stance (ST) phase. These trajectories are shown for the case of SEA by using the three spring optimization strategies and compared with the trajectory for the rigid actuation system during the three manoeuvres.

Even though, the effect of SEA on the kinetic requirements were not significant, the optimal elastic actuation system using SEA will be computed in the next section to investigate if the choice of the actuators can have any effect on the actuator design parameters in SEA as compared to the rigid actuation system.

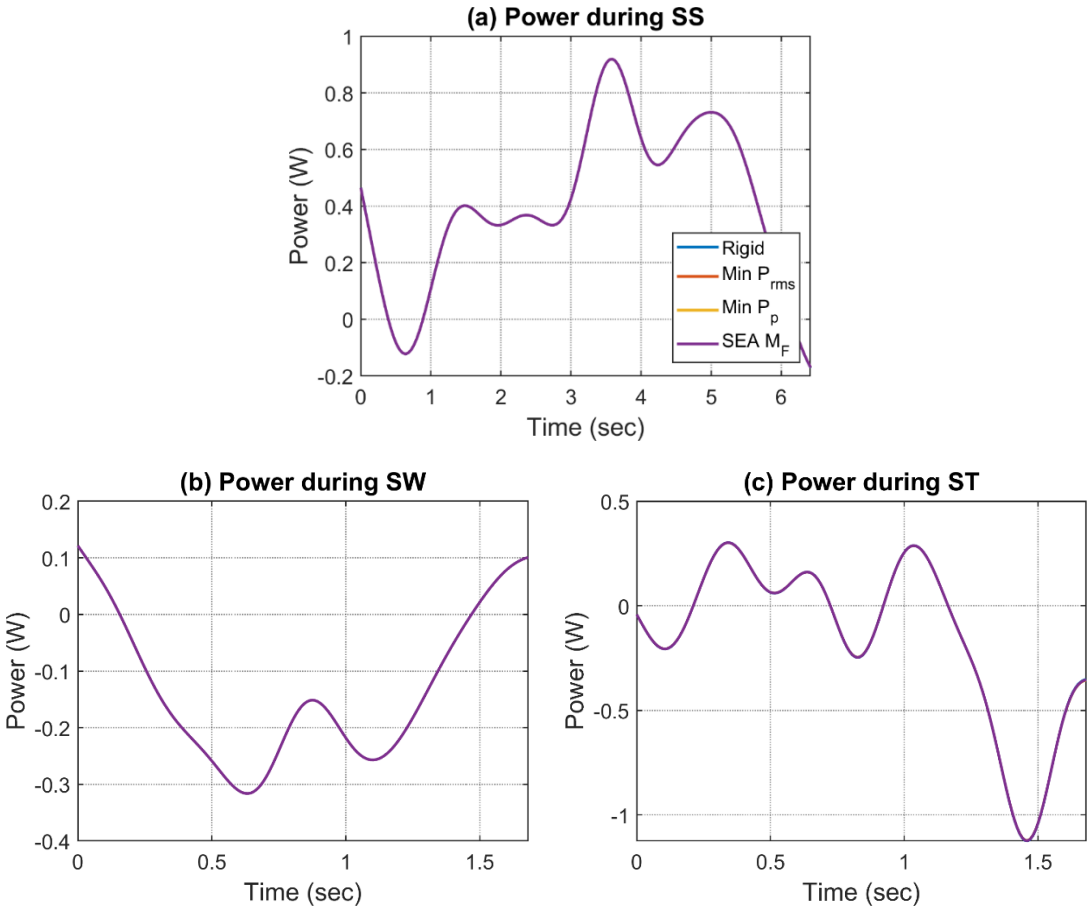

Figure 5.18: The power trajectory at the ankle joint during (a) sit to stand (SS), (b) swing (SW) and (c) stance (ST) phase. These trajectories are shown for the case of SEA by using the three spring optimization strategies and compared with the trajectory for the rigid actuation system during the three manoeuvres.

5.3.5 Optimal Elastic Actuation System

In this section, the optimal elastic actuation systems will be presented using the algorithm discussed in Section 5.2.8. These were assessed for PEA as well as for SEA. The results were separately analyzed for each type of the transmission system employed. However, the results are presented so that at least two of the lower limb joints have the same transmission system.

5.3.5.1 Parallel Elastic Actuation System

Tables 5.2 to 5.8 show the results of the optimal elastic actuation systems evaluated using different transmission systems at the joints. The results of the optimal parallel elastic actuation system using harmonic drives as the transmission systems at each of the lower limb joints are represented in Table 5.2 for each iteration of the algorithm.

Table 5.2: Optimal parallel elastic actuation system (PEA) assessed at each iteration of the optimization algorithm using harmonic drives as a type of the transmission system at each of the lower limb joint actuators.

Joint Optimization	Candidate Actuator			P_C (W)	W_{exo} (kg)	U_C (kg)
	Hip	Knee	Ankle			
Knee joint	Maxon ECX-speed-16M with CSD-14-50-2A	Maxon EC45-flat with CSD-20-160-2A	Maxon ECX-speed-16M with CSD-14-50-2A	10.6	25.6	100
Ankle joint	Maxon ECX-speed-16M with CSD-14-50-2A	Maxon EC45-flat with CSD-20-160-2A	Allied motion MF76008 with CPL-25-160-2A	22.1	25.3	100
Hip joint	Allied motion MF76008 with CSD-20-160-2A	Maxon EC45-flat with CSD-20-160-2A	Allied motion MF76008 with CPL-25-160-2A	32.5	25.5	100
Knee joint	Allied motion MF76008 with CSD-20-160-2A	Allied motion MF60020 with CSD-20-160-2A	Allied motion MF76008 with CPL-25-160-2A	28.1	25.6	100
Ankle joint	Allied motion MF76008 with CSD-20-160-2A	Allied motion MF60020 with CSD-20-160-2A	Allied motion MF76008 with CPL-25-160-2A	28.1	25.6	100
Hip joint	Allied motion MF76008 with CSD-20-160-2A	Allied motion MF60020 with CSD-20-160-2A	Allied motion MF76008 with CPL-25-160-2A	28.1	25.6	100

* P_C=Average Total Power consumption, W_{exo}=Total Weight of the exoskeleton and U_C= User's carrying capacity with 50% support

As previously mentioned, the algorithm is initially applied at the knee joint by assuming the most light weight actuators at the ankle and hip. The optimal knee actuator obtained during the first iteration of the knee joint was Maxon EC frameless-45-flat with the harmonic drive CSD-20-160-2A and a parallel spring with the stiffness shown in Table 5.1 using multi-factor optimization. The design parameters used for the optimal actuator selection i.e. the total power consumption, the total weight of the exoskeleton and the user carrying capacity were also shown for each iteration. When the algorithm was applied at the ankle joint, the optimum ankle actuator was estimated by considering the knee actuator from the previous step and hip actuator still the most lightweight from the list. The design parameters of the exoskeleton were obtained as shown. The algorithm was then operated at the hip joint to obtain the optimum actuation system for the hip as shown along with the design parameters of the exoskeleton. As mentioned during the explanation of the algorithm, it continues to repeat joint by joint iteration until same values started to appear for each of the joints from their respective previous iteration. As can be observed, the last three rows that corresponds to each

of the three lower limb joints were having the same actuation system and the values of the design parameters as compared to their respective previous iteration. The optimum actuation system using harmonic drive as the transmission system is shown in the last row of Table 5.2 for each of the joint with the total power, total weight and user carrying capacity also illustrated. These design parameters will be analyzed later in the next section.

Table 5.3: Optimal parallel elastic actuation system (PEA) assessed at each iteration of the optimization algorithm using harmonic drives combined with a belt and pulley drive system as a type of the transmission system at each of the lower limb joint actuators.

Joint Optimization	Candidate Actuator			P_C (W)	W_{exo} (kg)	U_C (kg)
	Hip	Knee	Ankle			
Knee joint	Maxon ECX-speed-16M with CSD-14-50-2A and a transmission ratio of 1:0.4	Maxon EC45-flat with CSD-20-160-2A and a transmission ratio of 1:350	Maxon ECX-speed-16M with CSD-14-50-2A and a transmission ratio of 1:0.4	5.2	25.6	100
Ankle joint	Maxon ECX-speed-16M with CSD-14-50-2A and a transmission ratio of 1:0.4	Maxon EC45-flat with CSD-20-160-2A and a transmission ratio of 1:350	Maxon EC45-flat with CPL-25-160-2A and a transmission ratio of 1:400	14.6	25.0	100
Hip joint	Maxon EC45-flat with CSD-20-160-2A and a transmission ratio of 1:400	Maxon EC45-flat with CSD-20-160-2A and a transmission ratio of 1:350	Maxon EC45-flat with CPL-25-160-2A and a transmission ratio of 1:400	23.9	24.8	100
Knee joint	Maxon EC45-flat with CSD-20-160-2A and a transmission ratio of 1:400	Maxon EC45-flat with CSD-20-160-2A and a transmission ratio of 1:350	Maxon EC45-flat with CPL-25-160-2A and a transmission ratio of 1:400	23.9	24.8	100
Ankle joint	Maxon EC45-flat with CSD-20-160-2A and a transmission ratio of 1:400	Maxon EC45-flat with CSD-20-160-2A and a transmission ratio of 1:350	Maxon EC45-flat with CPL-25-160-2A and a transmission ratio of 1:400	23.9	24.8	100

* P_C= Average Total Power consumption, W_{exo}=Total Weight of the exoskeleton and U_C= User's carrying capacity with 50% support

The transmission ratio of the harmonic drives were further exploited by combining it with a belt and pulley drive system. The results using this type of the transmission system can be observed in Table 5.3. The results were reported for each iteration starting from the knee joint and then continue to apply the optimization algorithm joint by joint until the values become similar as comparted to their previous iteration. The optimum actuation system

assessed using harmonic drive in combination with a belt and pulley drive mechanism were recorded in the last row. Using a transmission ratio of 1:350 at the knee joint and 1:400 at the hip and ankle joint by applying the belt and pulley drive mechanism with the harmonic drive, the elastic actuation system using PEA could be realized using smaller motors as compared to the previous case of using harmonic drives without the belt and pulley drive system.

Results were also achieved using only belt and drive system as the transmission mechanism coupled directly to the electric motor shown in Table 5.4. As can be observed, a larger and a heavier motor was required for this system but even though a larger motor was employed, it was not able to achieve the desired user carrying capacity. Consequently, the use of a belt and drive system without any other form of the transmission system is not recommended.

Table 5.4: Optimal parallel elastic actuation system (PEA) assessed at each iteration of the optimization algorithm using belt and pulley drive system directly coupled to the motor at each of the lower limb joint actuators.

Joint Optimization	Candidate Actuator			P_C (W)	W_{exo} (kg)	U_C (kg)
	Hip	Knee	Ankle			
Knee joint	Maxon ECX-speed-16M with a ratio of 1:0.4	Parker Hannifin K1781008Y with a ratio of 1:2.6	Maxon ECX-speed-16M with a ratio of 1:0.4	34.6	36.3	5.2
Ankle joint	Maxon ECX-speed-16M with a ratio of 1:0.4	Parker Hannifin K1781008Y with a ratio of 1:2.6	Parker Hannifin K1781008Y with a ratio of 1:2.6	696	46.0	6.1
Hip joint	Parker Hannifin K1781008Y with a ratio of 1:2.6	Parker Hannifin K1781008Y with a ratio of 1:2.6	Parker Hannifin K1781008Y	1224	56.4	11.5
Knee joint	Parker Hannifin K1781008Y with a ratio of 1:2.6	Parker Hannifin K1781008Y with a ratio of 1:2.6	Parker Hannifin K1781008Y with a ratio of 1:2.6	1224	56.4	11.5
Ankle joint	Parker Hannifin K1781008Y with a ratio of 1:2.6	Parker Hannifin K1781008Y with a ratio of 1:2.6	Parker Hannifin K1781008Y with a ratio of 1:2.6	1224	56.4	11.5

* P_C= Average Total Power consumption, W_{exo}=Total Weight of the exoskeleton and U_C= User's carrying capacity with 50% support

Table 5.5 shows the results for the case of ball screws. The transmission systems are represented with the configuration number of the ball screws.

These configurations are presented in Appendix C with their respective numbers. As previously mentioned, different configurations of ball screws were evaluated and specified in the optimization algorithm. The optimized actuation system using ball screws at the hip, knee and ankle joints are given in the last row of the table.

Table 5.5: Optimal parallel elastic actuation system (PEA) assessed at each iteration of the optimization algorithm using ball screws as a type of the transmission system at each of the lower limb joint actuators.

Joint Optimization	Candidate Actuator			P_C (W)	W_{exo} (kg)	U_C (kg)
	Hip	Knee	Ankle			
Knee joint	Maxon ECX-speed-16M with ball screw configuration no. 1	Allied motion MF76008 with ball screw configuration no. 185	Maxon ECX-speed-16M with ball screw configuration no. 1	19.2	24.1	100
Ankle joint	Maxon ECX-speed-16M with ball screw configuration no.1	Allied motion MF76008 with ball screw configuration no. 185	Allied motion MF60020 with ball screw configuration no. 14	26.9	24.5	100
Hip joint	Allied motion MF76008 with ball screw configuration no. 65	Allied motion MF76008 with ball screw configuration no. 185	Allied motion MF60020 with ball screw configuration no. 14	91.1	25.1	100
Knee joint	Allied motion MF76008 with ball screw configuration no. 65	Allied motion MF76008 with ball screw configuration no. 185	Allied motion MF60020 with ball screw configuration no. 14	91.1	25.1	100
Ankle joint	Allied motion MF60020 with ball screw configuration no. 11	Allied motion MF76008 with ball screw configuration no. 185	Allied motion MF60020 with ball screw configuration no. 11	92.6	25.0	100
Hip joint	Allied motion MF60020 with ball screw configuration no. 69	Allied motion MF76008 with ball screw configuration no. 185	Allied motion MF60020 with ball screw configuration no. 11	75.1	25.1	100
Knee joint	Allied motion MF60020 with ball screw configuration no. 69	Allied motion MF76008 with ball screw configuration no.185	Allied motion MF60020 with ball screw configuration no. 11	75.1	25.1	100
Ankle joint	Allied motion MF60020 with ball screw configuration no. 69	Allied motion MF76008 with ball screw configuration no. 185	Allied motion MF60020 with ball screw configuration no. 11	75.1	25.1	100

* P_C= Average Total Power consumption, W_{exo}=Total Weight of the exoskeleton and U_C= User's carrying capacity with 50% support

Tables E.4 to E.6 in Appendix E present the optimum actuation systems when different types of the transmission systems were utilized at each of the joints. Table E.4 shows the optimum actuation system with either the ball screws in a slider crank mechanism or the harmonic drives that were used as the transmission system for the three lower limb joints. These results are not represented for each iteration but only the final actuation systems from the optimization algorithm are illustrated. The optimum actuation system is recorded for each combination of the transmission mechanism. Similarly, Table E.5 shows the final selections of the actuation systems from the optimization algorithm with either the ball screws or the harmonic drives in combination with a belt and pulley drive system as the transmission system. These results are not represented for each iteration of the algorithm but only the final results for each combination are described. Finally, Table E.6 indicates the outcomes when either the belt and pulley drive system directly coupled to the electric motor was employed as the transmission system at the joints or a ball screw in a slider crank mechanism was used.

By using belt and pulley drive system without any other form of the transmission system at some of the joints whereas employing ball screws at the other joints, it was appropriate to explore if the overall user carrying capacity could be achieved since the total weight and power could be further reduced using belt and pulley drive system. This will be explained in the Section 5.3.6.

5.3.5.2 Series Elastic Actuation System

Tables 5.9 to 5.15 show the results of the optimum actuation systems computed using series elastic elements. Table 5.9 is presented for the case when harmonic drives were used as the transmission systems at each of the lower limb joints. The results were elaborated for each iteration of the algorithm. The optimum actuators can be observed in the last row. Similarly, when harmonic drives were designed to be applied with a belt and pulley drive system, the power consumption and the weight was reduced since the actuators can now be built with more efficient motors. Table 5.10 shows the optimum results using this type of the transmission mechanism.

Table 5.6: Optimal series elastic actuation system (SEA) assessed at each iteration of the optimization algorithm using harmonic drives as a type of the transmission system at each of the lower limb joint actuators.

Joint Optimization	Candidate Actuator			P_C (W)	W_{exo} (kg)	U_C (kg)
	Hip	Knee	Ankle			
Knee joint	Maxon ECX-speed-16M with CSD-14-50-2A	Allied motion MF60020 with CPL-20-160-2A	Maxon ECX-speed-16M with CSD-14-50-2A	9.8	25.8	100
Ankle joint	Maxon ECX-speed-16M with CSD-14-50-2A	Allied motion MF60020 with CPL-20-160-2A	Allied motion MF76008 with CPL-25-160-2A	20.9	25.5	100
Hip joint	Allied motion MF76008 with CSD-20-160-2A	Allied motion MF60020 with CPL-20-160-2A	Allied motion MF76008 with CPL-25-160-2A	31.1	25.6	100
Knee joint	Allied motion MF76008 with CSD-20-160-2A	Allied motion MF60020 with CPL-20-160-2A	Allied motion MF76008 with CPL-25-160-2A	31.1	25.6	100
Ankle joint	Allied motion MF76008 with CSD-20-160-2A	Allied motion MF60020 with CPL-20-160-2A	Allied motion MF76008 with CSD-14-50-2A	31.1	25.6	100

Table 5.7: Optimal series elastic actuation system (SEA) assessed at each iteration of the optimization algorithm using harmonic drives combined with a belt and pulley drive system as a type of the transmission system at each of the lower limb joint actuators.

Joint Optimization	Candidate Actuator			P_C (W)	W_{exo} (kg)	U_C (kg)
	Hip	Knee	Ankle			
Knee joint	Maxon ECX-speed-16M with CSD-14-50-2A and a ratio of 1:0.4	Maxon EC45-flat with CPL-20-160-2A and a ratio of 1:400	Maxon ECX-speed-16M with CSD-14-50-2A and a ratio of 1:0.4	7.3	25.7	100
Ankle joint	Maxon ECX-speed-16M with CSD-14-50-2A and a ratio of 1:0.4	Maxon EC45-flat with CPL-20-160-2A and a ratio of 1:400	Maxon EC45-flat with CPL-25-160-2A and a ratio of 1:400	16.3	25.0	100
Hip joint	Maxon EC45-flat with CSD-20-160-2A and a ratio of 1:400	Maxon EC45-flat with CPL-20-160-2A and a ratio of 1:400	Maxon EC45-flat with CPL-25-160-2A and a ratio of 1:400	24.4	24.8	100
Knee joint	Maxon EC45-flat with CSD-20-160-2A and a ratio of 1:400	Maxon EC45-flat with CPL-20-160-2A and a ratio of 1:400	Maxon EC45-flat with CPL-25-160-2A and a ratio of 1:400	24.4	24.8	100
Ankle joint	Maxon EC45-flat with CSD-20-160-2A and a ratio of 1:400	Maxon EC45-flat with CPL-20-160-2A and a ratio of 1:400	Maxon EC45-flat with CPL-25-160-2A and a ratio of 1:400	24.4	24.8	100

* P_C=Average Total Power consumption, W_{exo}=Total Weight of the exoskeleton and U_C= User's carrying capacity with 50% support

Results of a belt and pulley drive mechanism directly coupled with the electric motor can be investigated in Table 5.11. It was established that the required user carrying capacity cannot be achieved even though using larger and heavier motors. Table 5.12 represents the optimum actuators using ball screws as the form of the transmission system for each of the lower limb joints.

The results produced by using a different type of the transmission system at the compiled hip, knee and ankle joint are presented in Tables E.7 to E.9. These are illustrated for ball screws and the harmonic drives in Table E.7 for all of the possible combinations at the hip, knee and ankle joints. The results are not recorded here for each iteration. Table E.8 resulted when the harmonic drive was combined either with a belt and pulley drive system or ball screws were employed as the transmission system that represented for each possible combination at the hip, knee and ankle joint. Similarly, Table E.9 gives the results of the optimum actuation system when either the belt and pulley drive alone or the ball screws were used as the transmission system to confirm if any useful selection could be obtained similar to the case of PEA.

Table 5.8: Optimal series elastic actuation system (SEA) assessed at each iteration of the optimization algorithm using belt and pulley drive system directly coupled to the motor at each of the lower limb joint actuators.

Joint Optimization	Candidate Actuator			P_C (W)	W_{exo} (kg)	U_C (kg)
	Hip	Knee	Ankle			
Knee joint	Maxon ECX-speed-16M with a ratio of 1:0.4	Parker Hannifin K1781008Y with a ratio of 1:2.6	Maxon ECX-speed-16M with a ratio of 1:0.4	97.4	36.3	5.2
Ankle joint	Maxon ECX-speed-16M with a ratio of 1:0.4	Parker Hannifin K1781008Y with a ratio of 1:2.6	Parker Hannifin K1781008Y with a ratio of 1:2.6	709	46.0	6.1
Hip joint	Parker Hannifin K1781008Y with a ratio of 1:2.6	Parker Hannifin K1781008Y with a ratio of 1:2.6	Parker Hannifin K1781008Y with a ratio of 1:2.6	1227	56.4	11.5
Knee joint	Parker Hannifin K1781008Y with a ratio of 1:2.6	Parker Hannifin K1781008Y with a ratio of 1:2.6	Parker Hannifin K1781008Y with a ratio of 1:2.6	1227	56.4	11.5
Ankle joint	Parker Hannifin K1781008Y with a ratio of 1:2.6	Parker Hannifin K1781008Y with a ratio of 1:2.6	Parker Hannifin K1781008Y with a ratio of 1:2.6	1227	56.4	11.5

* P_C= Average Total Power consumption, W_{exo}=Total Weight of the exoskeleton and U_C= User's carrying capacity with 50% support

Table 5.9: Optimal series elastic actuation system (SEA) assessed at each iteration of the optimization algorithm using ball screws as a type of the transmission system at each of the lower limb joint actuators.

Joint Optimization	Candidate Actuator			P_C (W)	W_{exo} (kg)	U_C (kg)
	Hip	Knee	Ankle			
Knee joint	Maxon ECX-speed-16M with ball screw configuration no.1	Allied motion MF76008 with ball screw configuration no.190	Maxon ECX-speed-16M with ball screw configuration no.1	25.8	24.1	100
Ankle joint	Maxon ECX-speed-16M with ball screw configuration no.1	Allied motion MF76008 with ball screw configuration no.190	Allied motion MF60020 with ball screw configuration no.11	70.1	24.5	100
Hip joint	Allied motion MF95008 with ball screw configuration no.42	Allied motion MF76008 with ball screw configuration no.190	Allied motion MF60020 with ball screw configuration no.11	55.9	25.4	100
Knee joint	Allied motion MF95008 with ball screw configuration no.42	Allied motion MF76008 with ball screw configuration no.190	Allied motion MF60020 with ball screw configuration no.11	55.9	25.4	100
Ankle joint	Allied motion MF95008 with ball screw configuration no.42	Allied motion MF76008 with ball screw configuration no.190	Allied motion MF60020 with ball screw configuration no.11	55.9	25.4	100

* P_C= Average Total Power consumption, W_{exo}=Total Weight of the exoskeleton and U_C= User's carrying capacity with 50% support

Therefore, an optimum actuation system selection was established for different combinations of the transmission systems. The difference in the total weight and total power consumption of the exoskeleton using the optimum elastic actuation systems presented in this section for different categories of the transmission systems compared with the rigid actuators will be discussed in the next section.

5.3.6 Analysis of Elastic and Rigid actuation System categorized according to the Transmission Systems

The benefit of using the elastic actuators in an assistive robotic exoskeleton will be investigated in this section. The total weight and power of the exoskeleton in the parallel and series elastic actuators will be compared with the total weight and power of the exoskeleton using rigid actuators presented in Chapter 4. These results were separately analyzed for each category of the transmission system and are shown in Figures 5.19 to 5.21.

The outcomes in Figure 5.19 shows the total weight and average power consumption of the exoskeleton when either the harmonic drives or the ball screws in an inverted slider crank mechanism were employed as the transmission system. The weight and power consumption of the rigid, PEA and SEA differ significantly in most of the actuator combinations. However, a negligible difference was observed when harmonic drives were used at all of the joints. For some of the transmission system combinations, the power and weight of PEA and SEA were also noticed to be increased as compared to the rigid actuation system. For example, when ball screws were used at hip and knee joint and harmonic drives were used at the ankle joint, even though the total weight was decreased for the case of PEA but there was a significant increase in the total power consumption. There was a slight difference recorded for the case of SEA compared to the rigid system for this particular combination. The maximum decrease in the total power consumption of the exoskeleton for the case of PEA and SEA was observed when harmonic drives were employed at the hip and knee joint and ball screws at the ankle joint.

Figure 5.20 presents the comparison of the total weight and average power of the exoskeleton between elastic and rigid actuators when either the harmonic drive was utilized in combination with a belt and pulley drive system or ball screws were used. It was reported in Section 5.3.2 that the power requirements were further decreased when harmonic drives were combined with the belt and pulley drive system. This effect can also be noticed in Figure 5.20 where the total power consumption was decreased. The minimum value of the total mass for the case of PEA was revealed by using harmonic drives combined with a belt and pulley system at the knee joint and ball screws at the hip and ankle joint. But the total power consumption for this particular case was reported to be increased. Considering both the total mass and power consumption, the maximum reduction was recorded by using belt and pulley harmonic drive system at the hip and knee joint and ball screws at the ankle joint. This case was also true for SEA.

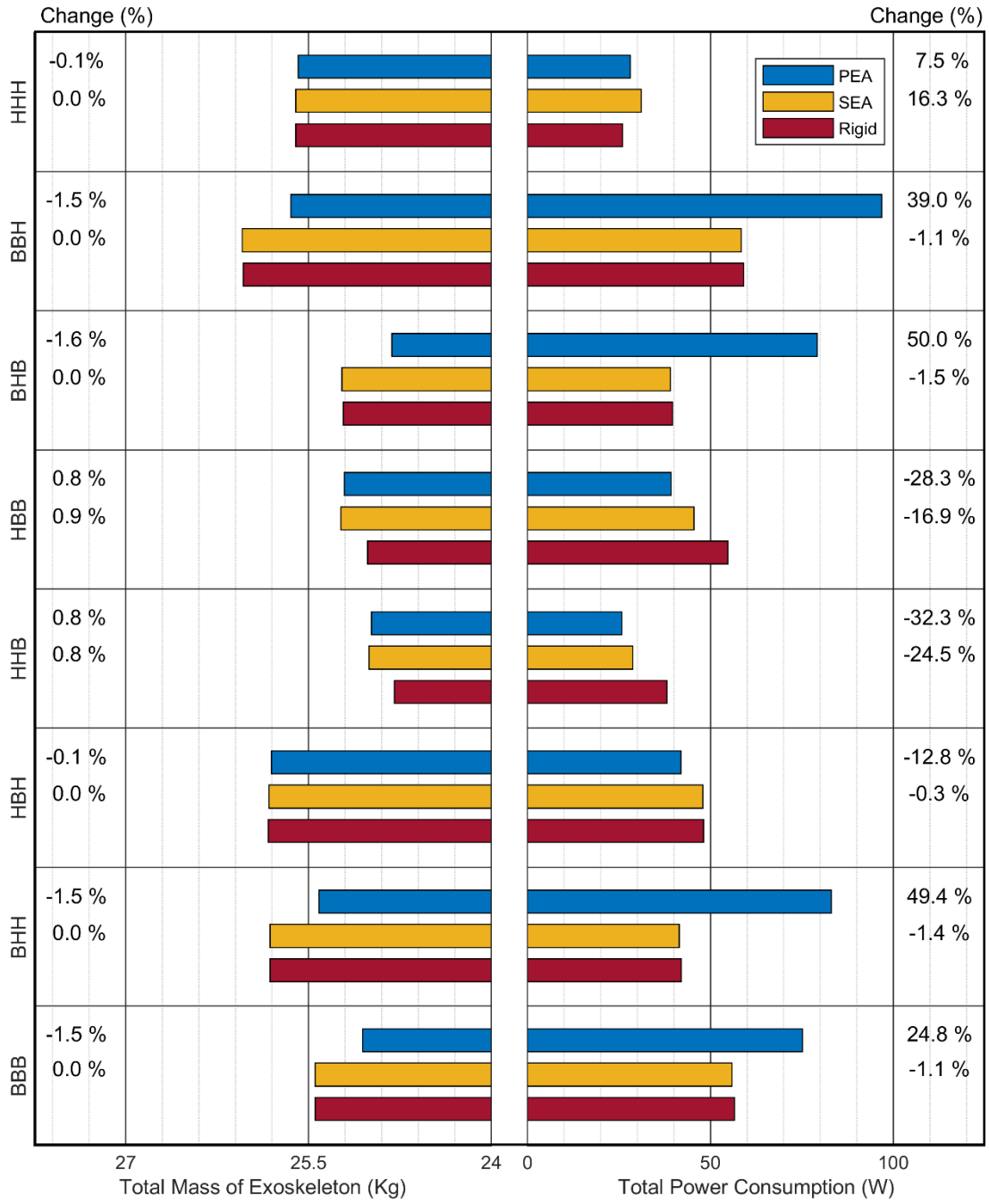

Figure 5.19: The total mass and average total power consumption of the exoskeleton of the optimal elastic and rigid actuation system compared with the single actuator rigid and elastic system using ball screws in an inverted slider mechanism and harmonic drives as the transmission mechanism. It examines the optimal actuation system for various combinations of these transmission systems at the joints.

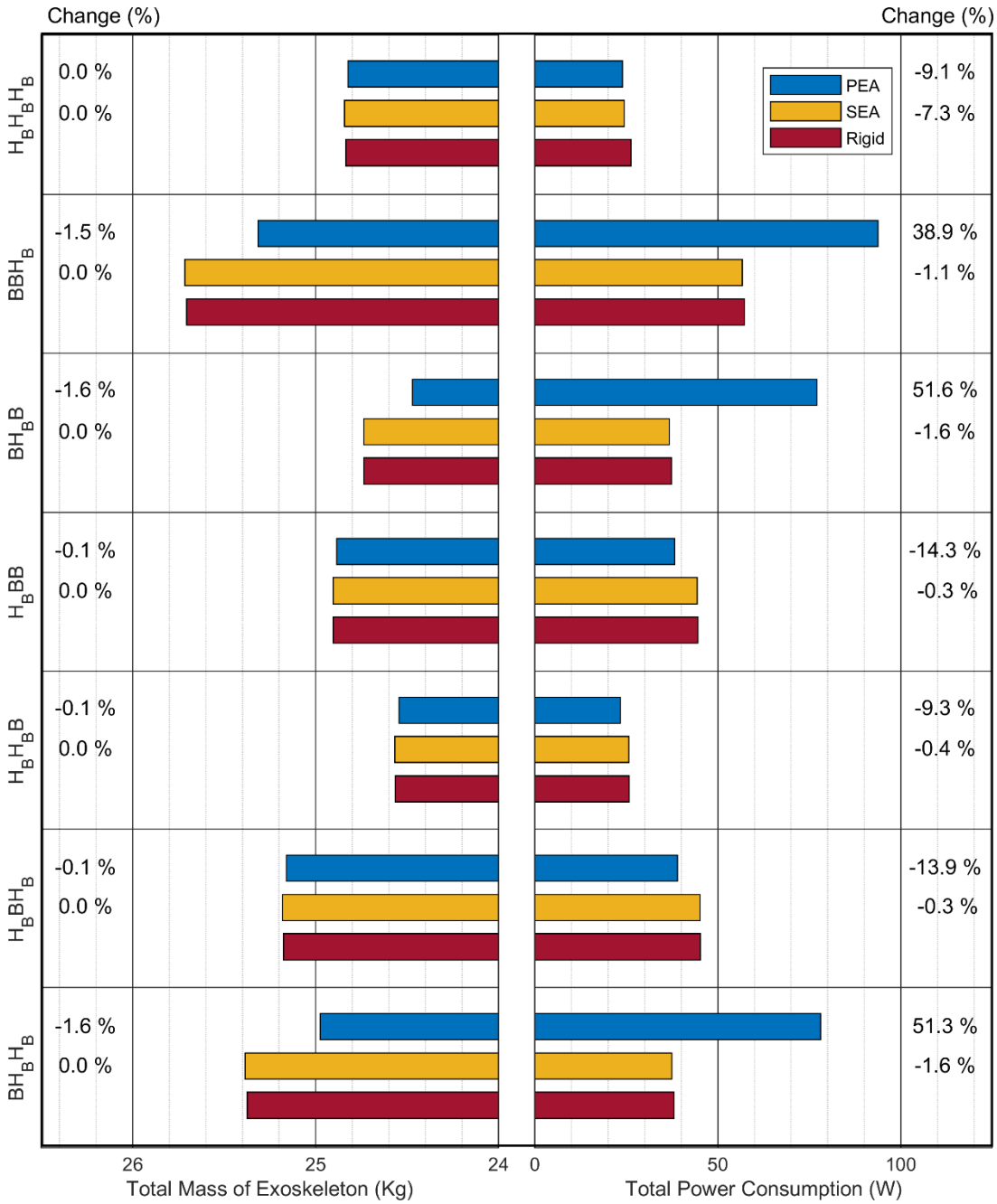

Figure 5.20: The total mass and average total power consumption of the exoskeleton of the optimal elastic and rigid actuation system using ball screws in an inverted slider mechanism and harmonic drives combined with belt and pulley drive system as the transmission mechanism. It examines the optimal actuation system for various combinations of these transmission systems at the joints.

It was mentioned in Section 5.3.5 that using belt and pulley drive system without any other form of the transmission system did not produce favorable results. This effect can be more clearly observed during the mass-power analysis in Figure 5.21. Since the belt and pulley drive system was directly coupled with the electric motor, therefore a larger and bulkier motor was required that also consumes a large amount of power for the desired kinetic

requirements. Therefore, the weight and average power consumption were recorded to be quite high as compared to previous combinations of the transmission systems. By comparing them with the same type of transmission systems for the case of rigid actuators, the total weight of the exoskeleton using elastic actuators were considerably decreased. A similar effect has also been observed on the power consumption of the system.

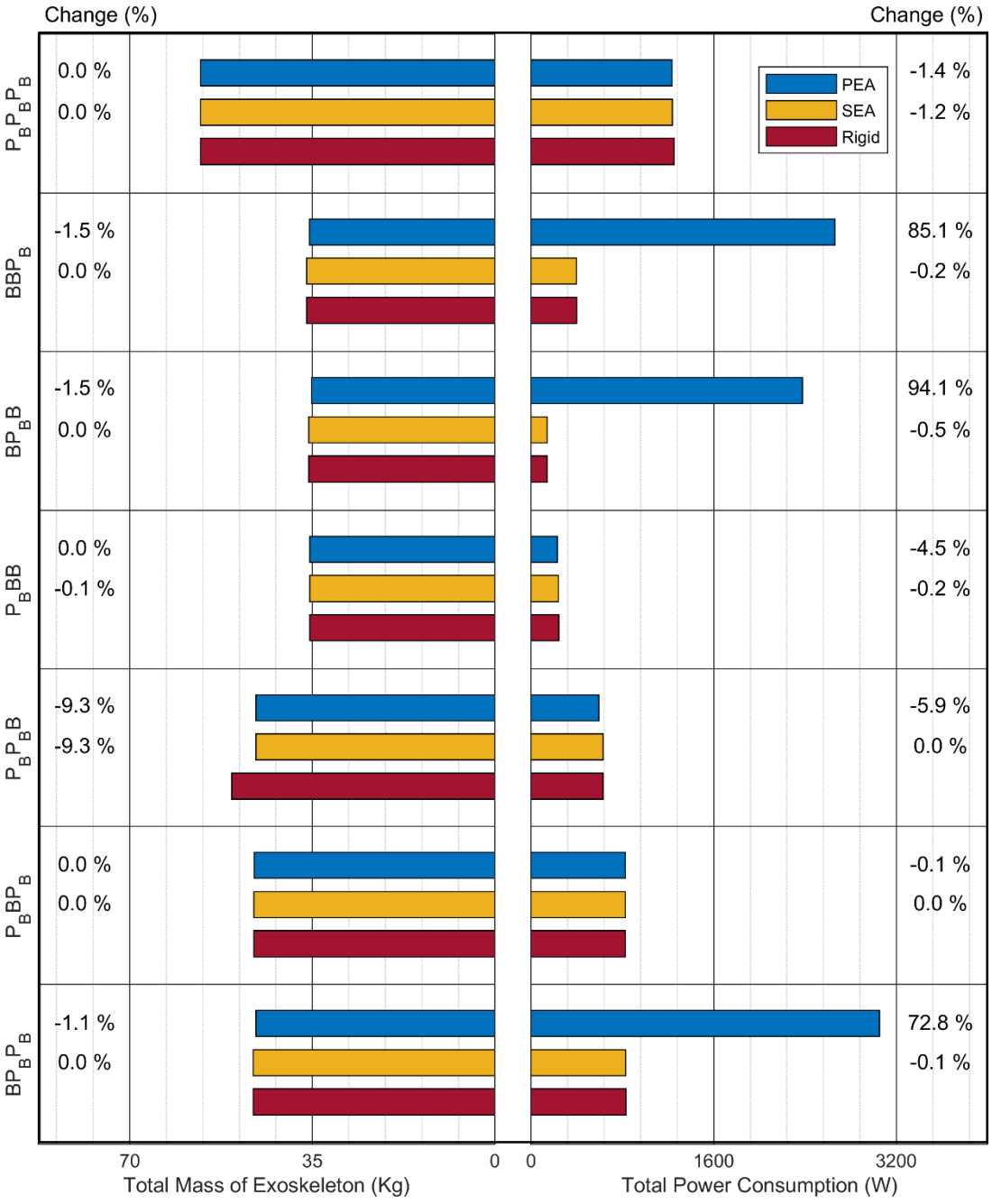

Figure 5.21: The total mass and average total power consumption of the exoskeleton of the elastic and rigid actuation system using ball screws in an inverted slider mechanism and a belt and pulley drive system directly coupled to the motor at some of the joints as the form of the transmission system. It examines the optimal actuation system for various combinations of these transmission systems at the joints.

The optimization algorithm of the elastic actuation system suggests significant weight and power consumption benefits of the assistive robotic exoskeleton. The power consumption was greatly reduced and hence the size of the required battery is decreased. It was observed that at some joints, the weight and power consumption of the individual actuator of the joints was increased but when compared it with the total weight and power of the three joints, it was reduced using PEA. Thus, the overall weight and power consumption of the exoskeleton was decreased. A slight effect on the requirement using SEA has also bring some favorable reductions in the weight and power of the system. Consequently, by using PEA and SEA, a more power efficient and a lightweight exoskeleton has been obtained.

5.4 Summary

This chapter presented an optimum elastic actuation system for an assistive robotic exoskeleton using series and parallel springs. A power efficient and a light weight system was evaluated using elastic actuation system as compared to the rigid actuation system. Different optimization strategies were defined to optimize the stiffness of the springs used in the elastic actuators. A multi-factor spring stiffness optimization approach was developed to optimize the spring based on a number of design factors. After selecting the components of the actuation system in the elastic optimization framework, the springs used in PEA and SEA were optimized to reduce the kinetic requirements of the system. SEA was not able to reduce the requirements significantly however, PEA can bring a significant reduction in the torque and power requirements of the system. A slow walking speed and the use of a fixed spring stiffness for all maneuvers was considered to be the main reason for not achieving large reductions for the case of SEA. Using a variable spring stiffness during the maneuvers could reduce the energy requirements. The spring stiffness obtained using the multi-factor approach was further used in the optimization algorithm to determine the best actuator selection in an elastic actuation system. There was a considerable effect on the weight and power of the system using elastic actuators as compared to the rigid actuation system. Hence, by using elastic actuators, even with a fixed spring stiffness, a more light weight and a power efficient system has been achieved.

Chapter 6
Optimal Design of Dual Actuation Systems

6.1 Introduction

This chapter describes the optimal actuation system for a dual motor and transmission system arranged in an antagonistic setup for assistive robotic exoskeleton. The antagonistic setup of the actuation system was motivated by the muscular system of the human joint working in an antagonistic manner. The concept of muscle redundancy was defined in [200]. The two opposing muscles called antagonist and agonist work together to move a joint but this muscular force is only able to exert a pulling force. When one muscle contracts and other expands, it produces a motion of the joint. Similarly, contracting both sides does not induce any motion but it changes the stiffness of the joint muscles. A similar transformation was realized in this setup of the exoskeleton actuation system. Two actuator units comprised of a pair of motor, the transmission system and a spring are connected to an output link. When a single actuator unit contracts, it produces an output torque but when both units contract, the stiffness of the spring is changed.

Several different architectures have been proposed for the actuators that involve dual motors and transmission systems [51, 201, 202]. In the general form, they can be classified in a parallel or serial classification. In the series classification, the dual actuation system could be realized by connecting the two actuators in a purely serial manner i.e. the ordinary connection of the output of one motor to the input of the other motor or it could be connected by a quasi-antagonistic arrangement. The parallel arrangement can be classified using a purely parallel connection or an agonistic/antagonistic arrangement of the two actuators. The work on this chapter will be based on the agonistic/antagonistic arrangement of the two motors that are connected in parallel, the case will be recorded for the rigid and elastic actuation systems in an assistive robotic exoskeleton, where each of the actuators in the elastic system will consist of a non-linear elastic element.

As introduced in the previous chapter, the variable stiffness elastic actuators could further reduce the torque and power requirements of the system. Therefore, by exploiting the elasticity of the elements, human gait could be performed in much more energy efficient way [51]. It has been recorded by several authors that the energy requirements could be reduced by using

redundant actuation concept when combined with the elastic elements such as springs [203-207]. Several authors implemented the dual elastic actuation concepts for a variable stiffness actuator [55, 170, 171, 208, 209]. The key point is to optimize the stiffness and equilibrium angle of the spring for each operational task. This chapter has employed dual actuators in an antagonistic arrangement for assistive exoskeleton robots that can also adapt the stiffness and equilibrium angle for each manoeuvre in the elastic actuators.

Part of the optimization problem for a dual actuation system using elastic components is to optimize the spring elements. Different optimization methods will be proposed in this study to optimize the parallel and series dual elastic actuators. An algorithm will be implemented to evaluate the optimized stiffness for series elastic actuators and also the equilibrium angle for parallel elastic actuators for each part of the manoeuvre. The spring stiffness optimization techniques recorded in the previous chapter will be applied for the case of dual actuation system but unlike the previous approach, the algorithm in this case will be applied for each set of manoeuvre separately. After recording the optimal spring for series and parallel elastic actuators, the algorithm to achieve the optimal actuation system using two motors and transmission systems will be implemented. The results will be discussed separately for each type of the transmission system employed at each of the joints of the lower limb assistive exoskeleton.

The optimal dual actuation system in an antagonistic arrangement introduces complexity into the system by adding an additional motor and a transmission system. The answers to several problems related to dual actuation in assistive robotic exoskeleton are still unknown. Does introducing the dual actuation concept in the assistive robotic exoskeleton bring benefits in terms of weight and power of the actuation system? How much compromise has to be made in the weight of the actuation system by adding an additional actuator in order to make it more power efficient? If the power requirements are reduced by introducing the variable stiffness actuators, does it also benefit in terms of a lightweight design by introducing lightweight motors? There has to be a criterion to choose an optimal dual actuation system in an antagonistic setup for assistive robotic exoskeleton that is more power efficient and lightweight.

6.2 Methodology

6.2.1 Data Collection using Motion Analysis

In the motion capture experiment, gait data of a healthy subject was collected that performed level ground walking and sit to stand manoeuvre as explained previously in Chapter 4. The torque and power were obtained at each of the joint of the exoskeleton by including the kinetic model of the exoskeleton. The kinetic model of the exoskeleton was adapted according to the actuation redundancy model.

6.2.2 Design Constraints and Components of a Dual Actuation System

The design requirements of the exoskeleton actuation system were explained in detail in Section 4.2 of Chapter 4. The design requirements have to be fulfilled using a dual actuation system in this work. The torque and power requirements at each of the joint of the exoskeleton can be assessed using Table 4.1. The motors and transmission systems in the optimization algorithm of the dual actuation system were formulated similar to those for the single motor case but the focus was on the lighter motors as compared to the single motor version. The complete list of motors and types of transmission systems with various configurations is given in Appendices B and C.

6.2.3 Antagonistic Arrangement of the Actuation System

To fulfil the design requirements, two motors and transmission systems were employed connected together in an antagonistic arrangement at each of the lower limb joints of the exoskeleton actuation system. The schematic diagrams of the antagonistic actuator set up is shown in Figure 6.1.

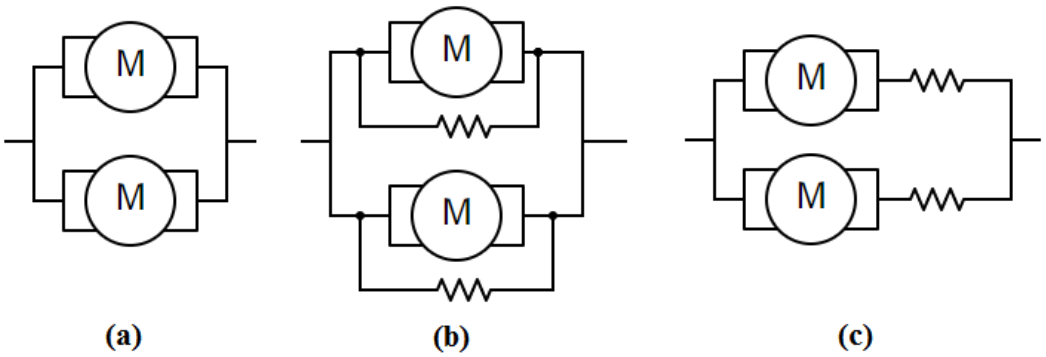

Figure 6.1: Schematic of dual actuators in a (a) rigid system (b) parallel elastic system and (c) series elastic system.

In this chapter, three types of the actuation systems are realised employing the antagonistic arrangement of the setup. This consists of a rigid actuation system as observed in Figure 6.1(a), a parallel elastic actuator (PEA) shown in Figure 6.1(b) and a series elastic actuator (SEA) displayed in Figure 6.1(c), all of them employing two motors and transmission systems. In PEA and SEA, each spring is connected to an individual set of motor and transmission system. Since the dual actuation system arranged in an antagonistic arrangement allows the system to be a variable stiffness actuation system, it was therefore appropriate to use the term (V-PEA) and (V-SEA) to mention the variable parallel elastic actuator and variable series elastic actuator respectively. Each set of a rigid, parallel or series actuator is connected in parallel to its similar pair so that the torque of each unit contributes to the overall torque as represented in Figure 6.2 and given by Eq. 6.1.

$$T_{eq} = T_{m1} + T_{m2} \tag{6.1}$$

Where T_{m1} is the torque from the first motor and T_{m2} is the torque from the second motor. Figure 6.2 shows the working operation of the motors in the antagonistic setup. When both motors rotate in the same direction, the above Eq. (6.1) results in which the two motors support each other and the output link is rotated. The stiffness of the mechanism can be varied by changing the torque contribution of the two motors. When the two motors are synchronised to move in the same direction for equal torque contribution, the highest achievable torque $T_{eq} = 2T_m$ can be obtained. On the other hand, moving the two motors in the opposite direction will result in generating the internal torques and when both motors are synchronized equally to move in the opposite direction, the external output torque at the link will be zero and thus, it will only change the stiffness of the spring. A pre-requisite for this type of the system is to use a non-linear stiffness-displacement characteristic of the spring.

The motor model to be used in this work is derived from the model developed in the previous chapter but modified here for the case of two motors. Hence, the derivation of the equations and notations used will not be discussed in detail here. The torque applied at the rotor of the first motor will be given by Eq. (6.2).

$$T_{m1} = T_{r1} + J_1\ddot{\theta}_{m1} + c_1\dot{\theta}_{m1} \tag{6.2}$$

In Eq. (6.2), T_{r1} is the output torque of the first motor, J_1 is the inertia of the mechanical parts including motor, shaft and the connecting parts related to

the first motor, c_1 is the viscous damping of the first motor. $\dot{\theta}_{m1}$ and $\ddot{\theta}_{m1}$ represents the required angular velocity and angular acceleration of the single motor respectively.

Similarly, the torque applied at the second motor is given by Eq. (6.3)

$$T_{m2} = T_{r2} + J_2\ddot{\theta}_{m2} + c_2\dot{\theta}_{m2} \quad (6.3)$$

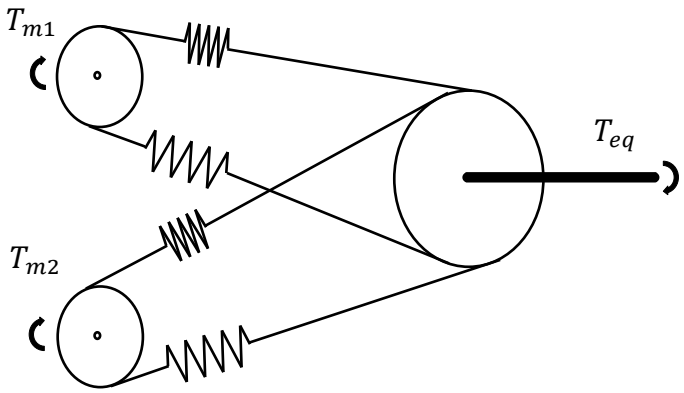

(a) Motors moving in the same direction

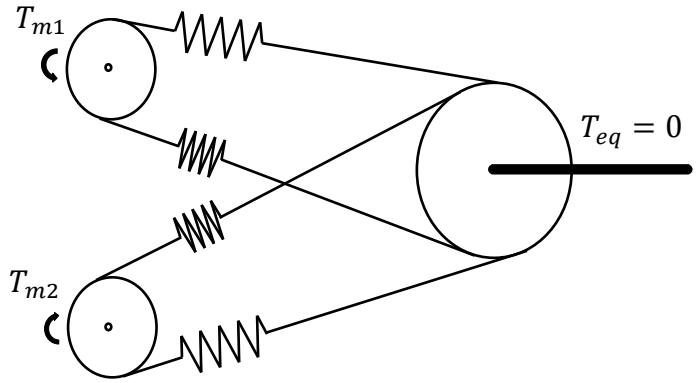

(b) Motors moving in the opposite direction

Figure 6.2: Illustration of the two modes of operation of the antagonistic setup of the actuators. In (a) the same direction rotation of motors induces higher torque to the output link. (b) opposite rotation of motors generates internal torque that is cancelled out and the stiffness of the spring is increased.

The torque from Eq. (6.2) and Eq. (6.3) applied on an individual motor will be substituted in Eq. (6.1) to account for the total equivalent torque that can be applied on the two motors, thus Eq. (6.4) results

$$T_{eq} = (T_{r1} + J_1\ddot{\theta}_{m1} + c_1\dot{\theta}_{m1}) + (T_{r2} + J_2\ddot{\theta}_{m2} + c_2\dot{\theta}_{m2}) \quad (6.4)$$

Since the two motors selected will be similar, therefore T_{m1}will be equal to T_{m2}. The torque applied on a single motor as given by Eq. (6.2) and Eq. (6.3) should fall within the allowable limits of that motor. The limits of the motors winding line, temperature line and current line is explained in detail in Section 4.7 and given by Eq. (4.2) to Eq. (4.4) in Chapter 4.

Similarly, the power consumption of a single motor can be calculated by Eq. (6.5)

$$P_{m1} = \begin{cases} \frac{T_{m1}^2}{K_{m1}^2 \gamma_1} + T_{m1}\dot{\theta}_{m1} \;\; P_{m1} \geq 0 \\ \frac{T_m^2 \gamma_1}{K_{m1}^2} + T_{m1}\dot{\theta}_{m1} \;\; P_{m1} < 0 \end{cases} \tag{6.5}$$

And for the second motor, Eq. (6.6) gives

$$P_{m2} = \begin{cases} \frac{T_{m2}^2}{K_{m2}^2 \gamma_2} + T_{m2}\dot{\theta}_{m2} \;\; P_{m2} \geq 0 \\ \frac{T_m^2 \gamma_2}{K_{m2}^2} + T_{m2}\dot{\theta}_{m2} \;\; P_{m2} < 0 \end{cases} \tag{6.6}$$

Therefore, the equivalent power will result in combining the powers from the two motors.

$$P_{eq} = \begin{cases} \frac{T_{m1}^2}{K_{m1}^2 \gamma_1} + T_{m1}\dot{\theta}_{m1} + \frac{T_{m2}^2}{K_{m2}^2 \gamma_2} + T_{m2}\dot{\theta}_{m2} \quad P_{eq} \geq 0 \\ \frac{T_{m2}^2 \gamma_1}{K_{m1}^2} + T_{m1}\dot{\theta}_{m1} + \frac{T_{m2}^2 \gamma_2}{K_{m2}^2} + T_{m2}\dot{\theta}_{m2} \quad P_{eq} < 0 \end{cases} \tag{6.7}$$

For the case of V-SEA, the power obtained is given by Eq. (6.8) and Eq. (6.9) for each motor respectively,

$$P1_{SEA} = T_{m1}\left(\dot{\theta}_{e1} + \frac{\dot{T}_{s1}}{K_{s1}}\right) \tag{6.8}$$

$$P2_{SEA} = T_{m2}\left(\dot{\theta}_{e2} + \frac{\dot{T}_{s2}}{K_{s2}}\right) \tag{6.9}$$

Where $\dot{\theta}_{e1}$ and $\dot{\theta}_{e2}$ are the total external angular velocity for the case of each motor, $\dot{T}_{s1}$ is the derivative of the spring torque related to the first series elastic actuator and $\dot{T}_{s2}$ is the derivative of the spring torque in the second V-SEA. K_{s1} and K_{s2} represent the spring stiffness.

The required peak power of V-SEA for each motor is calculated by Eq. (6.10) and Eq. (6.11),

$$P1_{SEA_{peak}} = \max\left(\left|T_{m1}\left(\dot{\theta}_{e1} + \frac{\dot{T}_{s1}}{K_{s1}}\right)\right|\right) \tag{6.10}$$

$$P2_{SEA_{peak}} = \max\left(\left|T_{m2}\left(\dot{\theta}_{e2} + \frac{\dot{T}_{s2}}{K_{s2}}\right)\right|\right) \quad (6.11)$$

The objective is to determine the spring stiffness that gives the minimum value of the required peak power in Eq. (6.10) and Eq. (6.11) for each motor. In order to estimate the required energy consumption, the RMS power of a single motor is used which is given by Eq. (6.12).

$$P_{SEA_{rms}} = \sqrt{\frac{\sum_{i=1}^{n}(P1_{SEA_i})}{n}} \quad (6.12)$$

As the two motors will be similar, therefore Eq. (6.12) can be calculated either using $P1_{SEA}$ given by Eq. (6.10) or $P2_{SEA}$ given by Eq. (6.11).

Similarly, the torque produced by each motor using V-PEA is given by Eq. (6.13) and Eq. (6.14) respectively, derivations of which can be found in Chapter 5.

$$T1_{PEA} = T_{m1} - K_{p1}(\Delta\theta_o - \theta_{e1}) \quad (6.13)$$

$$T2_{PEA} = T_{m2} - K_{p2}(\Delta\theta_o - \theta_{e2}) \quad (6.14)$$

Where K_{p1} and K_{p2} are the parallel spring stiffness related to first V-PEA and second V-PEA. $\Delta\theta_o$ is the equilibrium angle of the spring, θ_{e1} and θ_{e2} is the equilbruim angle of the first and second parallel spring.

The power required for the case of V-PEA by each motor can be obtained by using Eq. (6.15) and Eq. (6.16)

$$P1_{PEA} = \left(T_{m1} - K_{p1}(\Delta\theta_o - \theta_{e1})\right)\dot{\theta}_{e1} \quad (6.15)$$

$$P2_{PEA} = \left(T_{m2} - K_{p2}(\Delta\theta_o - \theta_{e2})\right)\dot{\theta}_{e2} \quad (6.16)$$

The peak and RMS value of torque and power can be calculated for V-PEA using Eq. (6.12) to Eq. (6.15) for each motor and is given by Eq. (6.17) to Eq. (6.22).

$$T1_{PEA_{peak}} = \max\left(\left|T_{m1} - K_{p1}(\Delta\theta_o - \theta_{e1})\right|\right) \quad (6.17)$$

$$T2_{PEA_{peak}} = \max\left(\left|T_{m2} - K_{p2}(\Delta\theta_o - \theta_{e2})\right|\right) \quad (6.18)$$

$$T_{PEA_{rms}} = \sqrt{\frac{\sum_{i=1}^{n}(T1_{PEA_i})}{n}} \quad (6.19)$$

$$P1_{PEA_{peak}} = \max\left(\left|T_{m1} - K_{p1}(\Delta\theta_o - \theta_{e1})\,\dot{\theta}_{e1}\right|\right) \quad (6.20)$$

$$P2_{PEA_{peak}} = \max\left(\left|T_{m2} - K_{p2}(\Delta\theta_o - \theta_{e2})\,\dot{\theta}_{e2}\right|\right) \quad (6.21)$$

$$P_{PEA_{rms}} = \sqrt{\frac{\sum_{i=1}^{n}(P1_{PEA_i})}{n}} \tag{6.22}$$

As the torque and power from both motors are the same, therefore the values related to the first V-PEA was only mentioned in Eq. (6.19) and Eq. (6.22) to calculate the RMS value.

6.2.4 Algorithm to Optimize the Stiffness of the Spring

An algorithm has been developed to optimize the stiffness of the spring. The spring stiffness optimization takes the advantage of the antagonistic setup of the actuation system in which the spring stiffness can be varied as it is composed of a non-linear spring. It was observed in Chapter 5, that although using a fixed spring stiffness during sit to stand and walking reduces the kinetic parameters of the exoskeleton joint but it also increased torque and power requirement of the joint at some instances during the operation. Hence, a variable spring stiffness is suggested that will significantly reduce the joint requirements. Adapting stiffness during the entire path was recorded to be inefficient during the simulation experiments conducted by [210], therefore, the spring stiffness was not varied during the complete trajectory but instead, it was only modified during the transition between sit to stand (SS), swing (SW) and stance phase (ST) of the gait and kept to a fixed stiffness value during each of these three manoeuvres.

It was analysed in [186], that PEA was able to reduce both the torque and power requirement of the joint while SEA was only able to reduce the power of the joint. Furthermore, in order to optimize the parallel spring, the stiffness and the equilibrium angle given by Eq. (6.13) to Eq. (6.16) needs to be optimized. Hence, five methods to optimize PEA were investigated. On the other hand, SEA requires only its spring stiffness to be optimized and it can only alter the power of the joint, therefore, three optimization methods for series spring were developed. Before explaining the spring optimization algorithm, the methods included in the spring optimization will be investigated in detail.

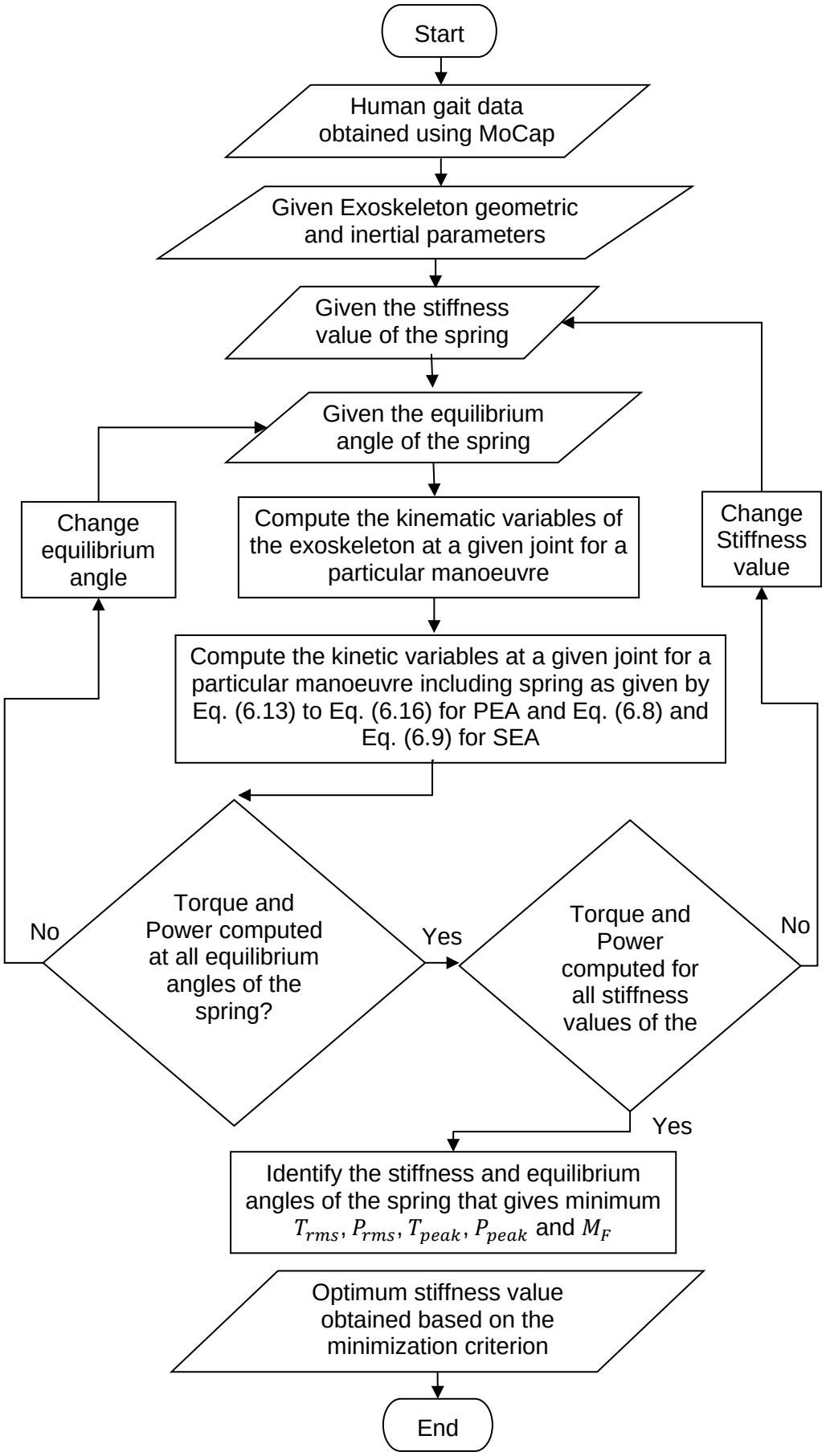

Figure 6.3: Algorithm for the optimization of the spring in a dual elastic actuator

The first method developed during parallel spring optimization is the determination of parallel spring stiffness and equilibrium angle that will minimize the peak torque of the joint. It uses Eq. (6.17) and Eq. (6.18) to determine the peak torque of the joint and then determines the stiffness and equilibrium angle that will minimize the peak torque of the joint. The second method makes use of the RMS torque of the joint and uses Eq. (6.19) to determine the RMS torque. The third method that was applied to both parallel and series spring was the peak power optimization method in which peak power was employed as the spring optimization criterion. The maximum torque can be calculated from Eq. (6.10) and Eq. (6.11) for the case of SEA and Eq. (6.20) and Eq. (6.21) for PEA. The fourth method put forward for SEA and PEA was the RMS power calculated from Eq. (6.12) and Eq. (6.22) respectively. Finally, a multi-factor optimization criterion M_F was developed that takes into account minimization of all variables together i.e. the peak and RMS torque and power of the joint calculated from Eq. (6.10) to Eq. (6.12) and Eq. (6.17) to Eq. (6.22) for SEA and PEA respectively and is given by Eq. (6.23).

$$M_F = T_{rms}/\max(T_{rms}) + P_{rms}/\max(P_{rms}) + P_{peak}/\max(P_{peak}) + T_{peak}/\max(T_{peak}) \quad (6.23)$$

Where $\max(T_{rms})$, $\max(P_{rms})$, $\max(P_{peak})$ and $\max(T_{peak})$ is the maximum RMS torque and power and peak power and torque respectively at a particular manoeuvre. As the two motors are similar, therefore, the torque and power from only one motor will be considered for the multi-factor optimization criterion in Eq. (6.23). The flow chart of the spring optimization algorithm is shown in Figure 6.3. The required human gait data and exoskeleton geometric and inertial parameters are fed into the spring optimization algorithm. It then computes the kinematic and kinetic variables at a given stiffness of the spring and if it computes for PEA, the algorithm also takes into account the given equilibrium angle of the spring at a particular joint for a particular manoeuvre i.e. SS, SW or ST. Depending upon the spring optimization method and also whether it was relevant to SEA or PEA, it then calculates the parameters of interest. This procedure is repeated for all manoeuvres and for all stiffness and equilibrium angles. Finally, the stiffness value of SEA and the stiffness value and the equilibrium angle for the case of PEA are obtained depending upon the optimization criteria. The same principle applies to all the three joints of the lower limb of assistive robotic exoskeleton system. The stiffness and equilibrium angle of the spring at a particular joint applies to both springs of the joints.

6.2.5 Algorithm to Optimize the Dual Actuation System

After determining the stiffness and equilibrium position of the spring, the motors and transmission systems were computed in the algorithm to optimize the actuation system based on the antagonistic arrangement of the system. The algorithm included list of motors and transmission systems as described earlier in Section 6.2.2. The three performance variables for the actuation system were the minimum total weight of the exoskeleton, the minimum total power consumption and to maximize the ability of the exoskeleton to carry user's weight.

Different weightage was given to the three variables to obtain the objective function of the optimization algorithm. The mathematical expression of the objective function for dual rigid $O_{f_{rg}}$ and dual elastic actuation system $O_{f_{els}}$ are shown respectively in Eq. (6.24) and Eq. (6.25).

$$O_{f_{rg}} = \left(0.3 \times \frac{U_c}{\max(U_c)}\right) - \left(0.3 \times \frac{P_c}{\max(P_c)}\right) - \left(0.5 \times \frac{W_{exo}}{\max(W_{exo})}\right) \quad (6.24)$$

$$O_{f_{els}} = \left(0.3 \times \frac{U_c}{\max(U_c)}\right) - \left(0.5 \times \frac{P_c}{\max(P_c)}\right) - \left(0.3 \times \frac{W_{exo}}{\max(W_{exo})}\right) \quad (6.25)$$

Where U_c is the user carrying capacity of the exoskeleton, P_c represents the total power consumption and W_{exo} is the total weight of the exoskeleton. In the formulation of the objective functions, the normalized values for each of the variables were used. The flowchart of the optimization algorithm was elaborated in Figure 6.4.

As can be observed in Figure 6.4, the human gait data of a healthy subject along with the exoskeleton geometric and inertial parameters were induced in the optimization algorithm. This algorithm was developed for rigid actuation, parallel elastic actuator (PEA) and a series elastic actuator (SEA). Depending upon the type of the actuation, it calculates the kinematic and kinetic parameters at a given joint. For the case of PEA and SEA, the spring stiffness and equilibrium angle were fed into the kinetic variables equation as determined from Section 6.2.4. According to the algorithm, it starts with the knee joint of the exoskeleton. Therefore, after evaluating the above parameters, the next step involves selection of the knee motor from the list of motors. Since it involves two actuators in an antagonistic setup, the algorithm will select two similar motors and then combine the two motors to obtain the equivalent motor torque, velocity and acceleration. After selecting two similar motors, the algorithm also selects two transmission systems and determine the required motor torque, velocity and acceleration.

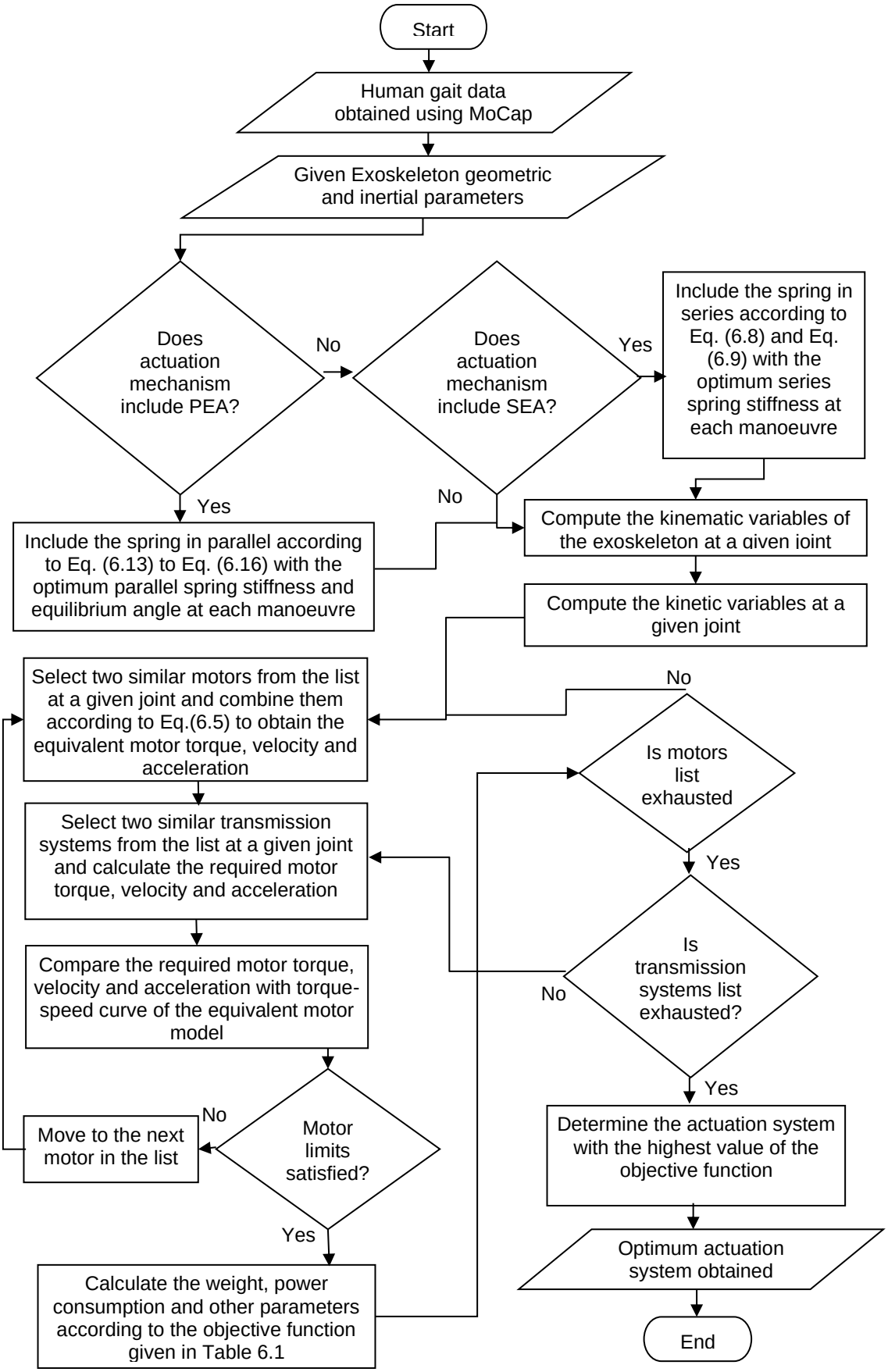

Figure 6.4: Optimization algorithm for the dual actuation system in an antagonistic arrangement of the lower limb exoskeleton at a particular joint

This required motor torque and velocity is compared with the equivalent torque speed curve of the two motors. If the equivalent motor limits obtained from the two motors are satisfied, it calculates the objective function of that particular candidate actuator giving weightage to the variables according to Table 6.1 and proceeds for the next available candidate actuator. If the motor limits are violated by any candidate actuator, the algorithm does not include that particular candidate actuator. The algorithm is repeated until all the candidate actuators are inspected and assigned a value of the objective function. The candidate actuator with the highest value of the objective function is the optimal solution at this phase.

As pointed out earlier, this algorithm is initially applied to determine the optimal system for the knee joint while assuming the hip and ankle actuators to be the most lightweight system in the list. After determining the optimal actuator at the knee joint, it advances to the ankle joint and the same above procedure of the algorithm is repeated. At this point, the knee actuator has already been obtained from the previous step but the hip actuator is again assumed to be the most lightweight system. As the algorithm finishes computing for the ankle joint, it proceeds towards the hip joint where the algorithm assumes the knee and ankle joint to be the ones obtained in the previous steps and determines the most optimal actuator for the hip joint by following the above procedure as depicted by the algorithm flow chart in Figure 6.4. This procedure is repeated again for the knee joint but this time the hip and ankle actuators are used from the already assessed actuators. The algorithm keeps on repeating until the actuators stops changing the candidate actuator at each of the individual joint.

Table 6.1: Weightage of the variables used in the objective function

Variables	Weightage	
	Dual Rigid actuation system	Dual Elastic actuation system
Power consumption	-0.3	-0.5
Mass of the exoskeleton	-0.5	-0.3
User carrying ability	0.3	0.3

It should be noted that in order to calculate the objective function, the three variables of interest are normalized first and then multiplied by the weighting factor given in Table 6.1. The power consumption is given a higher

weightage in the dual elastic actuation system than the rigid actuation system because a power efficient system is considered to be the main benefit of the dual actuation system with the elastic elements as will be explained later.

6.3 Results and Discussion

The results have been obtained by applying the algorithms described in Section 6.2.4 for spring stiffness optimization and Section 6.2.5 in order to determine the optimal actuation system in an antagonistic arrangement. The effect on the torque and power requirement at the hip, knee and ankle joint using different optimization criteria for spring stiffness will be discussed. The results of these requirements will be compared with the requirements of the rigid actuation system. Using the criteria for spring stiffness, optimal actuation system in an antagonistic arrangement will be determined and the outcomes of dual actuators will be discussed with the single motor optimization results.

6.3.1 Spring Stiffness Optimization

The criterion depicted in Figure 6.3 is applied based on the five optimization methods for parallel spring and three methods for the series spring. The optimal spring stiffness and the equilibrium angle of the spring assessed in each of the above cases is shown in Table 6.2.

The results depicted in Table 6.2 are for each of the three manoeuvres i.e. SS, SW and ST phase since the dual actuator system in an antagonistic arrangement allows the system to be a variable stiffness actuator. The stiffness of the parallel elastic actuator (V-PEA) was observed to be lower than the series elastic actuator (V-SEA). This is because the parallel elastic actuator has to follow the full trajectory along the joint motion. It was noticed that the torque and power required for the case of V-SEA was further reduced when compared with the case of fixed series elastic actuator that was evaluated in Chapter 5 because for the case of V-SEA, stiffness could vary while performing different manoeuvres. As the exoskeleton was intended for slow walking i.e. the speed of the user wearing a Rex Bionics exoskeleton was employed as a reference value as mentioned in the design requirements, therefore V-SEA was only able to partially reduce the requirements at the lower limb joints. For both the cases of V-SEA and V-PEA, the stiffness during the stance phase was recorded higher as compared to the other manoeuvres. The maximum torque at the joints was

minimized with a negative value of the equilibrium angle. This indicates that the spring should be preloaded before its operation. The stiffness value at the ankle joint was considerably lower for the case of V-PEA. The multi-factor optimization criterion determined the best possible value of the spring stiffness and equilibrium angle so that all the parameters get close to their lowest value as much as possible.

Table 6.2: The optimized spring stiffness and equilibrium angle of V-PEA and V-SEA for different spring optimization criterion

PEA		Hip		Knee		Ankle	
		K_p (Nm/rd)	θ (deg)	K_p (Nm/rd)	θ (deg)	K_p (Nm/rd)	θ (deg)
Minimizing τ_{peak}	Sit to Stand	7	-4	17	-4	1	-28
	Swing phase	46	21	1	134	1	51
	Stance phase	90	2	-	-	4	217
Minimizing τ_{rms}	Sit to Stand	8	3	17	-3	1	-172
	Swing phase	41	21	1	175	1	54
	Stance phase	3	74	-	-	3	269
Minimizing P_{peak}	Sit to Stand	8	1	18	-2	1	-146
	Swing phase	38	22	1	124	1	55
	Stance phase	-	-	-	-	3	332
Minimizing P_{rms}	Sit to Stand	9	7	17	-4	1	-176
	Swing phase	35	22	1	130	1	54
	Stance phase	-	-	-	-	3	318
Multi-factor Optimization M_F	Sit to Stand	8	2	17	-4	1	-146
	Swing phase	38	22	1	125	1	54
	Stance phase	90	2	-	-	3	289
SEA		K_s (Nm/rad)		K_s (Nm/rad)		K_s (Nm/rad)	
Minimizing P_{peak}	Sit to Stand	108		328		1803	
	Swing phase	4516		4478		4799	
	Stance phase	-		-		5711	
Minimizing P_{rms}	Sit to Stand	29		90		3639	
	Swing phase	4315		4569		4987	
	Stance phase	-		-		1691	
Multi-factor Optimization M_F	Sit to Stand	108		328		1799	
	Swing phase	4127		4987		4125	
	Stance phase	-		-		5711	

6.3.2 Torque and Power Requirements at the Hip Joint

The torque and power requirements at the hip joint evaluated for the five optimization methods during the three manoeuvres of V-PEA and V-SEA compared with the requirements of the rigid actuation system is shown in Figure 6.5. As V-SEA was only able to reduce the power, therefore, for the case of T_{peak} and T_{rms} minimization criteria, only V-PEA will be discussed. By using the method of T_{peak} minimization, the peak torque and power were significantly reduced using V-PEA at the hip joint. The RMS value of torque and power was also considerably less. The maximum reduction was recorded in the RMS power value i.e. 90% as compared to the requirement of P_{rms} for rigid actuation system. The outcomes for T_{rms} minimization were also similar with the maximum reduction of 95 % in the P_{rms} value. T_{rms} was also significantly reduced. With regards to the results evaluated during P_{peak} minimization, P_{rms} was the variable again that has attained the maximum reduction in its value both for V-PEA and V-SEA. All variables for V-PEA and V-SEA were reduced, however V-PEA and V-SEA have shown better reductions during sit to stand operation as compared to the walking phase. There was a reduction in the P_{peak} and P_{rms} value of 11% and 12% respectively during sit to stand manoeuvre.

When comparing the P_{rms} minimization criterion outcomes, all variables demonstrated a reduction in V-PEA, however, V-SEA has shown partial reductions during sit to stand and swing phase. Similar sequence of results have been assessed for the multi-factor optimization case in which V-PEA and V-SEA showed reduction in the variables. However, the highest reduction considering all the variables were evaluated to be the maximum in this case both for V-PEA and V-SEA. It should be noted here that the V-PEA and V-SEA were able to reduce the variables during all three manoeuvres as compared to the fixed elastic actuators. In the latter case, some variables were increased in PEA and SEA.

6.3.3 Torque and Power Requirements at the Knee Joint

Figure 6.6 depicts the torque and power requirement at the knee joint for different minimization criterion during each of the three manoeuvres. The torque and power analysed using V-PEA and V-SEA are compared with the torque and power requirements of the rigid actuation system. As recorded in Figure 6.6, the RMS value of torque and power was reduced to 96% as compared to the rigid actuation system during the T_{peak} minimization criteria.

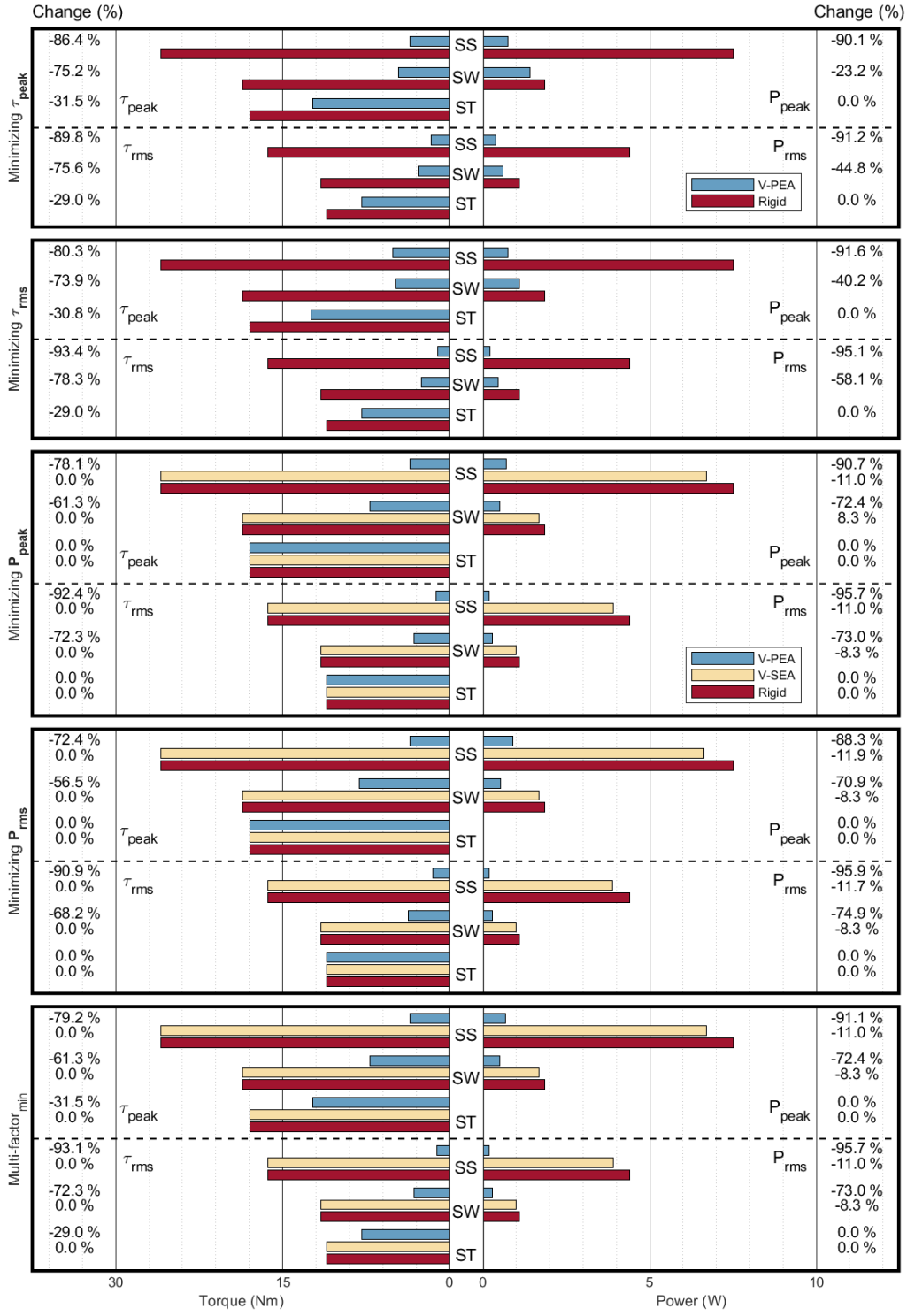

Figure 6.5: Torque and Power requirements at the hip joint during sit to stand (SS), swing (SW) and stance (ST) phase of the gait for V-PEA, V-SEA and rigid actuation system for various minimization criteria. The values of the variables T_{peak}, T_{rms}, P_{peak} and P_{rms} are shown with the spring stiffness and equilibrium angle optimized for each type of the minimization criterion.

The peak value of torque and power also indicated a reduction of 94% and 96% respectively during sit to stand. The swing and stance phase also

displayed a reduction in the peak and RMS value of the torque and power. The T_{rms} minimization criteria also revealed similar results with the torque and power reduced to 95% during sit to stand operation. The P_{peak} mimization showed a similar trend for the case of V-PEA, however, V-SEA showed a reduction of approximately 10% during the manoeuvres. A better reduction was observed during sit to stand than walking for the case of V-SEA. This was also true for P_{rms} minimization criteria. The multi-factor minimization criterion showed an advantage over other minimization criteria by reducing all variables as close to their minimum values as possible. At the knee joint, V-PEA and V-SEA estimated a reduction in all the manoeuvres for all minimization criteria similar to the hip joint.

6.3.4 Torque and Power Requirements at the Ankle Joint

The results at the ankle joint for V-PEA, V-SEA and rigid actuation system can be observed in Figure 6.7 relating the five minimization criteria. Although V-PEA and V-SEA were able to reduce the torque and power requirements of the joints but their benefits were noticed to be less prominent at the ankle joint as compared to the hip and knee joints. During T_{peak} minimization, the peak torque and power were reduced by 7% and 17% respectively while performing sit to stand manoeuvre but a substantial amount of reduction was observed during swing and stance phase.

The RMS value of torque and power revealed a slight decrease during sit to stand but a noticeable difference was observed during walking. The peak values of torque and power were increased during T_{rms} minimization criterion during the sit to stand manoeuvre. However, the swing and stance phase demonstrated a reduction. The RMS value of torque and power showed a decreasing trend in all the manoeuvres for this case. The maximum reduction was 84% for P_{peak} during swing phase. With regards to the minimization criterion of P_{peak}, V-SEA only showed a marginal difference to the torque and power requirements but V-PEA was able to bring significant reduction in all the variables as compared to rigid actuation system. The maximum difference of 85% in P_{rms} was specified during swing phase. Similar trend was observed for the case of P_{rms} minimization criteria. During the multi-factor minimization criteria, all variables were reduced similar to the case for hip and knee joint.

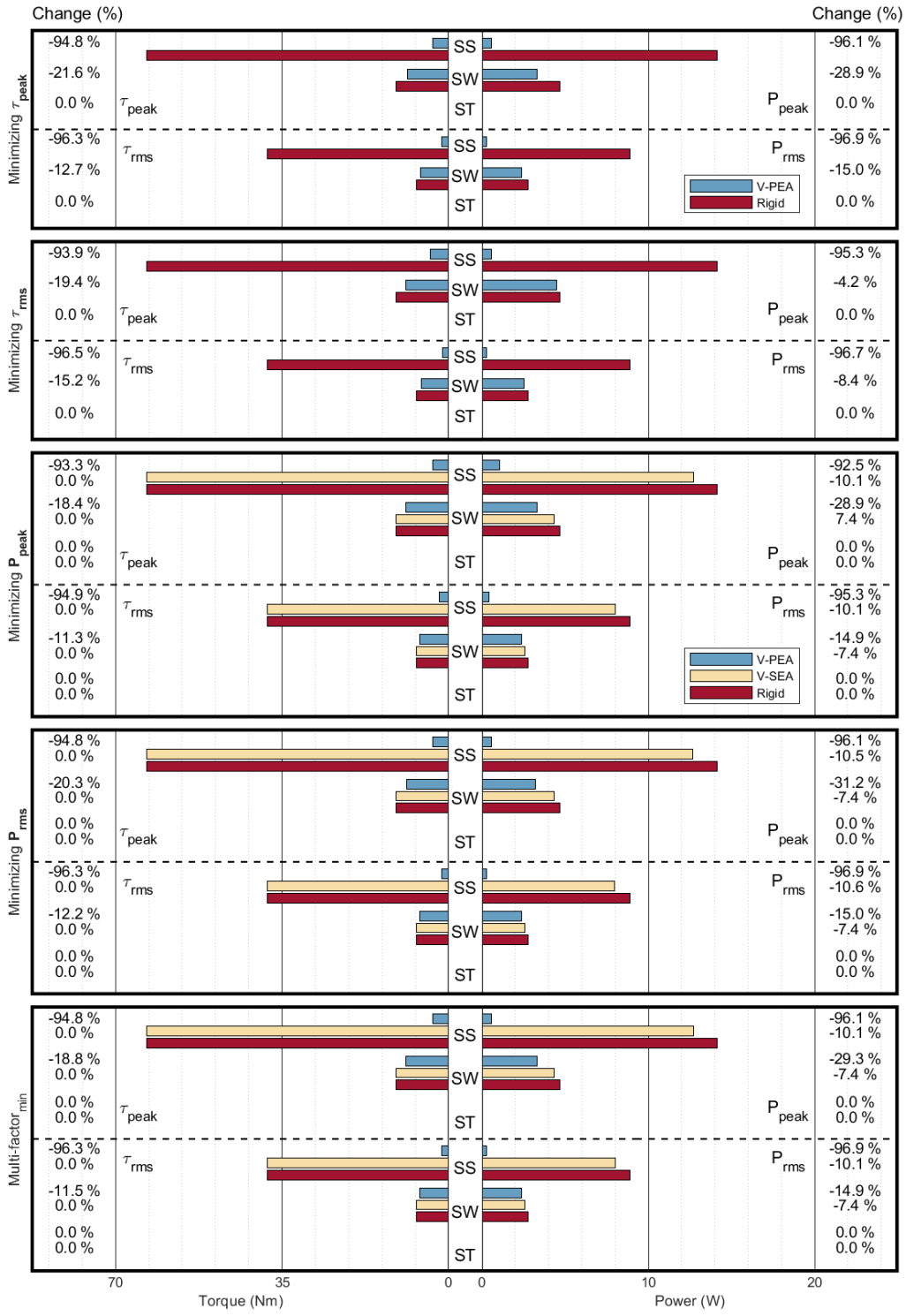

Figure 6.6: Torque and Power requirements at the knee joint during sit to stand (SS), swing (SW) and stance (ST) phase of the gait for V-PEA, V-SEA and rigid actuation system for various minimization criteria. The values of the variables T_{peak}, T_{rms}, P_{peak} and P_{rms} are shown with the spring stiffness and equilibrium angle optimized for each type of the minimization criterion.

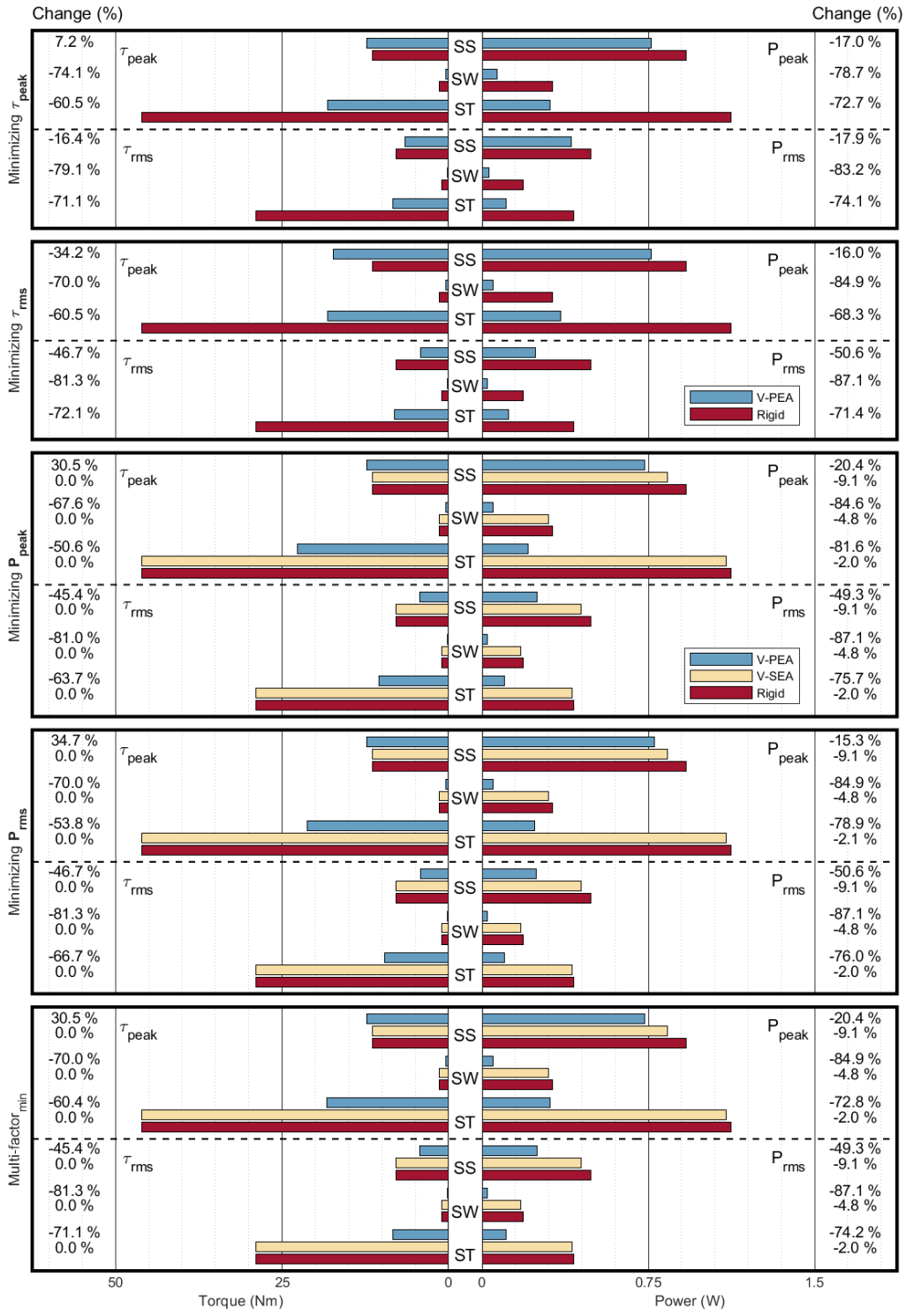

Figure 6.7: Torque and Power requirements at the ankle joint during sit to stand (SS), swing (SW) and stance (ST) phase of the gait for V-PEA, V-SEA and rigid actuation system for various minimization criteria. The values of the variables T_{peak}, T_{rms}, P_{peak} and P_{rms} are shown with the spring stiffness and equilibrium angle optimized for each type of the minimization criterion.

During the spring optimization, it appeared that V-PEA could drastically reduce the torque and power requirements at each of the joints. Although,

the reduction was indicated less at the ankle joint but still V-PEA demonstrated better results as compared to the fixed stiffness PEA. The reduction at the hip and knee joints was 90% as compared to the rigid actuation during most of the manoeuvres and hence it suggests that a smaller and less power consuming motors could be realized with V-PEA. The weight and power comparison of dual actuators with the single actuator case will be discussed in Section 6.3.7. On the other hand, V-SEA also reflected better and desirable results as compared to the fixed SEA. However, as pointed out earlier, the slow speed of the manoeuvres was the reason for V-SEA not producing large reduction in the torque and power requirements.

6.3.5 Simulation Results

Simulation results were obtained from the exoskeleton model as explained in Section 5.4 that was developed in SolidWorks. The torque and power requirements at the exoskeleton model were obtained at each of the lower limb joints by incorporating a rigid and elastic system into the model.

6.3.5.1 Variable Parallel Elastic Actuator (V-PEA)

The torque and power were evaluated at each of the joints of the lower limb of the exoskeleton by incorporating V-PEA for the five optimization methods discussed in Section 6.4.3. The simulation results recorded can be visualized in Figures 6.8 to 6.10 for the case of V-PEA. The results elaborated the torque and power requirements at the joints for each of the optimization methods employed to optimize the parallel spring.

Hip Joint

As it is clear from Figure 6.8, at the hip joint, the torque and power were reduced by employing V-PEA for each of the optimization methods used. The torque requirements of V-PEA by using T_{rms} optimization method showed the greatest reduction during sit to stand but the power reduction was not the highest by using this method. The graph of the torque and power using the multi-factor optimization method can be observed to be running in between the graphs by all other optimization methods. This showed that the multi-factor optimization method was able to reduce the overall requirement considering all variables. It is evident from Figure 6.8(a) and Figure 6.8(b) that V-PEA was able to significantly reduce the torque and power requirements during sit to stand manoeuvre.

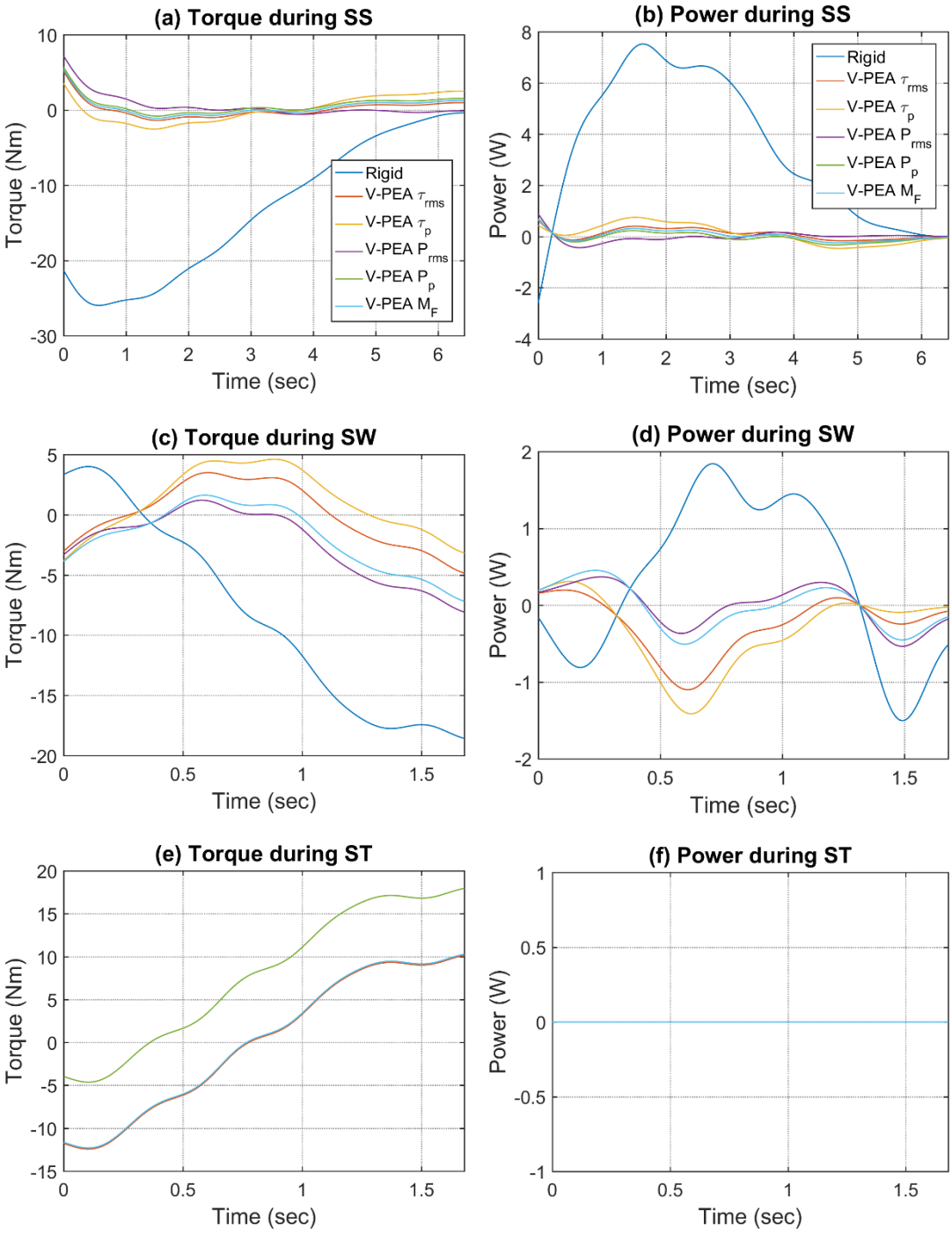

Figure 6.8: Torque and power trajectories at the hip joint during sit to stand (SS), swing (SW) and stance (ST) phase. Figures (a), (c) and (d) represent the torque trajectory of the joint and Figures (b), (d) and (f) represent power trajectories of the joint during the three manoeuvres. These trajectories are shown for the case of V-PEA by using each of the five spring optimization strategies and compared with the trajectory for the rigid actuation system.

The torque and power at the hip joint during swing phase highlighted a significant variation among the various optimization methods employed. For example, the T_{peak} optimization method established the results in which the

torque stays away from the peak torque as much as possible. Although all methods were able to reduce the requirements significantly, but this large variation showed the need to develop a multi-factor optimization strategy that reduces all variables simultaneously. Hence, the results of torque and power requirements for multi-factor optimization can be identified in which it runs in between the torque and power that were obtained by other optimization methods. The torque requirement during stance phase was also noticed to be significantly reduced. It appeared to follow the same pattern of the trajectory in the V-PEA as for the case of rigid one. However, no difference was observed between results of the different optimization methods. As mentioned previously, because of the knee locking mechanisms, the power requirement at the hip joint during stance phase was zero and hence spring mechanism should be disengaged during this phase.

Knee Joint

Figures 6.9 (a) to 6.9 (f) illustrates the simulation results at the knee joint using different optimization strategies during the three manoeuvres i.e. sit to stand, swing and stance phase. Similar to the previous figures for the hip joint, all torques trajectories are shown on the left and power diagrams on the right. As can be observed in Figure 6.9, the torque and power trajectories at the knee joint during sit to stand show significant reduction by all optimization strategies. The high peaks that were present during the rigid actuation were greatly reduced and the torque and power tries to stay within a constant range. The trajectory during the swing phase appears to be following the same pattern as the case for the rigid one but the high peaks in the rigid system are reduced. Knee gait during stance phase was recorded to be zero because of the knee locking mechanism.

Ankle Joint

By observing the ankle trajectory of the torque and power requirements in Figure 6.10, it is clear that the pattern of trajectory is similar when considering V-PEA and rigid actuation system, however, the peaks and the overall torque and power are reduced. A large variation exists in the torque and power trajectories of the ankle joint during sit to stand operation among different optimization strategies. The torque and power during T_{rms} and P_{rms} minimization criteria recorded to be the lowest one but the peaks observed were high. The ankle trajectories of torque and power during swing were significantly reduced with V-PEA.

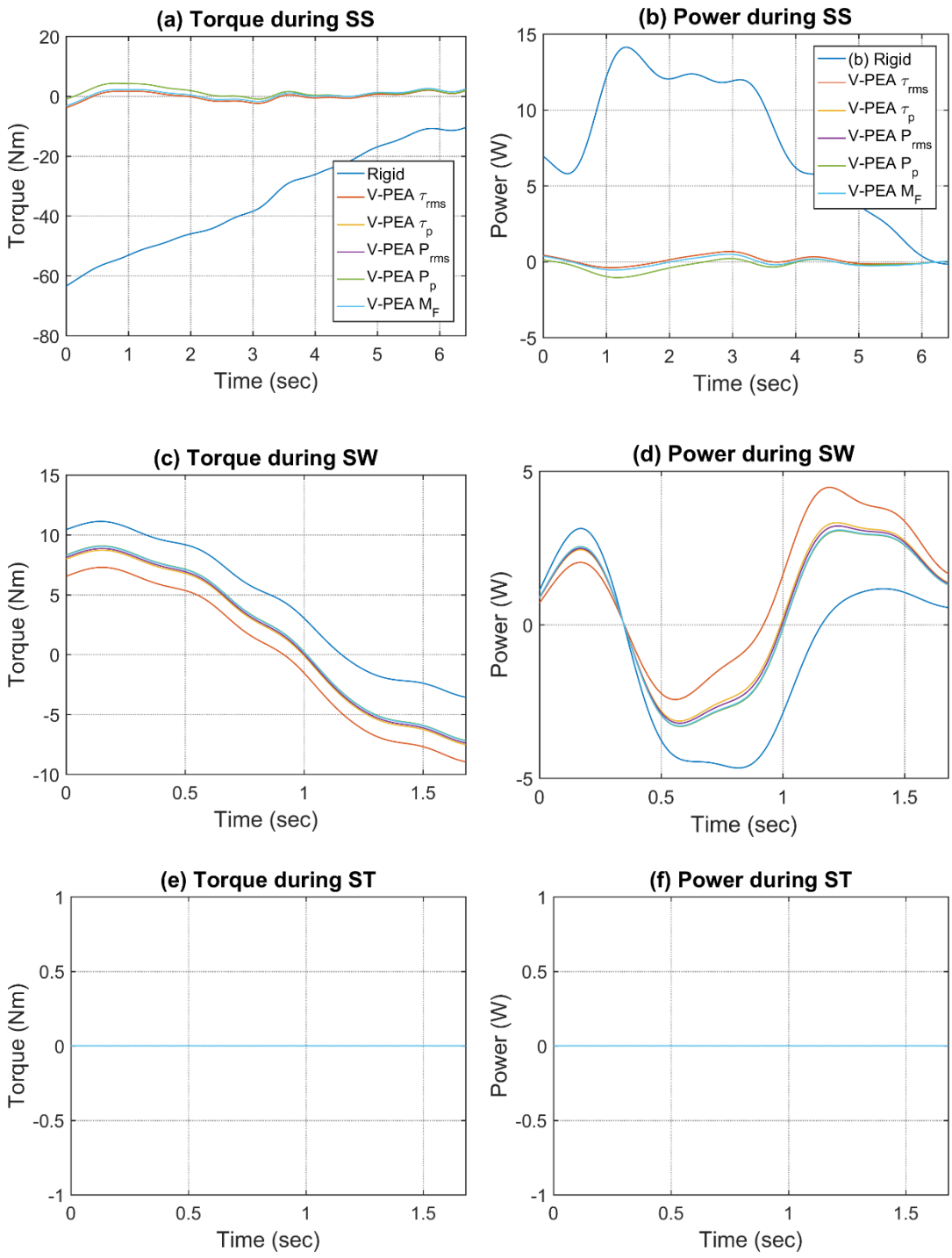

Figure 6.9: Torque and power trajectories at the knee joint during sit to stand (SS), swing (SW) and stance (ST) phase. Figures (a), (c) and (d) represent the torque trajectory of the joint and Figures (b), (d) and (f) represent power trajectories of the joint during the three manoeuvres. These trajectories are shown for the case of V-PEA by using each of the five spring optimization strategies and compared it with the trajectory for the rigid actuation system.

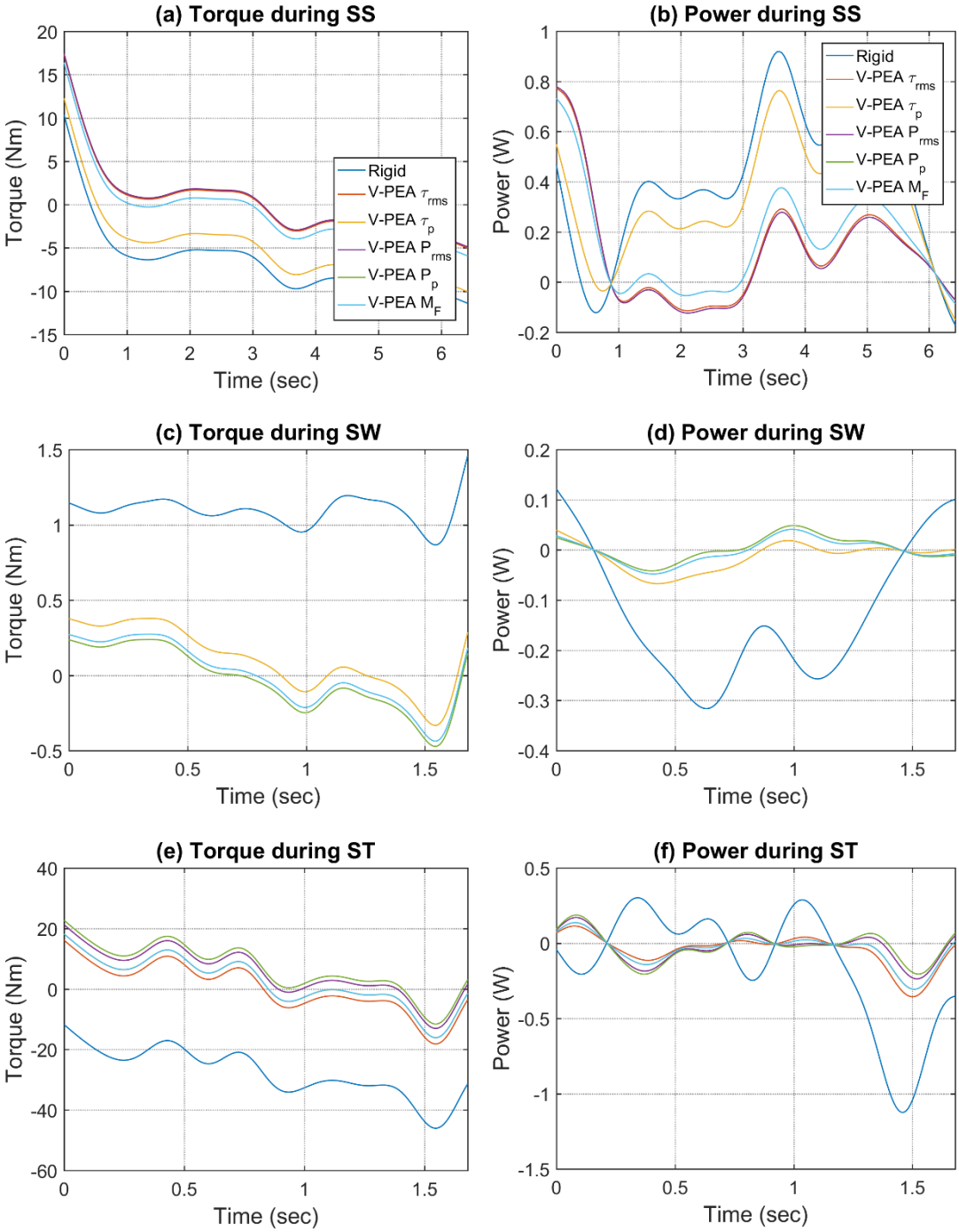

Figure 6.10: Torque and power trajectories at the ankle joint during sit to stand (SS), swing (SW) and stance (ST) phase. Figures (a), (c) and (d) represent the torque trajectory of the joint and Figures (b), (d) and (f) represent power trajectories of the joint during the three manoeuvres. These trajectories are shown for the case of V-PEA by using each of the five spring optimization strategies and compared it with the trajectory for the rigid actuation system.

No significant difference was observed among different optimization strategies during the trajectory of the swing phase in toque and power requirement. A significant reduction could also be seen during stance phase where the high peaks that were present in especially power requirement were greatly reduced and the power stayed within a smaller range using V-PEA.

It is evident from Figures 6.8 to 6.10 that V-PEA is able to reduce the torque and power requirement throughout the full trajectory during sit to stand and walking operation in an assistive exoskeleton. The advantages of using V-PEA during its operation could be observed in all phases for each of the joints. The maximum benefits of V-PEA was recorded during the trajectory of sit to stand manoeuvre for hip and knee joints and during stance phase at the ankle joint. The benefit of these significant reductions can be realized in the development of the actuation system with smaller motors and gears, therefore reducing the overall power consumption of the assistive robotic exoskeleton as will be explained later.

6.3.5.2 Variable-Series Elastic Actuator (V-SEA)

When a series spring is added to the dual actuation system, torque and power requirements were also recorded to be reduced at the joints during the operational phases. As mentioned previously, because of the slow walking speed of the gait, reductions in the torque and power were not significant. The results of the V-SEA at hip, knee and ankle joints are shown in Figures 6.11 to 6.13. These show the joint trajectories during the three optimization methods of V-SEA compared with the rigid actuation system. As V-SEA was only able to affect the power of the joint, therefore torque results are not considered with V-SEA. From Figure 6.11, the hip power trajectory during sit to stand, swing and stance phase was equally affected by all of the optimization methods employed. The power trajectory during sit to stand manoeuvre appeared to be more reduced as compared to the walking phase trajectories. Hip power during stance phase was observed to be zero. This is because of the knee locking mechanism as previously described that affects the hip angular velocity during stance phase and brings it close to zero.

A similar pattern was observed in Figure 6.12 for the knee joint. A slightly better reduction could be observed using V-SEA during sit to stand operation as compared to the swing phase of the gait. The trajectories obtained for V-SEA in all optimization strategies can be seen following the same gait pattern as for the case of rigid actuation system. The power during stance phase at the knee joint was zero as knee mechanism is locked during this

phase. Results from Figure 6.13 for the ankle joint also recorded similar outcomes with the sit to stand manoeuvre showing better results as compared to the swing and stance phase of walking. However, there was no significant difference obtained during the stance phase trajectory. As there was a slight movement of the ankle joint during most of the operations i.e. apart from the slow gait speed, there was only a slight movement of the ankle joint especially during sit to stand and stance phase, therefore, the results were not very significant for the case of V-SEA.

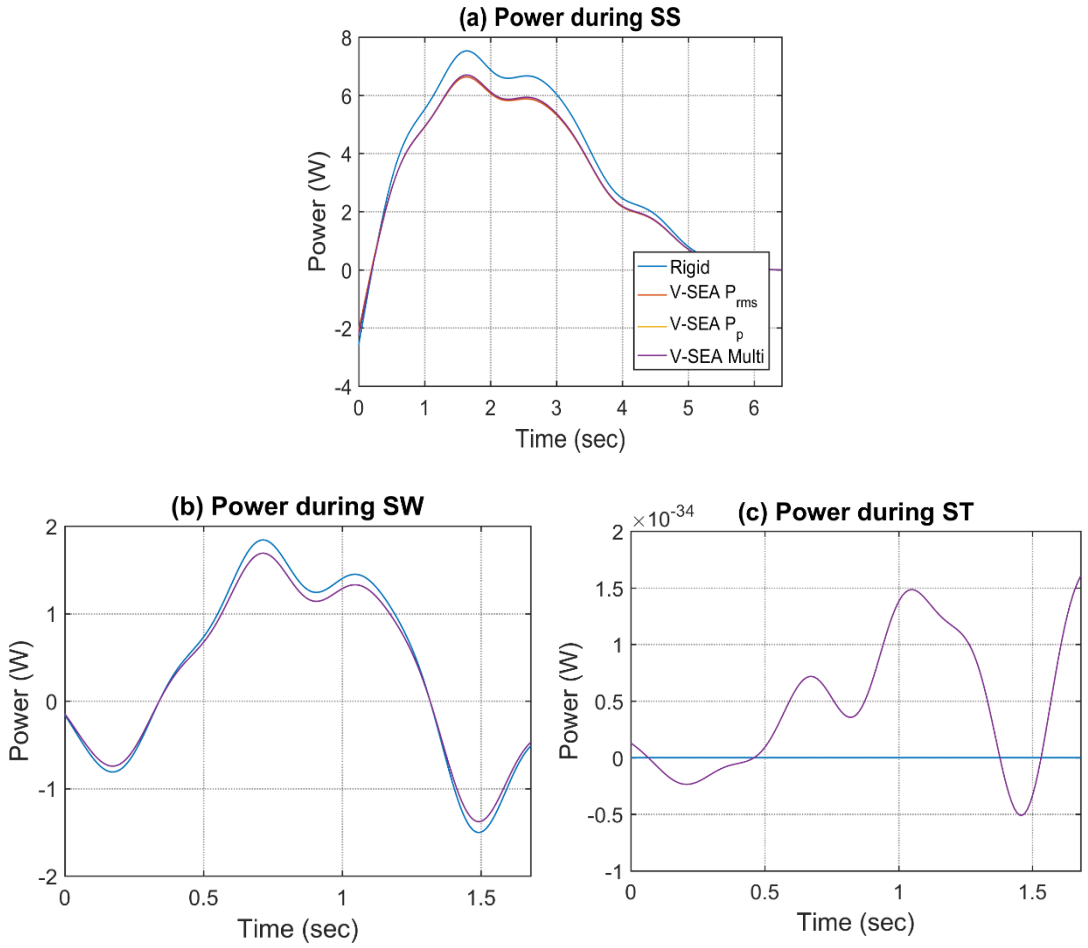

Figure 6.11: The power trajectory at the hip joint during (a) sit to stand (SS), (b) swing (SW) and (c) stance (ST) phase. These trajectories are shown for the case of V-SEA by using the three spring optimization strategies and compared it with the trajectory for the rigid actuation system during the three manoeuvres.

The results of V-PEA suggested a significant difference in the torque and power trajectories of the joints and V-SEA outcomes also suggested a slight difference in the power at the joints during the operations. Even though there was a slight reduction during different phases of the joints using V-SEA,

optimal actuation system using V-PEA and V-SEA will be determined to see if smaller motors could be realized using the above mentioned variable elastic actuators.

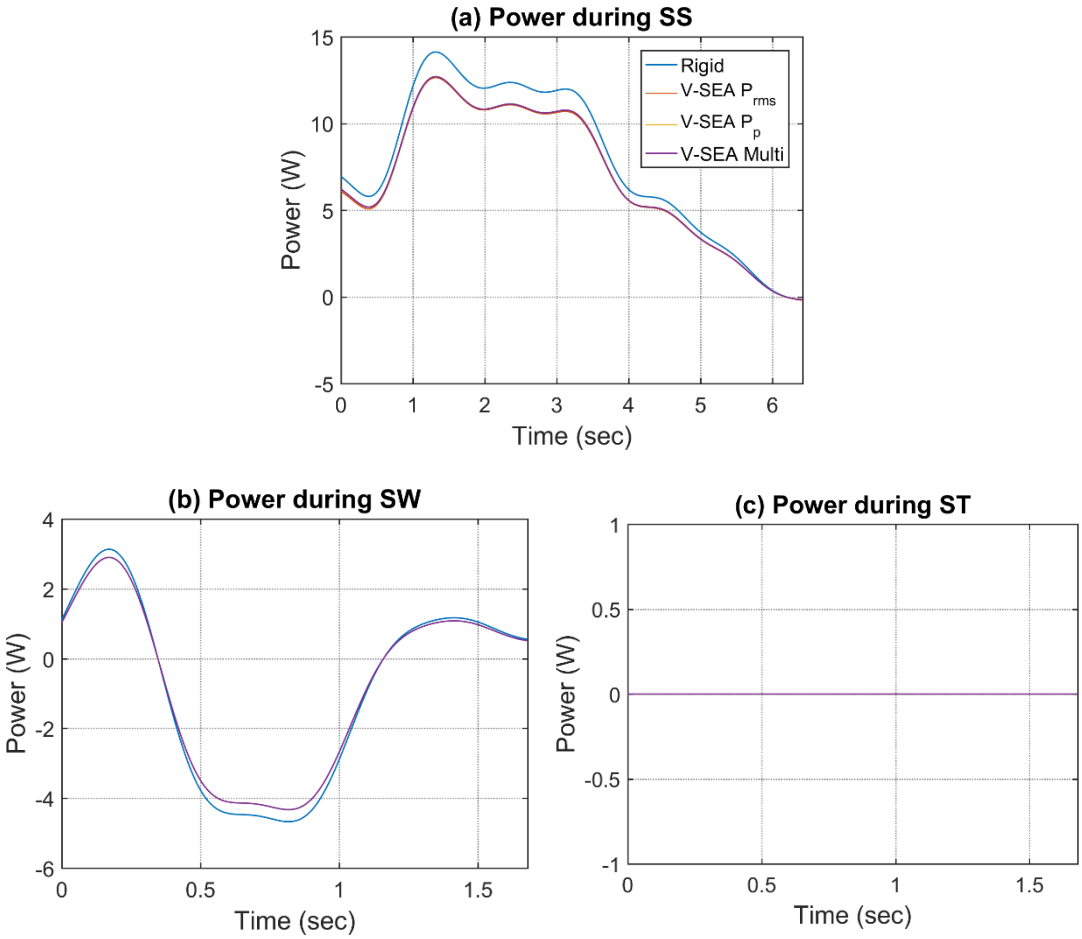

Figure 6.12: The power trajectory at the knee joint during (a) sit to stand (SS), (b) swing (SW) and (c) stance (ST) phase. These trajectories are shown for the case of V-SEA by using the three spring optimization strategies and compared it with the trajectory for the rigid actuation system during the three manoeuvres.

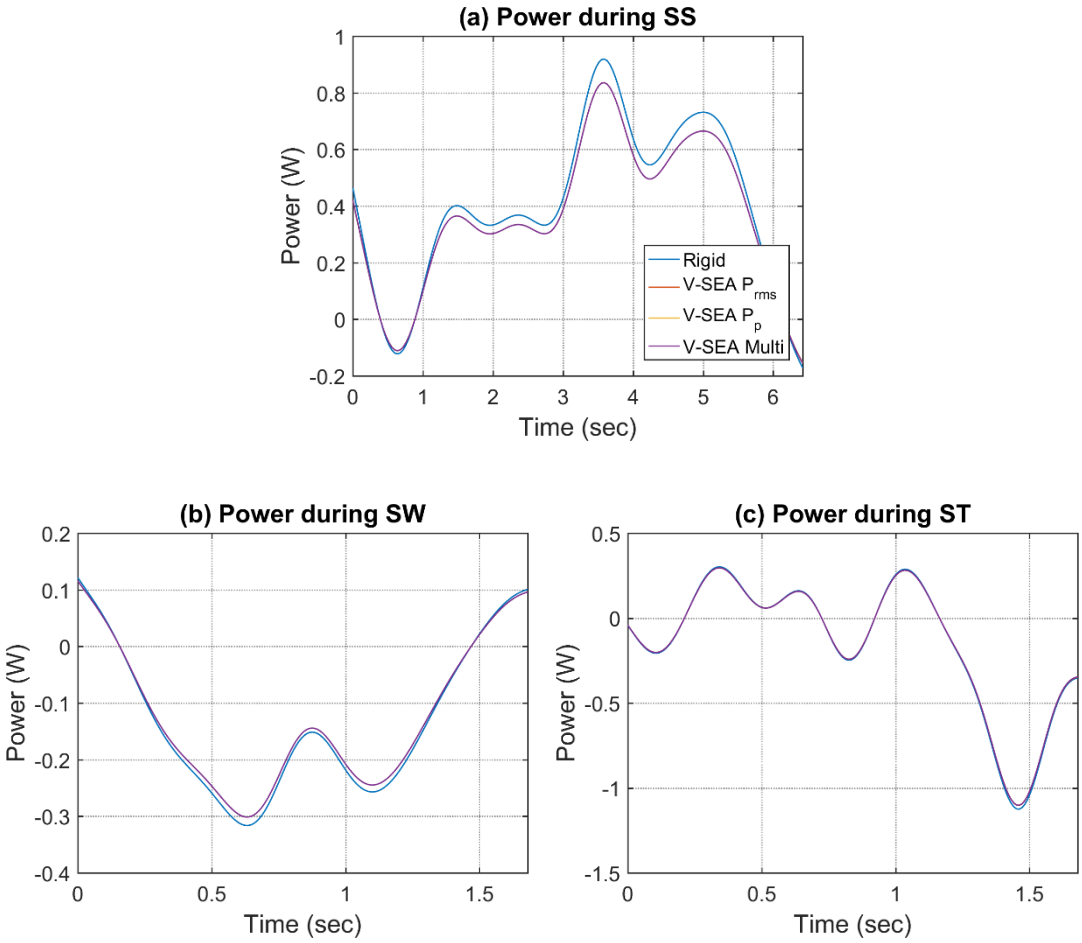

Figure 6.13: The power trajectory at the ankle joint during (a) sit to stand (SS), (b) swing (SW) and (c) stance (ST) phase. These trajectories are shown for the case of V-SEA by using the three spring optimization strategies and compared it with the trajectory for the rigid actuation system during the three manoeuvres.

6.3.6 Optimal Actuation System in an Antagonistic Arrangement

As discussed in Section 6.2.5, optimal actuation system in an antagonistic setup arrangement was obtained at each of the joints of the lower limb assistive robotic exoskeleton using algorithm shown in Figure 6.4. This has been assessed for the case of rigid actuation system, the parallel elastic actuation system (V-PEA) and the series elastic actuation system (V-SEA). The optimized spring stiffness employed for the case of V-SEA and also the equilibrium angle for the case of V-PEA has been tabulated in Table 6.2. In the evaluation of the optimal elastic actuators, the results were only investigated for the case of multi-factor optimization criterion of the spring stiffness. This is because the torque and power obtained using this case was the most optimal in terms of all variables as compared to the values of torque and power obtained by other criterion. The objective function used to

assess the various designs candidates was given Table 6.1. The algorithm was applied to each joint separately and the procedure continued until the motors and transmission systems ceased to alter in the iterations. For better understanding, it was found appropriate to record the results for each type of the transmission system separately. However, the results are presented so that at least two of the lower limb joints have the same transmission system. The optimized configuration of a particular transmission mechanism has also been found in the algorithm.

6.3.6.1 Dual Rigid Actuation System

Table 6.3 shows the results for the optimal rigid actuation system in an antagonistic arrangement for each iteration of the applied algorithm. The table has been subdivided for each type of the transmission system used. The first part of the table shows the results obtained by applying harmonic drive at each of the joints, therefore the algorithm determines the best motor combined with the harmonic drive that is most suitable from the list given in Table C.1 in Appendix C for a dual rigid actuation system.

The optimal actuation system was obtained first for the knee joint by assuming the lightweight designs possible for the hip and ankle actuator. The factors contributing to the objective function for each candidate actuator were recorded i.e. total power consumption, total weight of the exoskeleton and the ability to carry a user with 50% support. The knee actuator i.e. a pair of Maxon EC frameless-45-flat with harmonic drive CSD-20-160-2A was obtained as it was evaluated as a candidate actuator with the highest value of the objective function. After obtaining the knee actuator, results have been obtained for the ankle and hip joint to determine the most suitable actuator at this phase by recording the variables contributing to the objective function of the candidate actuators. Results were then repeated for the knee joint and during the second iteration, the optimal actuation system at the knee joint was different from the first one. Therefore, the ankle joint and hip joint is repeated with the new actuator at the knee joint. During the second iteration, identical results were noticed at each of the joint as it appeared in the last iteration. This can also be observed that the same values were obtained for the last three rows in Table 6.3 for the three variables. The second part of Table 6.3 shows the results recorded by using only belts and pulley drive with the various transmission ratios combined with the motor. As can be observed, heavy motors with a high power consumption were obtained at each of the joints. Even though with the heavy motors used, the actuation system was still not able to carry a user up to the required value.

Table 6.3: Optimal dual rigid actuation system in an antagonistic arrangement obtained at each iteration when similar type of the transmission system was used at each of the lower limb joints shown according to the type of transmission systems

Joint Optimization	Candidate Actuator			P_C (W)	W_{exo} (kg)	U_C (kg)
	Hip	Knee	Ankle			
Transmission type: Harmonic drives only						
Knee joint	Maxon ECX16M with CSD-14-50-2A	Maxon EC45 with CSD-20-160-2A	Maxon ECX16M with CSD-14-50-2A	19.59	12.25	100
Ankle joint	ECX16M with CSD-14-50-2A	Maxon EC45 with CSD-20-160-2A	Allied motion MF76008 with CPL-32-120-2A	42.68	11.93	100
Hip joint	Allied motion MF76008 with CSD-20-160-2A	Maxon EC45 with CSD-20-160-2A	Allied motion MF76008 with CPL-32-120-2A	63.02	12.08	100
Knee joint	Allied motion MF76008 with CSD-20-160-2A	Allied motion MF60020 with CSD-20-160-2A	Allied motion MF76008 with CPL-32-120-2A	55.34	14.78	100
Ankle joint	Allied motion MF76008 with CSD-20-160-2A	Allied motion MF60020 with CSD-20-160-2A	Allied motion MF76008 with CPL-32-120-2A	55.34	14.78	100
Hip joint	Allied motion MF76008 with CSD-20-160-2A	Allied motion MF60020 with CSD-20-160-2A	Allied motion MF76008 with CPL-32-120-2A	55.34	14.78	100
Transmission type: Ball screws and pulley and belt drive						
Knee joint	Maxon ECX16M with a ratio 1:0.4	Parker Hannifin K178100-8Y with a ratio 1:2.6	Maxon ECX16M with a ratio 1:0.4	52.50	36.12	10.1
Ankle joint	Maxon ECX16M with a ratio 1:0.4	Parker Hannifin K178100-8Y with a ratio 1:2.6	Parker Hannifin K178100-8Y with a ratio 1:2.6	1375	55.64	12.1
Hip joint	Parker Hannifin K178100-8Y with a ratio 1:2.6	Parker Hannifin K178100-8Y with a ratio 1:2.6	Parker Hannifin K178100-8Y with a ratio 1:2.6	2412	76.5	22.5
Knee joint	Parker Hannifin K178100-8Y with a ratio 1:2.6	Parker Hannifin K178100-8Y with a ratio 1:2.6	Parker Hannifin K178100-8Y with a ratio 1:2.6	2412	76.5	22.5
Ankle joint	Parker Hannifin K178100-8Y ratio 1:2.6	Parker Hannifin K178100-8Y ratio 1:2.6	Parker Hannifin K178100-8Y ratio 1:2.6	2412	76.5	22.5

Table 6.3: Optimal dual rigid actuation system (Cont.)

Joint Optimization	Candidate Actuator			P_C (W)	W_{exo} (kg)	U_C (kg)
	Hip	Knee	Ankle			
Transmission type: Ball screws and Harmonic drives with pulley and belt						
Knee joint	Maxon ECX16M with CSD-14-50-2A and a ratio 1:20	Maxon EC45 flat with a CSD-20-160-2A and a ratio 1:368	Maxon ECX16M with CSD-14-50-2A and a ratio 1:20	10.31	14.88	100
Ankle joint	Maxon ECX16M with CSD-14-50-2A and a ratio 1:20	Maxon EC45 with CSD-20-160-2A and a ratio 1:368	Allied motion MF76008 with CPL-32-120-2A and a ratio 1:400	29.37	13.62	100
Hip joint	Allied motion MF76008 with CSD-20-160-2A and a ratio 1:400	Maxon EC45 with CSD-20-160-2A and a ratio 1:368	Allied motion MF76008 with CPL-32-120-2A and a ratio 1:400	47.55	13.26	100
Knee joint	Allied motion MF76008 with CSD-20-160-2A and a ratio 1:400	Maxon EC45 with CSD-20-160-2A and a ratio 1:384	Allied motion MF76008 with CPL-32-120-2A and a ratio 1:400	47.53	13.26	100
Ankle joint	Allied motion MF76008 with CSD-20-160-2A and a ratio 1:400	Maxon EC45 with CSD-20-160-2A and a ratio 1:384	Allied motion MF76008 with CPL-32-120-2A and a ratio 1:400	47.53	13.26	100
Hip joint	Allied motion MF76008 with CSD-20-160-2A and a ratio 1:400	Maxon EC45 with CSD-20-160-2A and a ratio 1:384	Allied motion MF76008 with CPL-32-120-2A and a ratio 1:400	47.53	13.26	100
Transmission type: Ball screws only (B)						
Knee joint	Maxon ECX16M with ball screw no. 1	Allied motion MF76008 with ball screw no. 185	Maxon ECX16M with ball screw no. 1	33.28	11.74	100
Ankle joint	Maxon ECX16M with ball screw no. 1	Allied motion MF76008 with ball screw no. 185	Allied motion MF60020 with ball screw no. 11	52	12.56	100
Hip joint	Allied motion MF95008 with ball screw no. 42	Allied motion MF76008 with ball screw no. 185	Allied motion MF60020 with ball screw no. 11	94.37	14.46	100
Knee joint	Allied motion MF95008 with ball screw no. 42	Allied motion MF76008 with ball screw no. 185	Allied motion MF60020 with ball screw no. 11	94.37	14.46	100
Ankle joint	Allied motion MF95008 with ball screw 42	Allied motion MF76008 with ball screw 185	Allied motion MF60020 with ball screw 11	94.37	14.46	100

* P_C=Average Power consumption, W_{exo}= Weight of the exoskeleton and U_C= User's carrying capacity with 50% support

Therefore, using only belts and drive system as a transmission mechanism is not suggested. However, harmonic drives combined with a belt and pulley drive has obtained favourable results reducing further the total power consumption and weight of the exoskeleton as compared to a harmonic drive system only. These results were shown in Table 6.3 for the harmonic and a belt and pulley drive system. The results have been shown for each iteration of the joint. Finally ball screws in an inverted slider mechanism has been applied and obtained the suitable motors and the ball screws with a suitable configuration. The various configurations of the ball screws has been given in Appendix C. Table E.10 depicts the results obtained by applying different types of transmission systems at the joints. The motors and transmission systems obtained are found against each of the type of transmission system. However, results from each iteration were not shown in Table E.10 for various combinations of the transmission system at the lower limb joints. It only depicts the final optimal actuation system obtained.

6.3.6.2 Variable Parallel Dual Elastic Actuation System

Table 6.4 and Table E.11 show the results obtained for the case of parallel elastic actuator (V-PEA) and each table is also subdivided into parts to indicate the candidate actuators with various transmission types employed. The first part of Table 6.4 shows the results of the actuation system obtained when only harmonic drives were employed as the transmission mechanism. Results of the motors obtained along with the optimal harmonic drives recorded can be observed in the table. As can be seen in Table E.10, the optimal results were obtained during the second iteration. When only belts and pulley drives were used in combination with the motors, same actuation system was obtained at each of the joints. Harmonic drive combined with the belts and pulley system obtained the motor “Kollmorgen TBM(S)6051A” at each of the joints. The final actuation systems were obtained in the second iteration. Finally results using Ball screws as a transmission system at each of the joints were obtained. During the second iteration, candidate actuators started appearing same as the previous one for each of the joints.

Finally results for V-PEA with the various combinations of Ball screws, harmonic drives, belt and pulley drive and harmonic with belts and pulley drives were obtained and tabulated in Table E.11 for type of transmission system combination. These results are the final optimal actuation systems for the case of V-PEA.

Table 6.4: Variable parallel elastic actuation system (V-PEA) in an antagonistic arrangement obtained at each iteration when similar type of the transmission system was used at each of the lower limb joints shown according to the type of transmission systems

Joint Optimization	Candidate Actuator			P_C (W)	W_{exo} (kg)	U_C (kg)
	Hip	Knee	Ankle			
Transmission type: Harmonic drives only						
Knee joint	Maxon ECX16M with CSD-14-50-2A	Kollmorgen TBM(S)6051A with FR-25-160-2	Maxon ECX16M with CSD-20-160-2A	3.46	36.112	100
Ankle joint	Maxon ECX16M with CSD-14-50-2A	Kollmorgen TBM(S)6051A with FR-25-160-2	Allied motion MF76020 with FR-25-200-2	9.39	36.56	100
Hip joint	Allied motion MF76008 with CSD-20-160-2A	Kollmorgen TBM(S)6051A with FR-25-160-2	Allied motion MF76020 with FR-25-200-2	19.96	39.947	100
Knee joint	Allied motion MF76008 with CSD-20-160-2A	Kollmorgen TBM(S)6051A with FR-25-160-2	Allied motion MF76020 with FR-25-200-2	19.96	39.947	100
Ankle joint	Allied motion MF76008 with CSD-20-160-2A	Kollmorgen TBM(S)6051A with FR-25-160-2	Allied motion MF76020 with FR-25-200-2	19.96	39.947	100
Transmission type: Ball screws with pulley and belt drive						
Knee joint	Maxon ECX16M with a ratio 1:0.4	Parker Hannifin K178100-8Y with a ratio 1:2.6	Maxon ECX16M with a ratio 1:0.4	52.50	36.12	10.1
Ankle joint	Maxon ECX16M with a ratio 1:0.4	Parker Hannifin K178100-8Y with a ratio 1:2.6	Parker Hannifin K178100-8Y with a ratio 1:2.6	1375	55.64	12.1
Hip joint	Parker Hannifin K178100-8Y with a ratio 1:2.6	Parker Hannifin K178100-8Y with a ratio 1:2.6	Parker Hannifin K178100-8Y with a ratio 1:2.6	2412	76.5	22.5
Knee joint	Parker Hannifin K178100-8Y with a ratio 1:2.6	Parker Hannifin K178100-8Y with a ratio 1:2.6	Parker Hannifin K178100-8Y with a ratio 1:2.6	2412	76.5	22.5
Ankle joint	Parker Hannifin K178100-8Y with a ratio 1:2.6	Parker Hannifin K178100-8Y with a ratio 1:2.6	Parker Hannifin K178100-8Y with a ratio 1:2.6	2412	76.5	22.5

Table 6.4: Variable parallel elastic actuation system V-PEA (Cont.)

Joint Optimization	Candidate Actuator			P_C (W)	W_{exo} (kg)	U_C (kg)
	Hip	Knee	Ankle			
Transmission type: Ball screws and Harmonic drives with pulley and belt						
Knee joint	Maxon ECX16M with CSD-14-50-2A and a ratio 1:20	Kollmorgen TBM(S)6051 A with FR-25-160-2 and a ratio 1:178	Maxon ECX16M with CSD-14-50-2A and a ratio 1:	3.88	35.16	100
Ankle joint	Maxon ECX16M with CSD-14-50-2A and a ratio 1:20	Kollmorgen TBM(S)6051 A with FR-25-160-2 and a ratio 1:178	Kollmorgen TBM(S)6051A with FR-25-160-2 and a ratio 1:258	7.42	37.413	100
Hip joint	Kollmorgen TBM(S)6051A with CSD-20-160-2A and a ratio 1:400	Kollmorgen TBM(S)6051 A with FR-25-160-2 and a ratio 1:178	Kollmorgen TBM(S)6051A with FR-25-160-2 and a ratio 1:258	14.128	40.793	100
Knee joint	Kollmorgen TBM(S)6051A with CSD-20-160-2A and a ratio 1:400	Kollmorgen TBM(S)6051 A with FR-25-160-2 and a ratio 1:178	Kollmorgen TBM(S)6051A with FR-25-160-2 and a ratio 1:258	14.128	40.793	100
Ankle joint	Kollmorgen TBM(S)6051A with CSD-20-160-2A and a ratio 1:400	Kollmorgen TBM(S)6051 A with FR-25-160-2 and a ratio 1:178	Kollmorgen TBM(S)6051A with FR-25-160-2 and a ratio 1:258	14.128	40.793	100
Transmission type: Ball screws only (B)						
Knee joint	Maxon ECX16M with ball screw config.no. 1	Kollmorgen TBM(S)7646 A with ball screw config. no. 277	Maxon ECX16M with ball screw config. no. 1	7.38	33.89	100
Ankle joint	Maxon ECX16M with ball screw config. no. 1	Kollmorgen TBM(S)7646 A with ball screw config. no. 277	Kollmorgen TBM(S)6051A with ball screw config. no. 11	8.19	36.87	100
Hip joint	Parker Hannifin K089050-7Y with ball screw config. no. 49	Kollmorgen TBM(S)7646 A with ball screw config. no. 277	Kollmorgen TBM(S)6051A with ball screw config. no. 11	32.43	39.97	100
Knee joint	Parker Hannifin K089050-7Y with ball screw config. no. 49	Kollmorgen TBM(S)7646 A with ball screw config. no. 277	Kollmorgen TBM(S)6051A with ball screw config. no. 11	32.43	39.97	100
Ankle joint	Parker Hannifin K089050-7Y with ball screw config. no. 49	Kollmorgen TBM(S)7646 A with ball screw config. no. 277	Kollmorgen TBM(S)6051A with ball screw config. no. 11	32.43	39.97	100

* P_C= Average Total Power consumption, W_{exo}=Total Weight of the exoskeleton and U_C= User's carrying capacity with 50% support

6.3.6.3 Variable Series Dual Elastic Actuation System

As mentioned in the previous section, even though the simulation results obtained from the series elastic actuator (V-SEA) did not significantly differ with the case of rigid actuation system but there was a slight difference during some of the manoeuvres at the joints. The objective function of the candidate actuators were also modified as given in Table 6.1 to account more for power consumption reduction. Therefore, the results with V-SEA has been obtained with the various combinations and configurations of the transmission systems. These results are given in Tables 6.5 and Table E.12 for various types of transmission system employed by keeping it the same at each joint for a particular transmission type in Table 6.5 and depicting the various combinations of the transmission systems employed in Table E.12.

As can be observed in Table 6.5, the motors and transmission systems obtained are different from the rigid actuation system, since the power requirement was reduced, therefore the optimal actuation system in V-SEA consumed less power than rigid actuation system. This is true for each type and combination of the transmission system results. However, using belt and pulley drive only as a transmission system did not prove to be any beneficial for the case of V-SEA either. Even though with the heavy motors and transmission systems, the actuation system was not able to carry a user of up to 100 kg for any transmission value of the belt and pulley drive system. This is because a limited diameter of pulley could be employed in the actuation design otherwise the size of the actuator becomes very large. Table E.12 shows the various combinations of the transmission systems applied at each of the joints of the lower limb assistive robotic exoskeleton actuation system for V-SEA.

6.3.7 Mass and Power Analysis of the Actuation System

Since the main purpose of using the dual actuators in an assistive robotic exoskeleton is to realize the reduction in the power and observe the effect on the weight of the exoskeleton, it would be appropriate to discuss the results by comparing the total mass of the exoskeleton and the average power consumption of the dual actuation system with the single actuator case. Optimized results from three types of dual actuation system in an antagonistic arrangement have been obtained i.e. a rigid actuation system consisting of two motors and transmission systems, a parallel elastic actuator comprising two motors and transmission systems with a parallel spring and a series elastic actuator consisting of a series spring attached to each of the two motors and transmission system. The results of the

optimized actuation system for the above three cases will be compared with the three cases of single actuation system discussed in the previous chapters.

Table 6.5: Optimal variable series elastic actuation system (V-SEA)in an antagonistic arrangement obtained at each iteration when similar type of the transmission system was used at each of the lower limb joints shown according to the type of transmission systems

Joint Optimization	Candidate Actuator			P_C (W)	W_{exo} (kg)	U_C (kg)
	Hip	Knee	Ankle			
Transmission type: Harmonic drives only						
Knee joint	Maxon ECX16M with CSD-14-50-2A	Kollmorgen TBM(S)6051A with FR-25-160-2	Maxon ECX16M with CSD-20-160-2A	7.46	36.112	100
Ankle joint	Maxon ECX16M with CSD-14-50-2A	Kollmorgen TBM(S)6051A with FR-25-160-2	Allied motion MF76020 with FR-25-200-2	13.3	36.56	100
Hip joint	Allied motion MF76008 with CSD-20-160-2A	Kollmorgen TBM(S)6051A with FR-25-160-2	Allied motion MF76020 with FR-25-200-2	23.45	39.947	100
Knee joint	Allied motion MF76008 with CSD-20-160-2A	Kollmorgen TBM(S)6051A with FR-25-160-2	Allied motion MF76020 with FR-25-200-2	23.45	39.947	100
Ankle joint	Allied motion MF76008 with CSD-20-160-2A	Kollmorgen TBM(S)6051A with FR-25-160-2	Allied motion MF76020 with FR-25-200-2	23.45	39.947	100
Transmission type: Ball screws (B) with pulley and belt drive						
Knee joint	Maxon ECX16M with a ratio 1:0.4	Parker Hannifin K178100-8Y with a ratio 1:2.6	Maxon ECX16M with a ratio 1:0.4	53.23	36.12	10.1
Ankle joint	Maxon ECX16M with a ratio 1:0.4	Parker Hannifin K178100-8Y with a ratio 1:2.6	Parker Hannifin K178100-8Y with a ratio 1:2.6	1376	55.64	12.1
Hip joint	Parker Hannifin K178100-8Y with a ratio 1:2.6	Parker Hannifin K178100-8Y with a ratio 1:2.6	Parker Hannifin K178100-8Y with a ratio 1:2.6	2432	76.5	22.5
Knee joint	Parker Hannifin K178100-8Y with a ratio 1:2.6	Parker Hannifin K178100-8Y with a ratio 1:2.6	Parker Hannifin K178100-8Y with a ratio 1:2.6	2432	76.5	22.5
Ankle joint	Parker Hannifin K178100-8Y with a ratio 1:2.6	Parker Hannifin K178100-8Y with a ratio 1:2.6	Parker Hannifin K178100-8Y with a ratio 1:2.6	2432	76.5	22.5

Table 6.5: Optimal variable series elastic actuation system (Cont.)

Joint Optimization	Candidate Actuator			P_C (W)	W_{exo} (kg)	U_C (kg)
	Hip	Knee	Ankle			
Transmission type: Harmonic drives with pulley and belt system						
Knee joint	Maxon ECX16M with CSD-14-50-2A and a ratio 1:20	Kollmorgen TBM(S)6051A with FR-25-160-2 and a ratio 1:178	Maxon ECX16M with CSD-14-50-2A and a ratio 1:20	7.94	35.16	100
Ankle joint	Maxon ECX16M with CSD-14-50-2A and a ratio 1:20	Kollmorgen TBM(S)6051A with FR-25-160-2 and a ratio 1:178	Kollmorgen TBM(S)6051A with FR-25-160-2 and a ratio 1:258	11.396	37.41	100
Hip joint	Kollmorgen TBM(S)6051A with CSD-20-160-2A and a ratio 1:400	Kollmorgen TBM(S)6051A with FR-25-160-2 and a ratio 1:178	Kollmorgen TBM(S)6051A with FR-25-160-2 and a ratio 1:258	17.709	40.793	100
Knee joint	Kollmorgen TBM(S)6051A with CSD-20-160-2A and a ratio 1:400	Kollmorgen TBM(S)6051A with FR-25-160-2 and a ratio 1:178	Kollmorgen TBM(S)6051A with FR-25-160-2 and a ratio 1:258	17.709	40.793	100
Ankle joint	Kollmorgen TBM(S)6051A with CSD-20-160-2A and a ratio 1:400	Kollmorgen TBM(S)6051A with FR-25-160-2 and a ratio 1:178	Kollmorgen TBM(S)6051A with FR-25-160-2 and a ratio 1:258	17.709	40.793	100
Transmission type: Ball screws only (B)						
Knee joint	Maxon ECX16M with ball screw config. no. 1	Kollmorgen TBM(S)7646A with ball screw config. no. 277	Maxon ECX16M with ball screw config. no. 1	12.45	33.89	100
Ankle joint	Maxon ECX16M with ball screw config. no. 1	Kollmorgen TBM(S)7646A with ball screw config. no. 277	Kollmorgen TBM(S)6051A with ball screw config. no. 11	13.19	36.87	100
Hip joint	Parker Hannifin K089050-7Y with ball screw config. no. 49	Kollmorgen TBM(S)7646A with ball screw config. no. 277	Kollmorgen TBM(S)6051A with ball screw config. no. 11	35.76	39.97	100
Knee joint	Parker Hannifin K089050-7Y with ball screw config. no. 49	Kollmorgen TBM(S)7646A with ball screw config. no. 277	Kollmorgen TBM(S)6051A with ball screw config. no. 11	35.76	39.97	100
Ankle joint	Parker Hannifin K089050-7Y with ball screw config. no. 49	Kollmorgen TBM(S)7646A with ball screw config. no. 277	Kollmorgen TBM(S)6051A with ball screw config. no. 11	35.76	39.97	100

* P_C=Average Total Power consumption, W_{exo}=Total Weight of the exoskeleton and U_C= User's carrying capacity with 50% support

Figures 6.14 and 6.15 show the total exoskeleton mass and its power consumption during different optimized cases of the actuation system according to the transmission mechanisms used at the joints. These results of the weight and power of the exoskeleton are those obtained using the mentioned actuators in Tables 6.3 to 6.8. Figures 6.14 and 6.15 show the comparison of the results of the dual actuation system with the single actuation system.

6.3.7.1 Harmonic Drives and Ball Screws in an Inverted Slider Crank Mechanism as the Transmission Systems

It is evident from Figure 6.14, that the mass and power consumption of the exoskeleton was increased using dual antagonistic setup of the rigid actuation system as compared to the rigid actuation case of a single motor. Even though, the dual actuators used smaller motors but the sum of the mass and power of the two motors exceeded the mass and power of the single motor. Therefore, dual actuation system for the case of rigid system did not bring any advantages in terms of smaller batteries and a lightweight system but some advantages could still be valid for the dual case e.g. using smaller motors can reduce the noise that could otherwise resulted because of using large heavy motors. Therefore, a smooth and a less noisy system could be realized using dual actuation system in an antagonistic arrangement. On the other hand, using V-PEA in a dual antagonistic setup has shown benefits in the total power consumption of the exoskeleton as compared to single motor case of fixed stiffness (PEA). Even though, the total mass of the exoskeleton has increased as compared to a single actuator case of PEA but the total power consumption of the exoskeleton has significantly decreased. This is because the variable stiffness has decreased the torque and power requirement, thus the optimal dual actuation system was realized using more power efficient motors and hence decreasing the power requirement of the exoskeleton. This has also been proved to be true for the case of V-SEA where motors that were more power efficient were realized but compensating it on the total mass of the exoskeleton.

By a careful observation of Figure 6.14 (it shows the results for the optimized actuation systems where ball screws and harmonic drives were used as the transmission mechanism), the minimum overall power consumption of the exoskeleton for the case of rigid actuation, V-PEA and V-SEA was recorded when harmonic drives were used as the transmission mechanism at the hip and knee joint and ball screws were employed as the transmission

mechanism at the ankle joint. The minimum power consumption was also observed in V-PEA for this particular configuration of the transmission mechanisms. Details of the particular motor and particular ball screw and harmonic drive configuration obtained can be found in Tables 6.3 and 6.4. However, the maximum difference in the power consumption was observed between dual actuation system and single actuation system when ball screws were employed at hip and ankle joint and harmonic drives were used at the knee joint. These results can be observed in Figure 6.14 for various combinations with a percentage change in the total mass and power consumption indicated for each type of the dual actuation system and transmission mechanism.

6.3.7.2 Harmonic Drives Combined with a Belt and Pulley Drive System and Ball Screws in an Inverted Slider Crank Mechanism as the Transmission Systems

Harmonic drives combined with a belt and pulley mechanism could further vary the transmission ratio and hence optimized actuation system results were also obtained for this case. Therefore, this time either ball screws in an inverted slider crank mechanism were used or harmonic drives combined with a belt and pulley drive were used at each of the joints of the lower limb assistive robotic exoskeleton. The results of the total mass of the exoskeleton compared with the total power consumption for each type of dual actuation system and single actuation system for the transmission mechanism case mentioned is shown in Figure 6.15. The percentage change in the total mass and power consumption is also indicated. The dual actuation system for the case of rigid also showed a higher power consumption and total weight of the exoskeleton as compared to a single case. However, the benefits related to noise reduction still applies as discussed above. The reduction in the total power consumption in V-PEA and V-SEA could be observed as compared to PEA and SEA respectively but compensating it on the total mass of the exoskeleton. The minimum power consumption and weight was observed when the harmonic drive combined with a belt and pulley mechanism was used at the hip and knee joint and a ball screw mechanism was used at the ankle joint. The particular harmonic drive and the ball screw configuration obtained can be found in Tables 6.3 to 6.8. The difference in the power consumption between dual elastic actuation system and single elastic actuation system was obtained with harmonic drive linked with a belt and pulley at the hip joint and ball screws mechanisms at the knee and ankle joints.

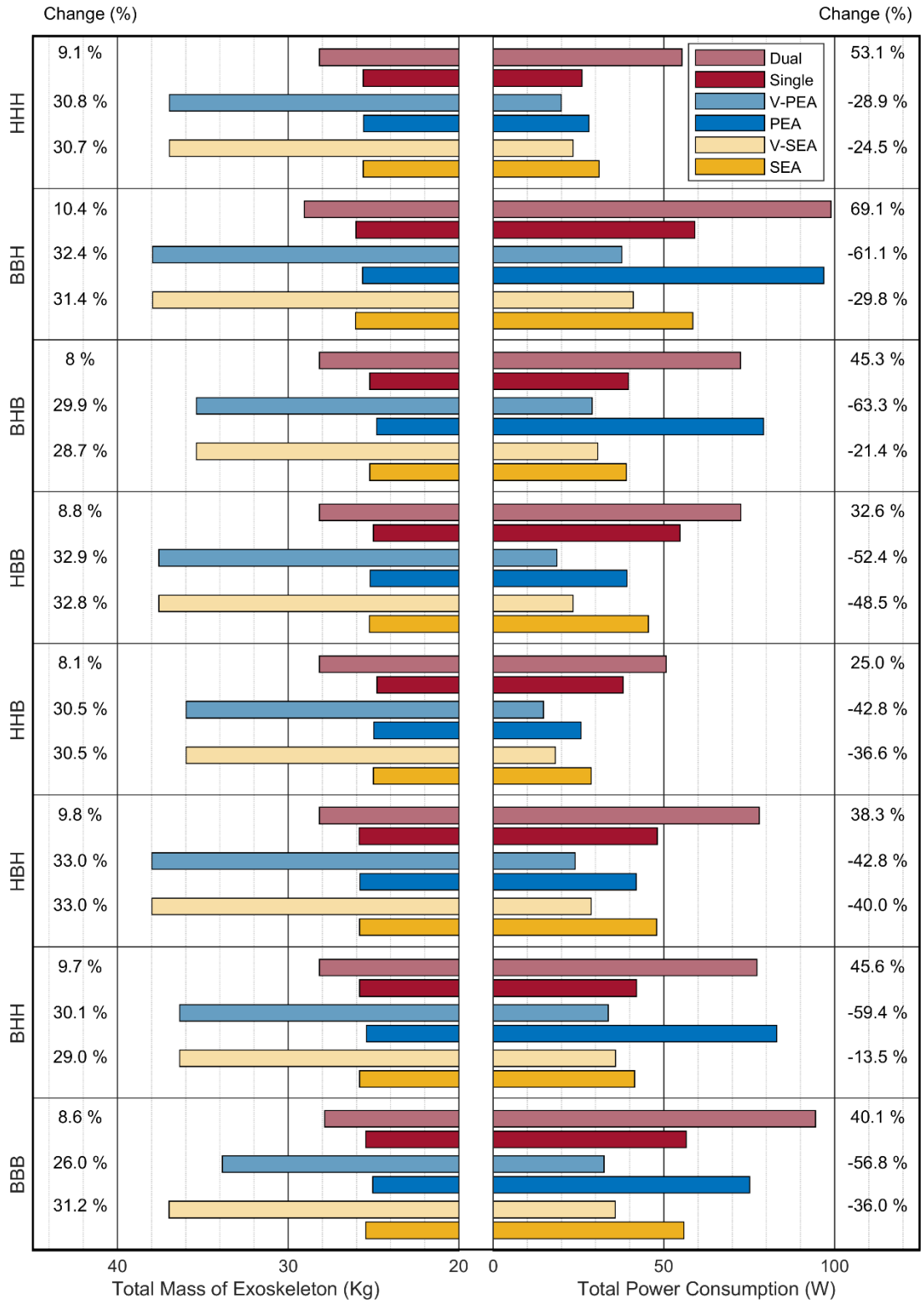

Figure 6.14: The total mass and average total power consumption of the exoskeleton of the optimal dual rigid and elastic actuation system compared with the single actuator rigid and elastic system when ball screws in an inverted slider mechanism and harmonic drives were used as the transmission mechanism. Figure shows the optimal actuation system for various combinations of these transmission systems at the lower limb joints of the assistive robotic exoskeleton

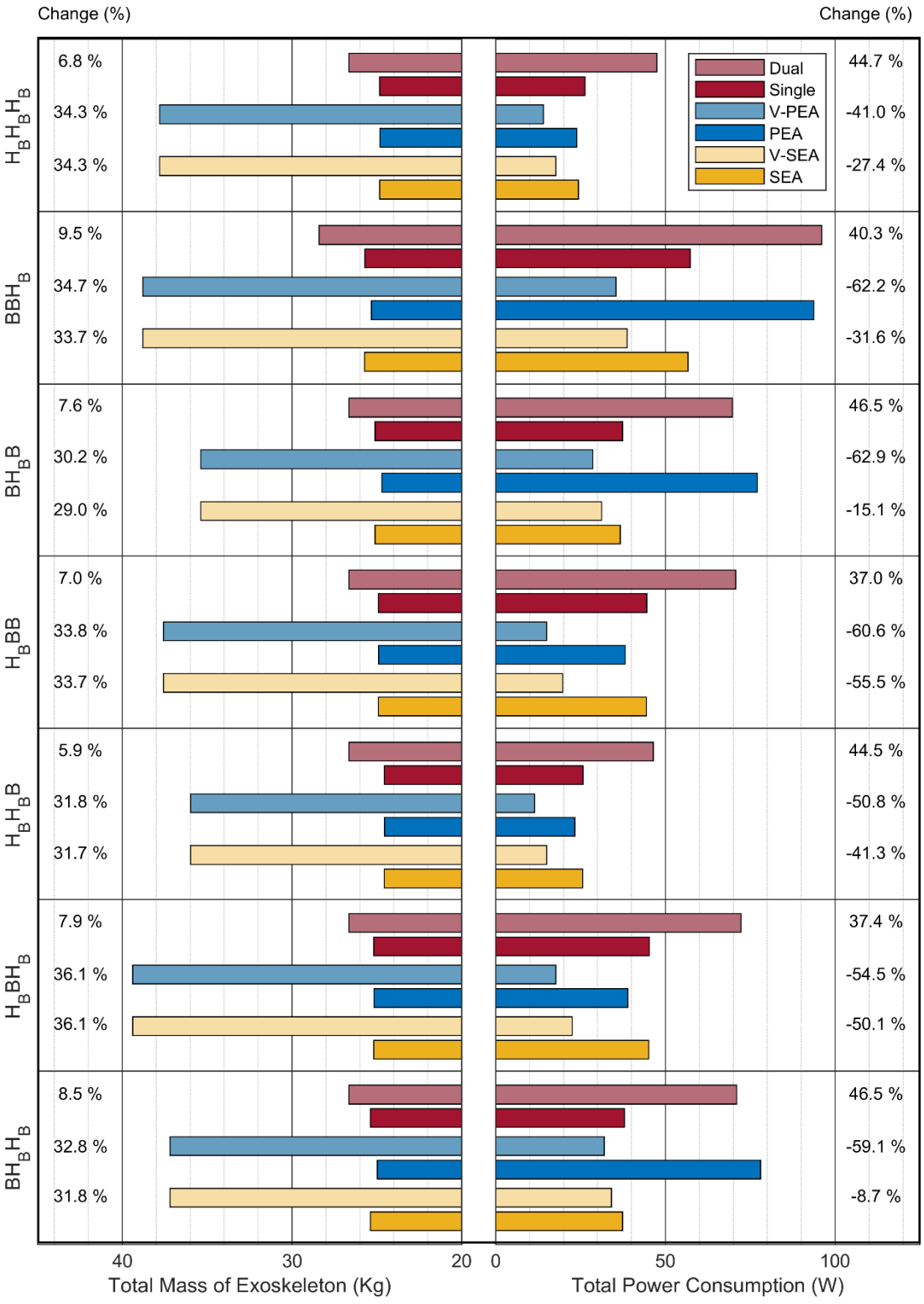

Figure 6.15: The total mass and average total power consumption of the exoskeleton of the optimal dual rigid and elastic actuation system compared with the single actuator rigid and elastic system when ball screws in an inverted slider mechanism and harmonic drives combined with belt and pulley drive system were used as the transmission mechanism. Figure shows the optimal actuation system for various combinations of these transmission systems at the lower limb joints of the assistive robotic exoskeleton

The results suggested that the total power consumption of the exoskeleton could be reduced by using dual elastic actuation system in an antagonistic arrangement. The main advantage found using dual elastic actuation system in an antagonistic arrangement was that the stiffness of the spring could be varied as the spring stiffness mechanism was non-linear and therefore, torque and power at the joint that demands a different stiffness for each type of manoeuvre could be decreased. Using V-PEA with a harmonic drive at the hip joint and ball screws at the knee and ankle as the transmission mechanism were found to be best choice. When the harmonic drive was combined with a belt and pulley drive system, the parameters of interests could further be reduced as the transmission ratio was factored by combining a belt and pulley drive mechanism. However, the transmission ratio in the belt and pulley system can only be increased up to a certain limit otherwise the diameter of the pulley will exceed our design limits. This was the reason why belt and pulley drive system cannot be used alone as the transmission mechanism.

6.4 Summary

In this chapter, the optimization of a dual actuation system arranged in an antagonistic setup for assistive robotic exoskeleton was presented. By using the concept of dual actuation system, a more power efficient system for assistive robotic exoskeletons has been realized. The optimization has been performed on three types of dual actuation system, a rigid system, a variable parallel elastic actuation system (V-PEA) and a variable series elastic actuation system (V-SEA). Section 6.2 described the methodology employed in the optimization of the dual actuation system. The spring stiffness has been optimized for V-PEA and V-SEA using the defined algorithm in Section 6.2.5. A multi-factor optimization criteria has been defined to optimize the spring stiffness. The algorithm to optimize the dual actuation system were introduced in Section 6.2.6.

The outcomes obtained for the dual actuation system of exoskeleton robots were recorded in Section 6.3. The torque and power requirement was considerably reduced using V-PEA and V-SEA at each of the joints of the lower limb. These results were described in Section 6.3.3. More favourable results were achieved using V-PEA than V-SEA. Slow walking speed was the main reason for not getting better results with V-SEA. The spring optimization results have shown a decrease of 96% on the torque and power during some of the operational modes. V-SEA has observed more reduction

in the power requirement during sit to stand manoeuvre. Section 6.3.4 highlighted the outcomes of the optimized dual actuation systems obtained for all of the three cases described. It also compared the results of the dual actuation system with the equivalent single motor actuation system. The rigid system using dual actuators however has not shown considerable difference in the overall lightweight design and power efficient system compared with the equivalent single motor system but the results of V-PEA and V-SEA has proved a more power efficient system using the concept of redundancy to realize a variable stiffness actuation system.

Chapter 7
Design Verification and Virtual Prototype Development

7.1 Introduction

In the previous chapters, a mathematical model of an assistive robotic exoskeleton was developed to achieve a lightweight, powerful and a power efficient design. This chapter will implement a virtual prototype of an assistive robotic exoskeleton for a rigid, elastic and a dual actuation system. The virtual prototype will be implemented using physical components of an actuator in a virtual environment. It will also serve to verify the actuator selection designs discussed in the previous chapters.

The design of an assistive exoskeleton recorded previously was controlled using a virtual prototype of the actuation models. Several actuation models were designed and tested at the joints of the exoskeleton to perform the desired tasks. The virtual model of an actuation system was realized by using the actual physical components within the Simscape environment of MATLAB. The virtual model was aimed to develop a true replica of an actual exoskeleton actuation system. The performance of different designs of an actuation system were investigated to ultimately achieve a virtual prototype of the system that will be developed for a rigid, elastic, dual rigid and dual elastic exoskeleton actuation system.

The development of the virtual prototype and its various components will be described in Section 7.2. Several designs of a DC motor will be implemented and these include operating the lower limb joints of an exoskeleton using a direct motion approach to a full actuator model and a trade-off will be defined in selecting the designs of the actuator. A DC motor controller will be utilized to control the speed of the DC motor. Several methods have been presented in the literature to control a DC motor [211-215]. The control technique will also be discussed to obtain a variable elastic actuator in a dual arrangement of the system. To achieve this, a distinction between the various phases of the maneuvers is required [71]. A smooth transition between different phases of the locomotion is often ignored [215]. Hence, a method will be investigated that will ensure a smooth behavior of the system. The transmission systems, elastic elements and sensing elements will be examined in a virtual protype of an exoskeleton actuation system. The spring stiffness of an elastic actuation system will be exploited since the energy

consumption can be reduced by optimizing the parameters of the spring [190, 216].

The performance and outcomes of the various designs of the actuation system will be presented in Section 7.3. Several designs of the actuator model will be tested and constraints and limitations applied to each of the them will be highlighted. The energy consumed by the virtual prototype during the performance of various locomotion tasks will be interpreted in Section 7.3.2. The design verification will be assessed by comparing the output of the virtual experimentation setup with the mathematical model of the exoskeleton actuation system analyzed previously so that a lightweight and power efficient system could be implemented.

7.2 Virtual Prototype of an actuation system

The components of a virtual prototype of an assistive robotic exoskeleton will be presented in this section. The virtual prototype of an exoskeleton was constructed by building a model in SolidWorks as represented in Figure 4.1 and then exporting the developed model in the Simscape environment of MATLAB. The length and weight of each individual component of the exoskeleton was defined to be similar as in the previous cases so that a comparison could be established. A virtual prototype of an assistive exoskeleton extracted in the Simscape environment of MATLAB by exporting the exoskeleton model from SolidWorks and then developing the actuation system in Simscape is shown in Figure 7.1. A global reference frame was attached to the left foot part and each component of the exoskeleton was linked to the other component according to the arrangement defined in the SolidWorks model of the exoskeleton. Each component of the model was described by a block in Simscape that defined completely the parameters related to that component. The parameters of the extracted model of SolidWorks will be automatically computed by Simscape and has exact mass, size, joint locations and inertia properties. Six actuators were developed and attached at each of the three lower limb joints of both legs. The modelling of the actuation system will be discussed in the upcoming sections. A joint mass block was assigned at each of the joint that represents the mass of the actuator at that joint. The two additional joint masses attached to the hip assembly indicated the upper mass of the exoskeleton and the upper body mass of the user. The lower body mass of the user was already specified at each of the lower limb part of the exoskeleton.

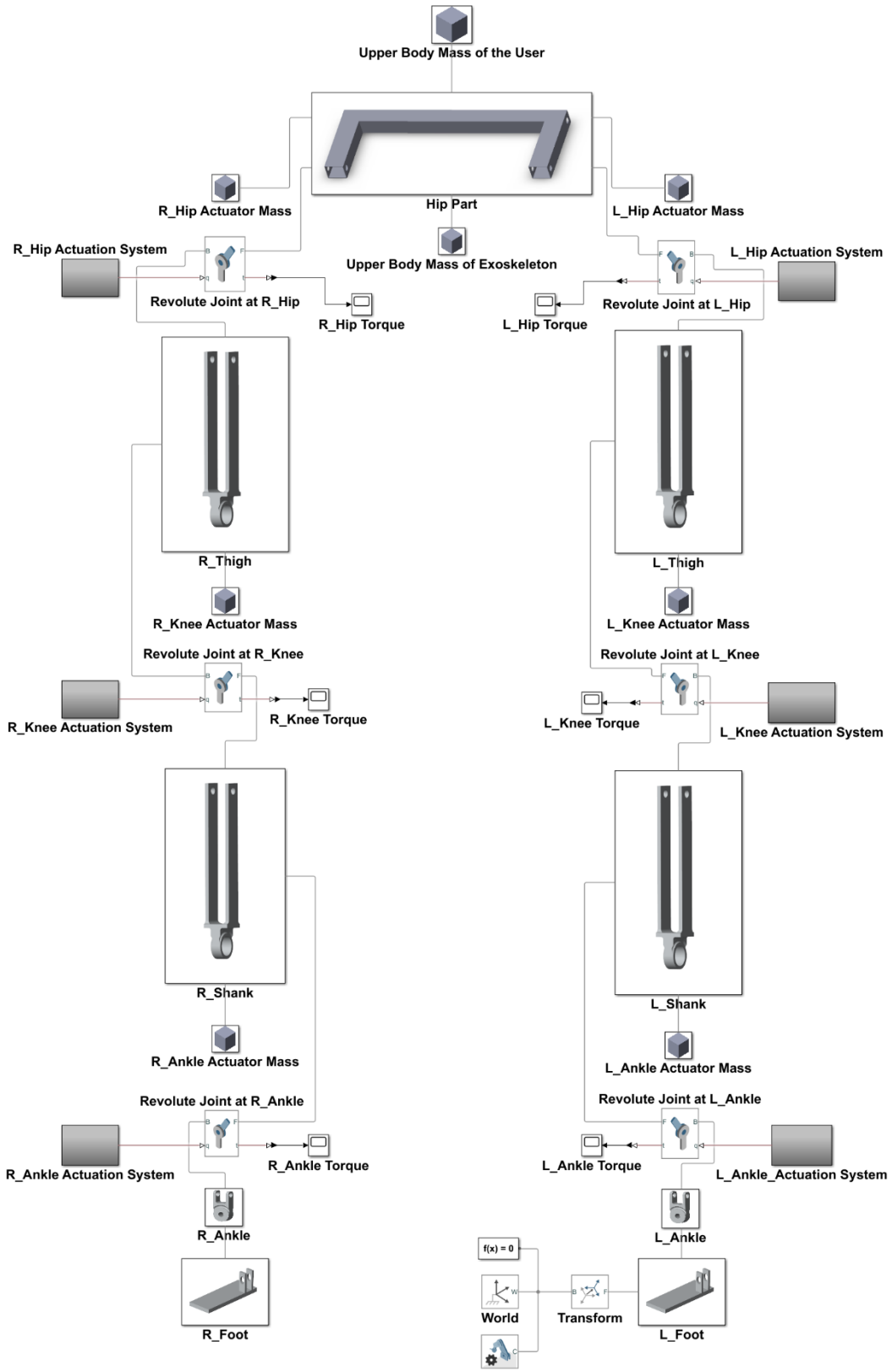

Figure 7.1: Virtual Model of an Assistive Robotic Exoskeleton

The actuator components were physically modelled in Simulink/Simscape and attached at each of the lower limb joints of the exoskeleton through a

revolute joint. These components include a controller that controls the speed of the motor so that the error between the desired speed and actual speed is minimum, a motor driver that conditions the signal to drive the DC motor by generating an output that is acceptable to be applied at the input terminals of the motor, a DC motor itself, a suitable transmission mechanism, an appropriate sensor and an elastic element (for the case of elastic actuators only). The individual components were built using the available components or a combination of the available components in Simulink/Simscape. A simplified block diagram of the actuation system of a virtual protype of an assistive exoskeleton is shown in Figure 7.2.

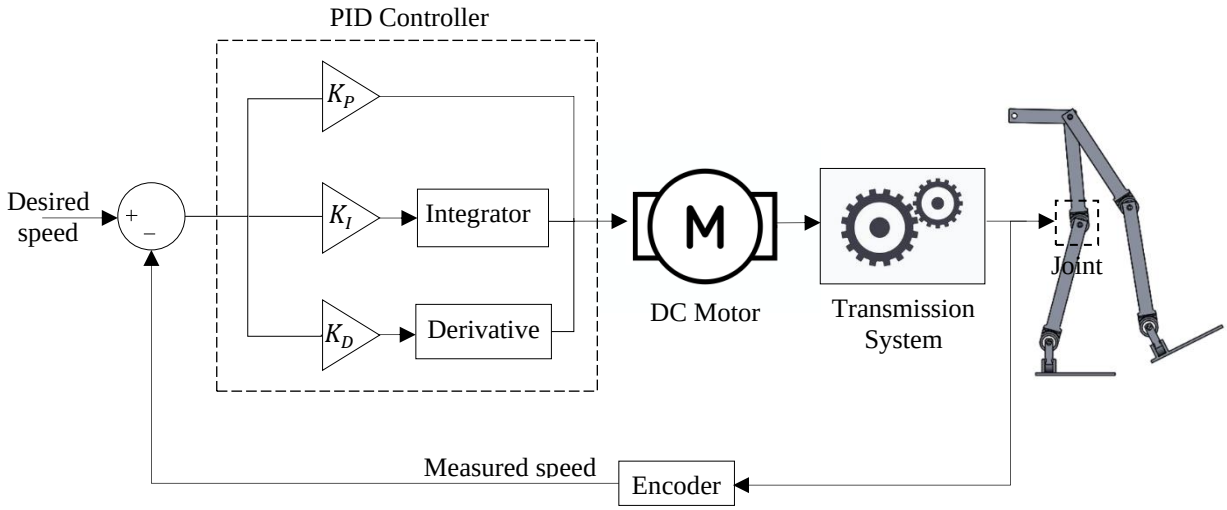

Figure 7.2: Block Diagram of a Virtual Prototype of an Actuation System of a Joint in an Assistive Exoskeleton

A PID controller was utilized to generate a speed controlled DC motor. The parameters of the PID controller were tuned to set the actual speed to the desired output. The parameters of the components of the DC motor were set to represent an actual DC motor. A voltage signal was given to its input terminals and based upon the physical parameters of the motor, a rotational speed was produced at its output. In order to reduce the size of the motor and to increase the torque produced, suitable types of the transmission systems were employed. The transmission systems applied were analyzed in detail in the previous chapters. These types of the transmission systems were modelled in Simscape to represent a virtual prototype of a transmission mechanism. In order to compare the desired output to the actual output, sensing elements were operated to measure the actual speed of the desired joint. The actuation systems were separately directed for each of the joint using the parameters of the recorded optimized systems. Each of the

individual component of the actuation system developed in Simulink/Simscape will be discussed in detail in the next section.

7.2.1 DC Motor

A DC motor is used as a form of an actuator in an assistive robotic exoskeleton actuation system. It can provide a rotary motion and when coupled with some of the transmission systems e.g. ball screws, it can also provide linear motion. A DC motor can be built in the Simscape environment of MATLAB using the actual physical components. Therefore, these models do not require any mathematical modelling of the components as is the case with Simulink. The circuit diagram of a DC motor along with the components employed to build a DC motor in Simscape in order to produce a rotational motion is shown in Figure 7.3.

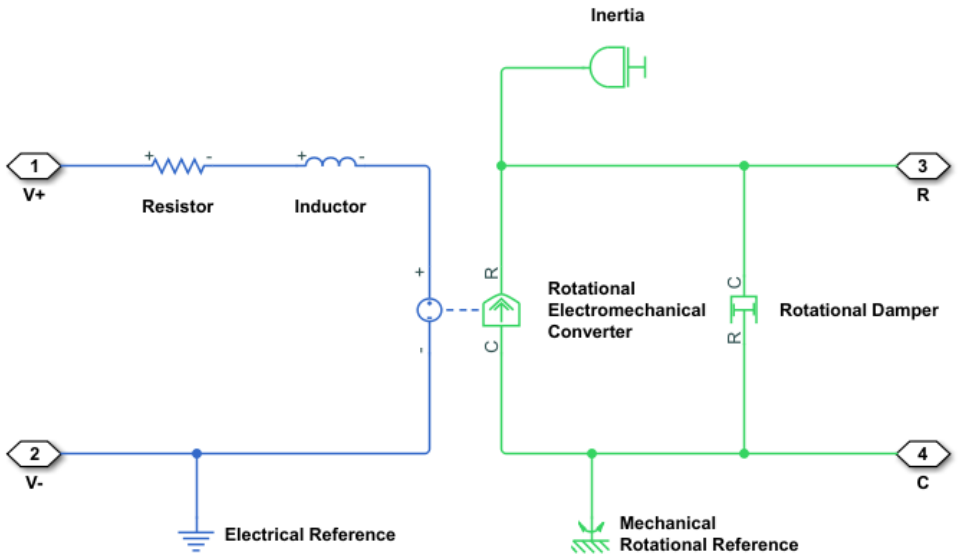

Figure 7.3: Circuit Diagram of a DC Motor Developed in Simscape

As indicated, the components include a resistor, an inductor, a rotational electromechanical convertor that defines the constant of proportionality, a rotational damper that represents the viscous friction of the motor and an inertia element with the required input and output ports. A voltage is applied at its input terminals V+ and V- and an output of a rotational angle θ and speed $\dot{\theta}$ is produced at its output. The relationship between the output speed and the input voltage is defined by the physical parameters of the components. The values of the individual components of the DC motor are given in the motors market search list in Appendix B. Therefore, for a given DC motor, the physical parameters of that specific motor were extracted from the list to be defined in the virtual model of that particular DC motor. The optimized motors were already defined in the previous chapters for each

of the type of the actuation system. Therefore, a similar or a different type of the DC motor (as the case maybe) was implemented in the virtual setup of the exoskeleton at each of the lower limb joint. It should be noted that the efficiency of the DC motor was also taken into account. It was expected that the motor will run in its maximum efficiency zone during most of the time but as noticed in [217], a DC motor in a robotic application can run through low efficiency zones as well and therefore, the average efficiency of the DC motor was evaluated to be lower than the maximum efficiency.

7.2.2 DC Motor with a Pulse Width Modulation (PWM) technique

The virtual prototype of a DC motor defined in the previous section is often suitable when there is a fixed voltage source and based on the physical parameters, it produces a rotational motion. However, for the case of varying speed, the input voltage will be fluctuating and hence a sophisticated system is required to regulate the amount of voltage at its input terminals. One such technique to achieve this is the pulse width modulation (PWM) method. In

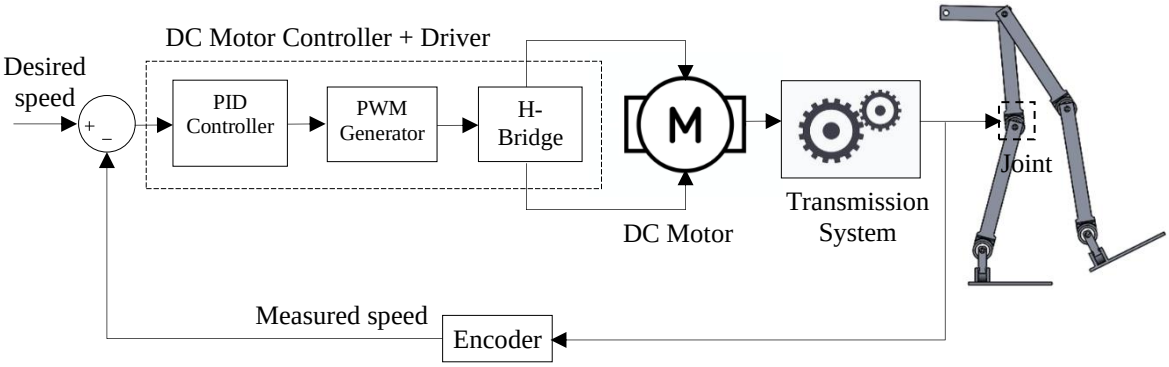

Figure 7.4: Block Diagram of a virtual prototype of an actuation system of a Joint using PWM technique

this method, the motor is driven by a series of ON/OFF pulses and by varying the duty cycle of the pulses, speed of the motor can be controlled i.e. larger the width of the pulse, the higher the average voltage that will be available for the motor and therefore, the voltage can be adjusted to alter the rotational speed of the motor. In order to realize this type of input for a DC motor, a microcontroller will be operated and by defining the desired speed curve required by the motor, the updated PWM modulated voltage could be extracted. Hence, a DC motor operated using the PWM technique was selected to drive the actuation system of the exoskeleton joints. The block diagram of a virtual DC motor using this technique is shown in Figure 7.4.

As represented, a controller and a DC motor driver consists of a PID controller along with a PWM generator and an H-bridge. The PID controller

will be explained in the next section. The PWM generator will define the pulses and its amplitude, phase and frequency of the signals are set to control the output voltage which is connected to an H-bridge that is used to control the direction of the speed of the motor. This type of a DC motor control system is complicated as compared to the previous model but it represents closely an actual DC motor system.

7.2.3 DC motor controller

As mentioned previously, a PID controller was used to develop a speed controlled DC motor system. In Simscape, a PID controller block is available that can also automatically tune the gain parameters or a combination of the components can also be used to develop a PID controller. It uses a closed loop feedback system to keep track of the actual output to the desired one. The proportional, derivative and integral terms were individually adjusted and tuned to achieve the desired output. As the speed of the selected maneuvers were slow, therefore, the integral gain could be small. However, during the PID tuning, a smaller value of integral gain did not correspond to an optimized gain. In order to develop a speed controller for a DC motor, the three terms of the PID controller were automatically tuned first and then some fine adjustments were made manually until it met the given design requirements. The gains of the individual terms used in the system are defined in Table 7.1.

Table 7.1: Gains of a PID Controller

Controller	Gains
Proportional (K_P)	82
Integral (K_I)	59
Derivative (K_D)	47

7.2.4 Gearing mechanism

The three types of the transmission systems used in the actuation system were harmonic drives, ball screws and belt and pulley drive system. The harmonic drive block was found available in the Simscape library. Therefore, it was combined with the output of the motor to increase the torque capacity of the system. The number of teeth on the circular ring gear and elliptical gear were defined to achieve the desired gear ratio N according to the relation given in Eq. (7.1) as,

$$N = \frac{n_e}{n_c - n_e} \tag{7.1}$$

Where n_e is the number of teeth of the elliptical gear and n_e is the number of teeth on the circular ring gear. The parameters that account for the power losses and efficiency of the transmission system were described. Since the efficiency was stated to be constant in Chapter 4, therefore, a constant efficiency was specified for the harmonic drive system. A virtual prototype of the actuation system built using a harmonic drive as the transmission system is shown in Figure 7.5.

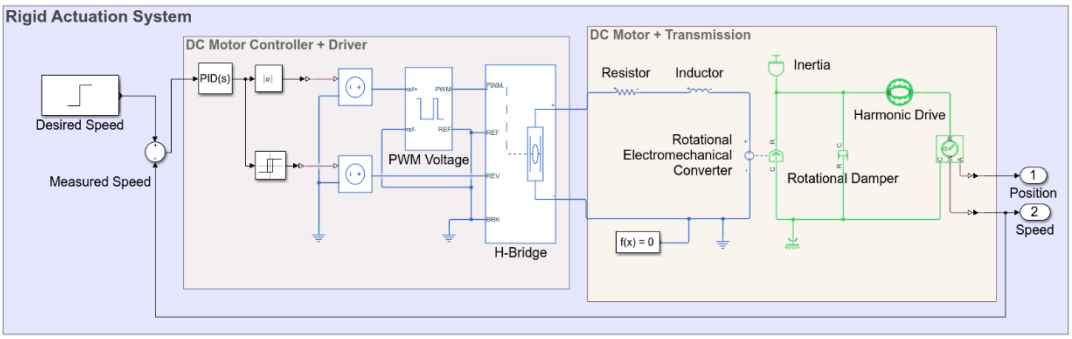

Figure 7.5: Virtual Rigid Actuation System using Harmonic drive as the Transmission system

The harmonic drive was also combined with a belt and pulley drive system to achieve an even better reduction ratio. A belt drive block in Simscape represents a pair of pulleys connected through a belt. This block was connected to the output of the motor as shown in Figure 7.6 to represent a virtual actuation system with a harmonic drive linked to a belt and pulley drive system. For the given system, an ideal pulley drive system was used in which the belt does not slip relative to the pulleys. The radii of the two pulleys were specified, since the maximum ratio obtained using belt and pulley drive system is 1:2.5 as defined in Chapter 4, therefore, this value was taken into account when defining the radius of the two pulleys.

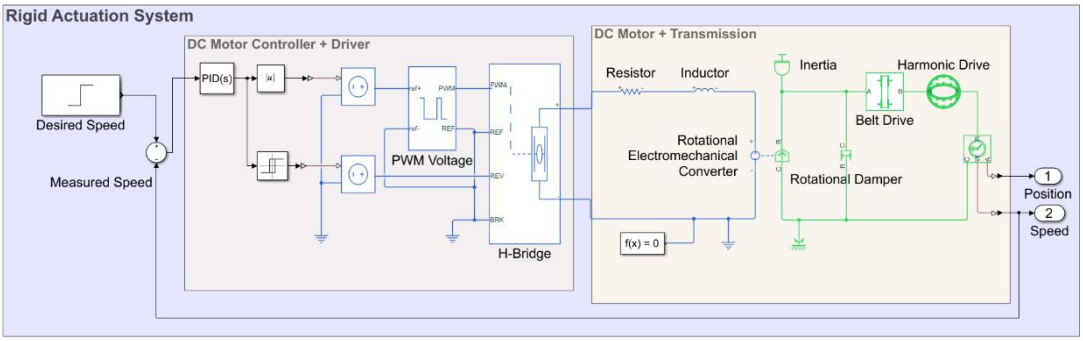

Figure 7.6: Virtual Rigid Actuation System using Harmonic drive linked to a belt and pulley drive system

The third type of the transmission system used in the actuation system is the ballscrews in an inverted slider crank mechanism. However, it was found not

available in the Simscape library but a different version known as Leadscrew was realized, since the ballscrews and leadscrews do not differ, therefore, leadscrew was employed to be used as a transmission system. This was combined with the output of the DC motor. Furthermore, to keep the system less complicated, it was not used in an inverted slider crank mechanism. A virtual actuation system built using the above transmission system is elaborated in Figure 7.7.

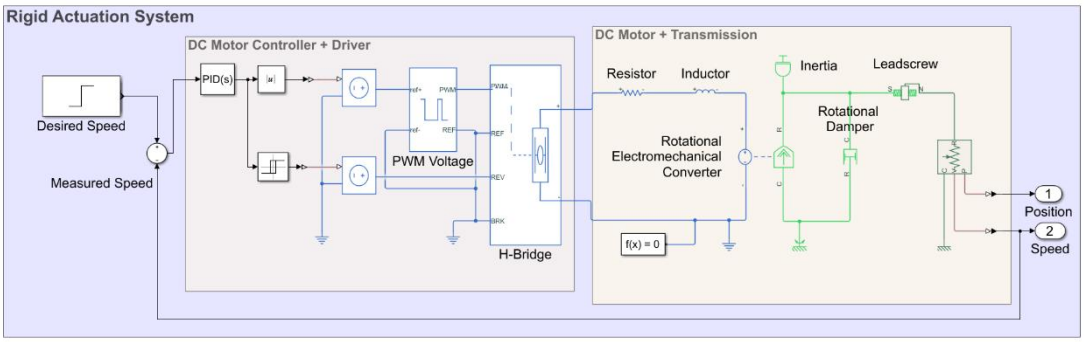

Figure 7.7: Rigid Actuation System using Lead Screw as the form of the Transmission Mechanism

7.2.5 Sensing elements

In order to measure the output parameters, various sensing elements were employed in the virtual model. These include the voltage sensor, that measures the voltage applied to the input terminals of the motor, the current sensor, that can yield the current flowing through the circuit with the given motor resistance and other parameters. Together the voltage and current will give the electrical power input of the system.

Since the DC motor controller works in a closed loop feedback system, therefore, sensing elements to measure the output parameters were required. In order to assess these parameters, rotational motion sensors were employed that can evaluate the speed and position of the motor. These represent an ideal sensors and subsequently they do not account for inertia, friction, efficiency and noise of the sensor. Since average power will be considered as will be explained in the next section, therefore the parameters considering the non-ideal behavior of the sensing elements will not have a large effect on the output of the sensor. A torque sensor was also employed to measure the output torque of the system.

7.2.6 Elastic elements

The torsional springs were employed in order to develop series and parallel elastic actuators that can be directly coupled to a DC motor. A rotational spring can be found in the Simscape library that were connected to a DC

motor in series or in parallel. The spring stiffness and its initial deformation can be defined in order to employ the spring in its optimized form. The series and parallel springs were optimized for their stiffness and equilibrium angle in Chapter 5, therefore, those values were applied in the virtual model of elastic actuators. This will also lead to the validation of the mathematical model developed previously. An example of a virtual elastic actuation system using a parallel spring is shown in Figure 7.8.

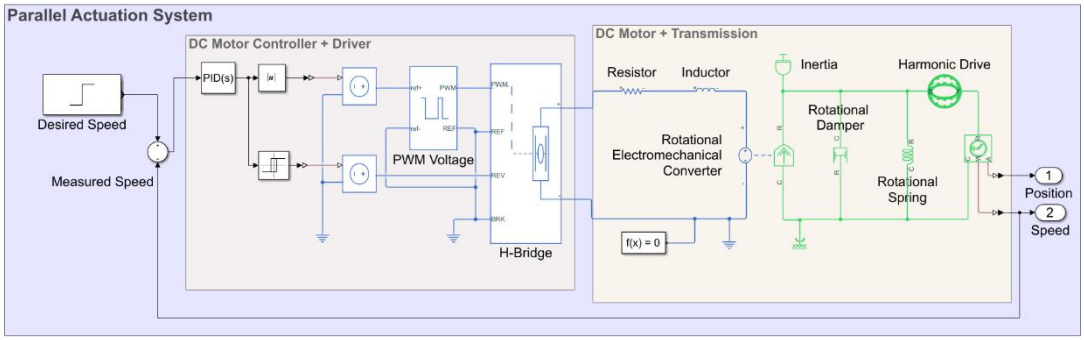

Figure 7.8: An elastic system using a parallel spring in a virtual prototype of an actuation system

7.2.7 Dual motor actuation system

A dual motor actuation system was implemented in Simscape that represented a virtual prototype of a rigid, variable series and variable parallel actuation system. A block diagram for a dual actuation system is shown in Figure 7.9. Each pair of a dual motor actuation system represents a controller and a driver that supplies the input to the two units of the DC motor and the transmission system. Since the two actuator units were identical and each unit is responsible to provide half of the actuation power, therefore, similar speed and power were supplied to both of the units by the controller keeping the desired speed to half of its original value. The two units were coupled together through a belt and pulley drive system. For the case of the transmission system where only harmonic drives were used, the radii of the two pulleys were kept similar but when harmonic drives were linked with a belt and pulley drive system, the radii of the two pulleys were made different to account for a further reduction ratio.

In a dual elastic actuation system, series and parallel elastic actuators were implemented in a way such that the stiffness could be varied. The spring variation mechanism in a dual elastic actuation system has been explained in Chapter 6. In a virtual prototype, this was implemented using a variable rotational spring in Simscape. For each specific maneuver, the two motors

were rotated first to set the stiffness of the spring to a desired value and then the particular maneuver was implemented.

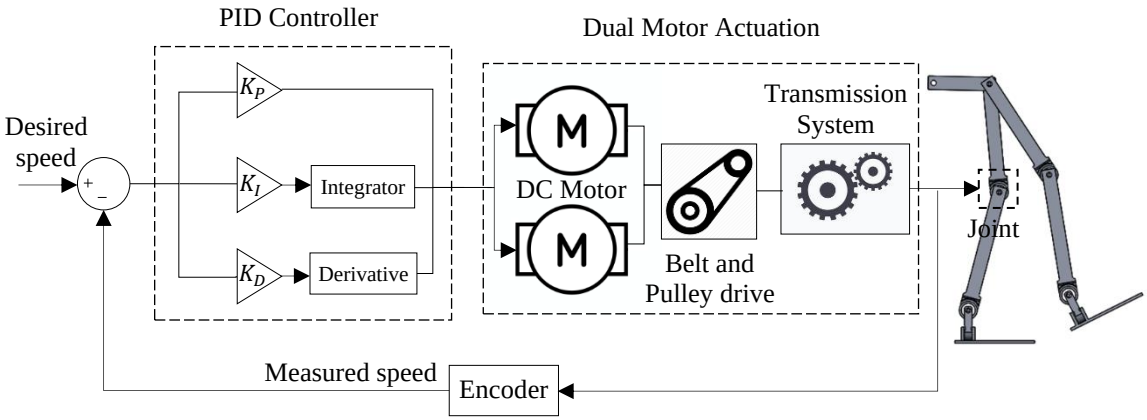

Figure 7.9: Block Diagram of a Virtual Prototype of a Dual Actuation System of a Joint in an Assistive Exoskeleton

Each unit of a virtual protype of an actuation system explained in this section was realized at each of the lower limb joints of an assistive robotic exoskeleton. In a dual actuation system, the two units of the actuators were operated at each of the joints. An example of a detailed virtual actuation system model represented with the prototype of an assistive exoskeleton is shown in Figure 7.10 . This model is demonstrated for one leg only with a single actuator to elaborate the virtual system realized at each of the three lower limb joints during the sit to stand maneuver. A DC motor speed controlled method was implemented and therefore, a desired speed of the joint was fed to the controller and a PWM technique was executed to regulate the amount of voltage to the DC motor. To carry out this process, a PWM voltage generator was applied whose output was given to an H-bridge that controls the direction of the motor depending upon whether the signal is positive or negative. If the signal is positive, a higher voltage is applied at the REV terminal of an H-bridge via a relay to rotate the motor in the positive direction but if the signal is negative, the voltage produced at the REV terminal is less than the threshold voltage level and consequently, the H-bridge moves the motor in the opposite direction. The block of the DC actuator represents the model of the DC motor and a suitable type of the transmission system in order to produce the desired position and speed at the revolute joint of the respective linkage. The position, speed, acceleration and torque of the respective joint can be measured using the actuation sensing elements.

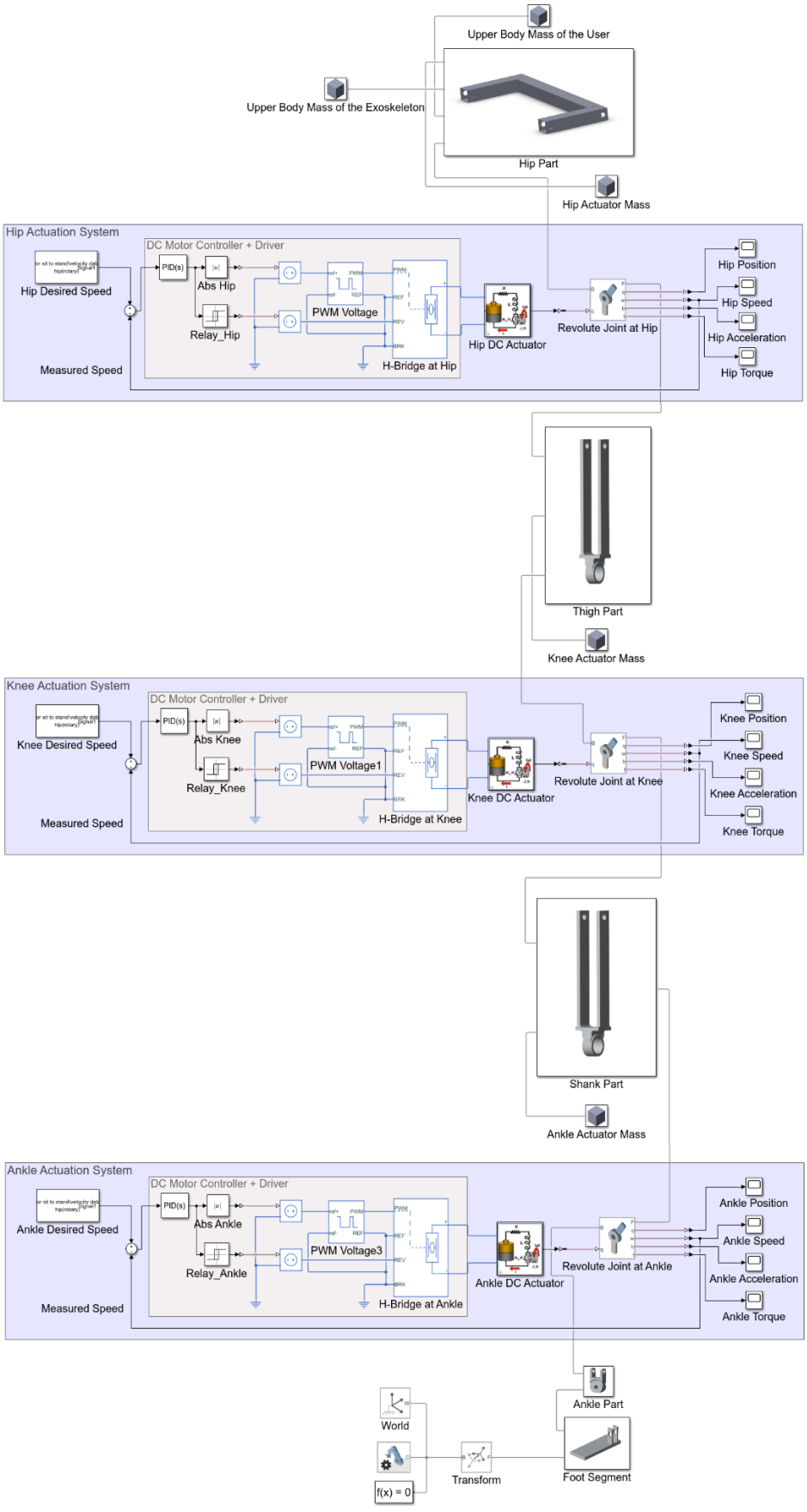

Figure 7.10: A detailed model of the actuation system at the hip, knee and ankle joints of an assistive exoskeleton

The virtual prototype of an assistive robotic exoskeleton actuation system will be used to study the rigid, elastic and dual actuation system in a virtual experimentation setup. The power consumption of the actuation system obtained mathematically and explained in the previous designs will be validated using the virtual setup. The optimal spring stiffness obtained will also be confirmed using a virtual model of an elastic actuation system. Similarly, the dual actuation concept was also implemented to obtain a power efficient system for a dual robotic exoskeleton actuation system.

7.3 Results and Discussion

The results obtained using a virtual experimentation setup will be discussed in this section. The performance identified using the variants of the actuation system developed and explained in the previous section will be analyzed followed by investigating the power consumption of the virtual actuation system. These will be examined for a rigid and elastic actuation system and also for a dual rigid and elastic actuation system.

7.3.1 Performance of different variants of an actuation system

In this section, the output of the actuation system using different models of the DC motor will be elaborated. It was mentioned in Section 7.2.1 and 7.2.2 that a DC motor was built using the available physical components in Simscape environment of MATLAB. The first variant of the actuation system was developed using the basic components in a DC motor. In the second type, the DC motor model was realized using a pulse width modulation (PWM) technique. The latter type of the model implements a more realistic approach in the development of the DC motor prototype. The output of the actuation system using the two types of the DC motor models will be evaluated. Furthermore, a direct approach in modelling the exoskeleton maneuvers was also implemented i.e. the desired speed of the joint was given directly to the joint of the exoskeleton prototype without any actuation system for comparison purposes. The output of the actuation systems will be analyzed during sit to stand and walking operation. For illustration purposes, the output will be depicted only during sit to stand transition. An STS maneuver for a complete transition time can be observed in Figure 7.11.

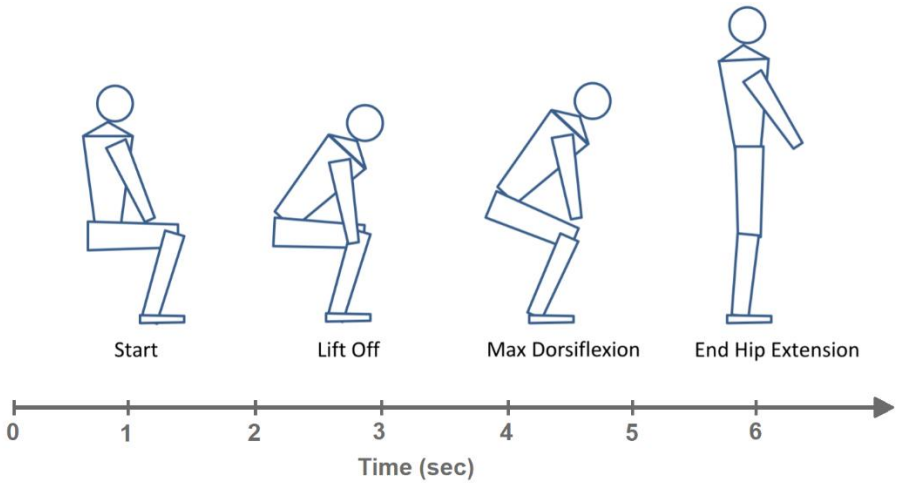

Figure 7.11: Movement during Sit-to-Stand (STS) Transition [218]

- **Hip Joint**

Figure 7.5 shows the mechanical power produced by the DC motor compared with the electrical power consumed by the DC motor at the hip joint during the sit to stand maneuver. The mechanical power was obtained using the rotational speed and torque of the motor. The electrical power was calculated using the voltage applied at its terminals and the current passing through its circuit. The output from the three actuation types in modelling the sit to stand maneuvers is depicted in Figure 7.12.

As can be observed in Figure 7.12 (a), (c) and (e), the speed, toque and mechanical power respectively were obtained using the three different variants of the actuation system. The output from the direct motion approach was observed to be noisy and oscillatory as compared to the outputs from the other variants. Using the second variant of the actuation system with a DC motor and the controller, the output torque was smooth as assessed with the previous case since the controller with the feedback loop keeps the actual output close to its desired value. The torque and power evaluated using the third variant of the actuation system i.e. a DC motor using a PWM technique produces an output that was also smooth with only some random noise signals. As the PWM generator runs at a specific frequency, therefore, output was fluctuating at some points. Furthermore, the simulation time was also noticed to be increased for the full actuation model since this variant of the actuation model was complicated and therefore, a trade-off was required between the model fidelity and the simulation speed that results in the generation of the random noise signals at some points.

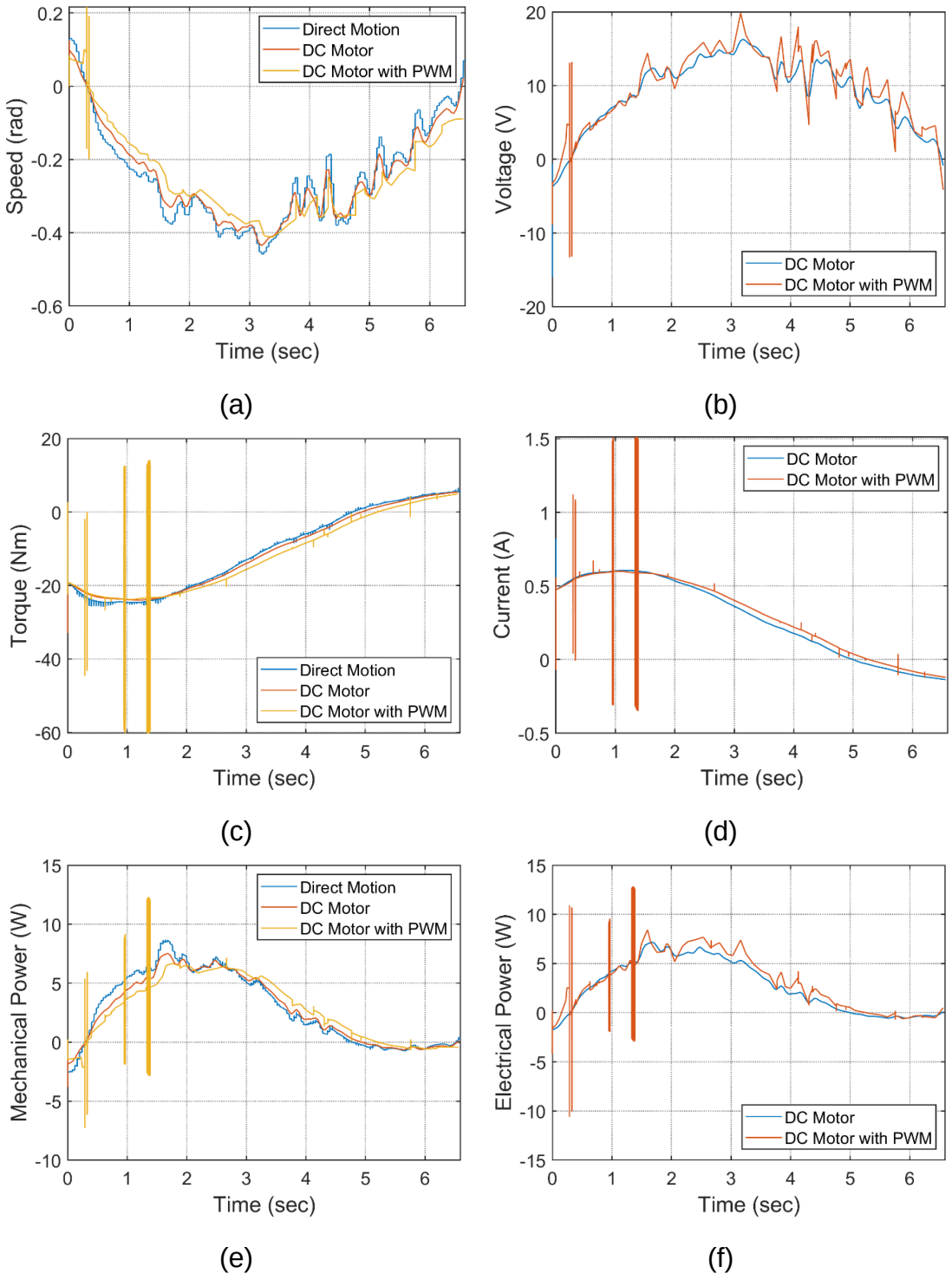

Figure 7.12: (a) Rotational Speed, (b) Voltage, (c) Torque, (d) Current, (e) Mechanical Power and (f) Electrical Power of Several Variants of the Virtual Prototype of an Actuation System at the Hip Joint in an Assistive Robotic Exoskeleton During Sit-to-Stand Manoeuvre.

The voltage and current graphs also showed a similar trend with some random spikes in the signal when moving towards the full actuation

variant. The trajectories of electrical and mechanical power were observed to be similar.

- **Knee Joint**

The output of the actuation system at the knee joint during sit to stand maneuver can be observed in Figure 7.13. The three models of the actuation system follow a similar trend at the knee joint as well. The speed of the system for the case of direct approach was observed to be smooth but spikes were observed during the toque trajectory. On the other hand, a smooth curve with less oscillations was realized by the second variant of the actuation system using a DC motor and a controller. This is true for each parameter of the actuation system. The simulation time was also less in the second variant since the model was not very complicated. The full actuator model shows a smooth curve for the speed and voltage but some random spikes and oscillations were observed for the toque and current of the motor. The electrical and mechanical power of the DC motor follows a similar trend.

- **Ankle Joint**

The mechanical and electrical parameters of the actuation system at the ankle joint during sit to stand maneuver are represented in Figure 7.14. In a direct motion model, the speed was realized to be smooth but the spikes were visible at the torque trajectory and therefore, at the mechanical power as well. Moving from the motion model to the actuator model, the parameters were smooth with less spikes. With the full actuator model, the graphs were also observed to be smooth with some random spikes but a trade-off was made in the running time of the simulation.

The trajectories were only shown for the case of sit to stand maneuver because the parameters of the actuation system follows similar pattern in other maneuvers as well. By observing the graphs of the parameters of the DC motor during sit to stand maneuver for the three actuator models, it was observed that even though the curves were not identical but they follow a similar trajectory pattern. This is true since similar actuator commands were given to the three variants. During the direct motion approach, the speed and angular position of the joint was idealized and therefore, smooth curves were appeared but some big spikes were noticed at the torque curve. These spikes tend to be less exaggerated as the system moves from the motion model to the actuator model. The speed and position was not similar to the

idealized speed of the motion model but overall a smooth curve with less oscillations was recorded for the toque and power curve. The exoskeleton was able to walk and follow the trajectory for all of the above three cases.

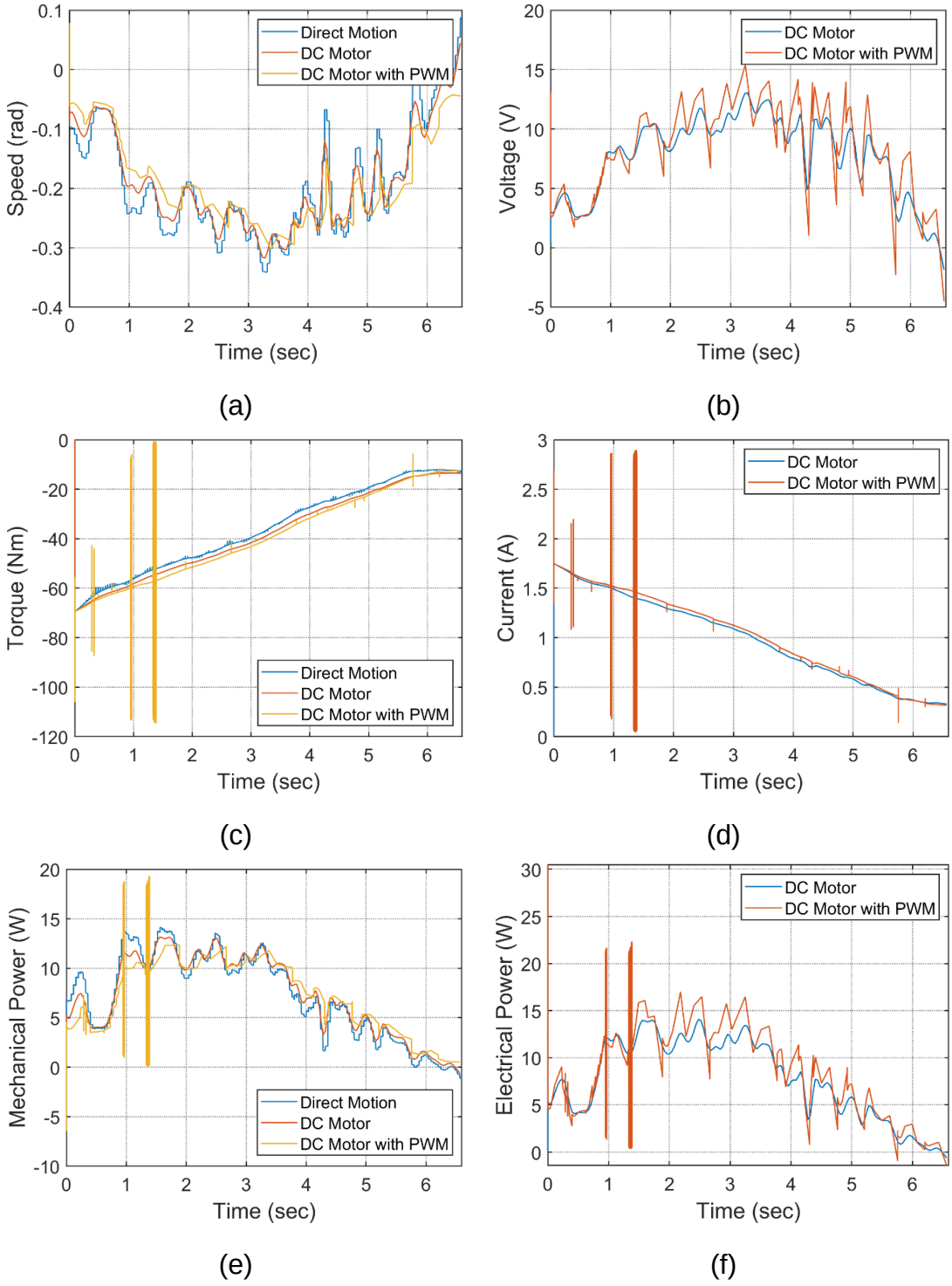

Figure 7.13: (a) Rotational Speed, (b) Voltage, (c) Torque, (d) Current, (e) Mechanical Power and (f) Electrical Power of Several Variants of the Virtual Prototype of an Actuation System at the Knee Joint in an Assistive Robotic Exoskeleton During Sit-to-Stand Manoeuvre.

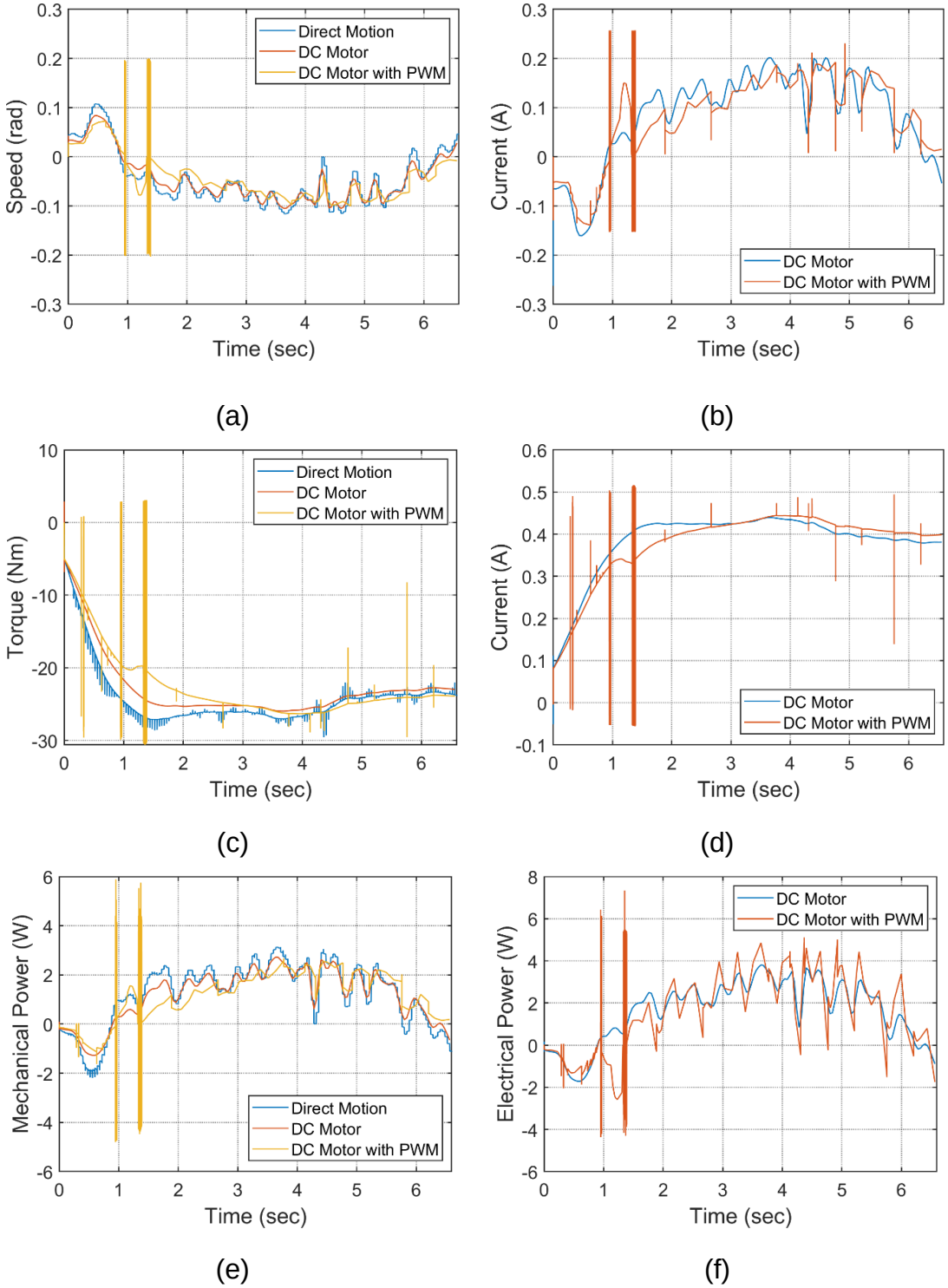

Figure 7.14: (a) Rotational Speed, (b) Voltage, (c) Torque, (d) Current, (e) Mechanical Power and (f) Electrical Power of Several Variants of the Virtual Prototype of an Actuation System at the Ankle Joint in an Assistive Robotic Exoskeleton During Sit-to-Stand Manoeuvre.

The optimization of the parameters of the actuation system is found to be a very challenging design task and requires a trade-off among different design aspects. It was revealed that the simulation time was much increased when moving towards the full actuation model. This was due to the reason that the system becomes more complicated with the addition of further physical details and power electronics to the system. The ideal motion actuator model helps to gain insight of the required torque and speed curve of the actuator that will be needed to perform the desired maneuvers.

In the above task, the controllers used were limited to a simple design otherwise the simulation time will add up with the complexity of the design. The coupling between the controllers was disregarded which alternatively could make the overall system more efficient. The trajectories of the robotic exoskeleton were also predefined and were not subjected to the environmental disturbances e.g. a rough terrain or if pushed by another force.

7.3.2 Design verification using a virtual experimentation model

The virtual experimentation model described in Section 7.2 was applied to compute the average power consumption of an assistive robotic exoskeleton. The virtual prototype was developed for a rigid actuation system, a series elastic actuation system, a parallel elastic actuation system, dual rigid actuation system and dual elastic actuation system. The performance of the three variants of the actuation systems was examined in the preceding section and it was revealed that the three variants yield similar power consumption patterns. Consequently, any variant of the actuation model could be utilized to assess the average power consumption of an assistive robotic exoskeleton actuation system. Furthermore, the full actuation model using a PWM technique reflected more specifically a real model of an actuation system, hence the full actuation model was used to evaluate the average power consumption of the actuation system for rigid, elastic and dual exoskeleton systems. It should be noted that the electrical power was used to determine the total power consumption of the system. The mathematical model of an assistive robotic exoskeleton actuation system developed and assessed in the previous chapters will also be verified with the virtual experimentation model. Results will be presented for each type of an assistive exoskeleton actuation system grouping them according to the type of transmission systems. For a particular type of the exoskeleton actuation system, results will be identified if the actuation systems at the lower limb joints are using harmonic drives or ball screws as

the form of the transmission mechanism or ball screws or harmonic drives combined with the belt and pulley drive system are used. The power consumption will be specified for every single combination of the transmission mechanism at the lower limb joints.

7.3.2.1 Rigid actuation system

The average power consumption was extracted using a virtual model of a rigid actuation system and compared with the power consumption obtained from the earlier developed mathematical model of a rigid actuation system. This was investigated for each combination of the transmission system used at the lower limb joints. Figure 7.15 shows the results of the average power consumption of the rigid actuation system for a range of the transmission systems. Figure 7.15(a) depicts the results for ball screws and harmonic drives as the transmission systems and Figure 7.15(b) illustrates them for harmonic drives combined with a belt and pulley drive system and ball screws as the form of the transmission system in the actuation system.

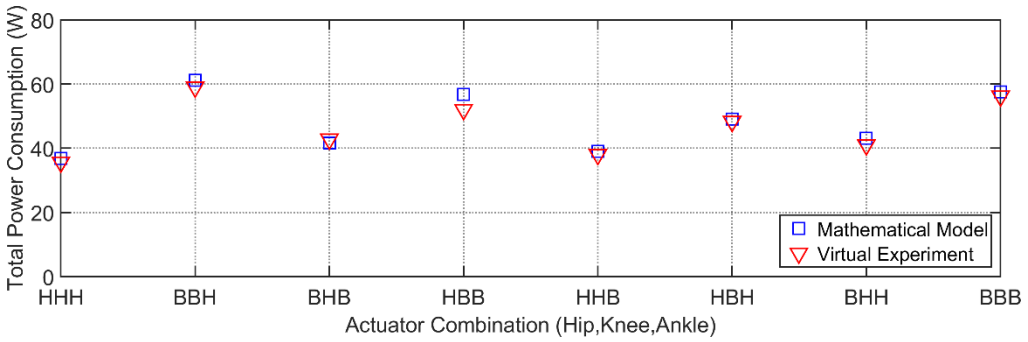

(a)

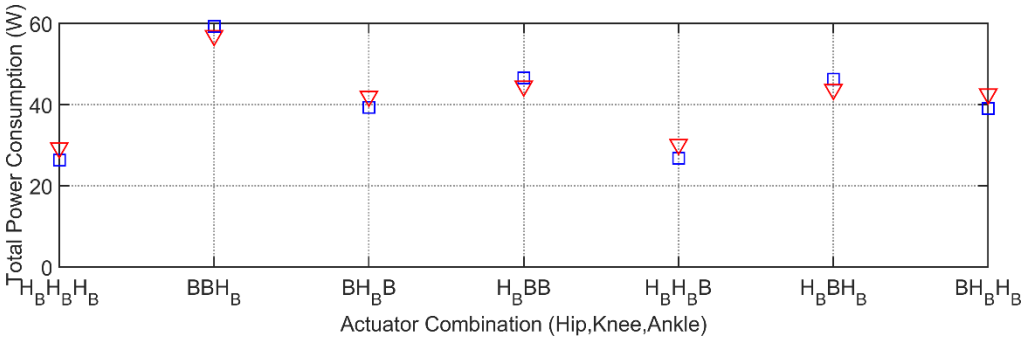

(b)

Figure 7.15: Average Total Power Consumption using a Virtual Prototype Compared with the Mathematical Model of an Optimal Rigid Actuation System when (a) Lead screws (B) and Harmonic drives (H) were used as the Transmission System and (b) Lead screws (B) and Harmonic Drives linked to a Belt and Pulley drive System (H_B) were used as the Transmission System. The first, second and third letter corresponds the mechanism at the hip, knee and ankle joints respectively.

The total power consumption assessed using a virtual experimentation setup was indicated close to the power attained using the mathematical model. A slight dissimilarity was evolved in the power consumption for the combination HBB but the difference was not observed to be significant. In some combinations, the power consumption was slightly higher for the virtual model as compared to the mathematical model and in other cases it was observed to be lower. But overall the difference was insignificant. Since the Pearson R-value squared (r^2) of 0.97 and 0.96 were revealed for the actuation systems represented in Figure 7.15(a) and (b) respectively, therefore, it indicates a high correlation between the two models for both of the transmission systems combinations. The correlation study for some of the actuation systems are represented in Figure 7.21. It is observed that by using a harmonic drive combined with a belt and pulley drive system reduces the amount of energy consumed in a virtual experimentation model.

7.3.2.2 Parallel elastic actuation system

Figure 7.15 refers to the total power consumption that corresponds to the virtual experimentation setup and the mathematical model of a parallel elastic actuation system. The outcomes of the power consumption of the actuation system while employing harmonic drives and ball screws as the transmission system are presented in Figure 7.16(a). Similarly, the results examined when harmonic drives were linked with the belt and pulley drive system or a ball screw was utilized solely as a form of the transmission system are shown in Figure 7.16(b).

The average total power consumption assessed for parallel elastic actuation system in a virtual experimentation setup revealed a similar trend according to the case of rigid elastic actuation system when compared with the mathematical model of the parallel elastic actuation system. The difference in the energy consumed between the virtual prototype and the mathematical model was insignificant. The Pearson R-value squared (r^2) for the two transmission systems combinations in PEA were 0.99 that also indicates a high correlation. The total power consumption was reduced to some extent when harmonic drives linked with a belt and pulley drive system were applied as the transmission system. In the exoskeleton setup, where ball screws/lead screws were implemented at the hip and ankle joint and harmonic drives were applied at the knee joint, a marginal difference was observed between the virtual setup and the mathematical model. However, the variation was insignificant as this was revealed by the correlation study. The total power consumption was slightly lessened in the virtual

experimentation setup as compared to the mathematical model of the parallel elastic actuation system.

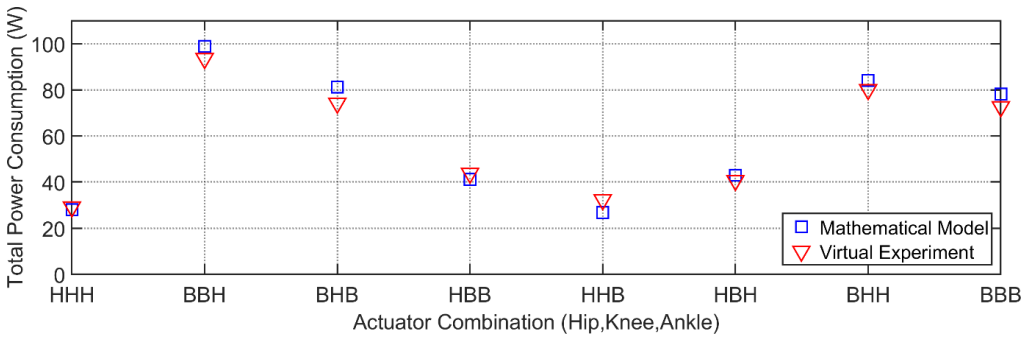

(a)

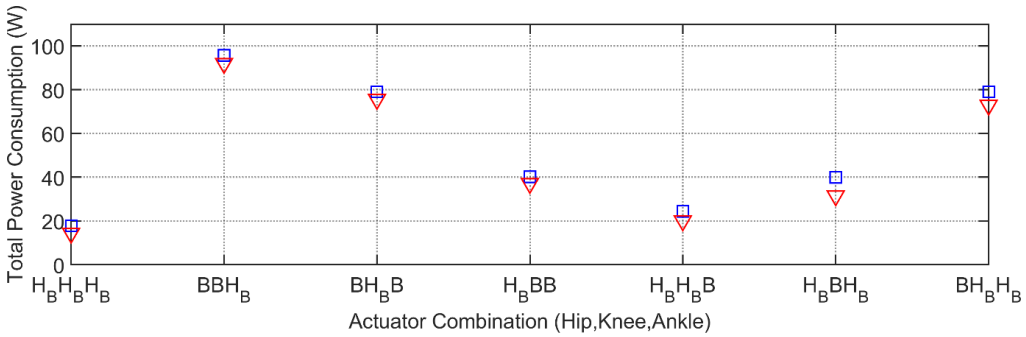

(b)

Figure 7.16: Average Total Power Consumption using a Virtual Prototype Compared with the Mathematical Model of an Optimal Parallel Elastic Actuation System when (a) Lead screws (B) and Harmonic drives (H) were used as the Transmission System and (b) Lead screws (B) and Harmonic Drives linked to a Belt and Pulley drive System (H_B) were used as the Transmission System. The first, second and third letter corresponds the mechanism at the hip, knee and ankle joints respectively.

7.3.2.3 Series Elastic Actuation system

The average total power consumption evaluated in a virtual experimentation setup of series elastic actuator in an assistive robotic exoskeleton is presented in Figure 7.17. Figure 7.17 (a) shows the results while using either the harmonic drive or ball screws at the joint as the form of the transmission system in a series elastic actuator. The results depicted in Figure 7.17 (b) were revealed when the harmonic drive was linked to the belt and pulley drive system.

The variation in the outcomes of the virtual protype and the mathematical model was not significant in any of the transmission system combinations in the series elastic actuator. The Pearson R-value squared (r^2) were 0.89 and

0.95 respectively for the two transmission system combinations in SEA. Nevertheless, a slight difference was observed for the following combination of the transmission system at the lower limb joints of the exoskeleton, ball screws at the hip and knee and harmonic drive at the ankle joint. However, the difference was less than 10W. For this specific combination, when the harmonic drives were linked to the belt and pulley system, a reduction in the power consumption was noticed. Furthermore, difference in the power consumption between the virtual experiment and the mathematical model was also diminished. In the virtual setup, the reduction in the total power consumption was only marginally reduced as compared to the rigid actuation system.

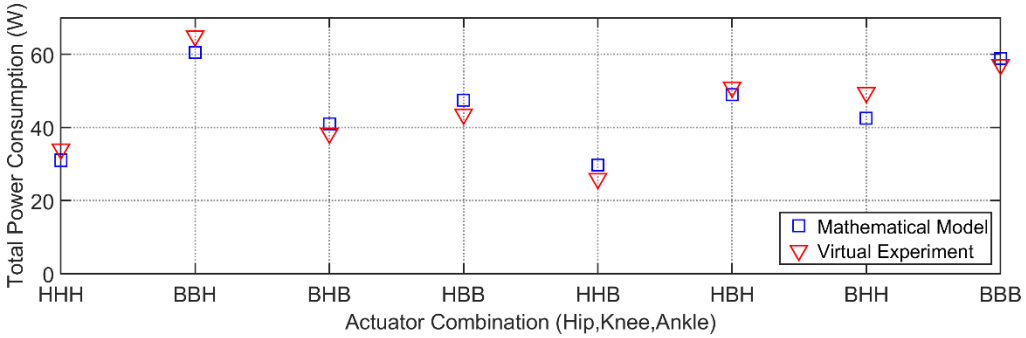

(a)

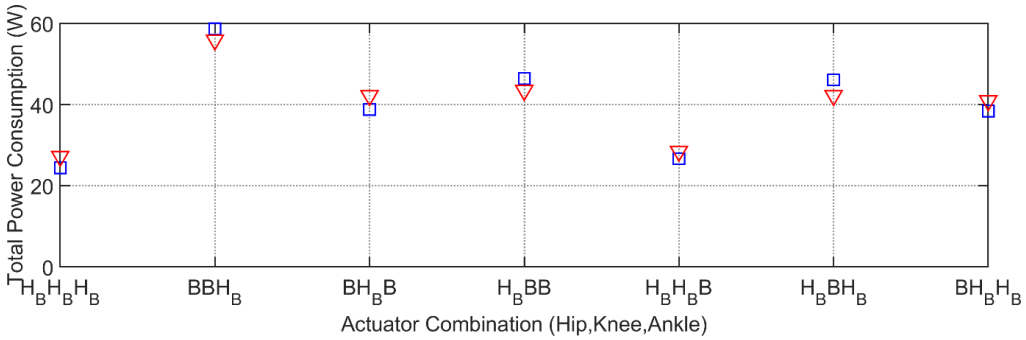

(b)

Figure 7.17: Average Total Power Consumption using a Virtual Prototype Compared with the Mathematical Model of an Optimal Series Elastic Actuation System when (a) Lead screws (B) and Harmonic drives (H) were used as the Transmission System and (b) Lead screws (B) and Harmonic Drives linked to a Belt and Pulley drive System (H_B) were used as the Transmission System. The first, second and third letter corresponds the mechanism at the hip, knee and ankle joints respectively.

7.3.2.4 Dual rigid and elastic actuation system

The average total power consumption examined in a virtual prototype of a dual actuation system in an assistive exoskeleton was interpreted in Figures 7.18 to 7.20. These were discussed for the case of rigid, parallel and series

elastic actuation system in a dual arrangement. In Figure 7.18(a), the average total power consumption was illustrated for a dual rigid actuation system using harmonic drives and ball screws as the transmission systems. Similarly, Figure 7.18(b) shows the results for the dual rigid actuation system using harmonic drives that were linked with a belt and pulley drive system or by using ball screws as the type of the transmission system. The energy consumed in a virtual setup of the dual actuation system was identical when assessed using a mathematical model with only a marginal difference in some of the transmission system combinations. The Pearson R-value squared (r^2) of 0.99 and 0.98 were revealed for the two transmission system combinations in a rigid, dual actuation system. The energy consumed was also lessened when harmonic drive was linked with a belt and pulley drive system.

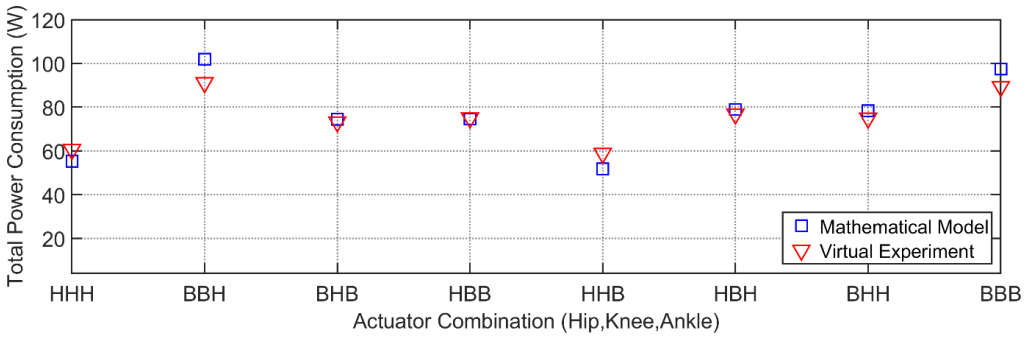

(a)

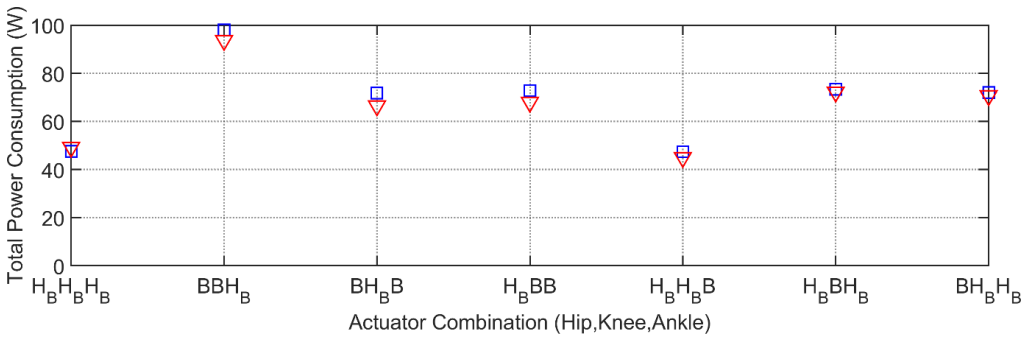

(b)

Figure 7.18: Average Total Power Consumption using a Virtual Prototype Compared with the Mathematical Model of an Optimal Dual Rigid Actuation System when (a) Lead screws (B) and Harmonic drives (H) were used as the Transmission System and (b) Lead screws (B) and Harmonic Drives linked to a Belt and Pulley drive System (H_B) were used as the Transmission System. The first, second and third letter corresponds the mechanism at the hip, knee and ankle joints respectively.

The average power consumption in a parallel elastic actuation system in a dual arrangement can be analyzed in Figure 7.19. Since one of the purposes

of the dual arrangement was to adjust the stiffness of the spring during its maneuver, therefore the average total power consumption was significantly reduced as compared to the single arrangement setup. When the results of the virtual prototype were examined with the mathematical model of the dual actuation system, the results were identical except in a limited number of cases i.e. using ball screws at the hip and ankle joint and harmonic drive at the knee joint and by using harmonic drive at the hip joint and ball screws at the knee and ankle joint. There was also a difference when ball screws were used at the hip joint and harmonic drives were employed at the knee and ankle joint. These outcomes hold true for the second case as well i.e. harmonic drives linked with the belt and pulley drive system. The Pearson R-value squared (r^2) for the two cases were 0.96 and 0.95 respectively that indicates a high correlation between the two models.

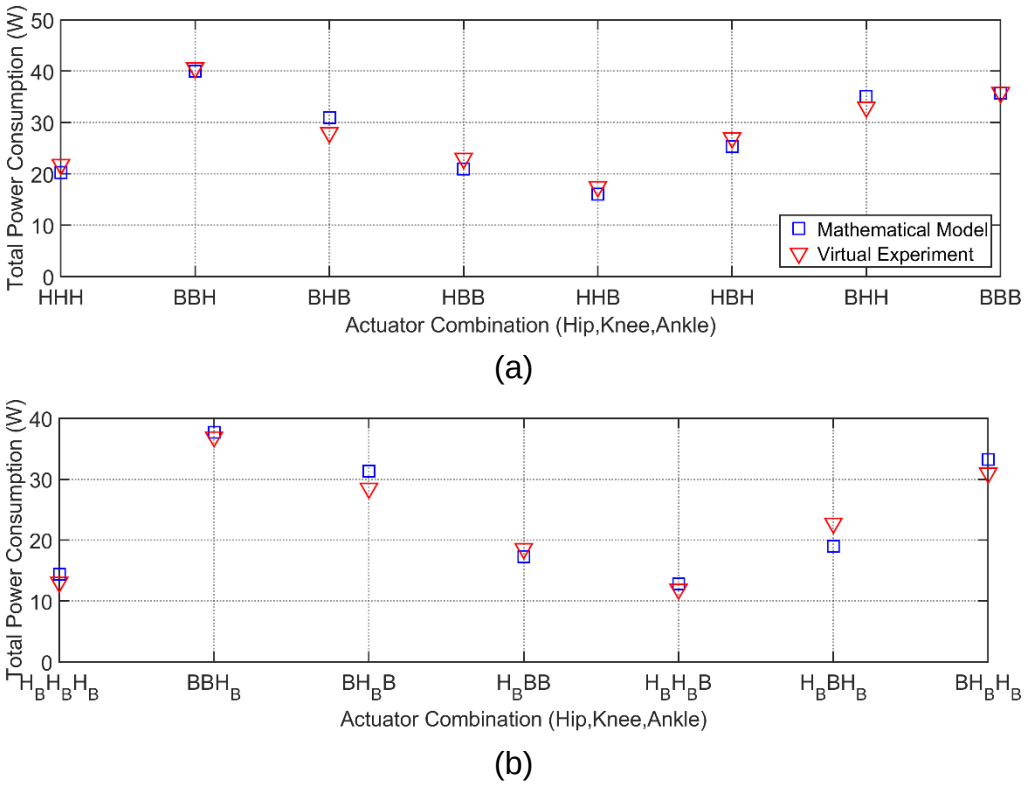

Figure 7.19: Average Total Power Consumption using a Virtual Prototype Compared with the Mathematical Model of an Optimal Dual Parallel Elastic Actuation System when (a) Lead screws (B) and Harmonic drives (H) were used as the Transmission System and (b) Lead screws (B) and Harmonic Drives linked to a Belt and Pulley drive System (H_B) were used as the Transmission System. The first, second and third letter corresponds the mechanism at the hip, knee and ankle joints respectively.

Similarly, the findings of the dual series elastic actuation system were elaborated in Figure 7.20. The harmonic drive and ball screws were used for

the case illustrated in Figure 7.20 (a) and ball screws and harmonic drive linked with a belt and pulley drive were evaluated in Figure 7.20 (b). The variable series elastic actuation system was not able to bring a significant reduction in the power consumption of the exoskeleton. This was also true when the power consumption was assessed using the mathematical model. The Pearson R-value squared (r^2) of 0.97 and 0.99 indicates a high correlation between the two models for both of the above cases of V-SEA.

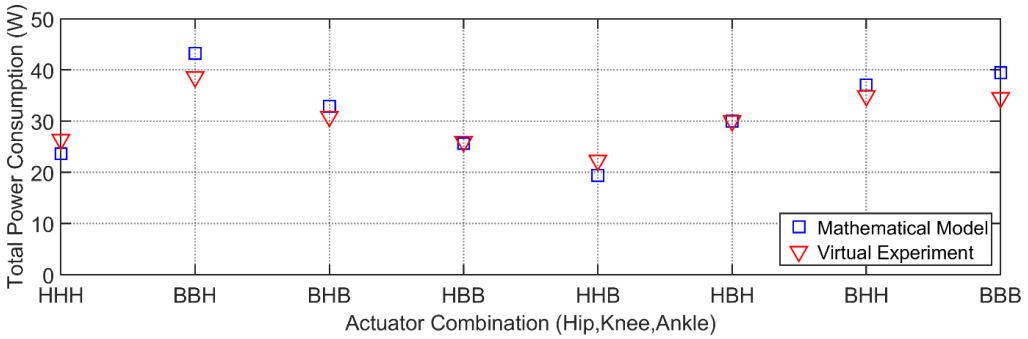

(a)

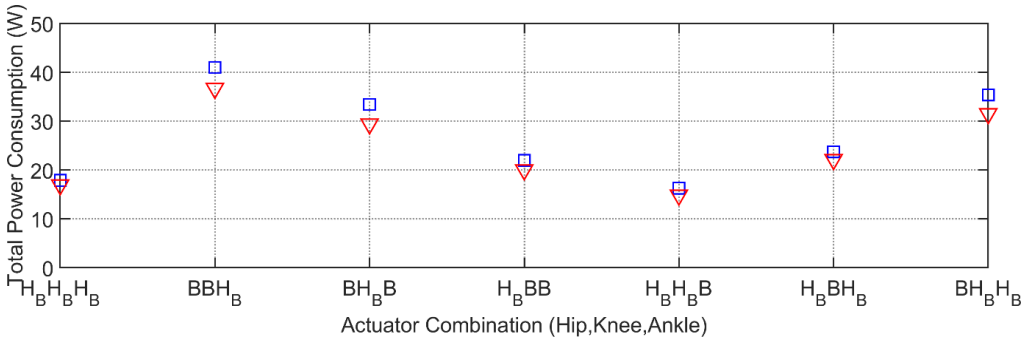

(b)

Figure 7.20: Average Total Power Consumption using a Virtual Prototype Compared with the Mathematical Model of an Optimal Dual Series Elastic Actuation System when (a) Lead screws (B) and Harmonic drives (H) were used as the Transmission System and (b) Lead screws (B) and Harmonic Drives linked to a Belt and Pulley drive System (H_B) were used as the Transmission System. The first, second and third letter corresponds the mechanism at the hip, knee and ankle joints respectively.

Figure 7.21 represents the correlation study of the average total power consumption of the exoskeleton between the virtual experimentation model and the mathematical model for some of the cases of the actuation systems. The Pearson R-value squared (r^2) shows a high correlation between the mathematical and virtual experimentation model and therefore, it indicates a good linearity. The correlation has been done for all different cases of the actuation systems but only few of them have been illustrated here. The

Pearson correlation coefficient of 0.89, 0.95, 0.97 and 0.99 reveals a high correlation between the two models.

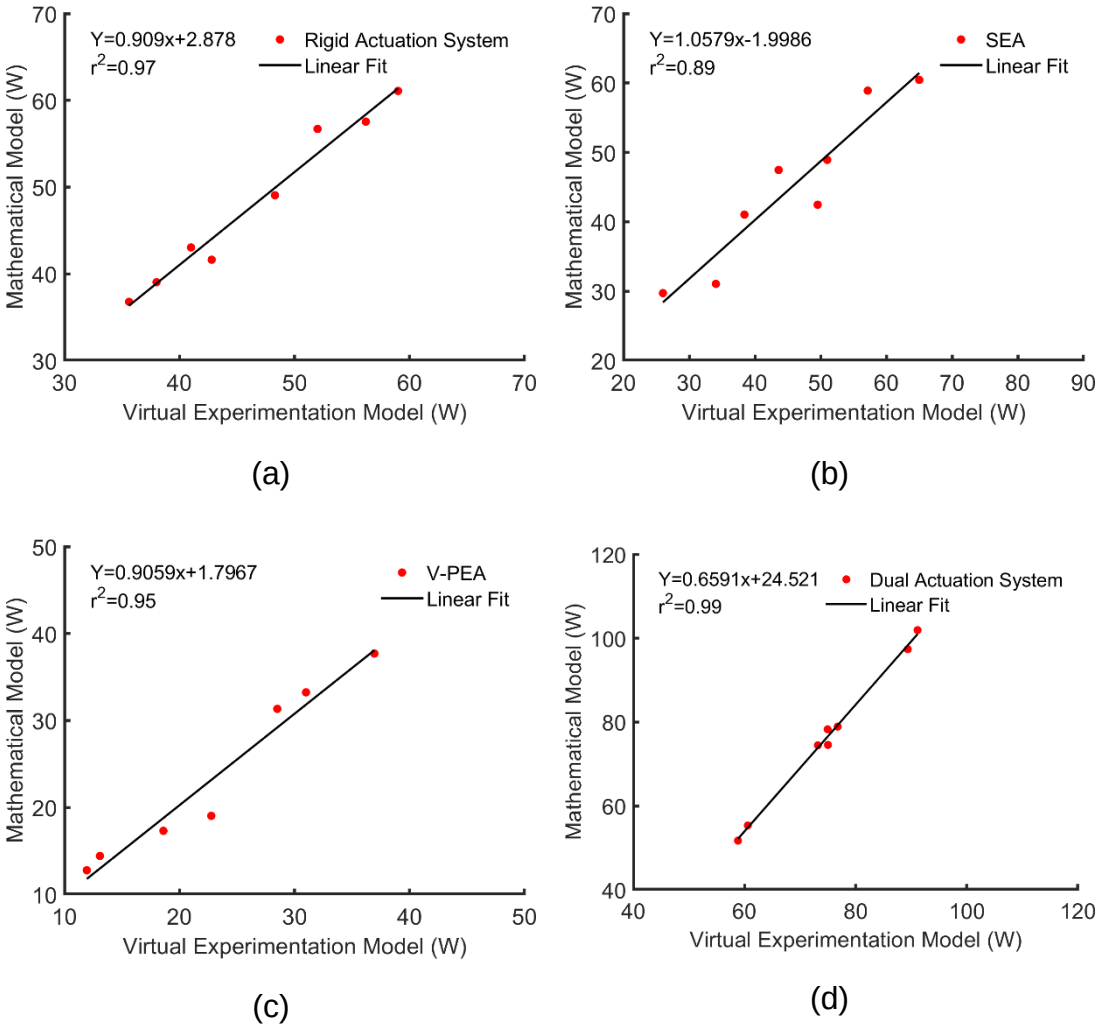

Figure 7.21: Correlation of Average Total Power Consumption of the Exoskeleton using Mathematical Model and Virtual Experimentation Model for (a) Rigid Actuation System (b) Series Elastic Actuation System (c) Parallel Elastic Actuation System and (d) Dual Actuation System, r^2: Pearson R-value squared.

The findings of the total power consumption using a virtual setup of an assistive robotic exoskeleton actuation system for a rigid, parallel and series arrangement in a single and dual setup were analyzed. These results were reported to be similar to the one demonstrated using the mathematical model in the previous chapters. A marginal difference was found in some of the transmission system combinations but the variation was not significant. It should be noted that in a virtual setup, lead screws were used without any linkage mechanism. The mathematical model was modified accordingly so that a comparison could be established since the ballscrews were previously assessed using an inverted slider crank mechanism. The identical values

using a virtual setup implies the integrity of the mathematical model developed and its verification and hence a lightweight and power efficient system was implemented using a virtual prototype of an assistive robotic exoskeleton.

By comparing the optimization results from the previous chapters, the actuator design consisting of a dual actuation system using V-PEA with harmonic drives combined with a belt and pulley mechanism at the hip and knee joint and ballscrews in an inverted slider crank mechanism at the ankle joint could be described as the best optimal combination for a detailed design. The energy requirements were found to be minimum using the above combination. However, adding an extra motor and the transmission system increases the complexity of the system in the practical design stage.

7.4 Summary

This chapter implements a virtual experimentation setup for an assistive robotic exoskeleton actuation system. The virtual prototype was realized in a rigid, elastic and dual configuration. Each component of the actuation system was virtually applied using physical components and connections in an interactive Simscape environment. Several designs of an actuator were considered and performance was assessed in accomplishing the desired manoeuvres of the exoskeleton. The actuator controller, transmission systems, elastic elements and sensors were established in the virtual setup of the prototype. The energy consumed by the virtual prototype in performing the desired manoeuvres was evaluated. By using the harmonic belt linked with a belt and pulley drive system, the power consumption is observed to be minimum in the virtual experimentation setup for all actuation systems. The design validation of the previously developed mathematical model was achieved using the virtual prototype and a light weight , powerful and power efficient system was realized for a rigid, parallel and series elastic actuator. Furthermore, the prototype was also applied to evaluate a dual rigid and elastic actuation system that was used to obtain a power efficient system. The statistical analysis revealed a high correlation between the mathematical and the virtual experimentation model of the exoskeleton.

Chapter 8
Summary, Conclusions and Future Work

8.1 Summary and Assessment of the Research Objectives

In Chapter 1, the research objectives were reported with the aim of designing and developing a lightweight, power efficient and powerful assistive robotic exoskeleton actuation system. In this chapter, the research objectives will be evaluated and the conclusions will be drawn from the obtained results.

- To establish the assistance requirements of the potential users of the lower limb exoskeleton robot.

  This is reported in Chapter 3. The analysis of the support requirements among different categories of the subjects is considered to be the primary step in the design of robot-assisted devices based on the needs of the end-users. A systematic approach was developed in identifying the support requirements among a broad category of potential users of the robot-assisted devices. The meta-analysis report shows a significant difference in the spatio-temporal, kinematic and kinetic gait parameters of elderly and neurological patients. A level of agreement was observed among most of the studies that reported the gait parameters but some controversies were also pointed out in the study. However, the fundamental needs of the potential users of the assistive devices were identified.

- To perform dynamic simulations to determine the joint kinematic and kinetic requirements.

  This is reported in Section 4.3 of Chapter 4. The basic manoeuvres for an elderly person are identified as sit-to-stand and level ground walking. The dynamic modelling defines the amount of power that will be required by the assistive exoskeleton in order to perform the desired tasks. The kinematic and kinetic requirements at the hip, knee and ankle joints during walking were obtained by several authors [173, 219, 220]. However, a significant amount of difference was noticed in reporting the kinetic characteristics and therefore, the manoeuvres were obtained using an experimental setup described in Section 4.3.1. These parameters are considered to be the most important design

specifications in exoskeleton robots as all of the design decisions are followed by these considerations. It is observed that the sit-to-stand phase is the most demanding part of the actuation system.

- To analyse the commercially available motors and transmission systems suitable for an assistive robotic exoskeleton

This is reported in Section 4.6 of Chapter 4. The actuator design solution evaluated consists of a state of the art motors and the available transmission systems obtained from an extensive market search. The list has been collected from different manufacturers of these devices. The parameters of these devices are collected from the provided datasheets and are used in the optimization algorithm for the best actuator selection. The selection is based on analysing the system's performance for the given tasks.

- To determine the optimal selection of the actuation system

This is presented in Section 4.8 of Chapter 4. An optimal actuation solution is presented to evaluate the performance of the actuation system for a given task. By using the optimization framework, a lightweight and power-efficient system is realized. A comparison was established based on the type of transmission system employed at each joint of the exoskeleton. The results show the efficiency of the system is increased when harmonic drives are linked to a belt and pulley drive system.

- To evaluate the spring optimization techniques.

This is reported in Chapter 5. The spring optimization techniques are investigated for the different minimization criteria. It was revealed that the torque and power of the actuator depend upon the spring stiffness optimization criterion. Consequently, the spring stiffnesses are optimized for each of the parameters involved. Furthermore, a combined criterion of the spring stiffness is also formulated that takes into account weightage from each of the parameters. The springs used in the elastic actuator design solution were adjusted using the developed combined criterion of spring optimization.

- To assess the optimal solution of an elastic actuation system.

This is reported in Chapter 5. The models of the elastic actuators are used in the elastic actuator design framework in order to assess the optimal elastic actuation systems. Using the elastic actuators, it is revealed that the weight and power consumption of the actuators is

increased at some of the joints nevertheless, it also brings benefits in terms of the weight and power efficiency of the system. It is reported that by using the elastic actuator design solution for PEA and SEA, a more power-efficient and a lightweight exoskeleton is achieved.

- To establish the variable spring stiffness optimization technique.

This is reported in Chapter 6. The techniques are investigated to evaluate a variable stiffness actuator. The actuation redundancy is introduced in which a dual actuation system is arranged in an antagonistic/agonistic arrangement that has also served to achieve a variable stiffness actuator. It is recorded that the stiffness of the spring in a dual actuation system yields best results when it is optimized for each phase of the manoeuvre separately.

- To investigate the optimal solution for a dual actuation system.

This is reported in Chapter 6. Section 6.2.5 presents the algorithm that is used to evaluate a dual actuation system for a rigid and elastic system. As the dual elastic actuation system is designed as a variable stiffness actuator, a significant advantage in terms of the weight and power efficiency of the actuators is reported as compared to the fixed stiffness actuators. Furthermore, the actuator design solution for the dual actuators also brings benefits in terms of the lightweight and power-efficient design. However, for the case of rigid systems using the dual arrangement of the actuators, no considerable advantages are reported.

- To build a virtual prototype and to validate the mathematical and simulation model.

This is presented in Chapter 7. The virtual prototype of an assistive exoskeleton is developed with a rigid and elastic, single and dual actuation systems by applying physical components and connections in a virtual environment. The performance is assessed using different designs of an actuation system. The energy consumed by the virtual prototype in performing the desired manoeuvres is evaluated. The design validations are achieved for the mathematical and simulation model of the assistive exoskeleton.

8.2 Conclusions

This research work has successfully presented a lightweight, power efficient and a powerful assistive robotic exoskeleton actuation system for a rigid,

elastic, single and dual actuator. The main conclusions obtained from this research are summarized below:

- The support requirement among different types of gait impairments were highlighted and it illustrates a strong need to develop assistive devices for the patients. The meta-analysis report suggests a significant difference between the impaired gait and the normal gait and hence assistive devices can help to overcome the altered gait biomechanics.
- Using the actuation design solution for a rigid actuation system, a harmonic drive linked to a belt and pulley drive system at the hip and ankle joint and ball screws in an inverted slider-crank mechanism at the knee joint is considered to be the most suited type of the transmission mechanism.
- A reduction of 35 % and 80 % in the total weight and the total power consumption respectively was achieved using the optimized rigid actuation system. These parameters were assessed with the parameters of the existing assistive exoskeletons.
- The kinematic and kinetic requirements of the system were significantly reduced by using a parallel elastic actuation system. However, the series elastic actuation system did not bring any significant difference in the requirements of the system. The slow walking speed was considered to be the main reason for not reducing any of the requirements in SEA. PEA was able to bring a reduction of up to 91 % at some of the lower limb joints during the sit-to-stand manoeuvre.
- The optimized actuation system using a parallel elastic actuator brings a reduction of up to 32% as compared to a rigid actuation system. This did not include the reduction that was already achieved using an optimized rigid actuation system.
- The dual actuators achieved a variable spring stiffness that has revealed a significant positive effect on the performance of the elastic actuation systems. This effect can be observed during all phases of the manoeuvres. However, no significant effect was observed on the rigid systems using dual actuation.
- As the variable spring stiffness of the actuators reduces the energy requirements, this effect was noticed when optimal dual actuation system was achieved using the developed dual actuation design solution and an increase of up to 60 % in the power efficiency of the dual actuators were identified. Using V-PEA, the optimal actuation

systems were recorded when harmonic drives were used at the hip joint and ball screws were employed at the knee and ankle joints. However, V-SEA could only bring an effect to a very limited extent.

- The optimal actuation systems were successfully implemented in a virtual prototype of an assistive exoskeleton. The PWM technique for the speed control of a DC motor was revealed to be the most realistic approach and therefore the systems were developed using that method. The findings reflected from the different models of the actuation systems correspond to similar outcomes.
- The energy consumption of the actuation systems of the virtual prototype yields similar results as were obtained using the mathematical and simulation models and therefore, it validates the actuator design solution for the rigid and elastic actuation systems for an assistive robotic exoskeleton.

8.3 Future Work

While there are several insights that have been presented in this thesis regarding an actuation system of exoskeleton robotics, there are several limitations and possible future directions of this work which are illustrated below.

- Some of the simplifications that were represented in this study related to the efficiency of the components used in the optimization algorithm which can indicate a good overall representation of the losses in the system but can also lead to an underestimated representation of the models, which on the other hand could be determined empirically for each of the components. This process requires an extra effort in terms of time but by no means guarantee any of a better representation of the inefficiencies because the components when linked to the other mechanisms, behave differently and the torque or speed dependent losses are typically distributed evenly and hence, this justifies the models used in this thesis.
- The list of the motors and the transmission systems used in the optimization algorithm although represented a good state of the art components and products but is not a comprehensive list and better actuator selection could still be possible with the addition of more and better actuators available in the market in the future.
- This study was limited to the sit-to-stand and level ground walking manoeuvres as they represented the basic tasks in performing the

activities of daily living. However, the future design could include extra tasks such as stair ascent/descent, walking on uneven terrain, faster walking speed and even running as well.

- In this work, the actuation system was considered to be in the sagittal plane in order to develop an optimal actuation system. While the walking and other activities of daily living are represented by the movements in the sagittal plane, there are other tasks e.g. maintaining balance of the user etc that could also be included in order to extend the functionalities of an assistive exoskeleton and hence, these movements could also be considered in the optimal design of an actuation system.
- The elastic elements used in this system comprised a single elastic system either in series or in parallel, however, studies have reported, although they are few in number that the efficiency of the system could be further increased by using a combination of the series and parallel elastic actuators in a single system [190]. Therefore, further fundamental investigations into the system will be required that will make a thorough evaluation of the strength and weaknesses of the elastic systems with a combination of different arrangements of two or more elastic elements.
- In this work, the primary advantage of using a dual elastic actuation system was to achieve a variable spring stiffness actuator. How the elastic actuation should be combined with a redundant system has many research options and is still an open question. An investigation into the study of the different techniques in order to achieve a variable stiffness actuator is required and the means for the elasticity and redundancy to be linked by evaluating the strength and limitations of each of the designs.
- The rigid actuation system in a dual arrangement did not show any significant power advantages. The slow speed was considered to be the main cause for this and therefore for faster walking speeds and running, the benefits of the dual rigid actuation system need further investigations. Furthermore, the efficiency of a dual system is highly dependent on the efficiency of the power distribution and therefore on the control algorithm. There is a need to develop efficient control schemes that can effectively control the power distribution of the dual actuators.
- In this work, the dual actuation system was designed using two motors as one of the motors represented the tension muscle, and the

other the contraction one. However, there are studies that reported about the movement of the human knee joint that is governed by 16 different types of muscles and each pair of muscles is responsible for some specific task. Therefore, this concept could be applied to the exoskeleton actuation system and further investigations are required to assess the addition of an extra actuator redundancy in which smaller actuators will be responsible to perform less energy-consuming tasks and larger actuators will perform the high energy demanding tasks e.g. stair climb in order to make it more power-efficient. Hence, a good assessment is required that will weigh the benefits of adding extra redundancy and extra complexity to the system against the power efficiency of the system. Furthermore, research will also be required for an optimal configuration for this type of redundant system.

- The actuator redundancy was used at the joint level in this study. Consequently, a more efficient way of using the kinematic redundancy of the motors could be to use them at the robot level. The variable spring stiffness could be achieved more efficiently if a single redundant motor could be used for all joints rather than using it for changing the spring stiffness at a single joint only at a cost of increasing the complexity of the control strategies. Further investigation is required for the assessment of the robot level redundancy concept and its optimal configuration.

References

1. Zoss, A.B., H. Kazerooni, and A. Chu, *Biomechanical design of the Berkeley lower extremity exoskeleton (BLEEX).* IEEE/ASME Transactions On Mechatronics, 2006. **11**(2): p. 128-138.
2. Tsukahara, A., et al., *Sit-to-stand and stand-to-sit transfer support for complete paraplegic patients with robot suit HAL.* Advanced robotics, 2010. **24**(11): p. 1615-1638.
3. Esquenazi, A., et al., *The ReWalk powered exoskeleton to restore ambulatory function to individuals with thoracic-level motor-complete spinal cord injury.* American journal of physical medicine & rehabilitation, 2012. **91**(11): p. 911-921.
4. Rose, J., *Human walking.* 1994.
5. Baker, R., *Temporal spatial data, the gait cycle and gait graphs.* university of salford: An Introduction to clinical gait analysis, 2013.
6. Dollar, A.M. and H. Herr, *Lower extremity exoskeletons and active orthoses: challenges and state-of-the-art.* IEEE Transactions on robotics, 2008. **24**(1): p. 144-158.
7. Hamill, J. and K.M. Knutzen, *Biomechanical basis of human movement*. 2006: Lippincott Williams & Wilkins.
8. Ishii, M., K. Yamamoto, and K. Hyodo, *Stand-alone wearable power assist suit–development and availability–.* Journal of robotics and mechatronics, 2005. **17**(5): p. 575-583.
9. Walsh, C.J., et al. *Development of a lightweight, underactuated exoskeleton for load-carrying augmentation*. in *Robotics and Automation, 2006. ICRA 2006. Proceedings 2006 IEEE International Conference on*. 2006. IEEE.
10. Walsh, C.J., *Biomimetic design for an under-actuated leg exoskeleton for load-carrying augmentation*. 2006: Massachusetts Institute of Technology.
11. Dollar, A.M. and H. Herr. *Design of a quasi-passive knee exoskeleton to assist running*. in *Intelligent Robots and Systems, 2008. IROS 2008. IEEE/RSJ International Conference on*. 2008. IEEE.
12. DE INGENIEURSWETENSCHAPPEN, I., *Design and control of a knee exoskeleton powered by pleated pneumatic artificial muscles for robot-assisted gait rehabilitation.*
13. Walsh, C.J., K. Endo, and H. Herr, *A quasi-passive leg exoskeleton for load-carrying augmentation.* International Journal of Humanoid Robotics, 2007. **4**(03): p. 487-506.
14. Colombo, G., et al., *Treadmill training of paraplegic patients using a robotic orthosis.* Journal of rehabilitation research and development, 2000. **37**(6): p. 693.
15. Karlin, S., *Raiding iron man's closet [Geek life].* IEEE Spectrum, 2011. **48**(8): p. 25-25.
16. Sasaki, D., T. Noritsugu, and M. Takaiwa. *Development of pneumatic lower limb power assist wear driven with wearable air supply system*. in *Intelligent Robots and Systems (IROS), 2013 IEEE/RSJ International Conference on*. 2013. IEEE.

17. Li, N., et al., *Review on lower extremity exoskeleton robot.* Open Automation and Control Systems Journal, 2015. **7**: p. 441-453.
18. Kawamoto, H. and Y. Sankai, *Power assist method based on phase sequence and muscle force condition for HAL.* Advanced Robotics, 2005. **19**(7): p. 717-734.
19. Kawamoto, H. and Y. Sankai, *Power assist system HAL-3 for gait disorder person.* Computers helping people with special needs, 2002: p. 19-29.
20. Fleischer, C., et al., *Application of EMG signals for controlling exoskeleton robots.* Biomedizinische technik, 2006. **51**(5/6): p. 314-319.
21. Fleischer, C., C. Reinicke, and G. Hommel. *Predicting the intended motion with EMG signals for an exoskeleton orthosis controller*. in *Intelligent robots and systems, 2005.(IROS 2005). 2005 IEEE/RSJ international conference on*. 2005. IEEE.
22. Fleischer, C. and G. Hommel, *Embedded control system for a powered leg exoskeleton.* Embedded Systems–Modeling, Technology, and Applications, 2006: p. 177-185.
23. Pons, J.L., *Wearable robots: biomechatronic exoskeletons*. 2008: John Wiley & Sons.
24. Reinkensmeyer, D.J. and M.L. Boninger, *Technologies and combination therapies for enhancing movement training for people with a disability.* Journal of neuroengineering and rehabilitation, 2012. **9**(1): p. 17.
25. Hintermüller, C., C. Guger, and G. Edlinger, *Brain-computer interface: generic control interface for social interaction applications.* Advances in Computational Intelligence, 2011: p. 386-392.
26. Do, A.H., et al., *Brain-computer interface controlled robotic gait orthosis.* Journal of neuroengineering and rehabilitation, 2013. **10**(1): p. 111.
27. De Rossi, S.M.M., et al., *Sensing pressure distribution on a lower-limb exoskeleton physical human-machine interface.* Sensors, 2010. **11**(1): p. 207-227.
28. Suzuki, K., et al., *Intention-based walking support for paraplegia patients with Robot Suit HAL.* Advanced Robotics, 2007. **21**(12): p. 1441-1469.
29. del-Ama, A.J., et al., *Online assessment of human-robot interaction for hybrid control of walking.* Sensors, 2011. **12**(1): p. 215-225.
30. Šlajpah, S., R. Kamnik, and M. Munih, *Kinematics based sensory fusion for wearable motion assessment in human walking.* Computer methods and programs in biomedicine, 2014. **116**(2): p. 131-144.
31. Kazerooni, H. and R. Steger, *The Berkeley lower extremity exoskeleton.* Journal of dynamic systems, measurement, and control, 2006. **128**(1): p. 14-25.
32. Pratt, G.A. and M.M. Williamson. *Series elastic actuators*. in *Intelligent Robots and Systems 95.'Human Robot Interaction and Cooperative Robots', Proceedings. 1995 IEEE/RSJ International Conference on*. 1995. IEEE.
33. Mohammed, S., Y. Amirat, and H. Rifai, *Lower-limb movement assistance through wearable robots: State of the art and challenges.* Advanced Robotics, 2012. **26**(1-2): p. 1-22.

34. Mosher, R.S., *Handyman to hardiman*. 1967, SAE Technical Paper.
35. Vukobratovic, M., D. Hristic, and Z. Stojiljkovic, *Development of active anthropomorphic exoskeletons.* Medical and Biological Engineering and Computing, 1974. **12**(1): p. 66-80.
36. Pratt, J., B. Krupp, and C. Morse, *Series elastic actuators for high fidelity force control.* Industrial Robot: An International Journal, 2002. **29**(3): p. 234-241.
37. Veale, A.J. and S.Q. Xie, *Towards compliant and wearable robotic orthoses: A review of current and emerging actuator technologies.* Medical engineering & physics, 2016. **38**(4): p. 317-325.
38. Yin, J., *Analysis and design of wearable lower extremity exoskeleton.* J Syst Simul, 2010. **12**: p. 7-18.
39. Jie, Z., *Study on the exoskeleton Leg for training paraplegic patients.* Master's degree paper of Zhejiang University, 2007.
40. Guizzo, E. and H. Goldstein, *The rise of the body bots [robotic exoskeletons].* IEEE spectrum, 2005. **42**(10): p. 50-56.
41. Huang, G.T., *Wearable robots.* Technology Review, 2004. **4**: p. 70-73.
42. Dzahir, M.A.M. and S.-i. Yamamoto, *Recent trends in lower-limb robotic rehabilitation orthosis: Control scheme and strategy for pneumatic muscle actuated gait trainers.* Robotics, 2014. **3**(2): p. 120-148.
43. Yamamoto, K., et al., *Development of power assisting suit for assisting nurse labor.* JSME International Journal Series C Mechanical Systems, Machine Elements and Manufacturing, 2002. **45**(3): p. 703-711.
44. Yamamoto, K., et al., *Development of Power assisting suit.* JSME International Journal Series C Mechanical Systems, Machine Elements and Manufacturing, 2003. **46**(3): p. 923-930.
45. Costa, N. and D.G. Caldwell. *Control of a biomimetic" soft-actuated" 10dof lower body exoskeleton*. in *Biomedical Robotics and Biomechatronics, 2006. BioRob 2006. The First IEEE/RAS-EMBS International Conference on*. 2006. IEEE.
46. Adam, B. and H. Kazerooni, *Design of an electrically actuated lower extremity.* Advan robot, 2006. **20**: p. 967-988.
47. Huo, W., et al., *Lower limb wearable robots for assistance and rehabilitation: A state of the art.* IEEE systems Journal, 2016. **10**(3): p. 1068-1081.
48. Kwa, H.K., et al. *Development of the IHMC mobility assist exoskeleton*. in *Robotics and Automation, 2009. ICRA'09. IEEE International Conference on*. 2009. IEEE.
49. Raj, A.K., et al., *Mina: A sensorimotor robotic orthosis for mobility assistance.* Journal of Robotics, 2011. **2011**.
50. Yu, H., et al. *Mechanical design of a portable knee-ankle-foot robot*. in *Robotics and Automation (ICRA), 2013 IEEE International Conference on*. 2013. IEEE.
51. Tagliamonte, N.L., et al., *Double actuation architectures for rendering variable impedance in compliant robots: A review.* Mechatronics, 2012. **22**(8): p. 1187-1203.

52. Verstraten, T., et al., *Modeling and design of an energy-efficient dual-motor actuation unit with a planetary differential and holding brakes.* Mechatronics, 2018. **49**: p. 134-148.
53. Wolf, S. and G. Hirzinger. *A new variable stiffness design: Matching requirements of the next robot generation*. in *2008 IEEE International Conference on Robotics and Automation*. 2008. IEEE.
54. Hollander, K. and T. Sugar. *Concepts for compliant actuation in wearable robotic systems*. in *US-Korea Conference (UKC) CDROM*. 2004.
55. Tonietti, G., R. Schiavi, and A. Bicchi. *Design and control of a variable stiffness actuator for safe and fast physical human/robot interaction*. in *Proceedings of the 2005 IEEE international conference on robotics and automation*. 2005. IEEE.
56. Kawamura, S., et al. *Development of passive elements with variable mechanical impedance for wearable robots*. in *Proceedings 2002 IEEE International Conference on Robotics and Automation (Cat. No. 02CH37292)*. 2002. IEEE.
57. Van Ham, R., et al., *MACCEPA, The mechanically adjustable compliance and controllable equilibrium position actuator: A 3DOF joint with two independent compliances.* International Applied Mechanics, 2007. **43**(4): p. 467-474.
58. Poole, A. and J. Booker, *Design methodology and case studies in actuator selection.* Mechanism and machine theory, 2011. **46**(5): p. 647-661.
59. Egbuna, C.C. and A.H. Basson. *Electric actuator selection design aid for low cost automation*. in *DS 58-6: Proceedings of ICED 09, the 17th International Conference on Engineering Design, Vol. 6, Design Methods and Tools (pt. 2), Palo Alto, CA, USA, 24.-27.08. 2009*. 2009.
60. Budinger, M., et al., *Optimal preliminary design of electromechanical actuators.* Proceedings of the Institution of Mechanical Engineers, Part G: Journal of Aerospace Engineering, 2014. **228**(9): p. 1598-1616.
61. Wang, S., C. Meijneke, and H. van der Kooij. *Modeling, design, and optimization of Mindwalker series elastic joint*. in *2013 IEEE 13th International Conference on Rehabilitation Robotics (ICORR)*. 2013. IEEE.
62. Kessels, J.T.B.A., *Energy management for automotive power nets*. 2007.
63. Chen, B., et al., *Recent developments and challenges of lower extremity exoskeletons.* Journal of Orthopaedic Translation, 2016. **5**: p. 26-37.
64. Kazerooni, H., et al. *On the control of the berkeley lower extremity exoskeleton (BLEEX)*. in *Robotics and automation, 2005. ICRA 2005. Proceedings of the 2005 IEEE international conference on*. 2005. IEEE.
65. Yang, Z., et al. *Impedance control of exoskeleton suit based on adaptive rbf neural network*. in *Intelligent Human-Machine Systems and Cybernetics, 2009. IHMSC'09. International Conference on*. 2009. IEEE.

66. Emken, J.L. and D.J. Reinkensmeyer, *Robot-enhanced motor learning: accelerating internal model formation during locomotion by transient dynamic amplification.* IEEE Transactions on Neural Systems and Rehabilitation Engineering, 2005. **13**(1): p. 33-39.
67. Ghan, J., R. Steger, and H. Kazerooni, *Control and system identification for the Berkeley lower extremity exoskeleton (BLEEX).* Advanced Robotics, 2006. **20**(9): p. 989-1014.
68. Anam, K. and A.A. Al-Jumaily, *Active exoskeleton control systems: State of the art.* Procedia Engineering, 2012. **41**: p. 988-994.
69. Rosen, J., M.B. Fuchs, and M. Arcan, *Performances of Hill-type and neural network muscle models—Toward a myosignal-based exoskeleton.* Computers and Biomedical Research, 1999. **32**(5): p. 415-439.
70. Chen, F., et al. *WPAL for human power assist during walking using dynamic equation*. in *Mechatronics and Automation, 2009. ICMA 2009. International Conference on*. 2009. IEEE.
71. Strausser, K.A. and H. Kazerooni. *The development and testing of a human machine interface for a mobile medical exoskeleton*. in *Intelligent Robots and Systems (IROS), 2011 IEEE/RSJ International Conference on*. 2011. IEEE.
72. Farris, R.J., H.A. Quintero, and M. Goldfarb, *Preliminary evaluation of a powered lower limb orthosis to aid walking in paraplegic individuals.* IEEE Transactions on Neural Systems and Rehabilitation Engineering, 2011. **19**(6): p. 652-659.
73. Belforte, G., L. Gastaldi, and M. Sorli, *Pneumatic active gait orthosis.* Mechatronics, 2001. **11**(3): p. 301-323.
74. Yan, T., et al., *Review of assistive strategies in powered lower-limb orthoses and exoskeletons.* Robotics and Autonomous Systems, 2015. **64**: p. 120-136.
75. He, H. and K. Kiguchi. *A study on emg-based control of exoskeleton robots for human lower-limb motion assist*. in *Information Technology Applications in Biomedicine, 2007. ITAB 2007. 6th International Special Topic Conference on*. 2007. IEEE.
76. Kong, K. and D. Jeon, *Design and control of an exoskeleton for the elderly and patients.* IEEE/ASME Transactions on mechatronics, 2006. **11**(4): p. 428-432.
77. Popovic, M.B., A. Goswami, and H. Herr, *Ground reference points in legged locomotion: Definitions, biological trajectories and control implications.* The International Journal of Robotics Research, 2005. **24**(12): p. 1013-1032.
78. Cowan, R.E., et al., *Recent trends in assistive technology for mobility.* Journal of neuroengineering and rehabilitation, 2012. **9**(1): p. 20.
79. Donelan, J.M., R. Kram, and A.D. Kuo, *Mechanical work for step-to-step transitions is a major determinant of the metabolic cost of human walking.* Journal of Experimental Biology, 2002. **205**(23): p. 3717-3727.
80. Griffin, T.M., T.J. Roberts, and R. Kram, *Metabolic cost of generating muscular force in human walking: insights from load-carrying and speed experiments.* Journal of Applied Physiology, 2003. **95**(1): p. 172-183.

81. Hausswirth, C., A.-X. Bigard, and J.-M. Le Chevalier, *The Cosmed K4 telemetry system as an accurate device for oxygen uptake measurements during exercise.* International Journal of Sports Medicine, 1997. **28**(06): p. 449-453.
82. Sawicki, G.S. and D.P. Ferris, *Powered ankle exoskeletons reveal the metabolic cost of plantar flexor mechanical work during walking with longer steps at constant step frequency.* Journal of Experimental Biology, 2009. **212**(1): p. 21-31.
83. Ohta, Y., et al., *A two-degree-of-freedom motor-powered gait orthosis for spinal cord injury patients.* Proceedings of the Institution of Mechanical Engineers, Part H: Journal of Engineering in Medicine, 2007. **221**(6): p. 629-639.
84. Blaya, J.A. and H. Herr, *Adaptive control of a variable-impedance ankle-foot orthosis to assist drop-foot gait.* IEEE Transactions on neural systems and rehabilitation engineering, 2004. **12**(1): p. 24-31.
85. Gregorczyk, K.N., et al., *Effects of a lower-body exoskeleton device on metabolic cost and gait biomechanics during load carriage.* Ergonomics, 2010. **53**(10): p. 1263-1275.
86. Akahira, H., et al., *Effect of dynamic knee motion on paralyzed lower limb muscle activity during orthotic gait: a test for the effectiveness of the motor-assisted knee motion device.* J Nov Physiother, 2012. **1**: p. 2-6.
87. Rupal, B., A. Singla, and G. Virk. *Lower limb exoskeletons: a brief review*. in *Conference on Mechanical Engineering and Technology (COMET-2016), IIT (BHU), Varanasi, India*. 2016.
88. Mohammed, S. and Y. Amirat. *Towards intelligent lower limb wearable robots: Challenges and perspectives-State of the art*. in *Robotics and Biomimetics, 2008. ROBIO 2008. IEEE International Conference on*. 2009. IEEE.
89. Kawamoto, H., et al. *Development of single leg version of HAL for hemiplegia*. in *Engineering in Medicine and Biology Society, 2009. EMBC 2009. Annual International Conference of the IEEE*. 2009. IEEE.
90. Viteckova, S., P. Kutilek, and M. Jirina, *Wearable lower limb robotics: A review.* Biocybernetics and Biomedical Engineering, 2013. **33**(2): p. 96-105.
91. Farris, R.J., H.A. Quintero, and M. Goldfarb. *Performance evaluation of a lower limb exoskeleton for stair ascent and descent with paraplegia*. in *2012 Annual International Conference of the IEEE Engineering in Medicine and Biology Society*. 2012. IEEE.
92. Kolakowsky-Hayner, S.A., et al., *Safety and feasibility of using the EksoTM bionic exoskeleton to aid ambulation after spinal cord injury.* J Spine, 2013. **4**(3).
93. Bionics, R., *Rex bionics.* Web Page (www. rexbionics. com), Accessed: Feb, 2017.
94. Neuhaus, P.D., et al. *Design and evaluation of Mina: A robotic orthosis for paraplegics*. in *2011 IEEE International Conference on Rehabilitation Robotics*. 2011. IEEE.
95. Kagawa, T. and Y. Uno. *Gait pattern generation for a power-assist device of paraplegic gait*. in *Robot and Human Interactive*

Communication, 2009. RO-MAN 2009. The 18th IEEE International Symposium on. 2009. IEEE.
96. Food and H. Drug Administration, *Medical devices; physical medicine devices; classification of the powered lower extremity exoskeleton; republication. Final order; republication.* Federal register, 2015. **80**(85): p. 25226.
97. Tsukahara, A., et al., *Restoration of gait for spinal cord injury patients using HAL with intention estimator for preferable swing speed.* IEEE Transactions on neural systems and rehabilitation engineering, 2014. **23**(2): p. 308-318.
98. Önen, Ü., et al., *Design and actuator selection of a lower extremity exoskeleton.* IEEE/ASME Transactions on Mechatronics, 2013. **19**(2): p. 623-632.
99. Aliman, N., R. Ramli, and S.M. Haris, *Design and development of lower limb exoskeletons: A survey.* Robotics and Autonomous Systems, 2017. **95**: p. 102-116.
100. Cestari, M., et al., *ARES, a variable stiffness actuator with embedded force sensor for the ATLAS exoskeleton.* Industrial Robot: An International Journal, 2014.
101. Yang, W., C.-j. Yang, and Q.-x. Wei. *Design of an anthropomorphic lower extremity exoskeleton with compatible joints*. in *2014 IEEE International Conference on Robotics and Biomimetics (ROBIO 2014)*. 2014. IEEE.
102. Rocon, E., et al., *Design and validation of a rehabilitation robotic exoskeleton for tremor assessment and suppression.* IEEE Transactions on neural systems and rehabilitation engineering, 2007. **15**(3): p. 367-378.
103. Whittle, M.W., *Gait analysis: an introduction*. 2014: Butterworth-Heinemann.
104. Morris, M.E., et al., *The pathogenesis of gait hypokinesia in Parkinson's disease.* Brain, 1994. **117**(5): p. 1169-1181.
105. Ebersbach, G., et al., *Comparative analysis of gait in Parkinson's disease, cerebellar ataxia and subcortical arteriosclerotic encephalopathy.* Brain, 1999. **122**(7): p. 1349-1355.
106. Palliyath, S., et al., *Gait in patients with cerebellar ataxia.* Movement disorders, 1998. **13**(6): p. 958-964.
107. Gage, J.R., et al., *Pre-and postoperative gait analysis in patients with spastic diplegia: a preliminary report.* Journal of Pediatric Orthopaedics, 1984. **4**(6): p. 715-725.
108. Bell, K.J., et al., *Natural progression of gait in children with cerebral palsy.* Journal of Pediatric Orthopaedics, 2002. **22**(5): p. 677-682.
109. Kurihara, S., et al., *An epidemiological genetic study of Charcot-Marie-Tooth disease in Western Japan.* Neuroepidemiology, 2002. **21**(5): p. 246-250.
110. Morocutti, C., et al., *Charcot-Marie-Tooth disease in Molise, a central-southern region of Italy: an epidemiological study.* Neuroepidemiology, 2002. **21**(5): p. 241-245.
111. Combarros, O., et al., *Prevalence of hereditary motor and sensory neuropathy in Cantabria.* Acta neurologica scandinavica, 1987. **75**(1): p. 9-12.

112. Rubenstein, L.Z., et al., *Falls and instability in the elderly.* Journal of the American Geriatrics Society, 1988. **36**(3): p. 266-278.
113. Gabell A, S.M.A., Nayak U S L, *Falls in the healthy elderly: Predisposing causes.* Ergonomics, 1986. **28**: p. 965-975.
114. Lilley, J.M., T. Arie, and C.E. Chilvers, *Accidents involving older people: a review of the literature.* Age Ageing, 1995. **24**(4): p. 346-65.
115. Quintero, H.A., R.J. Farris, and M. Goldfarb, *A method for the autonomous control of lower limb exoskeletons for persons with paraplegia.* Journal of medical devices, 2012. **6**(4): p. 041003.
116. Kuan, T.-S., J.-Y. Tsou, and F.-C. Su, *Hemiplegic gait of stroke patients: the effect of using a cane.* Archives of physical medicine and rehabilitation, 1999. **80**(7): p. 777-784.
117. Downs, S.H. and N. Black, *The feasibility of creating a checklist for the assessment of the methodological quality both of randomised and non-randomised studies of health care interventions.* Journal of Epidemiology & Community Health, 1998. **52**(6): p. 377-384.
118. Anderson, D.E. and M.L. Madigan, *Healthy older adults have insufficient hip range of motion and plantar flexor strength to walk like healthy young adults.* Journal of biomechanics, 2014. **47**(5): p. 1104-1109.
119. JudgeRoy, J.O., B. Davis, and S. Õunpuu, *Step length reductions in advanced age: the role of ankle and hip kinetics.* The Journals of Gerontology Series A: Biological Sciences and Medical Sciences, 1996. **51**(6): p. M303-M312.
120. Kerrigan, D.C., et al., *Reduced hip extension during walking: healthy elderly and fallers versus young adults.* Archives of physical medicine and rehabilitation, 2001. **82**(1): p. 26-30.
121. Kerrigan, D.C., et al., *Biomechanical gait alterations independent of speed in the healthy elderly: evidence for specific limiting impairments.* Archives of physical medicine and rehabilitation, 1998. **79**(3): p. 317-322.
122. Peppe, A., et al., *Does gait analysis quantify motor rehabilitation efficacy in Parkinson's disease patients?* Gait & posture, 2007. **26**(3): p. 452-462.
123. Ferrarin, M., et al., *Quantitative analysis of gait in Parkinson's disease: a pilot study on the effects of bilateral sub-thalamic stimulation.* Gait & posture, 2002. **16**(2): p. 135-148.
124. Roiz, R.d.M., et al., *Gait analysis comparing Parkinson's disease with healthy elderly subjects.* Arquivos de neuro-psiquiatria, 2010. **68**(1): p. 81-86.
125. Ferrarin, M., et al., *Effects of bilateral subthalamic stimulation on gait kinematics and kinetics in Parkinson's disease.* Experimental brain research, 2005. **160**(4): p. 517-527.
126. Hong, S., et al., *Analysis of Dynamics of Gait in Parkinson's Disease with 3-Demensional Gait Analysis System.* Journal of the Korean Neurological Association, 2005. **23**(5): p. 635-641.
127. Lewis, G.N., W.D. Byblow, and S.E. Walt, *Stride length regulation in Parkinson's disease: the use of extrinsic, visual cues.* Brain, 2000. **123**(10): p. 2077-2090.
128. Mitoma, H., et al., *Characteristics of parkinsonian and ataxic gaits: a study using surface electromyograms, angular displacements and*

floor reaction forces. Journal of the neurological sciences, 2000. **174**(1): p. 22-39.
129. Morris, M., et al., *Three-dimensional gait biomechanics in Parkinson's disease: Evidence for a centrally mediated amplitude regulation disorder.* Movement Disorders, 2005. **20**(1): p. 40-50.
130. Sofuwa, O., et al., *Quantitative gait analysis in Parkinson's disease: comparison with a healthy control group.* Archives of physical medicine and rehabilitation, 2005. **86**(5): p. 1007-1013.
131. Zijlmans, J., et al., *Quantitative gait analysis in patients with vascular parkinsonism.* Movement Disorders, 1996. **11**(5): p. 501-508.
132. Serrao, M., et al., *Gait pattern in inherited cerebellar ataxias.* The Cerebellum, 2012. **11**(1): p. 194-211.
133. Vasco, G., et al., *Functional and Gait Assessment in Children and Adolescents Affected by Friedreich's Ataxia: A One-Year Longitudinal Study.* PloS one, 2016. **11**(9): p. e0162463.
134. Stolze, H., et al., *Typical features of cerebellar ataxic gait.* Journal of Neurology, Neurosurgery & Psychiatry, 2002. **73**(3): p. 310-312.
135. Adolfsen, S.E., et al., *Kinematic and kinetic outcomes after identical multilevel soft tissue surgery in children with cerebral palsy.* Journal of Pediatric Orthopaedics, 2007. **27**(6): p. 658-667.
136. Davids, J.R., A.M. Bagley, and M. Bryan, *Kinematic and kinetic analysis of running in children with cerebral palsy.* Developmental Medicine & Child Neurology, 1998. **40**(8): p. 528-535.
137. Steinwender, G., et al., *Intrasubject repeatability of gait analysis data in normal and spastic children.* Clinical Biomechanics, 2000. **15**(2): p. 134-139.
138. Eek, M.N., R. Tranberg, and E. Beckung, *Muscle strength and kinetic gait pattern in children with bilateral spastic CP.* Gait & posture, 2011. **33**(3): p. 333-337.
139. Del Bianco, J. and S. Fatone, *Comparison of silicone and posterior leaf spring ankle-foot orthoses in a subject with Charcot-Marie-Tooth disorder.* JPO: Journal of Prosthetics and Orthotics, 2008. **20**(4): p. 155-162.
140. Ferrarin, M., et al., *Reliability of instrumented movement analysis as outcome measure in Charcot–Marie–Tooth disease: Results from a multitask locomotor protocol.* Gait & posture, 2011. **34**(1): p. 36-43.
141. Õunpuu, S., et al., *A comprehensive evaluation of the variation in ankle function during gait in children and youth with Charcot–Marie–Tooth disease.* Gait & posture, 2013. **38**(4): p. 900-906.
142. Rao, S., C. Saltzman, and H.J. Yack, *Ankle ROM and stiffness measured at rest and during gait in individuals with and without diabetic sensory neuropathy.* Gait & posture, 2006. **24**(3): p. 295-301.
143. Raspovic, A., *Gait characteristics of people with diabetes-related peripheral neuropathy, with and without a history of ulceration.* Gait & posture, 2013. **38**(4): p. 723-728.
144. Savelberg, H.H., et al., *Prolonged activity of knee extensors and dorsal flexors is associated with adaptations in gait in diabetes and diabetic polyneuropathy.* Clinical biomechanics, 2010. **25**(5): p. 468-475.

145. Sawacha, Z., et al., *Diabetic gait and posture abnormalities: a biomechanical investigation through three dimensional gait analysis.* Clinical biomechanics, 2009. **24**(9): p. 722-728.
146. Chen, G., et al., *Gait deviations associated with post-stroke hemiparesis: improvement during treadmill walking using weight support, speed, support stiffness, and handrail hold.* Gait & posture, 2005. **22**(1): p. 57-62.
147. Galli, M., et al., *Gait patterns in hemiplegic children with cerebral palsy: comparison of right and left hemiplegia.* Research in developmental disabilities, 2010. **31**(6): p. 1340-1345.
148. Winters, T., J. Gage, and R. Hicks, *Gait patterns in spastic hemiplegia in children and young adults.* J Bone Joint Surg Am, 1987. **69**(3): p. 437-441.
149. Buckon, C.E., et al., *Comparison of three ankle—foot orthosis configurations for children with spastic diplegia.* Developmental Medicine & Child Neurology, 2004. **46**(9): p. 590-598.
150. Carriero, A., et al., *Determination of gait patterns in children with spastic diplegic cerebral palsy using principal components.* Gait & posture, 2009. **29**(1): p. 71-75.
151. Langerak, N.G., et al., *A prospective gait analysis study in patients with diplegic cerebral palsy 20 years after selective dorsal rhizotomy.* 2008.
152. Saraph, V., et al., *Multilevel surgery in spastic diplegia: evaluation by physical examination and gait analysis in 25 children.* Journal of Pediatric Orthopaedics, 2002. **22**(2): p. 150-157.
153. Gomes, A.A., et al., *Electromyography and kinematic changes of gait cycle at different cadences in diabetic neuropathic individuals.* Muscle & nerve, 2011. **44**(2): p. 258-268.
154. Romkes, J. and R. Brunner, *Comparison of a dynamic and a hinged ankle–foot orthosis by gait analysis in patients with hemiplegic cerebral palsy.* Gait & posture, 2002. **15**(1): p. 18-24.
155. Bonnefoy-Mazure, A., et al., *Full body gait analysis may improve diagnostic discrimination between hereditary spastic paraplegia and spastic diplegia: a preliminary study.* Research in developmental disabilities, 2013. **34**(1): p. 495-504.
156. Morris, M.E., et al., *Stride length regulation in Parkinson's disease.* Brain, 1996. **119**(2): p. 551-568.
157. Brandstater, M., et al., *Hemiplegic gait: analysis of temporal variables.* Archives of physical medicine and rehabilitation, 1983. **64**(12): p. 583-587.
158. Carriero, A., et al., *Correlation between lower limb bone morphology and gait characteristics in children with spastic diplegic cerebral palsy.* Journal of Pediatric Orthopaedics, 2009. **29**(1): p. 73-79.
159. DeVita, P. and T. Hortobagyi, *Age causes a redistribution of joint torques and powers during gait.* Journal of applied physiology, 2000. **88**(5): p. 1804-1811.
160. Rosin, R., H. Topka, and J. Dichgans, *Gait initiation in Parkinson's disease.* Movement disorders, 1997. **12**(5): p. 682-690.
161. Morris, M.E., et al., *Constraints on the kinetic, kinematic and spatiotemporal parameters of gait in Parkinson's disease.* Human Movement Science, 1999. **18**(2): p. 461-483.

162. O'Byrne, J.M., A. Jenkinson, and T. O'brien, *Quantitative analysis and classification of gait patterns in cerebral palsy using a three-dimensional motion analyzer.* Journal of child neurology, 1998. **13**(3): p. 101-108.
163. Ballaz, L., S. Plamondon, and M. Lemay, *Ankle range of motion is key to gait efficiency in adolescents with cerebral palsy.* Clinical Biomechanics, 2010. **25**(9): p. 944-948.
164. Dallmeijer, A., et al., *Association between isometric muscle strength and gait joint kinetics in adolescents and young adults with cerebral palsy.* Gait & posture, 2011. **33**(3): p. 326-332.
165. Don, R., et al., *Foot drop and plantar flexion failure determine different gait strategies in Charcot-Marie-Tooth patients.* Clinical biomechanics, 2007. **22**(8): p. 905-916.
166. Ghaffar, A., A.A. Dehghani-Sanij, and S.Q. Xie, *A review of gait disorders in the elderly and neurological patients for robot-assisted training.* Disability and Rehabilitation: Assistive Technology, 2019: p. 1-15.
167. Gabell, A., M.A. Simons, and U.S.L. Nayak, *Falls in the healthy elderly: predisposing causes.* Ergonomics, 1985. **28**(7): p. 965-975.
168. Zeilig, G., et al., *Safety and tolerance of the ReWalk™ exoskeleton suit for ambulation by people with complete spinal cord injury: a pilot study.* The journal of spinal cord medicine, 2012. **35**(2): p. 96-101.
169. *Indego Powering People Forward*. 2012; Available from: http://www.parker.com/literature/Exoskeleton/Parker%20Indego%20Brochure.pdf.
170. Sonoda, T., et al., *Development of antagonistic wire-driven joint employing kinematic transmission mechanism.* Journal of Automation Mobile Robotics and Intelligent Systems, 2010. **4**: p. 62-70.
171. Koganezawa, K. *Mechanical stiffness control for antagonistically driven joints*. in *2005 IEEE/RSJ International Conference on Intelligent Robots and Systems*. 2005. IEEE.
172. Firouzy, S., *Optimal design of actuation systems for an enhancive robotic exoskeleton*. 2017, University of Leeds.
173. Winter, D.A., *Biomechanics and motor control of human movement*. 2009: John Wiley & Sons.
174. Brooks, T.L. *Telerobotic response requirements*. in *1990 IEEE International Conference on Systems, Man, and Cybernetics Conference Proceedings*. 1990. IEEE.
175. Liszka, M., *Mechanical design of a robotic arm exoskeleton for shoulder rehabilitation*. 2006.
176. Reshetov, D.N. and N. Weinstein, *Machine design*. 1978.
177. Grant, P.M., P.M. Dall, and A. Kerr, *Daily and hourly frequency of the sit to stand movement in older adults: a comparison of day hospital, rehabilitation ward and community living groups.* Aging clinical and experimental research, 2011. **23**(5-6): p. 437-444.
178. Kwon, J.W., S.M. Son, and N.K. Lee, *Changes of kinematic parameters of lower extremities with gait speed: a 3D motion analysis study.* Journal of physical therapy science, 2015. **27**(2): p. 477-479.
179. Haq, A., Y. Aoustin, and C. Chevallereau. *Effects of knee locking and passive joint stiffness on energy consumption of a seven-link planar*

biped. in *2012 IEEE International Conference on Robotics and Automation*. 2012. IEEE.
180. Hollander, K.W., et al., *An efficient robotic tendon for gait assistance.* Journal of biomechanical engineering, 2006. **128**(5): p. 788-791.
181. Zhu, Y., et al. *Design and evaluation of a parallel-series elastic actuator for lower limb exoskeletons*. in *2014 IEEE International Conference on Robotics and Automation (ICRA)*. 2014. IEEE.
182. Toxiri, S., et al., *A parallel-elastic actuator for a torque-controlled back-support exoskeleton.* IEEE Robotics and Automation Letters, 2018. **3**(1): p. 492-499.
183. Verstraten, T., et al., *Series and parallel elastic actuation: Impact of natural dynamics on power and energy consumption.* Mechanism and Machine Theory, 2016. **102**: p. 232-246.
184. Kim, H.-g., S. Park, and C. Han, *Design of a novel knee joint for an exoskeleton with good energy efficiency for load-carrying augmentation.* Journal of Mechanical Science and Technology, 2014. **28**(11): p. 4361-4367.
185. Velasco, A., et al. *Soft-actuators in cyclic motion: Analytical optimization of stiffness and pre-load*. in *2013 13th IEEE-RAS International Conference on Humanoid Robots (Humanoids)*. 2013. IEEE.
186. Wang, S., W. Van Dijk, and H. van der Kooij. *Spring uses in exoskeleton actuation design*. in *2011 IEEE International Conference on Rehabilitation Robotics*. 2011. IEEE.
187. Grimmer, M., M. Eslamy, and A. Seyfarth. *Energetic and peak power advantages of series elastic actuators in an actuated prosthetic leg for walking and running*. in *Actuators*. 2014. Multidisciplinary Digital Publishing Institute.
188. Hara, H. and Y. Sankai. *HAL equipped with passive mechanism*. in *2012 IEEE/SICE International Symposium on System Integration (SII)*. 2012. IEEE.
189. Grimmer, M., et al. *A comparison of parallel-and series elastic elements in an actuator for mimicking human ankle joint in walking and running*. in *2012 IEEE International Conference on Robotics and Automation*. 2012. IEEE.
190. Beckerle, P., et al., *Analysis of system dynamic influences in robotic actuators with variable stiffness.* Smart Structures and Systems, 2014. **13**(4): p. 711-730.
191. Mathijssen, G., et al., *Study on electric energy consumed in intermittent series–parallel elastic actuators (iSPEA).* Bioinspiration & biomimetics, 2017. **12**(3): p. 036008.
192. Hitt, J.K., et al., *An active foot-ankle prosthesis with biomechanical energy regeneration.* Journal of medical devices, 2010. **4**(1).
193. Yesilevskiy, Y., W. Xi, and C.D. Remy. *A comparison of series and parallel elasticity in a monoped hopper*. in *2015 IEEE International Conference on Robotics and Automation (ICRA)*. 2015. IEEE.
194. Grimmer, M. and A. Seyfarth. *Stiffness adjustment of a series elastic actuator in a knee prosthesis for walking and running: The trade-off between energy and peak power optimization*. in *2011 IEEE/RSJ International Conference on Intelligent Robots and Systems*. 2011. IEEE.

195. Bajelan, S. and M.R. Azghani. *Musculoskeletal analysis of sit-to-stand maneuver in order to compare the various standing up strategies*. in *2011 18th Iranian Conference of Biomedical Engineering (ICBME)*. 2011. IEEE.
196. Eslamy, M., M. Grimmer, and A. Seyfarth. *Effects of unidirectional parallel springs on required peak power and energy in powered prosthetic ankles: Comparison between different active actuation concepts*. in *2012 IEEE International Conference on Robotics and Biomimetics (ROBIO)*. 2012. IEEE.
197. Moore, A.W., D.J. Hill, and M.P. Johnson. *An empirical investigation of brute force to choose features, smoothers and function approximators*. in *Computational learning theory and natural learning systems*. 1992. Citeseer.
198. Rakib, M.I., et al., *Design and biomechanical performance analysis of a user-friendly orthotic device.* Materials & Design (1980-2015), 2015. **65**: p. 716-725.
199. Vanderborght, B., et al., *Variable impedance actuators: A review.* Robotics and autonomous systems, 2013. **61**(12): p. 1601-1614.
200. Marjaninejad, A. and F.J. Valero-Cuevas, *Should anthropomorphic systems be "redundant"?*, in *Biomechanics of Anthropomorphic Systems*. 2019, Springer. p. 7-34.
201. Tonietti, G. and A. Bicchi. *Adaptive simultaneous position and stiffness control for a soft robot arm*. in *IEEE/RSJ International Conference on Intelligent Robots and Systems*. 2002. IEEE.
202. Szufnarowski, F. and A. Schneider. *Compliant piezo-flexdrives for muscle-like, antagonistic actuation of robot joints*. in *2010 3rd IEEE RAS & EMBS International Conference on Biomedical Robotics and Biomechatronics*. 2010. IEEE.
203. Verstraten, T., et al., *Kinematically redundant actuators, a solution for conflicting torque–speed requirements.* The International Journal of Robotics Research, 2019. **38**(5): p. 612-629.
204. Verstraten, T., et al. *A series elastic dual-motor actuator concept for wearable robotics*. in *International Symposium on Wearable Robotics*. 2018. Springer.
205. Sugar, T.G. and M. Holgate. *Compliant mechanisms for robotic ankles*. in *ASME 2013 International Design Engineering Technical Conferences and Computers and Information in Engineering Conference*. 2013. American Society of Mechanical Engineers.
206. Alò, R., F. Bottiglione, and G. Mantriota, *An innovative design of artificial knee joint actuator with energy recovery capabilities.* Journal of Mechanisms and Robotics, 2016. **8**(1): p. 011009.
207. Mooney, L. and H. Herr. *Continuously-variable series-elastic actuator*. in *2013 IEEE 13th International Conference on Rehabilitation Robotics (ICORR)*. 2013. IEEE.
208. Migliore, S.A., E.A. Brown, and S.P. DeWeerth. *Biologically inspired joint stiffness control*. in *Proceedings of the 2005 IEEE international conference on robotics and automation*. 2005. IEEE.
209. Hurst, J.W., J.E. Chestnutt, and A.A. Rizzi, *The actuator with mechanically adjustable series compliance.* IEEE Transactions on Robotics, 2010. **26**(4): p. 597-606.

210. Vanderborght, B., et al., *Comparison of mechanical design and energy consumption of adaptable, passive-compliant actuators.* The International Journal of Robotics Research, 2009. **28**(1): p. 90-103.
211. Maheswararao, C.U., Y.K. Babu, and K. Amaresh. *Sliding mode speed control of a DC motor*. in *2011 International Conference on Communication Systems and Network Technologies*. 2011. IEEE.
212. Santana, J., et al., *Simulation and construction of a speed control for a DC series motor.* mechatronics, 2002. **12**(9-10): p. 1145-1156.
213. Ayasun, S. and G. Karbeyaz, *DC motor speed control methods using MATLAB/Simulink and their integration into undergraduate electric machinery courses.* Computer applications in engineering education, 2007. **15**(4): p. 347-354.
214. Ramesh, M., et al., *Speed control of brushless dc motor by using fuzzy logic pi controller.* ARPN Journal of Engineering and Applied Sciences, 2011. **6**(9): p. 55-62.
215. Ruiz Garate, V., et al., *Experimental validation of motor primitive-based control for leg exoskeletons during continuous multi-locomotion tasks.* Frontiers in neurorobotics, 2017. **11**: p. 15.
216. Grimmer, M. and A. Seyfarth, *Mimicking human-like leg function in prosthetic limbs*, in *Neuro-Robotics*. 2014, Springer. p. 105-155.
217. VERSTRATEN, T., *NEW ACTUATION PARADIGMS WITH HIGH EFFICIENCY FOR VARIABLE LOAD AT VARYING SPEED*. 2018, Technische Universität Darmstadt.
218. Schenkman, M., et al., *Whole-body movements during rising to standing from sitting.* Physical therapy, 1990. **70**(10): p. 638-648.
219. Ruthenberg, B.J., N.A. Wasylewski, and J.E. Beard, *An experimental device for investigating the force and power requirements of a powered gait orthosis.* Journal of rehabilitation research and development, 1997. **34**: p. 203-214.
220. Kim, C.M. and J.J. Eng, *Magnitude and pattern of 3D kinematic and kinetic gait profiles in persons with stroke: relationship to walking speed.* Gait & posture, 2004. **20**(2): p. 140-146.
221. Clauser, C.E., J.T. McConville, and J.W. Young, *Weight, volume, and center of mass of segments of the human body*. 1969, Antioch Coll Yellow Springs OH.
222. Lafond, D., M. Duarte, and F. Prince, *Comparison of three methods to estimate the center of mass during balance assessment.* Journal of biomechanics, 2004. **37**(9): p. 1421-1426.

Appendix A
Kinematic and Kinetic Modelling of an Assistive Robotic Exoskeleton

The dynamic modelling of the exoskeleton will be explained in this section. Figure A.1 shows the model of the exoskeleton that will be used to perform the kinematic and dynamic analysis of motion. The desired manoeuvres taken into account for an assistive device was sit to stand and level ground walking. The walking gait was further divided into swing and stance phase and the stance phase can be further subdivided into single limb stance phase and double limb stance phase. The modelling of the exoskeleton will also be discussed according to the above mentioned phases of the gait cycle.

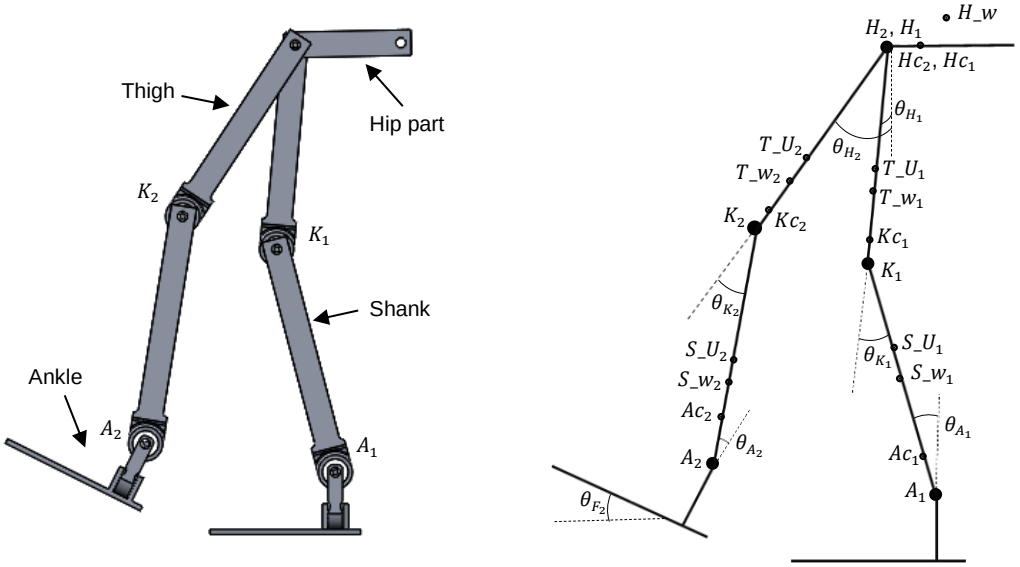

(a) **(b)**

Figure A.1: (a) Model of a Lower Limb Assistive Robotic Exoskeleton (b) Free Body Diagram of the exoskeleton model. Points S_U_1, S_w_1 shank segment during stance phase, T_U_1, T_w_1 for thigh segment during stance phase, T_U_2, T_w_2 for thigh segment during swing phase and S_U_2, S_w_2 for shank segment during swing phase represents the centre of gravity (COG) of the respective segment of user's limb mass and exoskeleton segment mass without actuators. Points H_1, K_1 A_1 and H_2, K_2 A_2 represents the joint actuators.

A.1 Single Limb Phase

A.1.1 Kinematic Analysis

The single limb phase starts with the toe-off of the swing leg and ends with the heel strike of the same leg. The inputs will be the position, velocity and acceleration of points A, K and H. The dynamic modelling of the swing and stance leg during single limb phase will be described as follows.

By using Figure A.1 and applying law of cosines at the stance leg, Eq. (A.1) will be obtained as:

$$\left(\overline{A_1H_1}\right)^2 = \left(\overline{A_1K_1}\right)^2 + \left(\overline{K_1H_1}\right)^2 - 2\left(\overline{A_1K_1}\right)\left(\overline{K_1H_1}\right)\cos\left(\pi - \boldsymbol{\theta}_{K_1}\right) \quad \text{(A.1)}$$

$$\boldsymbol{\theta}_{K_1} = \cos^{-1}\left(\frac{\left(\overline{A_1H_1}\right)^2 - \left(\overline{A_1K_1}\right)^2 - \left(\overline{K_1H_1}\right)^2}{2\left(\overline{A_1K_1}\right)^2\left(\overline{K_1H_1}\right)^2}\right) \quad \text{(A.2)}$$

The position of the ankle joint can be represented as follows

$$\boldsymbol{A}_{1_x} = \boldsymbol{H}_{1_x} + \left(\overline{H_1K_1}\right)\sin\left(\boldsymbol{\theta}_{H_1}\right) - \left(\overline{K_1A_1}\right)\sin\left(\boldsymbol{\theta}_{H_1} - \boldsymbol{\theta}_{K_1}\right) \quad \text{(A.3)}$$

$$\boldsymbol{A}_{1_y} = \boldsymbol{H}_{1_y} - \left(\overline{H_1K_1}\right)\cos\left(\boldsymbol{\theta}_{H_1}\right) - \left(\overline{K_1A_1}\right)\cos\left(\boldsymbol{\theta}_{H_1} - \boldsymbol{\theta}_{K_1}\right) \quad \text{(A.4)}$$

Using Eq. (A.3) to solve for the angular displacement of the hip joint

$$\begin{aligned}\boldsymbol{A}_{1_x} = \boldsymbol{H}_{1_x} &+ \left(\overline{H_1K_1}\right)\sin\left(\boldsymbol{\theta}_{H_1}\right) \\ &- \left(\overline{K_1A_1}\right)\left(sin\left(\boldsymbol{\theta}_{H_1}\right)cos\left(\boldsymbol{\theta}_{K_1}\right) - cos\left(\boldsymbol{\theta}_{H_1}\right)sin\left(\boldsymbol{\theta}_{K_1}\right)\right)\end{aligned} \quad \text{(A.5)}$$

$$\begin{aligned}\boldsymbol{A}_{1_x} = \boldsymbol{H}_{1_x} &+ \left(\overline{H_1K_1}\right)\sin\left(\boldsymbol{\theta}_{H_1}\right) \\ &- \left(\overline{K_1A_1}\right)\left(sin\left(\boldsymbol{\theta}_{H_1}\right)cos\left(\boldsymbol{\theta}_{K_1}\right)\right. \\ &\left. - \left(\sqrt{1 - sin^2\boldsymbol{\theta}_{H_1}}\right)sin\left(\boldsymbol{\theta}_{K_1}\right)\right)\end{aligned} \quad \text{(A.6)}$$

Re-arranging Eq. (A.6) results in Eq. (A.7) as:

$$\begin{aligned}-\left(\overline{K_1A_1}\right)&\left(\sqrt{1 - sin^2\boldsymbol{\theta}_{H_1}}\right)sin\left(\boldsymbol{\theta}_{K_1}\right) \\ &= \left(\boldsymbol{H}_{1_x} - \boldsymbol{A}_{1_x}\right) + \left(\overline{H_1K_1} - \overline{K_1A_1}\,cos\boldsymbol{\theta}_{K_1}\right)\sin\left(\boldsymbol{\theta}_{H_1}\right)\end{aligned} \quad \text{(A.7)}$$

Simplifying Eq. (A.7) in terms of variables $\boldsymbol{S}$, $\boldsymbol{T}$ and $\boldsymbol{U}$,

$$\boldsymbol{S}\sqrt{\left(1 - sin^2\boldsymbol{\theta}_{H_1}\right)} = \boldsymbol{T} + \boldsymbol{U}\,sin\left(\boldsymbol{\theta}_{H_1}\right) \quad \text{(A.8)}$$

Squaring Eq. (A.8)

$$\boldsymbol{S}^2 - \boldsymbol{S}^2\,sin^2\boldsymbol{\theta}_{H_1} = \boldsymbol{T}^2 + \boldsymbol{U}^2\,sin^2\boldsymbol{\theta}_{H_1} + 2\boldsymbol{TU}\,sin\boldsymbol{\theta}_{H_1} \quad \text{(A.9)}$$

$$(\boldsymbol{S}^2 + \boldsymbol{U}^2)sin^2\boldsymbol{\theta}_{H_1} + 2\boldsymbol{TU}\,sin\boldsymbol{\theta}_{H_1} + (\boldsymbol{S}^2 - \boldsymbol{T}^2) = 0 \quad \text{(A.10)}$$

Therefore,

$$\boldsymbol{\theta}_{H_1} = \sin^{-1}\left(\frac{-2\boldsymbol{TU} \pm \sqrt{4\boldsymbol{T}^2\boldsymbol{U}^2 - 4(\boldsymbol{S}^2 + \boldsymbol{U}^2)(\boldsymbol{T}^2 - \boldsymbol{S}^2)}}{2\,(\boldsymbol{S}^2 + \boldsymbol{U}^2)}\right) \tag{A.11}$$

Where Eq. (A.11) will yield the angular displacement of the hip joint of the stance leg during the single limb phase. It should be noted that the correct value of the angular displace of the hip joint will be obtained by using the positive value of the term $\sqrt{4\boldsymbol{T}^2\boldsymbol{U}^2 - 4(\boldsymbol{S}^2 + \boldsymbol{U}^2)(\boldsymbol{T}^2 - \boldsymbol{S}^2)}$. Hence, a positive value was considered.

Now, the joint angle of the swing leg denoted by subscript 2 will be calculated using a similar approach as above.

Eq. (A.12) will be obtained by applying law of cosines to yield the angular displacement of the knee joint of the swing leg.

$$\left(\overline{A_2H_2}\right)^2 = \left(\overline{A_2K_2}\right)^2 + \left(\overline{K_2H_2}\right)^2 - 2\left(\overline{A_2K_2}\right)\left(\overline{K_2H_2}\right)\cos\left(\pi - \boldsymbol{\theta}_{K_2}\right) \tag{A.12}$$

Re-arranging the above equation will give the angular displacement of the knee joint as given in Eq. (A.13).

$$\boldsymbol{\theta}_{K_2} = \cos^{-1}\left(\frac{\left(\overline{A_2H_2}\right)^2 - \left(\overline{A_2K_2}\right)^2 - \left(\overline{K_2H_2}\right)^2}{2\left(\overline{A_2K_2}\right)^2\left(\overline{K_2H_2}\right)^2}\right) \tag{A.13}$$

The linear position of the hip joint of the swing and stance leg can be represented as:

$$\boldsymbol{H}_{1_x} = \boldsymbol{H}_{2_x} = \boldsymbol{A}_{2_x} - \left(\overline{A_2K_2}\right)\cos\left(\theta_{S_2}\right) - \left(\overline{K_2H_2}\right)\cos\left(\theta_{T_2}\right) \tag{A.14}$$

and

$$\boldsymbol{H}_{1_y} = \boldsymbol{H}_{2_y} = \boldsymbol{A}_{2_y} + \left(\overline{A_2K_2}\right)\sin\left(\theta_{S_2}\right) + \left(\overline{K_2H_2}\right)\sin\left(\theta_{T_2}\right) \tag{A.15}$$

Where θ_{S_2} is the shin angle of the swing leg given be Eq. (A.16)

$$\boldsymbol{\theta}_{S_2} = \boldsymbol{\theta}_{F_2} + \frac{\pi}{2} - \boldsymbol{\theta}_{A_2} \tag{A.16}$$

Similarly, angular displacement of the thigh link $\boldsymbol{\theta}_{T_2}$ can be represented by Eq. (A.17).

$$\boldsymbol{\theta}_{T_2} = \boldsymbol{\theta}_{S_2} + \boldsymbol{\theta}_{K_2} \tag{A.17}$$

The angular displacement of the hip joint of the stance and swing leg is given by Eq. (A.18) and Eq. (A.19) respectively,

$$\boldsymbol{\theta}_{H_1} = \boldsymbol{\theta}_{K_1} - \boldsymbol{\theta}_{A_1} \tag{A.18}$$

$$\boldsymbol{\theta}_{H_2} = \boldsymbol{\theta}_{K_2} + \boldsymbol{\theta}_{A_2} - \boldsymbol{\theta}_{F_2} \tag{A.19}$$

Therefore, substituting Eq. (A.17) into Eq. (A.14) results in Eq. (A.20).

$$\boldsymbol{H}_{2_x} = \boldsymbol{A}_{2_x} - \left(\overline{A_2K_2}\right)\cos\left(\boldsymbol{\theta}_{s_2}\right) - \left(\overline{K_2H_2}\right)\cos\left(\boldsymbol{\theta}_{S_2} + \boldsymbol{\theta}_{K_2}\right) \tag{A.20}$$

$$\begin{aligned}\boldsymbol{H}_{2_x} = \boldsymbol{A}_{2_x} &- \left(\overline{A_2K_2}\right)\cos\left(\boldsymbol{\theta}_{s_2}\right) \\ &- \left(\overline{K_2H_2}\right)\left(\cos\left(\boldsymbol{\theta}_{S_2}\right)\cos(\boldsymbol{\theta}_{K_2}) \right. \\ &\left. - \sin(\boldsymbol{\theta}_{K_2})\sqrt{\left(1 - cos^2\boldsymbol{\theta}_{S_2}\right)}\right)\end{aligned} \tag{A.21}$$

Re-arranging Eq. (A.21) results in Eq. (A.22),

$$\begin{aligned}\left(\overline{A_2K_2} + \overline{K_2H_2}\,\cos\boldsymbol{\theta}_{K_2}\right)\cos(\boldsymbol{\theta}_s) + \left(\boldsymbol{H}_{2_x} - \boldsymbol{A}_{2_x}\right) \\ = \overline{K_2H_2}\,\sin\boldsymbol{\theta}_{K_2}\left(\sqrt{\left(1 - cos^2\boldsymbol{\theta}_{S_2}\right)}\right)\end{aligned} \tag{A.22}$$

Simplifying Eq. (A.22) by using variables P, Q and R gives,

$$\boldsymbol{P}\cos(\boldsymbol{\theta}_s) + \boldsymbol{Q} = \boldsymbol{R}\sqrt{\left(1 - cos^2\boldsymbol{\theta}_{S_2}\right)} \tag{A.23}$$

By Squaring Eq. (A.23),

$$\boldsymbol{P}^2 cos^2\boldsymbol{\theta}_{s_2} + \boldsymbol{Q}^2 + 2\boldsymbol{PQ}\cos\boldsymbol{\theta}_{s_2} = \boldsymbol{R}^2\left(1 - cos^2\boldsymbol{\theta}_{s_2}\right) \tag{A.24}$$

Re-arranging he above equation,

$$(\boldsymbol{P}^2 + \boldsymbol{R}^2)cos^2\boldsymbol{\theta}_{s_2} + 2\boldsymbol{PQ}\cos\boldsymbol{\theta}_{s_2} + (\boldsymbol{Q}^2 + \boldsymbol{R}^2) = 0 \tag{A.25}$$

Therefore,

$$\boldsymbol{\theta}_{s_2} = \cos^{-1}\left(\frac{-2\boldsymbol{PQ} \pm \sqrt{4\boldsymbol{P}^2\boldsymbol{Q}^2 - 4(\boldsymbol{P}^2 + \boldsymbol{R}^2)(\boldsymbol{Q}^2 - \boldsymbol{R}^2)}}{2(\boldsymbol{P}^2 + \boldsymbol{R}^2)}\right) \tag{A.26}$$

Using Eq. (A.26), the angular displacement of the shank segment will be determined. It should be noted that the correct value of the angular displacement of the shank segment will be obtained by using the positive value of the term $\sqrt{4\boldsymbol{P}^2\boldsymbol{Q}^2 - 4(\boldsymbol{P}^2 + \boldsymbol{R}^2)(\boldsymbol{Q}^2 - \boldsymbol{R}^2)}$. Similarly, by using the shank angular displacement, angular displacement of the thigh will be determined using Eq. (A.17).

After obtaining the expressions for the joint angular displacements, the angular velocities and accelerations of the lower limb joints will be calculated with the inputs as the linear velocities and accelerations of the joint. Figure A.2 shows the free body diagram of the shank segment of the stance leg.

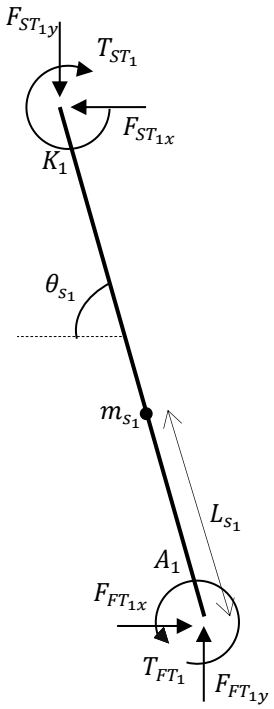

Figure A.2: Free body diagram of the shank segment of the stance leg

The linear velocity of the knee joint considering the stance leg can be written as:

$$\boldsymbol{V}_{K_1} = \boldsymbol{V}_{A_1} + \overline{A_1K_1}\,\boldsymbol{\omega}_{s_1}(-\sin(\boldsymbol{\theta}_{s_1}) - \cos(\boldsymbol{\theta}_{s_1})\,.\hat{\boldsymbol{j}} \tag{A.27}$$

Where,

$$\boldsymbol{\theta}_{s_1} = \left(\frac{\pi}{2} + \boldsymbol{\theta}_{H_1} - \boldsymbol{\theta}_{K_1}\right) \tag{A.28}$$

And,

$$\boldsymbol{V}_{A_1} = 0$$

Therefore, Eq. (A.27) can be written as:

$$\boldsymbol{V}_{K_1} = \overline{A_1K_1}\,\boldsymbol{\omega}_{s_1}\left(-\sin\left(\frac{\pi}{2} + \boldsymbol{\theta}_{H_1} - \boldsymbol{\theta}_{K_1}\right) - \cos\left(\frac{\pi}{2} + \boldsymbol{\theta}_{H_1} - \boldsymbol{\theta}_{K_1}\right).\hat{\boldsymbol{j}}\right. \tag{A.29}$$

$$\boldsymbol{V}_{K_1} = \overline{A_1K_1}\,\boldsymbol{\omega}_{s_1}(-\cos(\boldsymbol{\theta}_{H_1} - \boldsymbol{\theta}_{K_1}) + \sin(\boldsymbol{\theta}_{H_1} - \boldsymbol{\theta}_{K_1})\,.\hat{\boldsymbol{j}} \tag{A.30}$$

Also,

$$\boldsymbol{\theta}_{H_1} - \boldsymbol{\theta}_{K_1} = -\boldsymbol{\theta}_{A_1} \tag{A.31}$$

Eq. (A.30) in terms of θ_{A_1} can be given as:

$$\boldsymbol{V}_{K_1} = \overline{A_1K_1}\,\boldsymbol{\omega}_{s_1}(-\cos(\boldsymbol{\theta}_{A_1}) - \sin(\boldsymbol{\theta}_{A_1})\,.\hat{\boldsymbol{j}}) \tag{A.32}$$

As,

$$\boldsymbol{\omega}_{s_1} = -\dot{\boldsymbol{\theta}}_{A_1} \tag{A.33}$$

Therefore,

$$\boldsymbol{\omega}_{s_1} = \dot{\boldsymbol{\theta}}_{H_1} - \dot{\boldsymbol{\theta}}_{K_1} \tag{A.34}$$

Eq. (A.32) can be written as:

$$\left|\boldsymbol{V}_{K_1}\right| = \overline{A_1K_1}.\,\boldsymbol{\omega}_{s_1} \tag{A.35}$$

$$\boldsymbol{\omega}_{s_1} = \frac{\left|\boldsymbol{V}_{K_1}\right|}{\overline{A_1K_1}} \tag{A.36}$$

$$\boldsymbol{\omega}_{s_1} = \frac{real\left(\boldsymbol{V}_{K_1}\right)}{\overline{A_1K_1}\left(-\cos\left(\boldsymbol{\theta}_{A_1}\right)\right)} \tag{A.37}$$

Eq. (A.39) will yield the angular velocity of the shank leg during the stance phase.

Similarly, the acceleration of the shank segment during stance phase can be determined as follows:

The linear acceleration of the knee joint can be written according to Eq. (A.33)

$$\begin{aligned}\boldsymbol{A}_{K_1} = \overline{A_1K_1}\;\boldsymbol{\omega}_{s_1}{}^2\left(\sin\left(\boldsymbol{\theta}_{A_1}\right) - \cos\left(\boldsymbol{\theta}_{A_1}\right).\hat{\boldsymbol{j}}\right)\\ + \overline{A_1K_1}\;\alpha_{s_1}\left(-\cos\left(\boldsymbol{\theta}_{A_1}\right) - \sin\left(\boldsymbol{\theta}_{A_1}\right).\hat{\boldsymbol{j}}\right)\end{aligned} \tag{A.38}$$

where

$$\boldsymbol{\alpha}_{s_1} = -\ddot{\boldsymbol{\theta}}_{A_1} \tag{A.39}$$

$$\boldsymbol{\alpha}_{s_1} = \ddot{\boldsymbol{\theta}}_{H_1} - \ddot{\boldsymbol{\theta}}_{K_1} \tag{A.40}$$

Representing Eq. (A.38) in terms of real variables,

$$real\left(\boldsymbol{A}_{K_1}\right) = \overline{A_1K_1}\;\boldsymbol{\omega}_{s_1}{}^2\left(\sin\left(\boldsymbol{\theta}_{A_1}\right)\right) + \overline{A_1K_1}\;\boldsymbol{\alpha}_{s_1}\left(-\cos\left(\boldsymbol{\theta}_{A_1}\right)\right) \tag{A.41}$$

$$\boldsymbol{\alpha}_{s_1} = \frac{real\left(\boldsymbol{A}_{K_1}\right) - \overline{A_1K_1}\;\boldsymbol{\omega}_{s_1}{}^2\left(\sin\left(\boldsymbol{\theta}_{A_1}\right)\right)}{\overline{A_1K_1}\left(-\cos\left(\boldsymbol{\theta}_{A_1}\right)\right)} \tag{A.42}$$

Now the acceleration of the centre of gravity (COG) of shank segment will be calculated as:

$$\begin{aligned}\boldsymbol{A}_{s_1} = L_{\,s_1}\boldsymbol{\omega}_{s_1}{}^2\left(\cos\left(\boldsymbol{\theta}_{s_1}\right) - \sin\left(\boldsymbol{\theta}_{s_1}\right).\hat{\boldsymbol{j}}\right)\\ + L_{\,s_1}\,\boldsymbol{\alpha}_{s_1}\left(-\sin\left(\boldsymbol{\theta}_{s_1}\right) - \cos\left(\boldsymbol{\theta}_{s_1}\right).\hat{\boldsymbol{j}}\right)\end{aligned} \tag{A.43}$$

The mass and the location of COG of different segments of the human body in terms of the percentages of the respective total value is illustrated in Table A.1[221]. It should be noted that the mass each segment of the user will be added to the mass of the respective segment of the exoskeleton along with adding the masses of the actuators to yield the total mass of that segment.

Table A.1: The mass of each segment represented as a percentage of the total body mass and location of the centre of gravity of each segment represented as a percentage of the proximal end and the total respective segment length.

Segment	Mass (%)	COG location (%)
Head and Neck	8.26	36.3
Upper Arm	3.25	43.2
Forearm	1.87	41.8
Hand	0.65	47.4
Trunk	46.8	48.4
Thigh	10.5	43.3
Shank	4.75	43.4
Foot	1.43	42.9

The location of the COG of the shank segment will be analysed after incorporating the aforementioned mass of the user's limb and that of the motor and the transmission mechanism. The location of the COG of shank segment without the mass of the user and actuators will be represented by $L_{s\_w_1}$. The mass of the user is represented by $L_{S\_U_1}$ and calculated using Table A.1. After the addition of the mass of user and masses of the actuators, the new location of the COG (L_{s_1}) can be determined as:

$$L_{S\_U_1} m_{s\_u_1} + L_{S\_w_1} m_{s\_w_1} + \sum_n L_{AC_1}(n)\, m_{AC_1}(n) = \left(m_{s\_u_1} + m_{s\_w_1} + \sum_n m_{AC_1}(n) \right). L_{s_1} \tag{A.44}$$

$$L_{s_1} = \frac{L_{S\_U_1} m_{s\_u_1} + L_{S\_w_1} m_{s\_w_1} + \sum_n L_{AC_1}(n)\, m_{AC_1}(n)}{\left(m_{s\_u_1} + m_{s\_w_1} + \sum_n m_{AC_1}(n) \right)} \tag{A.45}$$

Similarly, the angular velocity and acceleration of the thigh part of the stance leg will be determined given the input as its linear velocity and acceleration. Figure A.3 represents the free body diagram of the thigh segment of the stance leg.

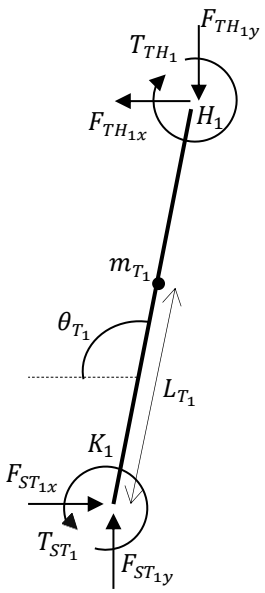

Figure A.3: Free body diagram of the thigh segment of the stance leg

The velocity of the knee joint can be represented by Eq. (A.46).

$$\boldsymbol{V}_{K_1} = \boldsymbol{V}_{H_1} + \overline{H_1K_1}\,\boldsymbol{\omega}_{T_1}(\cos(\boldsymbol{\theta}_{H_1}) - \sin(\boldsymbol{\theta}_{H_1}).\hat{\boldsymbol{j}}) \tag{A.46}$$

As,

$$\boldsymbol{\omega}_{T_1} = \dot{\boldsymbol{\theta}}_{H_1} \tag{A.47}$$

Therefore, Eq. (A.46) can be written as:

$$\boldsymbol{\omega}_{T_1} = \frac{real(\boldsymbol{V}_{K_1} - \boldsymbol{V}_{B_1})}{\overline{H_1K_1}\,\cos(\boldsymbol{\theta}_{H_1})} \tag{A.48}$$

Similarly, the linear acceleration of the knee joint can be given by Eq. (A.49)

$$\begin{aligned}\boldsymbol{A}_{K_1} = \boldsymbol{A}_{H_1} &+ \overline{H_1K_1}\,\boldsymbol{\omega}_{T_1}{}^2\,(\sin(\boldsymbol{\theta}_{H_1}) + \cos(\boldsymbol{\theta}_{H_1}).\hat{\boldsymbol{j}}) \\ &+ \overline{H_1K_1}\,\boldsymbol{\alpha}_{T_1}(\cos(\boldsymbol{\theta}_{H_1}) - \sin(\boldsymbol{\theta}_{H_1}).\hat{\boldsymbol{j}})\end{aligned} \tag{A.49}$$

Re-arranging and representing in terms of the real variables will yield Eq. (A.50)

$$\boldsymbol{\alpha}_{T_1} = \ddot{\boldsymbol{\theta}}_{H_1} = \frac{real(\boldsymbol{A}_{K_1} - \boldsymbol{A}_{B_1}) + \overline{H_1K_1}\,\boldsymbol{\omega}_{T_1}{}^2\,(-\sin(\boldsymbol{\theta}_{H_1}))}{\overline{H_1K_1}\,\cos(\boldsymbol{\theta}_{H_1})} \tag{A.50}$$

The linear acceleration of the thigh segment will be recorded in Eq. (A.51)

$$\begin{aligned}\boldsymbol{A}_{T_1} = \boldsymbol{A}_{K_1} &+ L_{T_1}\,\boldsymbol{\omega}_{T_1}{}^2\,(-\sin(\boldsymbol{\theta}_{H_1}) - \cos(\boldsymbol{\theta}_{H_1}).\hat{\boldsymbol{j}}) \\ &+ L_{T_1}\,\boldsymbol{\alpha}_{T_1}(-\cos(\boldsymbol{\theta}_{H_1}) + \sin(\boldsymbol{\theta}_{H_1}).\hat{\boldsymbol{j}})\end{aligned} \tag{A.51}$$

Similarly, the location of the COG of thigh segment after adding the mass of the user and that of the motor and the transmission mechanism will be given by Eq. (A.52).

$$L_{T_1} = \frac{L_{T\_U_1} m_{T\_U_1} + L_{T\_w_1} m_{T\_w_1} + \sum_n L_{KC_1}(n)\, m_{KC_1}(n)}{m_{T\_U_1} + m_{T\_w_1} + \sum_n m_{KC_1}(n)} \quad \text{(A.52)}$$

Where $L_{T\_w_1}$ represents the location of the COG of thigh segment of the exoskeleton without the mass of the actuator, $L_{T\_U_1}$ represents mass of the thigh segment of the user illustrated in Table A.1 and $m_{KC_1}(n)$ recorded the mass of the motor and the transmission systems.

Figure A.4 and A.5 represents the shank and thigh segment of the swing leg. The angular velocity and acceleration of the shank and thigh segment of the swing leg can be calculated as follows:

$$\boldsymbol{V}_{K_2} = \boldsymbol{V}_{A_2} + \overline{A_2K_2}\, \boldsymbol{\omega}_{s_2}(-\sin(\boldsymbol{\theta}_{s_2}) - \cos(\boldsymbol{\theta}_{s_2}).\hat{\boldsymbol{j}}) \quad \text{(A.53)}$$

Where $\boldsymbol{V}_{K_2}$ represents the linear velocity of the knee joint of the swing leg.

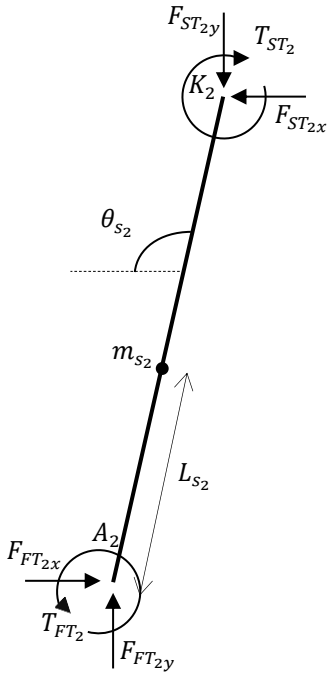

Figure A.4: Free body diagram of the shank segment of the swing leg

Eq. (A.53) can be written as:

$$\boldsymbol{\omega}_{s_2} = \dot{\boldsymbol{\theta}}_{s_2} = \frac{real(\boldsymbol{V}_{K_2} - \boldsymbol{V}_{A_2})}{-\overline{A_2K_2}\, \sin(\boldsymbol{\theta}_{s_2})} \quad \text{(A.54)}$$

Similarly, the linear acceleration of the knee joint of the swing leg will be recorded in Eq. (A.55) as:

$$\begin{aligned} \boldsymbol{A}_{K_2} = \boldsymbol{A}_{A_2} &+ \overline{A_2K_2}\, \boldsymbol{\omega}_{s_2}{}^2 \left(\cos(\boldsymbol{\theta}_{s_2}) - \sin(\boldsymbol{\theta}_{s_2}).\hat{\boldsymbol{j}}\right) \\ &+ \overline{A_2K_2}\, \boldsymbol{\alpha}_{s_2}\left(-\sin(\boldsymbol{\theta}_{s_2}) - \cos(\boldsymbol{\theta}_{s_2}).\hat{\boldsymbol{j}}\right) \end{aligned} \quad \text{(A.55)}$$

Therefore,

$$\boldsymbol{\alpha}_{s_2} = \ddot{\boldsymbol{\theta}}_{s_2} = \frac{real\left(\boldsymbol{A}_{K_2} - \boldsymbol{A}_{A_2}\right) - \overline{A_2K_2}\ \boldsymbol{\omega}_{s_2}{}^2\left(\cos\left(\boldsymbol{\theta}_{s_2}\right)\right)}{-\overline{A_2K_2}\ \sin\left(\boldsymbol{\theta}_{s_2}\right)} \tag{A.56}$$

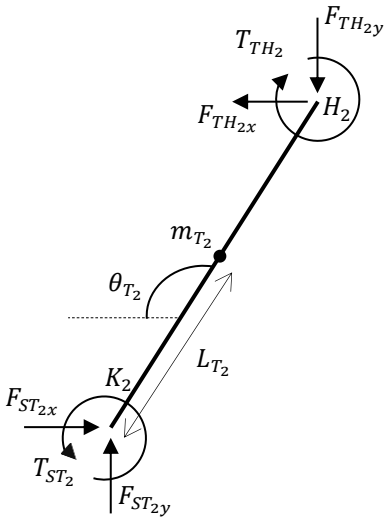

Figure A.5: Free body diagram of the thigh segment of the swing leg

For the thigh part of the swing leg, Eq. (A.57) represents the linear velocity of the knee joint of the swing leg in terms of hip velocity and angular displacement of the thigh segment.

$$\boldsymbol{V}_{K_2} = \boldsymbol{V}_{H_2} + \overline{H_2K_2}\ \boldsymbol{\omega}_{T_2}\left(\sin\left(\boldsymbol{\theta}_{T_2}\right) + \cos\left(\boldsymbol{\theta}_{T_2}\right).\hat{\boldsymbol{j}}\right) \tag{A.57}$$

$$\boldsymbol{\omega}_{T_2} = \dot{\boldsymbol{\theta}}_{T_2} = \frac{real\left(\boldsymbol{V}_{K_2} - \boldsymbol{V}_{H_2}\right)}{\overline{H_2K_2}\ \sin\left(\boldsymbol{\theta}_{T_2}\right)} \tag{A.58}$$

Similarly, the acceleration of the knee joint can be represented as:

$$\begin{aligned}\boldsymbol{A}_{K_2} = \boldsymbol{A}_{H_2} &+ \overline{H_2K_2}\ \boldsymbol{\omega}_{T_2}{}^2\left(-\cos\left(\boldsymbol{\theta}_{T_2}\right) + \sin\left(\boldsymbol{\theta}_{T_2}\right).\hat{\boldsymbol{j}}\right) \\ &+ \overline{H_2K_2}\ \boldsymbol{\alpha}_{T_2}\left(\sin\left(\boldsymbol{\theta}_{T_2}\right) + \cos\left(\boldsymbol{\theta}_{T_2}\right).\hat{\boldsymbol{j}}\right)\end{aligned} \tag{A.59}$$

$$\boldsymbol{\alpha}_{T_2} = \ddot{\boldsymbol{\theta}}_{T_2} = \frac{real\left(\boldsymbol{A}_{K_2} - \boldsymbol{A}_{H_2}\right) + \overline{H_2K_2}\ \boldsymbol{\omega}_{T_2}{}^2\left(\cos\left(\boldsymbol{\theta}_{T_2}\right)\right)}{\overline{H_2K_2}\ \sin\left(\boldsymbol{\theta}_{T_2}\right)} \tag{A.60}$$

Figure A.6 shows the free body diagram of the hip part that will be used to develop the equations of motion for the hip segment.

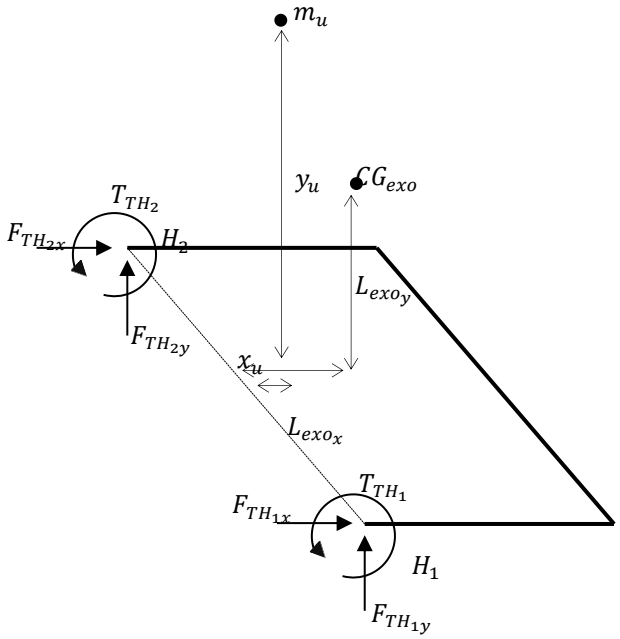

Figure A.6: Free body diagram of the hip part of the exoskeleton

Let CG_{exo} represents the location of the mass of the hip as well as the mass of the upper parts of the exoskeleton. m_U is the mass of the upper body of the user and G represents the centre of mass of the whole system. Therefore, x_G and y_G can be calculated using Eq. (A.61) and Eq. (A.62) respectively.

$$x_G = \frac{m_H L_{exo_x} + m_{HC_1} L_{HC_1} + m_{HC_2} L_{HC_2} + m_U x_U}{m_H + m_{HC_1} + m_{HC_2} + m_U} \tag{A.61}$$

$$y_G = \frac{-m_H L_{exo_y} - m_{HC_1}.0 - m_{HC_2}.0 + m_U y_U}{m_H + m_{HC_1} + m_{HC_2} + m_U} \tag{A.62}$$

The investigation of the location of COG of upper extremity (x_U, y_U) will be based on the segmentation method that states that the sum of the moments of the individual segment will be equal to the moment of the total body mass [222]. The mass and location of the COG of the upper extremity that does not include the thigh, shank and foot segment can be calculated as follows. Let m_{HN} be the mass of the head and neck, m_{Tr} be the mass of the trunk, m_{UA} be the mass of the upper arm, m_{FA} be the mass of the forearm and m_{Ha} be the mass of the hand. The total mass of the upper extremity m_u can therefore be represented as:

$$m_u = m_{HN} + m_{Tr} + 2.(m_{UA} + m_{FA} + m_{Ha}) \tag{A.63}$$

In order to calculate the location of the COG of the upper extremity (x_U, y_U), Eq. (A.64) and Eq. (A.65) will be used.

$$x_U = \frac{m_{HN}.L_{HN_x} + m_{Tr}.L_{Tr_x} + 2.(m_{UA}.L_{UA_x} + m_{FA}.L_{FA_x} + m_{Ha}.L_{Ha_x})}{m_{HN} + m_{Tr} + 2.(m_{UA} + m_{FA} + m_{Ha})} \quad \text{(A.64)}$$

$$y_U = \frac{m_{HN}.L_{HN_y} + m_{Tr}.L_{Tr_y} + 2.(m_{UA}.L_{UA_y} + m_{FA}.L_{FA_y} + m_{Ha}.L_{Ha_y})}{m_{HN} + m_{Tr} + 2.(m_{UA} + m_{FA} + m_{Ha})} \quad \text{(A.65)}$$

Where L_{HN_x} , L_{Tr_x} , L_{UA_x} , L_{FA_x} and L_{Ha_x} represents the x-component of the distance of the COG of head, trunk, upper arm, forearm and hand respectively and L_{HN_y} , L_{Tr_y} , L_{UA_y} , L_{FA_y} and L_{Ha_y} represents the y-component of the distance of the COG of head, trunk, upper arm, forearm and hand respectively from the ground in an upright position. These variables will be obtained from Table A.1.

Few more variables will be defined for the hip part because during the state of motion, the hip segment may be tilted towards a certain angle. Figure A.7 shows the free body diagram in a tilted position from a side view.

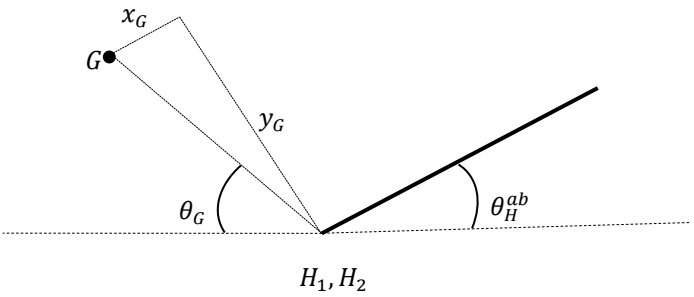

Figure A.7: Side View of the hip part

The absolute angle $\boldsymbol{\theta}_H^{ab}$ of the hip segment can be written as:

$$\boldsymbol{\theta}_H^{ab} = \boldsymbol{\theta}_A - \boldsymbol{\theta}_K + \boldsymbol{\theta}_H \quad \text{(A.66)}$$

Differentiating Eq. (A.66) results in Eq. (A.67)

$$\dot{\boldsymbol{\theta}}_H^{ab} = \dot{\boldsymbol{\theta}}_A - \dot{\boldsymbol{\theta}}_K + \dot{\boldsymbol{\theta}}_H \quad \text{(A.67)}$$

Similarly,

$$\ddot{\boldsymbol{\theta}}_H^{ab} = \ddot{\boldsymbol{\theta}}_A - \ddot{\boldsymbol{\theta}}_K + \ddot{\boldsymbol{\theta}}_H \quad \text{(A.68)}$$

From Figure A.6, $\boldsymbol{\theta}_G$ can be calculated as:

$$\boldsymbol{\theta}_G = \frac{\pi}{2} - \boldsymbol{\theta}_H^{ab} - \tan^{-1}\frac{x_G}{y_G} \quad \text{(A.69)}$$

The acceleration of point G can be given as:

$$\boldsymbol{A}_G = \boldsymbol{A}_{H_1} + L_G\,\dot{\boldsymbol{\theta}}_H^{ab\,2}\,(\cos(\boldsymbol{\theta}_G) - \sin(\boldsymbol{\theta}_G)\,.\hat{\boldsymbol{j}}) + L_G\,\ddot{\boldsymbol{\theta}}_H^{ab\,2}\,(-\sin(\boldsymbol{\theta}_G) - \cos(\boldsymbol{\theta}_G)\,.\hat{\boldsymbol{j}}) \tag{A.70}$$

where

$$L_G = \sqrt{x_G^2 + y_G^2} \tag{A.71}$$

The free body diagram of the foot of the swing leg is given in Figure A.8.

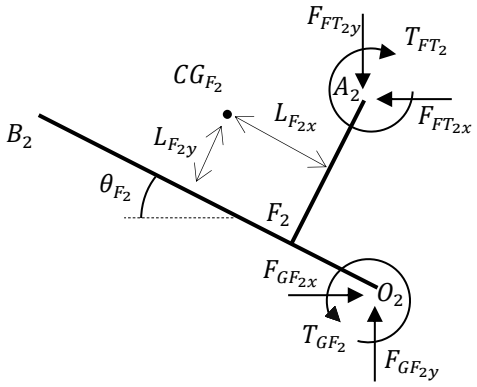

Figure A.8: Free body diagram of the swing foot

The velocity of point F_2 can be given by:

$$\boldsymbol{V}_{F_2} = \boldsymbol{V}_{H_2} + \overline{H_2F_2}\;\boldsymbol{\omega}_{F_2}(-\sin(\boldsymbol{\theta}_{F_2}) - \cos(\boldsymbol{\theta}_{F_2})\,.\hat{\boldsymbol{j}}) \tag{A.72}$$

Similarly, the velocity of the ankle in terms of the velocity of point F can be represented as:

$$\boldsymbol{V}_{A_2} = \boldsymbol{V}_{F_2} + \overline{F_2A_2}\;\boldsymbol{\omega}_{F_2}(-\cos(\boldsymbol{\theta}_{F_2}) + \sin(\boldsymbol{\theta}_{F_2})\,.\hat{\boldsymbol{j}}) \tag{A.73}$$

The linear acceleration of ankle $\boldsymbol{A}_{F_2}$ and point F can be given as in Eq. (A.74) and Eq. (A.75) respectively.

$$\boldsymbol{A}_{F_2} = \boldsymbol{A}_{H_2} + \overline{H_2F_2}\;\boldsymbol{\omega}_{F_2}{}^2\,(\cos(\boldsymbol{\theta}_{F_2}) - \sin(\boldsymbol{\theta}_{F_2})\,.\hat{\boldsymbol{j}}) + \overline{H_2F_2}\;\boldsymbol{\alpha}_{F_2}(-\sin(\boldsymbol{\theta}_{F_2}) - \cos(\boldsymbol{\theta}_{F_2})\,.\hat{\boldsymbol{j}}) \tag{A.74}$$

$$\boldsymbol{A}_{A_2} = \boldsymbol{A}_{F_2} + \overline{F_2A_2}\;\boldsymbol{\omega}_{F_2}{}^2\,(-\sin(\boldsymbol{\theta}_{F_2}) - \cos(\boldsymbol{\theta}_{F_2})\,.\hat{\boldsymbol{j}}) + \overline{F_2A_2}\;\boldsymbol{\alpha}_{F_2}(-\cos(\boldsymbol{\theta}_{F_2}) + \sin(\boldsymbol{\theta}_{F_2})\,.\hat{\boldsymbol{j}}) \tag{A.75}$$

The acceleration of the foot segment can be given as:

$$\boldsymbol{A}_{F_{t2}} = \boldsymbol{A}_{F_2} + L_{F_{2x}}\,\boldsymbol{\omega}_{F_2}{}^2\,(\cos(\boldsymbol{\theta}_{F_2}) - \sin(\boldsymbol{\theta}_{F_2})\,.\hat{\boldsymbol{j}}) + L_{F_{2y}}\,\boldsymbol{\omega}_{F_2}{}^2(-\sin(\boldsymbol{\theta}_{F_2}) - \cos(\boldsymbol{\theta}_{F_2})\,.\hat{\boldsymbol{j}}) + L_{F_{2x}}\,\boldsymbol{\alpha}_{F_2}\,(-\sin(\boldsymbol{\theta}_{F_2}) - \cos(\boldsymbol{\theta}_{F_2})\,.\hat{\boldsymbol{j}}) + L_{F_{2y}}\,\boldsymbol{\alpha}_{F_2}(-\cos(\boldsymbol{\theta}_{F_2}) + \sin(\boldsymbol{\theta}_{F_2})\,.\hat{\boldsymbol{j}}) \tag{A.76}$$

A.1.2 Kinetic Analysis

The forces and torques acting on the different segments of the exoskeleton are defined as follows, let $\boldsymbol{F}_{TH_{1x}}$ and $\boldsymbol{F}_{TH_{1y}}$ be the horizontal and vertical component of the force applied to the hip part by the thigh segment, $\boldsymbol{F}_{ST_{1x}}$and $\boldsymbol{F}_{ST_{1x}}$ be the horizontal and vertical segment of the forces applied to the thigh by the shank segment, $\boldsymbol{F}_{FS_{1x}}$and $\boldsymbol{F}_{FS_{1x}}$ be the horizontal and vertical component of the forces applied to the shank by the foot and $\boldsymbol{F}_{GF_{1x}}$ and $\boldsymbol{F}_{GF_{1x}}$ be the horizontal and vertical segment of the forces applied to the foot part by the ground. The joint torque are represented by $\boldsymbol{T}_{TH}$, $\boldsymbol{T}_{ST}$, $\boldsymbol{T}_{FS_1}$ and $\boldsymbol{T}_{GF_1}$ for the hip, knee, ankle and foot segment. These were represented for the case of stance leg. For the swing leg, a similar nomenclature was adopted except that the subscript 1 is replaced by 2.

Applying Newton's second law to the thigh segment of the stance leg.

$$\sum \boldsymbol{F}_x = \left(m_{T\_U_1} + m_{T\_w_1} + \sum_n m_{KC_1}(n) \right). \boldsymbol{A}_{T_1} \tag{A.77}$$

As,

$$m_{T_1} = m_{T\_U_1} + m_{T\_w_1} + \sum_n m_{KC_1}(n)$$

Therefore,

$$\boldsymbol{F}_{ST_{1x}} - \boldsymbol{F}_{TH_{1x}} = \left(m_{T_1}\right). \boldsymbol{A}_{T_1} \tag{A.78}$$

Similarly, applying along the y-direction

$$\sum \boldsymbol{F}_y = \left(m_{T\_U_1} + m_{T\_w_1} + \sum_n m_{KC_1}(n) \right). \left(\boldsymbol{A}_{T_1} + \boldsymbol{g}\right) \tag{A.79}$$

$$\boldsymbol{F}_{ST_{1y}} - \boldsymbol{F}_{TH_{1y}} = \left(m_{T_1}\right). \left(\boldsymbol{A}_{T_1} + \boldsymbol{g}\right) \tag{A.80}$$

The torque applied at the thigh segment is calculated as:

$$\sum \boldsymbol{T}_{T_1} = \boldsymbol{I}_{T_1}\, \boldsymbol{\alpha}_{T_1} \tag{A.81}$$

$$\begin{aligned} \boldsymbol{T}_{ST_1} + \boldsymbol{F}_{ST_{1x}}. L_{T_1} \cos\left(\boldsymbol{\theta}_{H_1}\right) - \boldsymbol{F}_{ST_{1y}}. L_{T_1} \sin\left(\boldsymbol{\theta}_{H_1}\right) - \boldsymbol{T}_{TH_1} \\ + \boldsymbol{F}_{TH_{1x}}. \left(L_{TF_1} - L_{T_1}\right) \cos\left(\boldsymbol{\theta}_{H_1}\right) \\ - \boldsymbol{F}_{TH_{1y}} \left(L_{TF_1} - L_{T_1}\right) \sin\left(\boldsymbol{\theta}_{H_1}\right) = \boldsymbol{I}_{T_1}\, \boldsymbol{\alpha}_{T_1} \end{aligned} \tag{A.82}$$

Where

$$\begin{aligned} \boldsymbol{I}_{T_1} = \boldsymbol{I}^0_{T_1} + \left(L_{T\_U_1} - L_{T_1}\right)^2. m_{T\_U_1} + \left(L_{T\_w_1} - L_{T_1}\right)^2. m_{T\_w_1} \\ + \sum_n \left(L_{KC_1}(n) - L_{T_1}\right)^2. m_{KC}(n) \end{aligned} \tag{A.83}$$

The $\boldsymbol{I}_{T_1}^0$ in Eq. (A.83) represents the moment of inertia of the thigh segment without the added mass of the user and the joint actuators.

For the case of shank segment during the stance phase,

$$\sum \boldsymbol{F}_x = \left(m_{s\_u_1} + m_{s\_w_1} + \sum_n m_{AC_1}(n) \right). \boldsymbol{A}_{S_1} \tag{A.84}$$

As,

$$m_{s_1} = m_{s\_u_1} + m_{s\_w_1} + \sum_n m_{AC_1}(n)$$

Therefore,

$$\boldsymbol{F}_{FS_{1x}} - \boldsymbol{F}_{ST_{1x}} = \left(m_{s_1}\right). \boldsymbol{A}_{S_1} \tag{A.85}$$

Similarly, Eq. (A.86) yields by applying along the vertical direction,

$$\sum \boldsymbol{F}_y = \left(m_{s\_u_1} + m_{s\_w_1} + \sum_n m_{AC_1}(n) \right). \left(\boldsymbol{A}_{S_1} + \boldsymbol{g}\right) \tag{A.86}$$

$$\boldsymbol{F}_{FS_{1y}} - \boldsymbol{F}_{ST_{1y}} = \left(m_{s_1}\right). \left(\boldsymbol{A}_{S_1} + \boldsymbol{g}\right) \tag{A.87}$$

Similarly, for the case of rotation,

$$\sum \boldsymbol{T}_{s_1} = \boldsymbol{I}_{s_1}\, \boldsymbol{\alpha}_{s_1} \tag{A.88}$$

where

$$\begin{aligned} \boldsymbol{I}_{s_1} = \boldsymbol{I}_{s_1}^0 + \left(L_{s\_u_1} - L_{s_1}\right)^2 . m_{s\_u_1} + \left(L_{s\_w_1} - L_{s_1}\right)^2 . m_{s\_w_1} \\ + \sum_n \left(L_{AC_1}(n) - L_{s_1}\right)^2 . m_{AC_1}(n) \end{aligned} \tag{A.89}$$

In Eq. (A.89), $\boldsymbol{I}_{s_1}^0$ represents the moment of inertia of the shank segment without the added mass of the user and the joint actuators.

$$\begin{aligned} \boldsymbol{T}_{FS_1} + \boldsymbol{F}_{s_{1x}} . L_{s_1} \sin\left(\theta_{s_1}\right) - \boldsymbol{F}_{s_{1y}} . L_{s_1} \cos\left(\boldsymbol{\theta}_{s_1}\right) - \boldsymbol{T}_{ST_1} \\ + \boldsymbol{F}_{ST_{1x}} . \left(L_{SK_1} - L_{s_1}\right) \sin\left(\boldsymbol{\theta}_{s_1}\right) \\ - \boldsymbol{F}_{ST_{1y}} \left(L_{SK_1} - L_{s_1}\right) \cos\left(\boldsymbol{\theta}_{s_1}\right) = \boldsymbol{I}_{s_1}\, \boldsymbol{\alpha}_{s_1} \end{aligned} \tag{A.90}$$

The aforementioned equations apply to the stance leg. For the swing leg, similar relations were formulated with only the difference of the subscript 1 which was replaced by subscript 2.

The foot of the swing leg will now be considered and Figure A.8 shows the free body diagram of the foot of the swing leg. The kinetic relations of the foot part will be as follows:

Applying Newton's law along x-direction

$$\sum (\boldsymbol{F}_x)_{Foot} = m_{F_1}\, \boldsymbol{A}_{Ft_x} \tag{A.91}$$

where

$$m_{F_1} = m_{F_E} + m_{F_U} \tag{A.92}$$

In Eq. (A.92), m_{F_E} represents mass of the foot segment of the exoskeleton and m_{F_U} represents mass of the foot of the user.

$$\boldsymbol{F}_{GF_{2x}} - \boldsymbol{F}_{SF_{2x}} = m_{F_1}\, \boldsymbol{A}_{Ft_x} \tag{A.93}$$

Along y-direction

$$\sum \left(\boldsymbol{F}_y\right)_{Foot} = m_{F_1}\, \boldsymbol{A}_{Ft_y} \tag{A.94}$$

$$\boldsymbol{F}_{GF_{2y}} - \boldsymbol{F}_{SF_{2y}} = m_{F_1}\, \boldsymbol{A}_{Ft_y} \tag{A.95}$$

The torque acting on the foot segment will be calculated as follows:

$$\sum \boldsymbol{T}_{Ft_2} = \boldsymbol{I}_{Ft_2}\, \ddot{\boldsymbol{\theta}}_{f_2} \tag{A.96}$$

$$\begin{aligned} \boldsymbol{T}_{GF_2} - \boldsymbol{T}_{FS_2} &+ \boldsymbol{F}_{FS_{2x}}.\left(\overline{F_2A_2} - LF_{2_y} - LF_{2_x}.\tan\boldsymbol{\theta}_{f_2}\right) \\ &+ \boldsymbol{F}_{FS_{2y}}.\left(\overline{F_2A_2} + \frac{LF_{2_x}}{\cos\theta_{F_2}} - LF_{2_x} - LF_{2_x}.\tan\boldsymbol{\theta}_{f_2}\right) \\ &+ \boldsymbol{F}_{GF_{2x}}.\left(\overline{F_2H_2} + LF_{2_x} - LF_{2_y}.\tan\boldsymbol{\theta}_{f_2}\right).\sin\boldsymbol{\theta}_{f_2} \\ &+ \frac{LF_{2_y}}{\cos\boldsymbol{\theta}_{f_2}} \\ &- \boldsymbol{F}_{GF_{2y}}.\left(\overline{F_2H_2} + LF_{2_x} - LF_{2_y}.\tan\boldsymbol{\theta}_{f_2}\right).\cos\boldsymbol{\theta}_{f_2} \\ &= \boldsymbol{I}_{Ft_2}\, \ddot{\boldsymbol{\theta}}_{f_2} \end{aligned} \tag{A.97}$$

It should be noted that the ground reaction forces are zero as the foot of the swing leg is not in contact with the ground.

The hip segment will be discussed next. The free body diagram of the hip segment is shown in Figure A.6. The forces and torques acting at the hip segment will be calculated as follows:

$$\sum (\boldsymbol{F}_x)_{hip} = \left(m_h + \sum_n m_{HC_1}(n) + \sum_n m_{HC_2}(n)\right).\boldsymbol{A}_G \tag{A.98}$$

$$\boldsymbol{F}_{TH_{1x}} - \boldsymbol{F}_{TH_{2x}} = \left(m_h + \sum_n m_{HC_1}(n) + \sum_n m_{HC_2}(n)\right).\boldsymbol{A}_G \tag{A.99}$$

Similarly, along the y-direction

$$\sum \left(\boldsymbol{F}_y\right)_{hip} = \left(m_h + \sum_n m_{HC_1}(n) + \sum_n m_{HC_2}(n)\right).(\boldsymbol{A}_G + \boldsymbol{g}) \tag{A.100}$$

$$\boldsymbol{F}_{TH_{1y}} - \boldsymbol{F}_{TH_{2y}} = \left(m_h + \sum_n m_{HC_1}(n) + \sum_n m_{HC_2}(n) \right). (\boldsymbol{A}_G + \boldsymbol{g}) \quad \text{(A.101)}$$

The torque applied at the hip joint will be determined as:

$$\sum \boldsymbol{T}_H = \boldsymbol{I}_G \, \ddot{\boldsymbol{\theta}}_H^{abs} \quad \text{(A.102)}$$

$$\begin{aligned} \left(-\boldsymbol{F}_{TH_{1y}} - \boldsymbol{F}_{TH_{2y}}\right) L_G \cos(\boldsymbol{\theta}_G) + \left(\boldsymbol{F}_{TH_{1x}} + \boldsymbol{F}_{TH_{2x}}\right) L_G \sin(\boldsymbol{\theta}_G) \\ + \boldsymbol{T}_{TH_1} + \boldsymbol{T}_{TH_2} = \boldsymbol{I}_G \, \ddot{\boldsymbol{\theta}}_H^{abs} \end{aligned} \quad \text{(A.103)}$$

Where,

$$\begin{aligned} \boldsymbol{I}_G = \boldsymbol{I}_{exo} + \left(L_{exo_x} - x_G\right)^2 . m_H + \left(L_{exo_y} - y_G\right)^2 . m_H \\ + \left(\left(L_{HC_1} + x_G\right)^2 + {y_G}^2\right) . m_{HC_1} \\ + \left(\left(L_{HC_2} + x_G\right)^2 + {y_G}^2\right) . m_{HC_2} \end{aligned} \quad \text{(A.104)}$$

In Eq. (A.104), $\boldsymbol{I}_{exo}$ is the moment of inertia of the upper part of the exoskeleton.

The above kinetic relations will be arranged in the matrix form as given by Eq. (A.105)

$$\boldsymbol{P}_n \boldsymbol{X}_n = \boldsymbol{Q}_n \quad \text{(A.105)}$$

Where $\boldsymbol{P}_n$ represents the coefficients matrix, $\boldsymbol{X}_n$ contains the unknown variables and $\boldsymbol{Q}_n$ records the input known variables. Therefore, Eq. (105) can be written as:

$$\boldsymbol{X}_n = \boldsymbol{P}_n^{-1} \boldsymbol{Q}_n \quad \text{(A.106)}$$

Eq. (106) will be used to solve for the unknown variables given the known input variables at each point of the trajectory.

A.2 Double limb phase

This phase starts with the heel strike of the swing leg and ends with the toe off of the other leg. Therefore, this phase can be divided into two further sub phases. The stage comprise of the heel strike to foot flat phase and from foot flat to toe off of the opposite leg.

During the first phase i.e. from heel strike to the foot flat phase, the heel of the foot (point H_2) will act as a pin joint and therefore torque $\boldsymbol{T}_{GF}$ at this point will be zero. The two components of the ground reaction forces will be unknown. To solve for these two unknowns, Eq. (A.107) to Eq. (A.108) will be considered.

$$\boldsymbol{F}_{TH_{1x}} = \boldsymbol{F}_{TH_{2x}} \tag{A.107}$$

$$\boldsymbol{F}_{TH_{1y}} = \boldsymbol{F}_{TH_{2y}} \tag{A.108}$$

During this phase, it is reasonable to consider the above equations as long as the sum of the two components will be equal to the previous calculated component elaborated in Eq. (A.92) and Eq. (A.94). During the double limb support phase, the two force components will not be equal but opposite that cancel out each other. It is approximated that the actuation force is equally divided between the two limbs and therefore, instead of one actuator limb pushing excessively during this phase, both actuators will contribute equally to push the hip forward. Therefore, using Eq. (A.107) and Eq. (108), the extra two unknowns during this phase can be calculated.

During the next sub-phase i.e. from foot flat to toe off of the opposite leg, there will be three unknowns, apart from the two unknown forces given in Eq. (107) and Eq. (108), there will be an unknown ground reaction torque $\boldsymbol{T}_{GF}$ as well. This can also be solved by considering Eq. (A.109) and assuming a similar approach as explained in the aforementioned sub phase.

$$\boldsymbol{T}_{TH_1} = \boldsymbol{T}_{TH_1} \tag{A.109}$$

A.3 Sit-to-Stand Manoeuvre

The kinematic and kinetic relations during this phase could be solved considering the formulations explained for the stance leg during single limb phase. As sit to stand manoeuvre can be considered to be of symmetry nature, therefore it could be solved considering only one leg. The mass of the hip part and the upper body mass of the user will also be considered half when solving for the kinetic formulation during this phase.

Appendix B
Electric Motors Market Search

Table B.1: Electric Motors Market Search List for an Assistive Robotic Exoskeleton Actuation System

Manufacturer	Model no.	Rated Power (W)	Rated Torque (Nm)	Weight (kg)	Torque Constant (Nm/A)
Moog	BN12-13AF-03	18	0.099	0.102	0.0208
Moog	BN12-13EU-03	18	0.099	0.102	0.0209
Moog	BN12-13IP-03	18	0.099	0.102	0.0208
Pittman Ametek	DCO54B-1	19	0.390	0.590	0.134
Pittman Ametek	DC030C-2	20	0.220	0.170	0.0624
Moons	R36BLB20L2	20	0.191	0.200	0.058
Nanotec	DB28L01	21	0.150	0.195	0.0356
Portescap	25GST2R82-216E	23	0.0300	0.111	0.042
Moog	BS12HS-13AF-02	24	0.035	0.142	0.009
Maxon	RE-40	25	0.818	0.480	0.17
Allied motion	CL66-13606	25	0.477	0.900	0.106
Nanotec	DS16L024240-A	25	0.030	0.065	0.0075
Pittman Ametek	DC030C-3	26	0.360	0.210	0.0752
Pittman Ametek	EC033A-2	26	0.160	0.180	0.0622
Cannon	FN38L	26	0.373	0.300	0.0402
Pittman Ametek	DCO54B-2	28	0.670	0.740	0.139
Maxon	DCX-max-26S	29	0.277	0.120	0.0522
Cannon	EN42	29	0.383	0.360	0.0339
Nanotec	DS28L024080-A	29	0.105	0.220	0.026
Buhler Motor	1.13.044.002	30	0.280	0.585	0.05
Moons	R42BLD30L3	30	0.240	0.340	0.048
Moog	BN12-18AF-03	32	0.275	0.156	0.0257
Nanotec	DBL36L024045-A	33	0.210	0.250	0.0368
Pittman Ametek	EC033A-3	34	0.190	0.240	0.0746
KOLLMORGEN	T-3912	35	1.63	0.86	3.905
Portescap	35NT2R32-416SP	35	0.0766	0.310	0.0516
Moog	C23-L33-50	35	0.883	0.765	0.1112
Portescap	16ECP52-8B-112	38	0.0296	0.062	0.0184
Pittman Ametek	DCO54B-3	38	1.000	0.880	0.165
Printed Motors Works	GPM9LR	39	1	0.7	0.0105
Moog	BS17-15AA-03	39	0.763	0.198	0.097
Moog	BSS09-28AB-02	40	0.230	0.119	0.021

Table B.1: Electric Motors Market Search List (Cont.)

Manufacturer	Model no.	Rated Power (W)	Rated Torque (Nm)	Weight (kg)	Torque Constant (Nm/A)
Moog	BN12-23AF-03	40	0.431	0.207	0.0283
Maxon	EC-max-30	40	0.157	0.195	0.0486
Moog	C23-L33-40	40	0.883	0.765	0.0724
Nanotec	DBL42L024032-A	40	0.360	0.350	0.054
Printed Motors Works	GPM9	41	1.3	0.7	0.022
Printed Motors GmbH	DC-Pancake Servomotor U 09 FS	41	1.2	0.54	0.023
Pittman Ametek	ES040A-1	41	0.260	0.400	0.0993
Printed Motors GmbH	DC-Servomotor KN 06 M4	43	1.44	0.6	0.03
Moons	65BLB43L2	43	0.318	0.520	0.04
Moog	BN12-28AF-03	44	0.508	0.261	0.0335
Moog	BN12-28IP-03	44	0.508	0.261	0.0335
Allied motion	HT01501-A00	44	0.415	0.120	0.05
Parker Hannifin	K032100-7Y	49	0.440	0.120	0.0458
Aerotech	BM22	50	0.480	0.400	0.032
Maxon	ECX-SPEED-16M	50	0.115	0.005	0.0081
Maxon	EC-i-30	50	0.909	0.240	0.0446
Pittman Ametek	ES040A-2	53	0.310	0.450	0.0964
Nanotec	DB43M024030-A	53	0.510	0.600	0.055
Maxon	ECX-SPEED-13L	54	0.151	0.034	0.0073
Moog	C23-L40-40	54	1.765	1.077	0.1306
Moog	C23-L40-40	54	1.765	1.077	0.1306
Portescap	22ECT48-10B-35	54	0.0648	0.098	0.0281
Parker Hannifin	K064050-8Y	58	1.860	0.290	0.1329
Parker Hannifin	K032050-7Y	59	0.260	0.070	0.0232
Maxon	RE-30	60	1.050	0.260	0.0538
Moons	57BLD60L4	60	0.435	0.640	0.09
Parker Hannifin	K044100-7Y	61	1.160	0.220	0.0921
Allied motion	HT02001-A00	63	1.130	0.220	0.089
Printed Motors Works	GPM12LR	64	2	0.8	0.022
Nanotec	DF45L024048	65	0.390	0.150	0.0369
Maxon	EC-frameless-45-flat	70	0.915	0.092	0.131
Buhler Motor	1.13.044.236	70	0.640	0.765	0.057
Allied motion	INB-15 (EN2400-509A100-1)	70	0.523	0.340	0.0237
Maxon	ECX-SPEED-19M	71	0.183	0.078	0.0078
Allied motion	HT01505-A00	71	1.300	0.370	0.081

Table B.1: Electric Motors Market Search List (Cont.)

Manufacturer	Model no.	Rated Power (W)	Rated Torque (Nm)	Weight (kg)	Torque Constant (Nm/A)
Pittman Ametek	ES040A-3	71	0.410	0.510	0.0993
Maxon	DCX 26L(Graphite)	74	0.750	0.170	0.0524
Printed Motors Works	GPN9LR	75	2.5	0.65	0.024
Allied motion	IM-21 (E2600)	77	0.671	0.737	0.0667
Parker Hannifin	K178100-8Y	77	48.000	3.710	1.5894
Maxon	EC32	80	0.353	0.270	0.04
Portescap	22ECP45-8B-82	80	0.0487	0.100	0.0146
Allied motion	HT02301-A00	81	1.470	0.330	0.2
Portescap	30GT2R82-234E	82	0.0920	0.310	0.0387
Allied motion	HT02003-A00	82	2.540	0.430	0.128
Parker Hannifin	K089050-7Y	82	4.660	0.500	0.2188
Printed Motors GmbH	DC-Pancake Servomotor U06FNC 24V80W	85	0.95	0.6	0.033
Moog	BN17-15AA-03	89	0.148	0.198	0.02
Moog	BN17-15IP-03	89	0.148	0.198	0.02
Maxon	RE-35	90	0.983	0.340	0.0622
Moons	42BLC90L4	90	0.645	0.830	0.089
Moog	BS17-15AA-03	91	2.344	0.454	0.071
Printed Motors Works	GPN9	94	3	0.65	0.048
Printed Motors GmbH	platinum U9DT-A	94	2.909	1.7	0.044
Printed Motors GmbH	DC-Pancake Servomotor U 09 FN	94	2	0.54	0.048
Aerotech	BMS35	96	1.07	0.6	0.15
Moog	BN17-20AA-03	97	0.318	0.291	0.031
Maxon	30	100	1.500	0.210	0.0261
Maxon	EC-60-flat	100	5.010	0.470	0.114
Maxon	EC-frameless-60-flat	100	5.010	0.333	0.114
Maxon	ECX-SPEED-16L	107	0.396	0.073	0.0071
Portescap	35NT2R82-426E	107	0.1774	0.310	0.099
Maxon	ECX-SPEED-16L (STERLIZER)	108	0.389	0.073	0.007
Printed Motors GmbH	platinum U9D-A	109	3.199	1.7	0.048
Printed Motors Works	GPM12	110	3	0.8	0.051
Printed Motors GmbH	U 12 FS	110	3	1.2	0.051
Maxon	DCX-32L	110	1.420	0.325	0.0975

Table B.1: Electric Motors Market Search List (Cont.)

Manufacturer	Model no.	Rated Power (W)	Rated Torque (Nm)	Weight (kg)	Torque Constant (Nm/A)
Moog	BS12-20AB-03	110	0.250	0.151	0.01
Moog	BS12-20ZAB-03	110	0.250	0.125	0.01
Aerotech	BMS60	112	1.31	1.1	0.2
KOLLMORGEN	TBM(S)-6013-A	114	1.653	0.221	0.087
Printed Motors GmbH	DC-Servomotor KN 09 M4 LR T	115	3.7	1.6	0.0266
Moog	BSG23-28AA-03	117	6.400	1.417	0.165
KOLLMORGEN	T-5403	120	1.76	0.54	0.5965
KOLLMORGEN	T-4412	120	2.030	0.680	1.0575
Moog	BMS09-23AB-03	123	0.141	0.116	0.005
Printed Motors GmbH	platinum U9DT-B	123	3.728	1.7	0.053
Moog	BSS09-23AB-03	124	0.177	0.094	0.0052
Printed Motors GmbH	DC-Servomotor KN 09 M4 LR	125	4	1.6	0.029
Printed Motors GmbH	platinum U9DT-C	128	3.863	1.7	0.055
Aerotech	1035	129	1.84	1.2	0.06
Moons	R57BLB130L3	130	0.990	1.000	0.062
Printed Motors GmbH	DC-Servomotor KN 09 M4 T	132	4.58	1.4	0.068
Printed Motors GmbH	platinum U9D-B	133	3.849	1.7	0.057
Aerotech	BMS100	133	2.26	1.5	0.38
Printed Motors GmbH	DC-Servomotor KN 09 M4	141	4.89	1.4	0.073
Printed Motors GmbH	platinum U9D-C	142	4.103	1.7	0.061
KOLLMORGEN	TBM(S)-6025-A	144	3.152	0.398	0.148
Aerotech	1050	146	2.52	1.6	0.07
Maxon	RE40(Graphite)	150	0.655	0.480	0.214
Moog	BMS09-28AB-03	154	0.194	0.142	0.0052
Printed Motors Works	GN9	154	3.673191401	1.8	0.0918
Allied motion	QB01701	158	0.590	0.150	0.036
KOLLMORGEN	TBM(S)-6051-A	159	5.790	0.571	0.193
Moog	BSG23-18AB-02	160	2.100	0.483	0.05
Printed Motors GmbH	platinum U9DT-F	160	4.802	1.7	0.069
Maxon	EC-90-flat	160	6.410	0.630	0.217
Maxon	ECX-SPEED-22L	162	1.120	0.148	0.008
Printed Motors GmbH	platinum U9DT-D	165	4.936	1.7	0.071
Printed Motors GmbH	platinum U9D-F	170	4.88	1.7	0.073
Maxon	EC40	170	2.760	0.580	0.0464
Allied motion	HT03800-A00	170	1.100	0.490	0.58

Table B.1: Electric Motors Market Search List (Cont.)

Manufacturer	Model no.	Rated Power (W)	Rated Torque (Nm)	Weight (kg)	Torque Constant (Nm/A)
Aerotech	S-50-39	171.5	0.82	0.32	0.04
Printed Motors GmbH	platinum U9D-D	179	5.134	1.7	0.076
Printed Motors GmbH	platinum U9DT-E	187	5.614	1.7	0.08
Portescap	30ECT64-10B-14	187	0.1330	0.263	0.0205
Printed Motors Works	GPN12LR	190	1.706734261	1.2	0.0474
Printed Motors GmbH	platinum U9D-E	190	5.459	1.7	0.081
Aerotech	BM75	192	1.300	1.100	0.06
Printed Motors Works	GM9H	197	3.0186774	2	0.0839
Allied motion	QB01702	199	1.680	0.220	0.044
Printed Motors Works	GPN12	200	3.578927926	1.2	0.0994
KOLLMORGEN	T-4601	200	1.09	0.369	0.325
Maxon	RE-50(Graphite)	200	4.340	1.100	0.242
Moons	70BLB200H2	200	2.160	1.600	0.26
Allied motion	MF0060020	204	3.800	0.130	0.23
Allied motion	MF0060032	210	7.500	0.420	0.17
KOLLMORGEN	QT-4602	211	1.15	0.369	0.271
KOLLMORGEN	QT-1401	217	0.388	0.125	0.0636
Printed Motors GmbH	DC-Pancake Servomotor U 12	220	6	1	0.114
Allied motion	QB01700	222	0.460	0.080	0.038
Aerotech	S-50-52	224.1	1.31	0.48	0.07
Moog	BN23HS-28HS-03	227	1.568	0.738	0.0298
Portescap	30ECT90-10B-8	244	0.2190	0.380	0.0211
HEINZMANN	SL 120-1NFB, coil: 17/56	250	40	1.8	0.16
Printed Motors GmbH	U12DT-A	250	8.319	3.1	0.106
Maxon	RE-65 (Graphite)	250	16.200	2.100	0.153
KOLLMORGEN	NT-1308	255	0.636	0.456	0.0685
KOLLMORGEN	TBM(S)-7615-A	258	3.672	0.435	0.102
KOLLMORGEN	QT-3102	263	3.390	0.910	0.6101
Allied motion	QB02301	268	5.560	0.540	0.094
Printed Motors GmbH	U12D-A	275	9.074	3.1	0.116
Printed Motors GmbH	U12DT-B	276	9.229	3.1	0.117
Aerotech	S-76-35	277.2	2.56	0.64	0.17
Allied motion	QB03400	291	4.270	0.680	0.112
Allied motion	MF0076008	292	4.000	0.200	0.26

Table B.1: Electric Motors Market Search List (Cont.)

Manufacturer	Model no.	Rated Power (W)	Rated Torque (Nm)	Weight (kg)	Torque Constant (Nm/A)
Printed Motors GmbH	U12D-B	298	9.907	3.1	0.126
Printed Motors GmbH	U12DT-C	301	10.133	3.1	0.129
KOLLMORGEN	TBM(S)-7631-A	307	6.192	0.738	0.172
Printed Motors GmbH	U12D-C	325	10.882	3.1	0.138
KOLLMORGEN	TBM(S)-7646-A	335	7.596	1.079	0.211
Printed Motors GmbH	U12DT-D	341	11.637	3.1	0.148
KOLLMORGEN	QT-1406	347	1.11	0.34	0.113
Aerotech	S-50-86	353.2	2.26	0.9	0.13
Moog	BN34-25AF-02	355	2.190	1.030	0.06
Moog	BN34-25EU-02	355	2.190	1.030	0.06
Moog	BN34-25IP-02	355	2.190	1.030	0.06
Allied motion	MF0060056	357	16.000	0.700	0.42
Printed Motors GmbH	U12D-D	362	12.315	3.1	0.157
Allied motion	QB02300	364	2.790	0.260	0.117
Printed Motors	U12DT-E	373	12.916	3.1	0.164
Printed Motors GmbH	U12D-F	380	13.664	3.1	0.174
Printed Motors GmbH	U12D-E	387	13.368	3.1	0.17
Printed Motors GmbH	U12DT-F	390	13.671	3.1	0.174
Allied motion	MF0060044	394	14.300	0.560	0.37
Moog	BN34HS-25AF-01	396	1.250	1.079	0.0137
Maxon	EC60	400	6.820	2.450	0.147
Allied motion	MF0095008	417	7.300	0.320	0.31
Allied motion	MF0076020	441	13.000	0.430	0.33
Moog	BN34-35EU-02	502	4.541	1.761	0.0701
KOLLMORGEN	KBM-10X01-C	575	1.23	0.425	0.097
KOLLMORGEN	KBM-10X02-B	785	2.48	0.703	0.307
KOLLMORGEN	KBM-10X03-D	850	3.69	0.99	0.259
KOLLMORGEN	KMB-17X01-C	855	6.35	1.16	0.355
KOLLMORGEN	KBM-10X04-D	910	4.91	1.26	0.345
KOLLMORGEN	KBM-14X01-C	915	3.59	1	0.199
KOLLMORGEN	KBM-14X02-D	975	7.31	1.68	0.374
Aerotech	S-130-39	986.9	9.42	1.87	0.44
KOLLMORGEN	KMB-17X02-D	1290	12.8	1.97	0.565

Appendix C
Characteristics of the Transmission Systems

Table C.1: List of Market Search of Harmonic Drives

Type	Rated Torque (Nm)	Moment of Inertia (*10^-6 kgm^2)	Repeatable Peak Torque (Nm)	Average Torque (Nm)	Weight (kg)
CSD-14-50-2A	4	2.1	12	4.8	0.06
CSD-14-100-2A	5	2.1	19	7.7	0.06
CPL-14-50-2A	5	2.0	18	6.9	0.06
CSG-14-50-2A	7	3.3	23	9.0	0.09
CPL-14-80-2A	8	2.0	23	11.0	0.06
CPL-14-100-2A	8	2.0	28	11.0	0.06
CSG-14-80-2A	10	3.3	30	14.0	0.09
CSG-14-100-2A	10	3.3	36	14.0	0.09
CSD-17-50-2A	11	5.4	23	18.0	0.10
CSD-17-100-2A	16	5.4	37	27.0	0.10
CPL-17-50-2A	16	4.9	34	26.0	0.10
CSD-20-50-2A	17	9.0	39	34.0	0.13
CSG-17-50-2A	21	7.9	44	34.0	0.15
SHG-17-50-2A	21	7.9	44	34.0	0.18
CPL-17-80-2A	22	4.9	43	27.0	0.10
FB-20-100-2	22	13.5	26	25.0	0.30
FB-25-50-2	23	36.0	30	30.0	0.50
CPL-17-100-2A	24	4.9	54	39.0	0.10
CPL-17-120-2A	24	4.9	54	39.0	0.10
FB-20-128-2	24	13.5	33	25.0	0.30
FB-20-160-2	24	13.5	38	25.0	0.30
CPL-20-50-2A	25	11.2	56	34.0	0.14
FR-20-50-2	25	32.0	34	34.0	0.30
CSD-25-50-2A	27	28.2	69	38.0	0.24
CSD-20-100-2A	28	9.0	57	34.0	0.13
CSD-20-160-2A	28	9.0	64	34.0	0.13
CSG-17-80-2A	29	7.9	56	35.0	0.15
SHG-17-80-2A	29	7.9	56	35.0	0.18
CSG-17-100-2A	31	7.9	70	51.0	0.15
CSG-17-120-2A	31	7.9	70	51.0	0.15
FB-25-80-2	31	36.0	39	39.0	0.50
SHG-17-100-2A	31	7.9	70	51.0	0.18
SHG-17-120-2A	31	7.9	70	51.0	0.18
CSG-20-50-2A	33	19.3	73	44.0	0.28
SHG-20-50-2A	33	19.3	73	44.0	0.31
CPL-20-80-2A	34	11.2	74	47.0	0.14
FR-20-80-2	34	32.0	41	41.0	0.30

Table C.1: List of Market Search of Harmonic Drives (Cont.)

Type	Rated Torque (Nm)	Moment of Inertia (*10^-6 kgm^2)	Repeatable Peak Torque (Nm)	Average Torque (Nm)	Weight (kg)
FB-25-100-2	39	36.0	52	52.0	0.50
FB-25-120-2	39	36.0	61	61.0	0.50
FB-25-160-2	39	36.0	76	61.0	0.50
FR-25-50-2	39	70.0	55	55.0	0.50
CPL-20-160-2A	40	11.2	92	49.0	0.14
FR-20-100-2	40	32.0	53	49.0	0.30
FR-20-128-2	40	32.0	67	49.0	0.30
FR-20-160-2	40	32.0	77	49.0	0.30
CSG-20-80-2A	44	19.3	96	61.0	0.28
SHG-20-80-2A	44	19.3	96	61.0	0.31
CSD-25-100-2A	47	28.2	110	75.0	0.24
CSD-25-160-2A	47	28.2	123	75.0	0.24
CSG-25-50-2A	51	41.3	127	72.0	0.42
SHG-25-50-2A	51	41.3	127	72.0	0.48
CSG-20-160-2A	52	19.3	120	64.0	0.28
SHG-20-120-2A	52	19.3	113	64.0	0.31
SHG-20-160-2A	52	19.3	120	64.0	0.31
FR-25-80-2	56	70.0	69	69.0	0.50
CPL-25-100-2A	67	26.3	157	108.0	0.24
CPL-25-120-2A	67	26.3	167	108.0	0.24
CPL-25-160-2A	67	26.3	176	108.0	0.24
FR-25-160-2	67	70.0	135	108.0	0.50
FR-25-200-2	67	70.0	147	108.0	0.50
CSG-25-80-2A	82	41.3	178	113.0	0.42
SHG-25-80-2A	82	41.3	178	113.0	0.48
CSG-25-100-2A	87	41.3	204	140.0	0.42
CSG-25-120-2A	87	41.3	217	140.0	0.42
CSG-25-160-2A	87	41.3	229	140.0	0.42
SHG-25-100-2A	87	41.3	204	140.0	0.48
SHG-25-120-2A	87	41.3	217	140.0	0.48
SHG-25-160-2A	87	41.3	229	140.0	0.48
CSD-32-100-2A	96	109.0	233	151.0	0.51
CSD-32-160-2A	96	109.0	261	151.0	0.51
CSG-32-50-2A	99	196.0	281	140.0	0.89
CPL-32-80-2A	118	92.4	304	167.0	0.54
CPL-32-120-2A	137	92.4	353	216.0	0.54
CPL-32-160-2A	137	92.4	372	216.0	0.54
CSG-32-80-2A	153	196.0	395	217.0	0.89
CSG-32-160-2A	178	196.0	484	281.0	0.89

Table C.2: Ballscrews for various configurations used at the hip joint

Config. number	r_p (mm)	r_d (m)	γ_d (rad)	Moment of Inertia (kg-m^2) x 10^{-4}	Weight for the max length (kg)	Weight per length (kg/m)	Max h (m)
Type: SKF SD 10x2							
1	0.081	0.079	1.850	2.880	0.057	0.617	0.069
2	0.085	0.083	2.158	2.880	0.047	0.617	0.089
3	0.088	0.087	2.158	2.880	0.049	0.617	0.097
4	0.098	0.096	1.850	2.880	0.070	0.617	0.082
5	0.099	0.100	1.850	2.880	0.071	0.617	0.088
6	0.104	0.100	2.158	2.880	0.057	0.617	0.107
Type: SKF SD 12x2							
7	0.083	0.083	1.850	2.880	0.085	0.888	0.075
8	0.084	0.087	1.850	2.880	0.087	0.888	0.081
9	0.091	0.092	2.158	2.880	0.073	0.888	0.105
10	0.093	0.096	2.158	2.880	0.075	0.888	0.113
Type: SKF SD 14x4							
31	0.081	0.079	1.850	2.880	0.112	1.208	0.069
32	0.085	0.083	2.158	2.880	0.093	1.208	0.089
33	0.088	0.087	2.158	2.880	0.096	1.208	0.097
34	0.098	0.096	1.850	2.880	0.136	1.208	0.082
35	0.099	0.100	1.850	2.880	0.140	1.208	0.088
36	0.104	0.100	2.158	2.880	0.112	1.208	0.107
Type: SKF SD 16x4							
37	0.083	0.083	1.850	2.880	0.150	1.578	0.075
38	0.084	0.087	1.850	2.880	0.155	1.578	0.081
39	0.091	0.092	2.158	2.880	0.129	1.578	0.105
40	0.093	0.096	2.158	2.880	0.133	1.578	0.113
41	0.096	0.100	2.158	2.880	0.137	1.578	0.121
Type: SKF SD 10x5							
42	0.081	0.079	1.850	2.880	0.057	0.617	0.069
43	0.085	0.083	2.158	2.880	0.047	0.617	0.089
44	0.088	0.087	2.158	2.880	0.049	0.617	0.097
45	0.098	0.096	1.850	2.880	0.070	0.617	0.082
46	0.099	0.100	1.850	2.880	0.071	0.617	0.088
47	0.104	0.100	2.158	2.880	0.057	0.617	0.107
Type: SKF SD 12x5							
48	0.083	0.083	1.850	2.880	0.085	0.888	0.075
49	0.084	0.087	1.850	2.880	0.087	0.888	0.081
50	0.091	0.092	2.158	2.880	0.073	0.888	0.105
51	0.093	0.096	2.158	2.880	0.075	0.888	0.113
52	0.096	0.100	2.158	2.880	0.077	0.888	0.121

Table C.2: Ballscrews for various configurations at the hip joint (Cont.)

Config. number	r_p (mm)	r_d (m)	γ_d (rad)	Moment of Inertia (kg-m^2) x 10^{-4}	Weight for the max length (kg)	Weight per length (kg/m)	Max h (m)
Type: SKF SD 14x5							
53	0.081	0.079	1.850	2.880	0.112	1.208	0.069
54	0.085	0.083	2.158	2.880	0.093	1.208	0.089
55	0.088	0.087	2.158	2.880	0.096	1.208	0.097
56	0.098	0.096	1.850	2.880	0.136	1.208	0.082
57	0.099	0.100	1.850	2.880	0.140	1.208	0.088
58	0.104	0.100	2.158	2.880	0.112	1.208	0.107
Type: SKF SD 16x5							
59	0.083	0.083	1.850	2.880	0.150	1.578	0.075
60	0.084	0.087	1.850	2.880	0.155	1.578	0.081
61	0.091	0.092	2.158	2.880	0.129	1.578	0.105
62	0.093	0.096	2.158	2.880	0.133	1.578	0.113
63	0.096	0.100	2.158	2.880	0.137	1.578	0.121
Type: SKF SD 10x10							
64	0.081	0.079	1.850	2.880	0.057	0.617	0.069
65	0.085	0.083	2.158	2.880	0.047	0.617	0.089
66	0.088	0.087	2.158	2.880	0.049	0.617	0.097
67	0.098	0.096	1.850	2.880	0.070	0.617	0.082
68	0.099	0.100	1.850	2.880	0.071	0.617	0.088
69	0.104	0.100	2.158	2.880	0.057	0.617	0.107
Type: SKF SD 12x10							
70	0.083	0.083	1.850	2.880	0.085	0.888	0.075
71	0.084	0.087	1.850	2.880	0.087	0.888	0.081
72	0.091	0.092	2.158	2.880	0.073	0.888	0.105
73	0.093	0.096	2.158	2.880	0.075	0.888	0.113
74	0.096	0.100	2.158	2.880	0.077	0.888	0.121

*It should be noted that some configurations that were not using in the optimization algorithm has not been shown.

*(SKF SD Diameter x Pitch size)

Table C.3: Ballscrews for various configurations used at the knee joint

Config. number	r_p (mm)	r_d (m)	γ_d (rad)	Moment of Inertia (kg-m^2) x 10^{-4}	Weight for the max length (kg)	Weight per length (kg/m)	Max h (m)
Type: SKF SD 10x2							
1	0.154	0.082	0.733	2.885	0.137	0.617	0.055
2	0.157	0.082	0.733	2.885	0.139	0.617	0.055
3	0.165	0.091	0.628	2.885	0.151	0.617	0.075
4	0.167	0.091	0.628	2.885	0.152	0.617	0.074
5	0.170	0.091	0.628	2.885	0.154	0.617	0.074
Type: SKF SD 12x2							
30	0.165	0.091	0.733	2.885	0.213	0.888	0.071
31	0.166	0.091	0.733	2.885	0.215	0.888	0.071
32	0.167	0.091	0.733	2.885	0.216	0.888	0.071
33	0.169	0.091	0.733	2.885	0.217	0.888	0.070
34	0.170	0.091	0.733	2.885	0.218	0.888	0.070
35	0.165	0.101	0.628	2.885	0.226	0.888	0.091
43	0.168	0.121	0.524	2.885	0.248	0.888	0.124
44	0.169	0.121	0.524	2.885	0.249	0.888	0.125
45	0.169	0.121	0.524	2.885	0.249	0.888	0.125
46	0.170	0.121	0.524	2.885	0.250	0.888	0.125
Type: SKF SD 14x2							
47	0.154	0.082	0.733	2.885	0.268	1.208	0.055
48	0.157	0.082	0.733	2.885	0.272	1.208	0.055
49	0.165	0.091	0.628	2.885	0.296	1.208	0.075
50	0.167	0.091	0.628	2.885	0.299	1.208	0.074
Type: SKF SD 16x2							
70	0.154	0.082	0.733	2.885	0.350	1.578	0.055
71	0.157	0.082	0.733	2.885	0.355	1.578	0.055
72	0.165	0.091	0.628	2.885	0.386	1.578	0.075
73	0.167	0.091	0.628	2.885	0.390	1.578	0.074
74	0.170	0.091	0.628	2.885	0.394	1.578	0.074
75	0.163	0.091	0.733	2.885	0.377	1.578	0.071
Type: SKF SD 16x2							
83	0.167	0.101	0.628	2.885	0.404	1.578	0.091
84	0.168	0.101	0.628	2.885	0.405	1.578	0.091
85	0.169	0.101	0.628	2.885	0.407	1.578	0.091
86	0.170	0.101	0.628	2.885	0.408	1.578	0.091
87	0.167	0.121	0.524	2.885	0.439	1.578	0.124
88	0.168	0.121	0.524	2.885	0.440	1.578	0.124
89	0.168	0.121	0.524	2.885	0.441	1.578	0.124
90	0.169	0.121	0.524	2.885	0.442	1.578	0.125
Type: SKF SD 10x4							
93	0.154	0.082	0.733	2.885	0.137	0.617	0.055
94	0.157	0.082	0.733	2.885	0.139	0.617	0.055
95	0.165	0.091	0.628	2.885	0.151	0.617	0.075
96	0.167	0.091	0.628	2.885	0.152	0.617	0.074
97	0.170	0.091	0.628	2.885	0.154	0.617	0.074

Table C.3: Ballscrews various configurations at the knee joint (Cont.)

Config. number	r_p (mm)	r_d (m)	γ_d (rad)	Moment of Inertia (kg-m^2) x 10^{-4}	Weight for the max length (kg)	Weight per length (kg/m)	Max h (m)
Type: SKF SD 10x4							
98	0.163	0.091	0.733	2.885	0.147	0.617	0.071
99	0.165	0.091	0.733	2.885	0.148	0.617	0.071
100	0.166	0.091	0.733	2.885	0.149	0.617	0.071
Type: SKF SD 12x4							
116	0.154	0.082	0.733	2.885	0.197	0.888	0.055
117	0.157	0.082	0.733	2.885	0.200	0.888	0.055
118	0.165	0.091	0.628	2.885	0.217	0.888	0.075
119	0.167	0.091	0.628	2.885	0.220	0.888	0.074
120	0.170	0.091	0.628	2.885	0.222	0.888	0.074
Type: SKF SD 14x4							
139	0.154	0.082	0.733	2.885	0.268	1.208	0.055
140	0.157	0.082	0.733	2.885	0.272	1.208	0.055
141	0.165	0.091	0.628	2.885	0.296	1.208	0.075
142	0.167	0.091	0.628	2.885	0.299	1.208	0.074
143	0.170	0.091	0.628	2.885	0.302	1.208	0.074
144	0.163	0.091	0.733	2.885	0.289	1.208	0.071
145	0.165	0.091	0.733	2.885	0.290	1.208	0.071
Type: SKF SD 16x4							
170	0.167	0.091	0.733	2.885	0.383	1.578	0.071
171	0.169	0.091	0.733	2.885	0.386	1.578	0.070
172	0.170	0.091	0.733	2.885	0.388	1.578	0.070
173	0.165	0.101	0.628	2.885	0.401	1.578	0.091
174	0.166	0.101	0.628	2.885	0.402	1.578	0.091
175	0.167	0.101	0.628	2.885	0.404	1.578	0.091
Type: SKF SD 10x10							
185	0.154	0.082	0.733	2.885	0.137	0.617	0.055
186	0.157	0.082	0.733	2.885	0.139	0.617	0.055
187	0.165	0.091	0.628	2.885	0.151	0.617	0.075
188	0.167	0.091	0.628	2.885	0.152	0.617	0.074
189	0.170	0.091	0.628	2.885	0.154	0.617	0.074
190	0.163	0.091	0.733	2.885	0.147	0.617	0.071
Type: SKF SD 10x12.7							
277	0.154	0.082	0.733	2.885	0.137	0.617	0.055
278	0.157	0.082	0.733	2.885	0.139	0.617	0.055
279	0.165	0.091	0.628	2.885	0.151	0.617	0.075
280	0.167	0.091	0.628	2.885	0.152	0.617	0.074

*It should be noted that some configurations that were not using in the optimization algorithm has not been shown.

*(SKF SD Diameter x Pitch size)

Table C.4: Ballscrews for various configurations used at the ankle joint

Config. number	r_p (mm)	r_d (m)	γ_d (rad)	Moment of Inertia (kg-m^2) x 10^{-4}	Weight for the max length (kg)	Weight per length (kg/m)	Max h (m)
Type: SKF SD 10x2							
1	0.068	0.062	2.220	2.885	0.036	0.617	0.058
2	0.084	0.062	2.220	2.885	0.042	0.617	0.064
3	0.101	0.062	2.220	2.885	0.049	0.617	0.069
4	0.117	0.062	2.220	2.885	0.058	0.617	0.071
5	0.134	0.062	2.220	2.885	0.067	0.617	0.071
6	0.150	0.062	2.220	2.885	0.076	0.617	0.071
7	0.088	0.100	1.665	2.885	0.078	0.617	0.065
8	0.108	0.100	1.665	2.885	0.087	0.617	0.065
9	0.129	0.100	1.665	2.885	0.096	0.617	0.063
10	0.150	0.100	1.665	2.885	0.106	0.617	0.059
11	0.084	0.100	2.220	2.885	0.046	0.617	0.153
12	0.097	0.100	2.220	2.885	0.051	0.617	0.122
13	0.110	0.100	2.220	2.885	0.057	0.617	0.101
14	0.124	0.100	2.220	2.885	0.062	0.617	0.098
15	0.137	0.100	2.220	2.885	0.068	0.617	0.104
16	0.150	0.100	2.220	2.885	0.074	0.617	0.109
Type: SKF SD 12x2							
17	0.068	0.062	2.220	2.885	0.051	0.888	0.058
18	0.084	0.062	2.220	2.885	0.060	0.888	0.064
19	0.101	0.062	2.220	2.885	0.071	0.888	0.069
20	0.117	0.062	2.220	2.885	0.083	0.888	0.071
21	0.134	0.062	2.220	2.885	0.096	0.888	0.071
22	0.150	0.062	2.220	2.885	0.109	0.888	0.071
23	0.088	0.100	1.665	2.885	0.112	0.888	0.065
24	0.108	0.100	1.665	2.885	0.125	0.888	0.065
25	0.129	0.100	1.665	2.885	0.138	0.888	0.063
26	0.150	0.100	1.665	2.885	0.153	0.888	0.059
27	0.084	0.100	2.220	2.885	0.066	0.888	0.153
28	0.097	0.100	2.220	2.885	0.074	0.888	0.122
29	0.110	0.100	2.220	2.885	0.082	0.888	0.101
30	0.124	0.100	2.220	2.885	0.090	0.888	0.098
31	0.137	0.100	2.220	2.885	0.098	0.888	0.104
32	0.150	0.100	2.220	2.885	0.106	0.888	0.109
Type: SKF SD 14x2							
33	0.068	0.062	2.220	2.885	0.070	1.208	0.058
34	0.084	0.062	2.220	2.885	0.082	1.208	0.064
35	0.101	0.062	2.220	2.885	0.097	1.208	0.069
36	0.117	0.062	2.220	2.885	0.113	1.208	0.071
37	0.134	0.062	2.220	2.885	0.131	1.208	0.071
38	0.150	0.062	2.220	2.885	0.148	1.208	0.071
39	0.088	0.100	1.665	2.885	0.153	1.208	0.065
40	0.108	0.100	1.665	2.885	0.170	1.208	0.065
41	0.129	0.100	1.665	2.885	0.188	1.208	0.063

Table C.4: Ballscrews configurations at the ankle joint (Cont.)

Config. number	r_p (mm)	r_d (m)	γ_d (rad)	Moment of Inertia (kg-m^2) x 10^{-4}	Weight for the max length (kg)	Weight per length (kg/m)	Max h (m)
Type: SKF SD 14x2							
42	0.150	0.100	1.665	2.885	0.208	1.208	0.059
43	0.084	0.100	2.220	2.885	0.090	1.208	0.153
44	0.097	0.100	2.220	2.885	0.100	1.208	0.122
45	0.110	0.100	2.220	2.885	0.111	1.208	0.101
46	0.124	0.100	2.220	2.885	0.122	1.208	0.098
47	0.137	0.100	2.220	2.885	0.133	1.208	0.104
48	0.150	0.100	2.220	2.885	0.145	1.208	0.109
Type: SKF SD 16x2							
49	0.068	0.062	2.220	2.885	0.091	1.578	0.058
50	0.084	0.062	2.220	2.885	0.107	1.578	0.064
55	0.088	0.100	1.665	2.885	0.200	1.578	0.065
56	0.108	0.100	1.665	2.885	0.222	1.578	0.065
57	0.129	0.100	1.665	2.885	0.246	1.578	0.063
58	0.150	0.100	1.665	2.885	0.272	1.578	0.059
59	0.084	0.100	2.220	2.885	0.117	1.578	0.153
60	0.097	0.100	2.220	2.885	0.131	1.578	0.122
61	0.110	0.100	2.220	2.885	0.145	1.578	0.101
62	0.124	0.100	2.220	2.885	0.159	1.578	0.098
63	0.137	0.100	2.220	2.885	0.174	1.578	0.104
64	0.150	0.100	2.220	2.885	0.189	1.578	0.109
Type: SKF SD 10x10							
65	0.068	0.062	2.220	2.885	0.036	0.617	0.058
66	0.084	0.062	2.220	2.885	0.042	0.617	0.064
67	0.101	0.062	2.220	2.885	0.049	0.617	0.069
68	0.117	0.062	2.220	2.885	0.058	0.617	0.071
69	0.134	0.062	2.220	2.885	0.067	0.617	0.071
70	0.150	0.062	2.220	2.885	0.076	0.617	0.071
75	0.084	0.100	2.220	2.885	0.046	0.617	0.153
76	0.097	0.100	2.220	2.885	0.051	0.617	0.122
77	0.110	0.100	2.220	2.885	0.057	0.617	0.101
78	0.124	0.100	2.220	2.885	0.062	0.617	0.098
79	0.137	0.100	2.220	2.885	0.068	0.617	0.104
80	0.150	0.100	2.220	2.885	0.074	0.617	0.109
Type: SKF SD 14x10							
100	0.117	0.062	2.220	2.885	0.113	1.208	0.071
101	0.134	0.062	2.220	2.885	0.131	1.208	0.071
102	0.150	0.062	2.220	2.885	0.148	1.208	0.071
103	0.088	0.100	1.665	2.885	0.153	1.208	0.065
104	0.108	0.100	1.665	2.885	0.170	1.208	0.065
105	0.129	0.100	1.665	2.885	0.188	1.208	0.063

*It should be noted that some configurations that were not using in the optimization algorithm has not been shown.

*(SKF SD Diameter x Pitch size)

Appendix D

Table D.1: Study Quality Assessment (Downs and Black [117])

Downs and black questions	Anderson et al. [118]	Judge et al. [119]	Kerrigan et al. [120]	Kerrigan et al. [121]	Peppe et al. [122]	Ferrain et al. [123]	Roiz et al. [124]	Ferrarin et al. [125]
1	Y	Y	Y	Y	N	N	Y	N
2	Y	Y	Y	Y	Y	Y	Y	Y
3	Y	Y	Y	Y	Y	Y	Y	Y
4	NR	NR	NR	NR	NR	NR	NR	NR
5	N	Y	Y	Y	Y	Y	Y	Y
6	Y	Y	Y	Y	Y	Y	Y	Y
7	N	Y	Y	N	Y	Y	Y	Y
8	NR	NR	NR	NR	NR	NR	NR	NR
9	NR	NR	NR	NR	NR	NR	NR	NR
10	N	N	Y	N	N	N	Y	N
11	UTD	Y	Y	N	Y	Y	Y	UTD
12	UTD	Y	Y	UTD	Y	Y	UTD	UTD
13	UTD	UTD	NR	Y	Y	Y	UTD	UTD
14	NR	NR	NR	NR	NR	NR	NR	NR
15	NR	NR	NR	NR	NR	NR	NR	NR
16	Y	Y	Y	Y	Y	N	Y	Y
17	NR	NR	NR	NR	NR	NR	NR	NR
18	Y	Y	Y	N	Y	N	Y	N
19	NR	NR	NR	NR	NR	NR	NR	NR
20	UTD	Y	Y	Y	Y	Y	Y	Y
21	UTD	UTD	N	Y	UTD	Y	Y	Y
22	UTD	UTD	UTD	Y	UTD	UTD	UTD	UTD
23	NR	NR	NR	NR	Y	NR	NR	NR
24	NR	NR	NR	NR	UTD	NR	NR	NR
25	UTD	UTD	UTD	UTD	Y	Y	Y	Y
26	NR	NR	NR	NR	NR	NR	NR	NR
27	NR	NR	NR	NR	NR	NR	NR	NR
Total score	6	11	12	10	13	11	13	9

Downs and black questions	Sofuwa et al. [130]	Zijlmans et al. [131]	Lewis et al. [127]	Morris et al. [129]	Mitoma et al. [128]	Vasco et al. [133]	Serraro et al. [132]	Stolze et al. [134]
1	Y	Y	Y	Y	Y	Y	Y	Y
2	Y	Y	Y	Y	Y	Y	Y	Y
3	Y	Y	Y	Y	Y	Y	Y	Y
4	NR	NR	NR	NR	NR	NR	NR	NR

Table D.1: Study Quality Assessment (Cont.)

Downs and black questions	Sofuwa et al. [130]	Zijlmans et al. [131]	Lewis et al. [127]	Morris et al. [129]	Mitoma et al. [128]	Vasco et al. [133]	Serraro et al. [132]	Stolze et al. [134]
5	Y	Y	NR	Y	Y	Y	Y	Y
6	Y	Y	Y	Y	Y	Y	Y	Y
7	Y	Y	Y	Y	Y	Y	Y	Y
8	NR	NR	NR	NR	NR	NR	NR	NR
9	NR	NR	NR	NR	NR	NR	NR	NR
10	Y	NR	Y	Y	N	N	Y	N
11	Y	Y	Y	Y	N	UTD	UTD	UTD
12	Y	Y	UTD	Y	Y	UTD	Y	UTD
13	UTD	UTD	Y	UTD	UTD	UTD	Y	UTD
14	NR	NR	NR	NR	NR	NR	NR	NR
15	NR	NR	NR	NR	NR	NR	NR	NR
16	Y	Y	Y	Y	Y	Y	Y	Y
17	NR	NR	NR	NR	NR	NR	NR	NR
18	Y	N	Y	Y	Y	Y	Y	N
19	NR	NR	NR	NR	NR	NR	NR	NR
20	Y	Y	Y	Y	Y	Y	Y	Y
21	Y	Y	Y	Y	Y	Y	N	Y
22	UTD	UTD	UTD	UTD	Y	Y	Y	Y
23	NR	NR	NR	NR	NR	NR	NR	NR
24	NR	NR	NR	NR	NR	NR	NR	NR
25	N	Y	Y	N	Y	Y	N	Y
26	NR	NR	NR	NR	NR	NR	NR	NR
27	NR	NR	NR	NR	NR	NR	NR	NR
Total score	13	12	13	13	13	12	13	11

Downs and black questions	Palliyath et al. [106]	Chen et al. [146]	Galli et al. [147]	Kuan et al. [116]	Mazure et al. [155]	Romkes et al. [154]	Adolfsen et al. [135]	Gomes et al. [153]
1	Y	y	Y	Y	N	Y	Y	Y
2	Y	Y	Y	Y	Y	Y	Y	Y
3	Y	Y	Y	Y	Y	Y	Y	Y
4	NR	NR	NR	NR	NR	NR	NR	NR
5	Y	Y	Y	Y	Y	Y	Y	Y
6	Y	Y	Y	Y	Y	Y	Y	Y
7	Y	Y	Y	Y	Y	Y	Y	Y
8	NR	NR	NR	NR	NR	NR	NR	NR
9	NR	NR	NR	NR	NR	NR	NR	NR
10	Y	N	N	Y	Y	N	Y	Y
11	UTD	Y	UTD	UTD	Y	Y	Y	N

Table D.1: Study Quality Assessment (Cont.)

Downs and black questions	Palliyath et al. [106]	Chen et al. [146]	Galli et al. [147]	Kuan et al. [116]	Mazure et al. [155]	Romkes et al. [154]	Adolfsen et al. [135]	Gomes et al. [153]
12	UTD	Y	Y	UTD	UTD	Y	Y	Y
13	Y	Y	Y	UTD	UTD	Y	Y	Y
14	NR	NR	NR	NR	NR	NR	NR	NR
15	NR	NR	NR	NR	NR	NR	NR	NR
16	Y	Y	Y	Y	Y	Y	Y	Y
17	NR	NR	NR	NR	NR	NR	NR	NR
18	Y	Y	N	Y	Y	N	Y	Y
19	NR	NR	NR	NR	NR	NR	NR	NR
20	Y	Y	Y	Y	Y	Y	Y	Y
21	Y	UTD	N	Y	Y	Y	N	Y
22	Y	UTD	Y	Y	Y	Y	UTD	UTD
23	NR	NR	NR	NR	NR	NR	NR	NR
24	NR	NR	NR	NR	NR	NR	NR	NR
25	UTD	Y	Y	Y	N	Y	Y	Y
26	NR	NR	NR	NR	NR	NR	NR	NR
27	NR	NR	NR	NR	NR	NR	NR	NR
Total score	13	13	12	13	12	14	14	14
Downs and black questions	**Davids et al. [136]**	**Steinwender et al. [137]**	**Eek et al. [138]**	**Sawacha et al. [145]**	**Carreiro et al. [150]**	**Langrak et al. [151]**	**Saraph et al. [152]**	**Bianco et al. [139]**
1	Y	Y	Y	Y	Y	Y	Y	Y
2	Y	Y	Y	Y	Y	Y	Y	Y
3	N	Y	Y	Y	Y	Y	Y	Y
4	NR	NR	NR	NR	NR	NR	NR	NR
5	N	Y	Y	Y	Y	Y	Y	Y
6	Y	Y	Y	Y	Y	Y	Y	Y
7	Y	Y	Y	Y	Y	N	Y	Y
8	NR	NR	NR	NR	NR	NR	NR	NR
9	NR	NR	NR	NR	NR	NR	NR	NR
10	N	N	Y	Y	Y	Y	Y	N
11	Y	N	Y	Y	Y	N	Y	N
12	Y	UTD	Y	Y	Y	Y	UTD	Y
13	Y	UTD	Y	Y	Y	Y	UTD	Y
14	NR	NR	NR	NR	NR	NR	NR	NR
15	NR	NR	NR	NR	NR	NR	NR	NR
16	Y	Y	Y	Y	Y	Y	Y	Y
17	NR	NR	NR	NR	NR	NR	NR	NR

Table D.1: Study Quality Assessment (Cont.)

Downs and black questions	Davids et al. [136]	Steinwender et al. [137]	Eek et al. [138]	Sawacha et al. [145]	Carreiro et al. [150]	Langrak et al. [151]	Saraph et al. [152]	Bianco et al. [139]
18	N	Y	Y	Y	Y	Y	Y	N
19	NR	NR	NR	NR	NR	NR	NR	NR
20	Y	Y	Y	Y	Y	Y	Y	Y
21	N	Y	Y	Y	Y	Y	Y	Y
22	Y	Y	N	N	UTD	N	Y	Y
23	NR	NR	NR	NR	NR	NR	NR	NR
24	NR	NR	NR	NR	NR	NR	NR	NR
25	N	Y	UTD	N	UTD	N	Y	Y
26	NR	NR	NR	NR	NR	NR	NR	NR
27	NR	NR	NR	NR	NR	NR	NR	NR
Total score	10	12	14	14	14	12	14	13

Downs and black questions	Ferrain et al. [140]	Onupuu et al. [141]	Rao et al. [142]	Raspovic et al. [143]
1	Y	Y	Y	Y
2	Y	Y	Y	Y
3	Y	Y	Y	Y
4	NR	NR	NR	NR
5	Y	Y	Y	Y
6	Y	Y	Y	Y
7	Y	Y	N	Y
8	NR	NR	NR	NR
9	NR	NR	NR	NR
10	Y	Y	Y	Y
11	N	N	Y	Y
12	Y	Y	Y	Y
13	Y	Y	Y	Y
14	NR	NR	NR	NR
15	NR	NR	NR	NR
16	Y	Y	Y	Y
17	NR	NR	NR	NR
18	Y	Y	Y	Y
19	NR	NR	NR	NR
20	Y	Y	UTD	Y
21	Y	Y	UTD	UTD
22	Y	N	Y	Y

Table D.1: Study Quality Assessment (Cont.)

Downs and black questions	Ferrain et al. [140]	Onupuu et al. [141]	Rao et al. [142]	Raspovic et al. [143]
23	NR	NR	NR	NR
24	NR	NR	NR	NR
25	N	N	Y	N
26	NR	NR	NR	NR
27	NR	NR	NR	NR
Total score	14	13	13	14

*Y=1, N=0, NR=not relevant, UTD=unable to determine

Appendix E

Table E.1: Optimal rigid actuation system obtained using different combinations of the transmission systems at the lower limb joints. The transmission systems used in the joint actuators were either the ball screws or the harmonic drives.

Joint Optimization	Candidate Actuator		
	Hip	**Knee**	**Ankle**
BBH	Allied motion MF95008 with ball screw configuration no. 42	Allied motion MF76008 with ball screw configuration no. 190	Allied motion MF76008 with harmonic drive CPL-25-160-2A
BHB	Allied motion MF95008 with ball screw configuration no. 42	Allied motion MF60020 with harmonic drive CPL-20-160-2A	Allied motion MF60020 with ball screw configuration no. 11
HBB	Allied motion MF60020 with harmonic drive CSD-20-160-2A	Allied motion MF76008 with ball screw configuration no. 190	Allied motion MF60020 with ball screw configuration no. 11
HHB	Allied motion MF60020 with harmonic drive CSD-20-160-2A	Allied motion MF60020 with harmonic drive CPL-20-160-2A	Allied motion MF60020 with ball screw configuration no. 11
HBH	Allied motion MF76008 with harmonic drive CSD-20-160-2A	Allied motion MF76008 with ball screw configuration no. 190	Allied motion MF76008 with harmonic drive CPL-25-160-2A
BHH	Allied motion MF95008 with ball screw configuration no. 42	Allied motion MF60020 with harmonic drive CPL-20-160-2A	Allied motion MF76008 with harmonic drive CPL-25-160-2A

*B=Ball screws, H=Harmonic drives, the first letter in the actuator symbols represents the transmission mechanism at the hip joint, second letter represents at the knee joint and third letter represents at the ankle joint

Table E.2: Optimal rigid actuation system obtained using different combinations of the transmission systems at the lower limb joints. The transmission systems used in the joint actuators were either the ball screws in a slider crank mechanism or the harmonic drives combined with a belt and pulley drive system.

Joint Optimization	Candidate Actuator		
	Hip	**Knee**	**Ankle**
BBH_B	Allied motion MF95008 with ball screw configuration no. 42	Allied motion MF76008 with ball screw configuration no. 190	Maxon EC45 with harmonic drive CPL-25-160-2A and a transmission ratio of 1:400 in a belt and pulley drive system
BH_BB	Allied motion MF95008 with ball screw configuration no. 42	Maxon EC45 with harmonic drive CPL-20-160-2A and a transmission ratio of 1:400 in a belt and pulley drive system	Allied motion MF60020 with ball screw configuration no. 11
H_BBB	Maxon EC45 with harmonic drive CSD-20-160-2A and a transmission ratio of 1:400 in a belt and pulley drive system	Allied motion MF76008 with ball screw configuration no. 190	Allied motion MF60020 with ball screw configuration no. 11
H_BH_BB	Maxon EC45 with harmonic drive CSD-20-160-2A and a transmission ratio of 1:400 in a belt and pulley drive system	Maxon EC45 with harmonic drive CPL-20-160-2A and a transmission ratio of 1:400 in a belt and pulley drive system	Allied motion MF60020 with ball screw configuration no. 11
H_BBH_B	Maxon EC45 with harmonic drive CSD-20-160-2A and a transmission ratio of 1:400 in a belt and pulley drive system	Allied motion MF76008 with ball screw configuration no. 190	Maxon EC45 with harmonic drive CPL-25-160-2A and a transmission ratio of 1:400 in a belt and pulley drive system
BH_BH_B	Allied motion MF95008 with ball screw configuration no. 42	Maxon EC45 with harmonic drive CPL-20-160-2A and a transmission ratio of 1:400 in a belt and pulley drive system	Maxon EC45 with harmonic drive CPL-25-160-2A and a transmission ratio of 1:400 in a belt and pulley drive system

*B=Ball screws, H_B=Harmonic drives combined with a belt and pulley drive, the first letter in the actuator symbols represents the transmission mechanism at the hip joint, second letter represents at the knee joint and third letter represents at the ankle joint

Table E.3: Optimal rigid actuation system obtained using different combinations of the transmission systems at the lower limb joints. The transmission systems used in the joint actuators were either the ball screws in a slider crank mechanism or a belt and pulley drive system.

Joint Optimization	Candidate Actuator		
	Hip	Knee	Ankle
BBP_B	Allied motion MF95008 with ball screw configuration no. 42	Allied motion MF76008 with ball screw configuration no. 190	Parker Hannifin K1781008Y with pulley and belt drive of ratio 1:2.6
BP_BB	Allied motion MF95008 with ball screw configuration no. 42	Parker Hannifin K1781008Y with pulley and belt drive of ratio 1:2.6	Allied motion MF60020 with ball screw configuration no. 11
P_BBB	Parker Hannifin K1781008Y with pulley and belt drive of ratio 1:2.6	Allied motion MF76008 with ball screw configuration no. 190	Allied motion MF60020 with ball screw configuration no. 11
P_BP_BB	Parker Hannifin K1781008Y with pulley and belt drive of ratio 1:2.6	Parker Hannifin K1781008Y with pulley and belt drive of ratio 1:2.6	Allied motion MF60020 with ball screw configuration no. 11
P_BBP_B	Parker Hannifin K1781008Y with pulley and belt drive of ratio 1:2.6	Allied motion MF76008 with ball screw configuration no. 190	Parker Hannifin K1781008Y with pulley and belt drive of ratio 1:2.6
BP_BP_B	Allied motion MF95008 with ball screw configuration no. 42	Parker Hannifin K1781008Y with pulley and belt drive of ratio 1:2.6	Parker Hannifin K1781008Y with pulley and belt drive of ratio 1:2.6

Table E.4: Optimal parallel elastic actuation system (PEA) assessed using different combinations of the transmission systems at the lower limb joints. The transmission systems analysed in the joint actuators were either the ball screws or the harmonic drives.

Joint Optimization	Candidate Actuator		
	Hip	Knee	Ankle
BBH	Allied motion MF76008 with ball screw configuration no.65	Allied motion MF76008 with ball screw configuration no.185	Allied motion MF76008 with harmonic drive CPL-25-160-2A
BHB	Allied motion MF76008 with ball screw configuration no.65	Allied motion MF60020 with harmonic drive CSD-20-160-2A	Allied motion MF60020 with ball screw configuration no.11
HBB	Allied motion MF76008 with harmonic drive CSD-20-160-2A	Allied motion MF76008 with ball screw configuration no.185	Allied motion MF60020 with ball screw configuration no.11
HHB	Allied motion MF76008 with harmonic drive CSD-20-160-2A	Allied motion MF60020 with harmonic drive CSD-20-160-2A	Allied motion MF60020 with ball screw configuration no.11
HBH	Allied motion MF76008 with harmonic drive CSD-20-160-2A	Allied motion MF76008 with ball screw configuration no.185	Allied motion MF76008 with harmonic drive CPL-25-160-2A
BHH	Allied motion MF76008 with ball screw configuration no.65	Allied motion MF60020 with harmonic drive CSD-20-160-2A	Allied motion MF76008 with harmonic drive CPL-25-160-2A

Table E.5: Optimal parallel elastic actuation system (PEA) assessed using different combinations of the transmission systems at the lower limb joints. The transmission systems analysed in the joint actuators were either the ball screws or the harmonic drives combined with a belt and pulley drive system.

Joint Optimization	Candidate Actuator		
	Hip	**Knee**	**Ankle**
BBH_B	Allied motion MF76008 with ball screw configuration no.65	Allied motion MF76008 with ball screw configuration no.185	Maxon EC45-flat with harmonic drive CPL-25-160-2A with a transmission ratio of 1:400 in a belt and pulley drive system
BH_BB	Allied motion MF76008 with ball screw configuration no.65	Maxon EC45-flat with harmonic drive CSD-20-160-2A with a transmission ratio of 1:350 in a belt and pulley drive system	Allied motion MF60020 with ball screw configuration no.11
H_BBB	Maxon EC45-flat with harmonic drive CSD-20-160-2A with a transmission ratio of 1:400 in a belt and pulley drive system	Allied motion MF76008 with ball screw configuration no.185	Allied motion MF60020 with ball screw configuration no.11
H_BH_BB	Maxon EC45-flat with harmonic drive CSD-20-160-2A with a transmission ratio of 1:400 in a belt and pulley drive system	Maxon EC45-flat with harmonic drive CSD-20-160-2A with a transmission ratio of 1:350 in a belt and pulley drive system	Allied motion MF60020 with ball screw configuration no.11
H_BBH_B	Maxon EC45-flat with harmonic drive CSD-20-160-2A with a transmission ratio of 1:400 in a belt and pulley drive system	Allied motion MF76008 with ball screw configuration no.185	Maxon EC45-flat with harmonic drive CPL-25-160-2A with a transmission ratio of 1:400 in a belt and pulley drive system
BH_BH_B	Allied motion MF76008 with ball screw configuration no.11	Maxon EC45-flat with harmonic drive CSD-20-160-2A with a transmission ratio of 1:350 in a belt and pulley drive system	Maxon EC45-flat with harmonic drive CPL-25-160-2A with a transmission ratio of 1:400 in a belt and pulley drive system

*B=Ball screws, H_B=Harmonic drives combined with a belt and pulley drive, the first letter in the actuator symbols represents the transmission mechanism at the hip joint, second letter represents at the knee joint and third letter represents at the ankle joint

Table E.6: Optimal parallel elastic actuation system (PEA) assessed using different combinations of the transmission systems at the lower limb joints. The transmission systems analysed in the joint actuators were either the ball screws in a slider crank mechanism or a belt drive system directly coupled to the motor.

Joint Optimization	Candidate Actuator		
	Hip	**Knee**	**Ankle**
BBP_B	Allied motion MF60020 with ball screw configuration no.11	Allied motion MF76008 with ball screw configuration no.185	Parker Hannifin K1781008Y with pulley and belt drive of ratio 1:2.6
BP_BB	Allied motion MF60020 with ball screw configuration no.11	Parker Hannifin K1781008Y with pulley and belt drive of ratio 1:2.6	Allied motion MF60020 with ball screw configuration no.11
P_BBB	Parker Hannifin K1781008Y with pulley and belt drive of ratio 1:2.6	Allied motion MF76008 with ball screw configuration no.185	Allied motion MF60020 with ball screw configuration no.11
P_BP_BB	Parker Hannifin K1781008Y with pulley and belt drive of ratio 1:2.6	Parker Hannifin K1781008Y with pulley and belt drive of ratio 1:2.6	Allied motion MF60020 with ball screw configuration no.11
P_BBP_B	Parker Hannifin K1781008Y with pulley and belt drive of ratio 1:2.6	Allied motion MF76008 with ball screw configuration no.185	Parker Hannifin K1781008Y with pulley and belt drive of ratio 1:2.6
BP_BP_B	Allied motion MF60020 with ball screw configuration no.11	Parker Hannifin K1781008Y with pulley and belt drive of ratio 1:2.6	Parker Hannifin K1781008Y with pulley and belt drive of ratio 1:2.6

*B=Ball screws, P_B =Belt and pulley drive, the first letter in the actuator symbols represents the transmission mechanism at the hip joint, second letter represents at the knee joint and third letter represents at the ankle joint

Table E.7: Optimal series elastic actuation system (SEA) assessed using different combinations of the transmission systems at the lower limb joints. The transmission systems analysed in the joint actuators were either the ball screws or the harmonic drives.

Joint Optimization	Candidate Actuator		
	Hip	**Knee**	**Ankle**
BBH	Allied motion MF95008 with ball screw configuration no.42	Allied motion MF76008 with ball screw configuration no.190	Allied motion MF76008 with harmonic drive CPL-25-160-2A
BHB	Allied motion MF95008 with ball screw configuration no.42	Allied motion MF60020 with harmonic drive CPL-20-160-2A	Allied motion MF60020 with ball screw configuration no.11
HBB	Allied motion MF76008 with harmonic drive CSD-20-160-2A	Allied motion MF76008 with ball screw configuration no. 190	Allied motion MF60020 with ball screw configuration no.11
HHB	Allied motion MF76008 with harmonic drive CSD-20-160-2A	Allied motion MF60020 with harmonic drive CPL-20-160-2A	Allied motion MF60020 with ball screw configuration no.11
HBH	Allied motion MF76008 with harmonic drive CSD-20-160-2A	Allied motion MF76008 with ball screw configuration no. 190	Allied motion MF76008 with harmonic drive CPL-25-160-2A
BHH	Allied motion MF95008 with ball screw configuration no.42	Allied motion MF60020 with harmonic drive CPL-20-160-2A	Allied motion MF76008 with harmonic drive CPL-25-160-2A

*B=Ball screws, H=Harmonic drives, the first letter in the actuator symbols represents the transmission mechanism at the hip joint, second letter represents at the knee joint and third letter represents at the ankle joint

Table E.8: Optimal series elastic actuation system (SEA) assessed using different combinations of the transmission systems at the lower limb joints. The transmission systems analysed in the joint actuators were either the ball screws or the harmonic drives combined with a belt and pulley drive system.

Joint Optimization	Candidate Actuator		
	Hip	Knee	Ankle
BBH_B	Allied motion MF95008 with ball screw configuration no.42	Allied motion MF76008 with ball screw configuration no.190	Maxon EC45-flat with harmonic drive CPL-25-160-2A and a transmission ratio of 1:400 in a belt and pulley drive system
BH_BB	Allied motion MF95008 with ball screw configuration no.42	Maxon EC45-flat with harmonic drive with a transmission ratio CPL-20-160-2A of 1:400 in a belt and pulley drive system	Allied motion MF60020 with ball screw configuration no.11
H_BBB	Maxon EC45-flat with harmonic drive CSD-20-160-2A with a transmission ratio of 1:400 in a belt and pulley drive system	Allied motion MF76008 with ball screw configuration no.190	Allied motion MF60020 with ball screw configuration no.11
H_BH_BB	Maxon EC45-flat with harmonic drive CSD-20-160-2A with a transmission ratio of 1:400 in a belt and pulley drive system	Maxon EC45-flat with harmonic drive CPL-20-160-2A with a transmission ratio of 1:400 in a belt and pulley drive system	Allied motion MF60020 with ball screw configuration no.11
H_BBH_B	Maxon EC45-flat with harmonic drive CSD-20-160-2A with a transmission ratio of 1:400 in a belt and pulley drive system	Allied motion MF76008 with ball screw configuration no.190	Maxon EC45-flat with harmonic drive CPL-25-160-2A with a transmission ratio of 1:400 in a belt and pulley drive system
BH_BH_B	Allied motion MF95008 with ball screw configuration no.42	Allied motion MF95008 with harmonic drive CPL-20-160-2A with a transmission ratio of 1:400 in a belt and pulley drive system	Maxon EC45-flat with harmonic drive CPL-25-160-2A with a transmission ratio of 1:400 in a belt and pulley drive system

*B=Ball screws, H_B=Harmonic drives combined with a belt and pulley drive, the first letter in the actuator symbols represents the transmission mechanism at the hip joint, second letter represents at the knee joint and third letter represents at the ankle joint

Table E.9: Optimal series elastic actuation system (SEA) assessed using different combinations of the transmission systems at the lower limb joints. The transmission systems analysed in the joint actuators were either the ball screws in a slider crank mechanism or a belt drive system directly coupled to the motor.

Joint Optimization	Candidate Actuator		
	Hip	**Knee**	**Ankle**
BBP$_B$	Allied motion MF95008 with ball screw configuration no.42	Allied motion MF76008 with ball screw configuration no.190	Parker Hannifin K1781008Y with pulley and belt drive of ratio 1:2.6
BP$_B$B	Allied motion MF95008 with ball screw configuration no.42	Parker Hannifin K1781008Y with pulley and belt drive of ratio 1:2.6	Allied motion MF60020 with ball screw configuration no.11
P$_B$BB	Parker Hannifin K1781008Y with pulley and belt drive of ratio 1:2.6	Allied motion MF76008 with ball screw configuration no.190	Allied motion MF60020 with ball screw configuration no.11
P$_B$P$_B$B	Parker Hannifin K1781008Y with pulley and belt drive of ratio 1:2.6	Parker Hannifin K1781008Y with pulley and belt drive of ratio 1:2.6	Allied motion MF60020 with ball screw configuration no.11
P$_B$BP$_B$	Parker Hannifin K1781008Y with pulley and belt drive of ratio 1:2.6	Allied motion MF76008 with ball screw configuration no.190	Parker Hannifin K1781008Y with pulley and belt drive of ratio 1:2.6
BP$_B$P$_B$	Allied motion MF95008 with ball screw configuration no.42	Parker Hannifin K1781008Y with pulley and belt drive of ratio 1:2.6	Parker Hannifin K1781008Y with pulley and belt drive of ratio 1:2.6

*B=Ball screws, P$_B$ =Belt and pulley drive, the first letter in the actuator symbols represents the transmission mechanism at the hip joint, second letter represents at the knee joint and third letter represents at the ankle joint

Table E.10: Optimal dual rigid actuation system in an antagonistic arrangement obtained using different combinations of the transmission systems at the lower limb joints shown according to the type of transmission systems

Joint Optimization	Candidate Actuator		
	Hip	Knee	Ankle
Transmission type: Ball screws (B) and Harmonic drives (H)			
BBH	Allied motion MF95008 with ball screw configuration no. 42	Allied motion MF76008 with ball screw configuration no. 185	Allied motion MF76008 with harmonic drive CPL-32-120-2A
BHB	Allied motion MF95008 with ball screw configuration no. 42	Allied motion MF60020 with harmonic drive CSD-20-160-2A	Allied motion MF60020 with ball screw configuration no. 11
HBB	Allied motion MF76008 with harmonic drive CSD-20-160-2A	Allied motion MF76008 with ball screw configuration no. 185	Allied motion MF60020 with ball screw configuration no. 11
HHB	Allied motion MF76008 with harmonic drive CSD-20-160-2A	Allied motion MF60020 with harmonic drive CSD-20-160-2A	Allied motion MF60020 with ball screw configuration no. 11
HBH	Allied motion MF76008 with harmonic drive CSD-20-160-2A	Allied motion MF76008 with ball screw configuration no. 185	Allied motion MF76008 with harmonic drive CPL-32-120-2A
BHH	Allied motion MF95008 with ball screw configuration no. 42	Allied motion MF60020 with harmonic drive CSD-20-160-2A	Allied motion MF76008 with harmonic drive CPL-32-120-2A
Transmission type: Ball screws (B) and Harmonic drives with pulley and belt (H_B)			
BBH_B	Allied motion MF95008 with ball screw configuration no. 42	Allied motion MF76008 with ball screw configuration no. 185	Allied motion MF76008 with harmonic drive CPL-32-120-2A with a ratio 1:400 in a belt and pulley drive
BH_BB	Allied motion MF95008 with ball screw configuration no. 42	Maxon EC45 with harmonic drive CSD-20-160-2A with a ratio 1:384 in a belt and pulley drive	Allied motion MF60020 with ball screw configuration no. 11
H_BBB	Allied motion MF76008 with harmonic drive CSD-20-160-2A with a ratio 1:400 in a belt and pulley drive	Allied motion MF76008 with ball screw configuration no. 185	Allied motion MF60020 with ball screw configuration no. 11
H_BH_BB	Allied motion MF0076008 with harmonic drive CSD-20-160-2A with a transmission ratio 1:400 in a belt and pulley drive	Maxon EC45 with harmonic drive CSD-20-160-2A with a ratio 1:384 in a belt and pulley drive	Allied motion MF60020 with ball screw configuration no. 11
H_BBH_B	Allied motion MF76008 with harmonic drive CSD-20-160-2A with a ratio 1:400 in a belt and pulley drive	Allied motion MF76008 with ball screw configuration no. 185	Allied motion MF76008 with harmonic drive CPL-32-120-2A with a ratio 1:400 in a belt and pulley drive
BH_BH_B	Allied motion MF95008 with ball screw configuration no. 42	Maxon EC45 flat with harmonic drive CSD-20-160-2A with a ratio 1:384 in a belt and pulley drive	Allied motion MF76008 with harmonic drive CPL-32-120-2A with a ratio 1:400 in a belt-pulley

Table E.10: Optimal dual rigid actuation system in an antagonistic arrangement obtained using different combinations of the transmission systems at the lower limb joints shown according to the type of transmission systems (Cont.)

Joint Optimization	Candidate Actuator		
	Hip	**Knee**	**Ankle**
Transmission type: Ball screws (B) with pulley and belt drive (P_B)			
BBP_B	Allied motion MF95008 with ball screw configuration no. 42	Allied motion MF76008 with ball screw configuration no. 185	Parker Hannifin K178100-8Y with pulley and belt drive of ratio 1:2.6
BP_BB	Allied motion MF95008 with ball screw configuration no. 42	Parker Hannifin K178100-8Y with pulley and belt drive of ratio 1:2.6	Allied motion MF60020 with ball screw configuration no. 11
P_BBB	Parker Hannifin K178100-8Y with pulley and belt drive of ratio 1:2.6	Allied motion MF76008 with ball screw configuration no. 185	Allied motion MF60020 with ball screw configuration no. 11
P_BP_BB	Parker Hannifin K178100-8Y with pulley and belt drive of ratio 1:2.6	Parker Hannifin K178100-8Y with pulley and belt drive of ratio 1:2.6	Allied motion MF60020 with ball screw configuration no. 11
P_BBP_B	Parker Hannifin K178100-8Y with pulley and belt drive of ratio 1:2.6	Allied motion MF76008 with ball screw configuration no. 185	Parker Hannifin K178100-8Y with pulley and belt drive of ratio 1:2.6
BP_BP_B	Allied motion MF95008 with ball screw configuration no. 42	Parker Hannifin K178100-8Y with pulley and belt drive of ratio 1:2.6	Parker Hannifin K178100-8Y with pulley and belt drive of ratio 1:2.6

*In the symbols above, the first letter represents the transmission mechanism at the hip joint, second letter represents at the knee joint and third letter represents at the ankle joint

Table E.11: Optimal variable parallel elastic actuation system (V-PEA) in an antagonistic arrangement obtained using different combinations of the transmission systems at the lower limb joints shown according to the type of transmission systems

Joint Optimization	Candidate Actuator		
	Hip	**Knee**	**Ankle**
Transmission type: Ball screws (B) and Harmonic drives (H)			
BBH	Parker Hannifin K089050-7Y with ball screw configuration no. 49	Kollmorgen TBM(S)7646A with ball screw configuration no. 277	Allied motion MF76020 with harmonic drive FR-25-200-2
BHB	Parker Hannifin K089050-7Y with ball screw configuration no. 49	Kollmorgen TBM(S)6051A with harmonic drive FR-25-160-2	Kollmorgen TBM(S)6051A with ball screw configuration no. 11
HBB	Allied motion MF 0076008 with harmonic drive CSD-20-160-2A	Kollmorgen TBM(S)7646A with ball screw configuration no. 277	Kollmorgen TBM(S)6051A with ball screw configuration no. 11
HHB	Allied motion MF 0076008 with harmonic drive CSD-20-160-2A	Kollmorgen TBM(S)6051A with harmonic drive FR-25-160-2	Kollmorgen TBM(S)6051A with ball screw configuration no. 11
HBH	Allied motion MF 0076008 with harmonic drive CSD-20-160-2A	Kollmorgen TBM(S)7646A with ball screw configuration no. 277	Allied motion MF76020 with harmonic drive FR-25-200-2
BHH	Parker Hannifin K089050-7Y with ball screw configuration no. 49	Kollmorgen TBM(S)6051A with harmonic drive FR-25-160-2	Allied motion MF76020 with harmonic drive FR-25-200-2
Transmission type: Ball screws (B) and Harmonic drives with pulley and belt (H_B)			
BBH_B	Parker Hannifin K089050-7Y with ball screw configuration no. 49	Kollmorgen TBM(S)7646A with ball screw configuration no. 277	Kollmorgen TBM(S)6051A with harmonic drive FR-25-160-2 with a ratio 1:258 in a belt and pulley drive
BH_BB	Parker Hannifin K089050-7Y with ball screw configuration no. 49	Kollmorgen TBM(S)6051A with harmonic drive FR-25-160-2 with a ratio 1:178 in a belt and pulley drive	Kollmorgen TBM(S)6051A with ball screw configuration no. 11
H_BBB	Kollmorgen TBM(S)6051A with harmonic drive CSD-20-160-2A with a ratio 1:400 in a belt and pulley drive	Kollmorgen TBM(S)7646A with ball screw configuration no. 277	Kollmorgen TBM(S)6051A with ball screw configuration no. 11
H_BH_BB	Kollmorgen TBM(S)6051A with harmonic drive CSD-20-160-2A with a ratio 1:400 in a belt and pulley drive	Kollmorgen TBM(S)6051A with harmonic drive FR-25-160-2 with a ratio 1:178 in a belt and pulley drive	Kollmorgen TBM(S)6051A with ball screw configuration no. 11
H_BBH_B	Kollmorgen TBM(S)6051A with harmonic drive CSD-20-160-2A with a ratio 1:400 in a belt and pulley drive	Kollmorgen TBM(S)7646A with ball screw configuration no. 277	Kollmorgen TBM(S)6051A with harmonic drive FR-25-160-2 with a ratio 1:258 in a belt-pulley

Table E.11: Optimal variable parallel elastic actuation system (Cont.)

Joint Optimization	Candidate Actuator		
	Hip	**Knee**	**Ankle**
BH_BH_B	Parker Hannifin K089050-7Y with ball screw configuration no. 49	Kollmorgen TBM(S)6051A with harmonic drive FR-25-160-2 with a ratio 1:178 in a belt and pulley drive	Kollmorgen TBM(S)6051A with harmonic drive FR-25-160-2 with a ratio 1:258 in a belt and pulley drive
Transmission type: Ball screws (B) with pulley and belt drive (P_B)			
BBP_B	Parker Hannifin K089050-7Y with ball screw configuration no. 49	Kollmorgen TBM(S)7646A with ball screw configuration no. 277	Parker Hannifin K178100-8Y with pulley and belt drive of ratio 1:2.6
BP_BB	Parker Hannifin K089050-7Y with ball screw configuration no. 49	Parker Hannifin K178100-8Y with pulley and belt drive of ratio 1:2.6	Kollmorgen TBM(S)6051A with ball screw configuration no. 11
P_BBB	Parker Hannifin K178100-8Y with pulley and belt drive of ratio 1:2.6	Kollmorgen TBM(S)7646A with ball screw configuration no. 277	Kollmorgen TBM(S)6051A with ball screw configuration no. 11
P_BP_BB	Parker Hannifin K178100-8Y with pulley and belt drive of ratio 1:2.6	Parker Hannifin K178100-8Y with pulley and belt drive of ratio 1:2.6	Kollmorgen TBM(S)6051A with ball screw configuration no. 11
P_BBP_B	Parker Hannifin K178100-8Y with pulley and belt drive of ratio 1:2.6	Kollmorgen TBM(S)7646A with ball screw configuration no. 277	Parker Hannifin K178100-8Y with pulley and belt drive of ratio 1:2.6
BP_BP_B	Parker Hannifin K089050-7Y with ball screw configuration no. 49	Parker Hannifin K178100-8Y with pulley and belt drive of ratio 1:2.6	Parker Hannifin K178100-8Y with pulley and belt drive of ratio 1:2.6

*In the symbols above, the first letter represents the transmission mechanism at the hip joint, second letter represents at the knee joint and third letter represents at the ankle joint

Table E.12: Optimal variable series elastic actuation system (V-SEA) in an antagonistic arrangement obtained using different combinations of the transmission systems at the lower limb joints shown according to the type of transmission systems

Joint Optimization	Candidate Actuator		
	Hip	**Knee**	**Ankle**
Transmission type: Ball screws (B) and Harmonic drives (H)			
BBH	Parker Hannifin K089050-7Y with ball screw configuration no. 49	Kollmorgen TBM(S)-7646A with ball screw configuration no. 277	Allied motion MF76020 with harmonic drive FR-25-200-2
BHB	Parker Hannifin K089050-7Y with ball screw configuration no. 49	Kollmorgen TBM(S)-6051A with harmonic drive FR-25-160-2	Kollmorgen TBM(S)-6051A with ball screw configuration no. 11
HBB	Allied motion MF76008 with harmonic drive CSD-20-160-2A	Kollmorgen TBM(S)-7646A with ball screw configuration no. 277	Kollmorgen TBM(S)-6051A with ball screw configuration no. 11
HHB	Allied motion MF76008 with harmonic drive CSD-20-160-2A	Kollmorgen TBM(S)-6051A with harmonic drive FR-25-160-2	Kollmorgen TBM(S)-6051A with ball screw configuration no. 11
HBH	Allied motion MF76008 with harmonic drive CSD-20-160-2A	Kollmorgen TBM(S)-7646A with ball screw configuration no. 277	Allied motion MF76020 with harmonic drive FR-25-200-2
BHH	Parker Hannifin K089050-7Y with ball screw configuration no. 49	Kollmorgen TBM(S)-6051A with harmonic drive FR-25-160-2	Allied motion MF76020 with harmonic drive FR-25-200-2
Transmission type: Ball screws (B) and Harmonic drives with pulley and belt (H_B)			
BBH_B	Parker Hannifin K089050-7Y with ball screw configuration no. 49	Kollmorgen TBM(S)7646A with ball screw configuration no. 277	Kollmorgen TBM(S)6051A with harmonic drive FR-25-160-2 with a ratio 1:258 in a belt and pulley drive
BH_BB	Parker Hannifin K089050-7Y with ball screw configuration no. 49	Kollmorgen TBM(S)6051A with harmonic drive FR-25-160-2 with a ratio 1:178 in a belt and pulley drive	Kollmorgen TBM(S)6051A with ball screw configuration no. 11
H_BBB	Kollmorgen TBM(S)6051A with harmonic drive CSD-20-160-2A with a ratio 1:400 in a belt and pulley drive	Kollmorgen TBM(S)7646A with ball screw configuration no. 277	Kollmorgen TBM(S)6051A with ball screw configuration no. 11
H_BH_BB	Kollmorgen TBM(S)6051A with harmonic drive CSD-20-160-2A with a ratio 1:400 in a belt and pulley drive	Kollmorgen TBM(S)6051A with harmonic drive FR-25-160-2 with a ratio 1:178 in a belt and pulley drive	Kollmorgen TBM(S)6051A with ball screw configuration no. 11
H_BBH_B	Kollmorgen TBM(S)6051A with harmonic drive CSD-20-160-2A with a ratio 1:400 in a belt and pulley drive	Kollmorgen TBM(S)7646A with ball screw configuration no. 277	Kollmorgen TBM(S)6051A with harmonic drive FR-25-160-2 with a ratio 1:258 in a belt and pulley drive
BH_BH_B	Parker Hannifin K089050-7Y with ball screw configuration no. 49	Kollmorgen TBM(S)6051A with harmonic drive FR-25-160-2 with a ratio 1:178 in a belt and pulley drv	Kollmorgen TBM(S)6051A with harmonic drive FR-25-160-2 with a ratio 1:258 in a belt and pulley drive

Table E.12: Optimal variable series elastic actuation system (Cont.)

Joint Optimization	Candidate Actuator		
	Hip	**Knee**	**Ankle**
Transmission type: Ball screws (B) with pulley and belt drive (P_B)			
BBP_B	Parker Hannifin K089050-7Y with ball screw configuration no. 49	Kollmorgen TBM(S)7646A with ball screw configuration no. 277	Parker Hannifin K178100-8Y with pulley and belt drive of ratio 1:2.6
BP_BB	Parker Hannifin K089050-7Y with ball screw configuration no. 49	Parker Hannifin K178100-8Y with pulley and belt drive of ratio 1:2.6	Kollmorgen TBM(S)6051A with ball screw configuration no. 11
P_BBB	Parker Hannifin K178100-8Y with pulley and belt drive of ratio 1:2.6	Kollmorgen TBM(S)7646A with ball screw configuration no. 277	Kollmorgen TBM(S)6051A with ball screw configuration no. 11
P_BP_BB	Parker Hannifin K178100-8Y with pulley and belt drive of ratio 1:2.6	Parker Hannifin K178100-8Y with pulley and belt drive of ratio 1:2.6	Kollmorgen TBM(S)6051A with ball screw configuration no. 11
P_BBP_B	Parker Hannifin K178100-8Y with pulley and belt drive of ratio 1:2.6	Kollmorgen TBM(S)7646A with ball screw configuration no. 277	Parker Hannifin K178100-8Y with pulley and belt drive of ratio 1:2.6
BP_BP_B	Parker Hannifin K089050-7Y with ball screw configuration no. 49	Parker Hannifin K178100-8Y with pulley and belt drive of ratio 1:2.6	Parker Hannifin K178100-8Y with pulley and belt drive of ratio 1:2.6

*In the symbols above, the first letter represents the transmission mechanism at the hip joint, second letter represents at the knee joint and third letter represents at the ankle joint